Titre: Title:	Natural Pore Pressure Fluctuations in a Champlain Clay Deposit
Auteur: Author:	Vahid Marefat
Date:	2016
Type:	Mémoire ou thèse / Dissertation or Thesis
Référence: Citation:	Marefat, V. (2016). Natural Pore Pressure Fluctuations in a Champlain Clay Deposit [Ph.D. thesis, École Polytechnique de Montréal]. PolyPublie. https://publications.polymtl.ca/2099/

URL de PolyPublie: PolyPublie URL:	https://publications.polymtl.ca/2099/
Directeurs de recherche: Advisors:	Robert P. Chapuis, & François Duhaime
Programme: Program:	Génie civil

UNIVERSITÉ DE MONTRÉAL

NATURAL PORE PRESSURE FLUCTUATIONS IN A CHAMPLAIN CLAY DEPOSIT

VAHID MAREFAT

DÉPARTEMENT DES GÉNIES CIVIL, GÉOLOGIQUE ET DES MINES

ÉCOLE POLYTECHNIQUE DE MONTRÉAL

THÈSE PRÉSENTÉE EN VUE DE L'OBTENTION

DU DIPLÔME DE PHILOSOPHIAE DOCTOR

(GÉNIE CIVIL)

AVRIL 2016

UNIVERSITÉ DE MONTRÉAL

ÉCOLE POLYTECHNIQUE DE MONTRÉAL

Cette thèse intitulée :

NATURAL PORE PRESSURE FLUCTUATIONS IN A CHAMPLAIN CLAY DEPOSIT

présentée par : MAREFAT Vahid

en vue de l'obtention du diplôme de : Philosophiae Doctor

a été dûment acceptée par le jury d'examen constitué de :

M. SILVESTRI Vincenzo, Ph. D., président

M. CHAPUIS Robert P., D. Sc. A., membre et directeur de recherche

M. DUHAIME François, Ph. D., membre et codirecteur de recherche

M. COURCELLES Benoît, Doctorat, membre

M. CUISINIER Olivier, Ph. D., membre

DEDICATION

To my beloved parents, my family, and Samira

ACKNOWLEDGEMENTS

RÉSUMÉ

Les argiles Champlain recouvrent les basses terres de la vallée du Saint-Laurent au Québec, dans l'est du Canada. Ces argiles ont été déposées il y a approximativement 12000 à 8500 ans dans la mer Champlain, tard dans la période du Quaternaire. Les argiles Champlain jouent un rôle crucial dans le contrôle des écoulements souterrains. Ces argiles contrôlent et protègent les aquifères sous-jacents des contaminants en provenance de la surface ou des couches plus perméables près de la surface. La conductivité hydraulique (K) est un paramètre fondamental pour estimer la vitesse d'écoulement, la vitesse de migration des contaminants et la consolidation des argiles. Du point de vue de la géotechnique, des valeurs représentatives des paramètres élastiques de l'argile applicables à de très faibles déformations sont nécessaires pour comprendre le comportement de l'argile sous des sollicitations dynamiques.

Les essais standards de laboratoire fournissent des valeurs pour les propriétés élastiques de l'argile qui dépendent du remaniement et des changements d'état de contrainte. Ces essais surestiment la compressibilité et sous-estiment le module élastique des argiles pour de très faibles déformations. Les essais conventionnels réalisés sur le terrain (p.ex. pressiomètre) sous-estiment aussi le module élastique pour les dépôts d'argile. Cette sous-estimation peut être causée par une augmentation des déformations due à l'installation de l'équipement pour la réalisation de l'essai. Des essais dynamiques spécifiques (p.ex. analyse multimodale des ondes de surface) sont utilisés pour mesurer les modules élastiques applicables à de très faibles déformations. La variation de la pression interstitielle causée par les changements de pression atmosphérique est une avenue prometteuse pour la mesure des propriétés élastiques des argiles pour de très faibles déformations.

Les essais de perméabilité in situ sont à privilégier pour la mesure de K dans les argiles. L'obtention de valeurs in situ de K par la réalisation d'essais à niveau variable dans des puits d'observation est une procédure commune. Toutefois, ce type d'essai produit des valeurs de K qui sont des estimations de la perméabilité horizontale autour du massif filtrant, pas de la perméabilité verticale à grande échelle. Cette dernière est plus importante pour l'étude de la protection des aquifères. Quand la perméabilité est anisotrope, les deux composantes, verticale et horizontale (K_h et K_v), doivent être déterminées. L'interprétation d'un essai de pompage réalisé dans un aquifère en tenant compte du débit de fuite en provenance de l'aquitard permet en théorie

de déterminer K_v. Toutefois, ce type d'essai ne s'applique pas toujours aux conditions réelles sur le terrain et il ne peut pas toujours être utilisé sur les sites contaminés. Une analyse combinée, basse et haute fréquences, des variations naturelles des pressions interstitielles dans l'argile, par exemple en raison des cycles annuels d'infiltration et des variations de la pression atmosphérique, peut être utilisée pour mesurer la valeur in situ de K et son anisotropie.

Les variations à long terme de la charge hydraulique dans la couche d'argile sont aussi importantes pour l'estimation de la vitesse de l'eau souterraine dans la couche d'argile. Le suivi à long terme de la pression interstitielle permet d'étudier les variations de la charge hydraulique. Dans un système hydrogéologique où les gradients hydrauliques sont faibles, les variations de la pression interstitielle causées par les changements de pression atmosphérique peuvent mener à des valeurs erronées du gradient. De plus, les changements de pression atmosphérique influencent la charge de pression pour les essais de perméabilité in situ. Par conséquent, les fluctuations de la pression interstitielle causées par les changements de pression atmosphérique devraient être corrigées avant l'interprétation de ces essais.

Les fluctuations naturelles de la pression interstitielle dans les dépôts d'argile peuvent être mesurées avec des piézomètres à corde vibrante (VWP), un type de capteur qui répond rapidement aux changements de pression. Les VWP peuvent être installés dans l'argile selon la méthode conventionnelle avec un massif filtrant, ou selon la méthode avec scellement complet du forage (*fully grouted*). La méthode de scellement complet reçoit depuis quelques temps plus d'attention. Selon certains, cette méthode a les avantages suivants : coûts plus faibles, pas de risque de rupture du massif filtrant et facilité d'installation. Toutefois, la performance des piézomètres installés selon cette méthode (temps de réponse et précision) n'a pas encore été validée.

Dans cette thèse, une solution analytique a été combinée avec la méthode des éléments finis pour déterminer l'erreur piézométrique en régime permanent pour des piézomètres installés dans l'argile avec la méthode du scellement complet. Les performances des piézomètres installés avec cette méthode dépendent de trois paramètres : le rapport entre la perméabilité du coulis et la perméabilité de l'argile (K_g/K_c), la composante verticale du gradient hydraulique naturel dans l'aquitard, et la profondeur du capteur dans l'aquitard. Pour un gradient hydraulique vertical inférieur à 1, l'erreur piézométrique est négligeable lorsque la perméabilité du coulis est jusqu'à

un ordre de grandeur plus grande que celle de l'argile. Pour un rapport K_g/K_c inférieur à 10, la position du capteur a une influence négligeable sur l'erreur piézométrique. Toutefois, lorsque le rapport K_g/K_c est supérieur à 100, l'erreur augmente avec la profondeur du forage et du capteur.

Les paramètres élastiques applicables pour de très faibles déformations ont été calculés à partir de la mesure in situ de l'efficacité de chargement (LE). Le paramètre LE représente la portion de la pression atmosphérique qui est portée par l'eau interstitielle d'un aquitard. Ce paramètre peut être déterminé à partir de plusieurs méthodes. Cette thèse a comparé trois méthodes de calcul : régression linéaire, inspection visuelle et fonction de réponse de la charge hydraulique (BHRF). Des valeurs de LE entre 0.8 et 0.95 ont été obtenues pour le dépôt d'argile de Lachenaie. La méthode de régression linéaire a produit des valeurs de LE plus élevées que les deux autres méthodes. L'analyse des BHRF a révélé que le paramètre LE est influencé par le délai hydraulique ou la fréquence de la sollicitation. Les BHRF ont fourni des valeurs stables de LE. On note que les trois méthodes testées dans la thèse ont fournies des valeurs de LE qui diffèrent par moins de 10 % pour un piézomètre donné.

En se basant sur la mesure in situ du paramètre LE, la compressibilité verticale et l'emmagasinement spécifique de l'argile ont respectivement été évalués à 1×10^{-6} kPa^{-1} et 1×10^{-5} m^{-1}. Le module de rigidité pour des déformations latérales empêchées a aussi été calculé et comparé à des valeurs déduites de la littérature en supposant un coefficient de Poisson entre 0.3 et 0.5. Une comparaison des paramètres élastiques obtenus à partir de l'analyse in situ de LE présentée dans cette thèse avec ceux qui ont été obtenus avec le pressiomètre, l'œdomètre et les essais de choc hydraulique confirme que la compressibilité de l'argile dépend des déformations. Le paramètre LE fournit des modules élevés qui sont valides pour de très faibles déformations et pour de l'argile non remaniée, alors que les essais conventionnels sur le terrain et au laboratoire produisent des modules plus faibles.

La valeur de K_h de l'argile a été obtenue à partir de la réponse des pressions interstitielles pour des variations de la pression atmosphérique à haute fréquence. La faible perméabilité de l'argile de Lachenaie produit des BHRF qui montrent une variation exponentielle de la charge semblable à celle qui est observée lors d'un essai de perméabilité à niveau variable. L'allure générale des BHRF correspond au comportement observé pour un aquifère à nappe captive affecté par l'emmagasinement du puits. La méthode des éléments finis a été utilisée pour simuler

l'écoulement autour des massifs filtrants et des capteurs à corde vibrante pour un changement instantané de la pression (essai à charge variable) comme analogue aux BHFR observées. L'ajustement de courbes-types numériques et des BHRF observées sur le terrain a fourni des valeurs de K_h semblables aux valeurs de K_v. Comme pour les essais de perméabilité in situ, l'analyse des BHRF évalue K_h à proximité du massif filtrant.

Les valeurs de K_v et K_h produites par l'analyse temporelle multiéchelle des variations naturelles de la pression d'eau sont à la limite inférieure des valeurs de K obtenues auparavant pour la région couverte par les sites expérimentaux. Ces valeurs de K plus faibles peuvent être expliquées dans une certaine mesure par l'effet de la compressibilité des gaz à l'intérieur de la cavité. À Lachenaie, on observe un dégazage pour certains puits installés dans le roc et on sait que l'argile contient de la matière organique et qu'elle peut produire du gaz.

Une comparaison des valeurs de K_v et K_h obtenues respectivement à partir des variations naturelles de la pression d'eau sur une base annuelle et à partir des variations de la pression atmosphérique ne montrent pas d'anisotropie pour l'argile de Lachenaie. Le rapport d'anisotropie varie entre 0.45 et 1.67. Cette observation est en accord avec les déterminations précédentes de l'anisotropie pour le dépôt de Lachenaie et pour le reste du bassin de la mer Champlain. De plus, les valeurs de K_h et K_v présentées dans cette thèse ont respectivement été obtenues à l'échelle du mètre et à l'échelle de la dizaine de mètres. La similitude des valeurs obtenues pour ces deux échelles montre le haut degré d'intégrité du dépôt d'argile de Lachenaie.

Le gradient hydraulique naturel à l'intérieur de la couche d'argile a présenté des changements significatifs pour certains sites durant la période de suivi. Pendant la période de suivi, le gradient hydraulique est passé de -0.01 à 0.6 sur le site 6 à proximité de la rivière des Mille-Îles, et de 0.01 à 0.1 sur les autres sites. La régression multiple et la méthode par inspection visuelle ont été utilisées pour corriger les données de pression interstitielle pour les changements de pression atmosphérique. Pour la plupart des piézomètres, les deux méthodes ont fourni des résultats presque identiques. Toutefois, pour les piézomètres avec une fonction BHRF montrant une réponse plus lente, la méthode de régression-multiple a fourni des courbes de la pression en fonction du temps qui sont plus lisses que celles de la méthode par inspection visuelle.

ABSTRACT

Champlain clays cover the lowlands of the Saint Lawrence River valley in Quebec, in eastern Canada. The clays were deposited approximately from 12000 to 8500 BP (before present) in the Champlain Sea, during the late Quaternary Period. Champlain clay aquitards play a crucial role in defining groundwater regimes; they control recharge and protect underlying aquifers from surface contamination. The clay K value is a fundamental parameter to estimate flow velocity, the rates of contaminant migration, and time-dependent clay deformation. From a geotechnical standpoint, representative values of the clay elastic parameters for very small-strain are needed to understand the dynamic behaviour of clay deposits.

Standard laboratory tests often yield elastic properties that depend upon sample disturbance and stress changes in clay samples: they are known to overestimate the compressibility and underestimate the elastic moduli for clay deposits. Conventional field tests (e.g., pressuremeter test) also underestimate very small-strain elastic moduli for clay deposits. This may be caused by an increase in strain due to soil disturbance during installation of testing equipment. Specific field dynamic tests (e.g., multi-modal analysis of surface wave) are recommended to estimate very-small strain elastic moduli. Pore pressure response to barometric pressure changes can be envisioned as a very small-strain test which can be used to estimate the elastic properties of the clay deposits.

In-situ permeability tests are preferred to measure K in clay deposits. Variable-head tests conducted in observation wells are common in-situ testing procedure. Nevertheless, the obtained hydraulic conductivity mainly represents the horizontal component around the intake zone (medium-scale) rather than the large-scale vertical one. The vertical hydraulic conductivity is appropriate in aquifer vulnerability assessment. When hydraulic conductivity anisotropy is present, both the vertical and horizontal components (K_v and K_h) must be determined. Aquifer pumping tests with leakage through the aquitard may yield, in theory, the clay deposit K_v. However, these tests cannot be adapted to a wide range of field conditions and may not always be used where groundwater is contaminated. A combined analysis of low- and high-frequency natural pore pressure response to in-situ loading, such as barometric pressure changes and annual groundwater recharge cycle, can be used to measure in-situ hydraulic conductivity and its anisotropy.

Long-term variations of hydraulic head within the clay layer are also of importance to estimate flow velocity within the clay layer. Baseline pore pressure monitoring allows the natural hydraulic head variations to be investigated. In an aquifer and aquitard system with a low hydraulic gradient, pore pressure fluctuations associated with barometric pressure changes may lead to erroneous gradient estimates. In addition, barometric pressure changes influence pressure head responses and in-situ permeability tests results. Therefore, pore pressure fluctuations caused by barometric pressure change should be removed from data series prior to test interpretation.

Natural pore pressure fluctuations in clay deposits can be measured with a quick response vibrating wire pressure transducer (VWP). The VWP can be installed in a clay deposit with either the conventional sand pack procedure or the fully grouted method. The fully grouted method has recently received more interest and is said to have advantages including reduced cost, no risk of failure for the sand pack, and ease of installation. However, piezometer performance (piezometer response time and measurement accuracy) is still questioned.

In this thesis, an analytical solution was combined with a finite element analysis to determine the piezometric error for fully grouted piezometers installed within clay deposits under steady state conditions. The success of a fully grouted piezometer installed in a clay deposit depends upon three parameters: permeability ratio (ratio of grout permeability K_g to surrounding aquitard permeability K_c), natural vertical hydraulic gradient within the aquitard, and installation depth within the aquitard. For field conditions with a vertical hydraulic gradient of less than 1, the piezometric error is insignificant for a grout permeability by up to one order of magnitude greater than the surroundig soil permeability. For a lower permeability ratio (i.e., $K_g/K_c \leq 10$) borehole geometry has no significant impact on piezometric error. However, for permeability ratios greater than 100, the error increases with borehole depth.

Very small strain elastic parameters were calculated based on in-situ loading efficiency (LE) analysis. LE is a portion of the barometric pressure borne by aquitard pore fluid. It can be calculated with several methods. This thesis examined three methods to determine LE including linear regression, visual inspection, and barometric head response function (BHRF). LE values between 0.8 and 0.95 were obtained for the Lachenaie clay deposit. The linear regression method provided greater LE values than the other two methods. The BHRF analysis revealed that the LE

in clay is time-lag or frequency dependent and delivered stable LE values. Nevertheless, the three methods provided values for LE within a 10% range for a given piezometer.

The vertical compressibility and specific storage were about 1×10^{-6} kPa^{-1} and 1×10^{-5} m^{-1} respectively, based on in-situ LE analysis approach. The constrained modulus was also calculated and compared with values obtained from literature by assuming a Poisson's ratio between 0.3 and 0.5. A comparison of the clay elastic parameters derived from the in situ LE analysis in this thesis with those obtained with pressuremeter, oedometer, and pulse tests confirmed that the clay compressibility is strain dependent. The LE calculation yields a high modulus for a very small-strain (undisturbed conditions), whereas the field and laboratory tests provide a lower modulus.

Values on the order of 1×10^{-5} m^2/s and 1×10^{-10} m/s were obtained for vertical hydraulic diffusivity and conductivity respectively, in the Lachenaie clay deposit. The vertical hydraulic diffusivity was determined from spectral frequency analysis of downward low-frequency cyclic groundwater recharge through the clay layer. Analysis of low-frequency pore pressure cycles provides hydraulic properties that are representative of the large-scale field condition. Spectral analysis utilizing Fast Fourier Transform provided the pressure head amplitude associated with an annual cycle which is required for hydraulic diffusivity calculation. Applying direct in-situ values of specific storage in the definition of the vertical hydraulic diffusivity yielded an in-situ K_v for the clay aquitard.

The clay K_h was obtained from analysis of pore pressure response to high-frequency barometric pressure fluctuations. For low permeability Lachenaie clay, BHRF shows an exponential pattern similar to a slug test response. The general shape of BHRF conforms to the pressure behaviour of a composite confined aquifer with a wellbore storage model. A finite element model was used to simulate the groundwater seepage around the sealed cavity caused by an instantaneous pressure change (i.e., slug test), as analogue to the observed BHRF. Curve fitting between observed BHRF and numerical simulation, both in type curve format, provided a horizontal hydraulic conductivity close to the vertical one. Similar to in-situ variable-head tests, BHRF analysis measures K_h in the immediate vicinity of the intake zone.

The K_v and K_h values provided with the multi-timescale analysis of natural pore pressure response (pore pressure responses to short-term barometric pressure change and long-term vertical groundwater recharge cycle) are at the lower bound of previously obtained K values for

the same study area. The low hydraulic conductivity values could be explained to some extent by the effects of gas compressibility within closed piezometer cavity. In Lachenaie, some wells installed in the underlying bedrock are continuously degassing and the clay contains some organic matter known to produce gas.

A comparison between K_v and K_h obtained respectively from natural pore pressure response to groundwater recharge cycles and barometric pressure changes shows insignificant permeability anisotropy for Lachenaie clay. The anisotropy ratio (K_v/K_h) was between 0.45 and 1.67. This agrees with previous works at laboratory scale and previous findings for the same study area and for other localities in the former Champlain Sea basin. In addition, K_v and K_h represent clay hydraulic conductivity for large- and medium-scale respectively. Matching permeability values obtained from analyses conducted at different scales show a high degree of integrity for the Lachenaie clay deposit.

The natural hydraulic gradient within the clay layer changes significantly on some test sites due to their hydrogeological characteristics. During this study, there was a significant change in natural gradient from -0.01 to 0.9 at site 6 next to Mille-Iles River and from 0.01 to 0.1 at the other sites. The multiple-regression and visual inspection methods were applied to correct the pore pressure data series for barometric pressure fluctuations. For most piezometers, both methods provided nearly identical results. However, for piezometers with slow BHRF response, the multiple-regression method provided smoother pore pressure time series than the visual inspection method.

TABLE OF CONTENTS

LIST OF TABLES

LIST OF FIGURES

LIST OF SYMBOLS AND ABBREVIATIONS

Symbols

α_s amplitude of the pore pressure wave at the top of the aquitard

α_z amplitude of the pore pressure wave at depth (z)

α_0 regression intercept (-)

α_1 best-fit coefficient (-)

b thickness of the clay layer (m)

B_{ave} average barometric pressure at test site (kPa)

B_{sea} average barometric pressure head at sea level (kPa)

B observed barometric pressure (kPa)

BE barometric efficiency (-)

β_w compressibility of the water (kPa^{-1})

C geometric shape factor (m)

C_c compression index (-)

C_r recompression index (-)

C_s swelling index (-)

C_U coefficient of uniformity (-)

D diameter of the borehole (m)

D_{cavity} cavity diameter (m)

D_v vertical hydraulic diffusivity (m^2/s)

δ_0 regression coefficient relating to time lag of 0 (-)

δ_i coefficients of the multiple linear regression (-)

$\hat{\delta}$ least square estimator matrix

ΔB_t change in barometric pressure, B_t-B_{t-1} (kPa)

$(\Delta B)_{t-1}$ change in pore water pressure for a previous time step (kPa)

$(\Delta B)_{t-m}$ change in pore water pressure for m previous time steps (kPa)

$\Delta \sigma$ change in total stress (kPa)

$\Delta \sigma'$ change in effective stress (kPa)

Δu_t change in pore water pressure, u_t-u_{t-1} (kPa)

Δp change in cavity pressure (kPa)

Δu_w transient pore pressure in excess of the hydrostatic pressure (kPa)

ΔV_{cavity} change in cavity volume (m3)

$\mathbf{\Delta X}$ explanatory variable matrix

$\mathbf{\Delta Y}$ dependent variable matrix

ΔW change in well water level (m)

e	void ratio (-)
ε	error (m)
ε_T	earth tide components
ET	evapotranspiration
E_{max}	low-strain elastic modulus (kPa)
F	complex Fourier component
g	gravitational acceleration (m/s^2)
G	shear modulus (kPa)
G_{ma}	very small-strain shear modulus (kPa)
G_0	low strain shear modulus (kPa)
G_s	average specific gravity of solid (-)
G_{XX}	one-side autospectral density function
H	difference in hydraulic head between the soil in natural condition and the borehole bottom (m)
$H(t)$	difference in hydraulic head (m)
$H(t=0)$	initial difference in hydraulic head (m)
h_1	hydraulic head in the upper aquifer (m)
h_3	hydraulic head in the lower aquifer (m)

h^* natural hydraulic head in the clay before installation of a piezometer (m)

h_p measured hydraulic head in the fully grouted borehole (m)

i_{AB} vertical hydraulic gradients between levels A and B (-)

i_{BC} vertical hydraulic gradients between levels B and C (-)

i^* vertical hydraulic gradient in the clay layer (-)

J fluid source or sink

K hydraulic conductivity matrix

K_1 hydraulic conductivity of the upper sandy aquifer (m/s)

K_c hydraulic conductivity of the clay layer (m/s)

K_2 hydraulic conductivity of the lower sandy aquifer (m/s)

K_g hydraulic conductivity of the cement-bentonite grout (m/s)

K_v vertical hydraulic conductivity (m/s).

K_h horizontal hydraulic conductivity (m/s)

L depth of the fully grouted borehole in the clay layer (m)

L_{cavity} cavity length (m)

LE loading efficiency (-).

m maximum number of lag (-)

m_v	compressibility of the formation (kPa^{-1})
M	constrained modulus (MPa)
n	porosity of the formation (-)
OCR	preconsolidation ratio (-)
ρ_w	unit mass of water (kg/m^3)
Q_0	flow rate coming from upper sandy layer into the borehole (m^3/s)
Q_1	flow rate injected to the clay layer from borehole side wall (m^3/s)
q	flow rate for unit length of the borehole (m^2/s)
σ	total stress (kPa)
$\boldsymbol{\sigma}$	total stress matrix
$\boldsymbol{\sigma}'$	effective stress matrix
σ'_v	vertical effective stress (kPa)
σ'_P	preconsolidation pressure (kPa)
r_0	radius of influence (m)
r_w	radius of the borehole (m)
R	runoff
S	specific surface of solid mass (m^2/kg)

S_{inj} internal cross section of piezometer (m^2)

S_s specific storage (m^{-1})

S_{XX} two-sided autospectral density function

t time (s)

T transmissivity (m^2/s)

T_P fluctuation period (s)

Tm temperature ($^{\circ}$C)

u observed pore pressure head (m).

u^* corrected relative pore pressure (kPa)

u_t observed absolute pore water pressure at time step t (kPa)

u_{t-1} observed absolute pore water pressure at previous time step (kPa)

u_w hydrostatic pore water pressure (kPa)

$\mathbf{V}$ Darcy's velocity vector

V_{cavity} volume of sand cavity (m^3)

V_s shear wave velocity (m/s)

v Poisson's ratio (-)

w natural gravimetric water content of the clay (-)

w_L liquid limit (-)

ω cyclical frequency

z elevation (m)

z_1 elevation of the top of the clay layer (m)

z_3 elevation of the bottom of the clay layer (m)

z^* elevation of the fully grouted piezometer in the clay layer (m)

Abbreviations

APT   Atmospheric Pressure Transducer

BHRF   barometric head response function

BRF   barometric response function

BETCO   Barometric and earth Tide Response Correction

BRF   Barometric Response Function

FFT   Fast Fourier transformation

KGS-BRF   Kansas Geological Survey Barometric Response Function

MMASW   multi-modal analysis of surface wave

MRCX   Multiple Regression in Excel

MW   Monitoring Well

PT   Pressure Transducer

SBPM   self-boring pressuremeter tests

SPSS   Statistical Package for the Social Sciences

VWP   Vibrating Wire piezometer

HFT   Hydraulic fracture test

PMT   Prebored pressuremeter test

ISCT   instrumented sharp cone test

LIST OF APPENDICES

CHAPTER 1   INTRODUCTION

1.1 Background

The southern lowlands of the Saint Lawrence River valley in Quebec, in eastern Canada, are covered with sensitive soft marine clay referred to as Champlain clay. The clay layer plays an important role in defining groundwater regimes; it controls recharge and protect underlying groundwater from surface contamination. Champlain clay can also be a safe location for hazardous waste storage. Meanwhile, clay aquitards in general are a poorly understood constituent of groundwater systems (Cherry et al., 2004). In geotechnical engineering, clay layers are often the most challenging components of foundation engineering problems and slope stability analyses. Representative values of their mechanical (e.g., compressibility and shear modulus) and hydraulic properties (e.g., hydraulic conductivity and diffusivity) are required for site hydrogeological characterisation and engineering applications.

The elastic and hydraulic properties of clay layers can be determined from both small core samples and in-situ tests. Laboratory tests are known to overestimate the compressibility of geological materials (Klohn, 1965; Clark, 1998; van der Kamp, 2001b). Due to sample disturbance and stress change in clay samples (Clark, 1998), laboratory tests often yield elastic properties that are questionable. This is often the case for sensitive Champlain clays (e.g., La Rochelle and Lefebvre, 1971; Tavenas et al., 1974; La Rochelle et al., 1981). In addition, when heterogeneities are present within an aquitard, the standard laboratory tests often yield matrix permeability values which are not representative of large-scale in-situ conditions (Bradbury and Muldoon, 1990; Bredehoeft et al., 2008). In-situ tests are recommended to determine clay hydraulic and elastic properties.

There are several standard methods to determine in-situ elastic and hydraulic properties of clay deposits. For example, the in-situ elastic properties of clay can be determined directly from self-boring pressuremeter tests or using correlations with cone penetration test and vane shear test results (e.g., Silvestri and Abou-Samra, 2008). The common in-situ tests that allows clay hydraulic conductivity and diffusivity to be measured include variable-head tests in monitoring wells (MWs), and pulse tests (e.g., van der Kamp, 2001b). These conventional field tests mainly provide values for the horizontal hydraulic conductivity for immediate vicinity of the MW intake

zone (Hussein et al., 2013; Odling et al., 2015). When the hydraulic conductivity is anisotropic in an aquitard, the vertical component of permeability is an important factor in assessing contaminant migration. The vertical hydraulic conductivity of clay aquitards can be obtained in the field by conducting aquifer pumping tests that considers leakage from clay aquitard (Hantush, 1956). Such a test can be costly and time consuming and may not be adaptable for a wide-range of field test conditions.

This thesis propose to use analysis of in-situ natural pore pressure response to barometric pressure change and vertical groundwater recharge cycle to calculate clay aquitard horizontal and vertical hydraulic conductivity and its anisotropy. Pore pressure in clay layers reacts to various natural phenomena including barometric pressure change, Earth and ocean tide fluctuations, precipitations, ground water recharge and discharge events (Timms and Acworth, 2005; Anochikwa et al., 2012; Hussein et al., 2013; Smith et al., 2013; Smerdon et al., 2014). Among the variety of natural stress sources, pore pressure response to barometric stress changes deserves more attention. Atmospheric pressure changes are continuous and ubiquitous and the solicitation and response data can be obtained with relative ease (Seo, 1999). Hydrogeologists taken advantage of these naturally occurring pore pressure fluctuations to estimate aquitard properties (e.g., Timms and Acworth, 2005; Anochikwa et al., 2012; Hussein et al., 2013; Smith et al., 2013). This approach is useful for example where groundwater is contaminated and conventional in-situ tests are limited (Furbish, 1991).

Long-term low-frequency vertical groundwater recharge cycles can be used to estimate large-scale clay vertical hydraulic properties (Keller et al., 1989; Neuman and Gardner, 1989). The amplitude of the groundwater recharge cycle imposed by the surficial aquifer is attenuated and lagged while propagating downward within the clay aquitard. The amplitude attenuation for a given signal period is required for vertical hydraulic diffusivity calculation. Previous studies performed by Keller et al. (1989) and Timms and Acworth (2005) simply subtracted the associated well hydrographs to calculate the attenuation in the groundwater recharge amplitude. This graphical method is inaccurate because it depends upon scale and visual appreciations. However, a more accurate method is needed to calculate pressure head amplitude corresponding to a given signal frequency.

Measuring pore pressure fluctuations within a clay layer is rarely a straightforward task in

geotechnical, mining, and groundwater engineering. Due to the appreciable response time of open standpipe piezometers, faster diaphragm-type transducers (e.g., vibrating wire piezometers) are preferred to monitor pore pressures within clay formations. The conventional sand pack procedure for standpipe piezometer has been adapted and used with fast diaphragm-type piezometers by the geotechnical and mining industry for decades (Hvorslev, 1951; Dunnicliff, 1988). Some practitioners have proposed to eliminate the sand filter around the piezometer, and to grout completely the borehole after having positioned the sensor. This method is referred to as the fully grouted installation method. Nevertheless, the performance of fully grouted piezometers is still questioned by some practitioners in hydrogeology and geotechnique. Previous investigators have noted that the success of fully grouted piezometers depends only on grout permeability and a few authors have tried to prove that a grout more permeable than the target formation induces a small error (e.g., Vaughan, 1969; Mikkelsen and Green, 2003; Contreras et al., 2008). However, from field results, McKenna (1995) concluded that the grout permeability should be lower than surrounding soil permeability in order to reduce piezometric error. One can see that there are inconsistencies in the grout criteria.

Clay elastic parameters associated with very small strain deformations are required to understand the dynamic behaviour of clay deposits (e.g., Lefebvre et al., 1994; Youd et al., 2001). For example, the very small strain shear modulus allows sites to be classified according to their response to earthquakes (Canadian Geotechnical Society, 2006). In this context, the need to study very-small strain parameters for clay deposits is becoming more significant. These parameters can be determined by in-situ geophysical methods (e.g., multi-modal analysis of surface wave) and laboratory methods (e.g., resonant column tests). Loading efficiency measurements from the analysis of the natural pore pressure response to barometric pressure changes can be envisioned as a very small-strain test. Loading efficiency is the ratio of change in aquifer total head to the change in barometric pressure (i.e., that portion of the barometric pressure borne by aquitard pore fluid). Loading efficiency analysis provides clay elastic parameters that are associated with very small strains and very low clay disturbance.

Most of the previous studies dealing with the analysis of loading efficiency and the natural pore pressure response in clay aquitards were limited to simple linear regression models or visual inspection methods (Timms and Acworth, 2005; Smith et al., 2013; Smerdon et al., 2014). However, for cases involving a time lag between barometric pressure change and piezometer

response, these methods do not model the complex relationship between pressure head response and barometric pressure change (Weeks, 1979; Furbish, 1991; Rasmussen and Crawford, 1997). For such cases, barometric response functions, BRF, or barometric head response functions, BHRF can be used to analyze the time-dependent pore pressure response to barometric pressure change (Furbish, 1991; Rasmussen and Crawford, 1997).

In time domain, BRF and BHRF are impulse functions which represent well water-level/aquifer total head response for a unit change in barometric pressure (Spane, 2002). The BRF and BHRF can be determined from slug and pulse test solutions (Rasmussen and Crawford, 1997). The obtained model can be used to estimate the permeability of geological units (Spane, 2002). In time domain, BRF is calculated by performing a multiple regression. BRF has been presented in a type-curve format to determine hydraulic properties for a few aquifer/aquitard systems. Previous studies performed by Butler et al. (2011) and Hussein et al. (2013) fitted BRF from an underlying confined aquifer response with an analytical model to determine the vertical hydraulic diffusivity for the overlying confining layer. None of the previous studies utilized actual aquitard pressure responses obtained from partially penetrating wells within clay aquitards as a basis for estimating in-situ aquitard hydraulic properties.

The influence of barometric pressure changes on well water-level/pore pressure have been used to monitor contaminated aquifer and aquitard systems (Hare and Morse, 1997; Hare and Morse, 1999), and as an indicator of underlying aquifer vulnerability (Hussein et al., 2013; Odling et al., 2015). Major fluctuations in well water-level associated with barometric stress changes lead to hydraulic gradients and flow velocities that are inaccurate (Rasmussen and Crawford, 1997; Seo, 1999; Spane, 2002). In addition, barometric pressure change can disguise the results of in-situ permeability tests (Supardi, 1993; Rasmussen and Crawford, 1997; Spane, 2002). An appropriate technique should be selected for various field conditions in order to eliminate the influence of such fluctuations on pore pressure response.

Natural, even homogenous, soils are known to develop some hydraulic conductivity anisotropy during deposition and the densification process (Chan and Kenney, 1973; Olson and Daniel, 1981; Al-Tabbaa and Wood, 1987; Chapuis and Gill, 1989; Chapuis et al., 1989; Scholes et al., 2007). Permeability anisotropy is an important parameter for the analysis of seepage through earth dams and dykes, contaminant migration, settlement rates for clays, design of drainage

systems, and optimum design of oil or water well fields (e.g., Chapuis and Gill, 1989). In clay-rich sediments, the permeability anisotropy is caused by changes in particle orientation, size and shape of pores (Neuzil, 1994). The in-situ anisotropy of clay aquitards can be assessed based on conventional slug tests in partially penetrating wells of different aspect ratios (Hvorslev, 1951) and from aquifer pumping tests with leakage from clay aquitards (Hantush, 1956). These field tests however, may not be adaptable for a wide-range of field conditions and can be cost intensive. The assessment of permeability anisotropy for Champlain clay has been limited to laboratory work (Tavenas et al., 1983a; Leroueil et al., 1990; Duhaime, 2012) which may not be representative of field conditions.

Despite previous research efforts regarding the analysis of the natural pore pressure response in clay aquitards, some gaps remain. They can be summarized as follows:

- The capacity and limitations of fully grouted piezometers for pore pressure measurements in clay aquitards are not fully understood.

- For clay aquitards, time lag is not taken into account when evaluating the loading efficiency and when correcting raw pore pressure data for barometric effect. The impact of the time lag on these estimates is not well understood.

- The factors impacting the BHRF shape for clay aquitards and the link between this shape and the in-situ horizontal hydraulic conductivity remains unclear.

- For low-frequency groundwater cycle, the spectral frequency analysis was not used when calculating hydraulic diffusivity and conductivity. The isolated groundwater recharge for a period of year was not clearly analyzed.

- The link between natural pore pressure response and hydraulic conductivity anisotropy in large-scale remains unclear.

1.2 Objectives

The main and specific objectives of this thesis can be summarized as follows:

1. Determining the limitations of the fully grouted installation method when it is deployed for pore pressures measurement within clay layers (Paper 1).

2. Estimating the in-situ elastic parameters of Lachenaie clay for very small strains from the natural pore pressure response to barometric pressure changes (Paper 2).

The specific objectives of paper 2 were:

2.1. Calculating the loading efficiency for the Lachenaie clay aquitard using three methods of linear regression, visual inspection and BHRF.

2.2. Investigating the capability of BHRF to remove barometric pressure effects on pore pressure response in a soft clay aquitard.

2.3. Monitoring long-term variations of vertical hydraulic gradient within a Champlain clay layer.

3. Estimating the in-situ vertical and horizontal hydraulic diffusivity and conductivity from multi-timescale analysis of a combined low- to high-frequency natural pore pressure response (Paper 3).

The specific objectives of paper 3 were:

3.1. Determining the in-situ vertical hydraulic diffusivity and conductivity for Lachenaie clay aquitard from analysis of long-term pore pressure response to low-frequency vertical groundwater recharge cycle.

3.2. Determining the in-situ horizontal hydraulic conductivity for Lachenaie clay aquitard from analysis of short-term pore pressure response to high-frequency barometric pressure change (BHRF analysis).

3.3. Assessing the in-situ hydraulic conductivity anisotropy for Lachenaie clay based on a multi-timescale analysis of the natural pore pressure response (i.e., pore pressure responses to short-term barometric loading and long-term groundwater recharge cycle).

1.3 Scope and content

It is proposed in this study that the in-situ elastic and hydraulic properties of soft and sensitive Champlain clay can be determined by a combined analysis of low- and high-frequency pore

pressure response to barometric pressure change and groundwater recharge cycle. This dissertation includes seven chapters: Chapter 1 presents the background, gaps in knowledge, and objectives of the study. Chapter 2 of this dissertation presents a state of art and practice literature review on the following themes:

- ✓ In-situ pore pressure measurement,

- ✓ Effective stress principle,

- ✓ Stress-strain relationship,

- ✓ Pore pressure response to natural loading in clay layer,

- ✓ In-situ estimation of clay aquitard elastic properties,

- ✓ Methods for loading efficiency calculation,

- ✓ Barometric response function,

- ✓ Mathematical equations for multiple-regression,

- ✓ BRF/BHRF and groundwater vulnerability,

- ✓ Methods for eliminating the effects of barometric pressure fluctuations,

- ✓ Clay hydraulic conductivity,

- ✓ Hydraulic conductivity anisotropy,

- ✓ Simple spectral frequency analysis and filtering,

- ✓ Champlain clay and its mechanical properties.

Chapters 3 through 5 are the main part of this dissertation which includes three manuscripts. One of them was published and the others two were submitted to peer-reviewed journals:

- ➢ Chapter 3: "Fully grouted piezometers: Implications for pore pressure monitoring in clay layers," submitted to Engineering Geology on September, 2015.

- ➢ Chapter 4: "Pore pressure response to barometric pressure change in Champlain clay: Prediction of the clay elastic properties," published in Engineering Geology on November, 2015.

➢ Chapter 5: "Estimates of in-situ vertical and horizontal hydraulic diffusivity and conductivity for a shallow clay aquitard, using a combined natural recharge and barometric pressure response approach," submitted to Journal of Hydrology on January, 2016.

Four conference papers (Marefat et al. 2013, 2014, 2015a, and 2015b) were also published in the course of this doctoral work.

In summary, the main chapters (chapters 3 through 5) of this thesis include the followings:

Chapter 3 present presents analytical and numerical models to predict piezometric error for fully grouted piezometers installed within clay layer under steady state condition. With the fully grouted installation method, there is no sand filter around the piezometer. This method is said to have the following advantages: reduced cost, no risk of failure for the sand pack, and ease of installation, especially for nested piezometers. A closed-form equation for the piezometric error was derived and verified with the finite element code of SEEP/W. More than 300 numerical simulations were completed to assess the piezometric error equations. For a steady state flow, the piezometer performance is controlled by three factors: a) the permeability ratio, ratio of grout permeability to surrounding aquitard permeability, b) the natural vertical hydraulic gradient, and c) the borehole geometry. This paper is an introduction to the fully grouted installation method for a steady state groundwater flow condition. The piezometer performance under transient flow condition was not addressed in this paper. The problem was introduced in Marefat et al. (2015c) and orally presented in the 68th Canadian Geotechnical Conference, Quebec, Canada.

Chapter 4 discusses a detailed baseline natural pore pressure monitoring program on 5 study sites with a combined area of 50 km^2 near Montreal in Quebec, Canada. This chapter provides very small-strain elastic properties for Lachenaie clay based on analysis of natural pore pressure response to barometric pressure changes. The compressibility values obtained in this thesis are up to two orders of magnitude smaller than those given by previous results of oedometer and pulse tests. This indicates strain dependency of clay elastic properties. This chapter also provides long-term variation for the natural vertical hydraulic gradient in the clay layer. The methods to extract the influence of barometric pressure changes on pore pressure response are discussed.

Chapter 5 presents a numerical and analytical model to assess in-situ vertical and horizontal hydraulic diffusivities-conductivities for clay deposits. A combined multi-timescale analysis of

groundwater recharge cycles and barometric pressure responses was used. Analysis of pore pressure response to the downward low-frequency (annual term) groundwater recharge cycles yielded large-scale values for the vertical hydraulic diffusivity. Applying direct in-situ values of specific storage in the definition of the vertical hydraulic diffusivity yielded a large-scale vertical hydraulic conductivity for the clay deposit. The clay horizontal hydraulic conductivity was determined from pore pressure response to short-term (high-frequency) barometric pressure change in terms of BHRF. In time domain, BHRF is an impulse response that describes pore pressure imbalance between borehole and surrounding clay associated with a unit change in barometric pressure. The pore pressure imbalance creates a transient flow between borehole and clay aquitard which is essentially horizontal for a partially penetrating well in the clay aquitard. The finite element code of SEEP/W was used to simulate the transient flow around the borehole as an analogue to BHRF. The horizontal hydraulic conductivity was estimated by curve matching between BHRF and predicted numerical model results. The obtained horizontal hydraulic conductivity from BHRF represents the value for the clay adjacent to the piezometer cavity zone, thus a local value, similar to in-situ variable head test results. However, the vertical hydraulic conductivity determined from analysis of low-frequency pore pressure cycles is a large-scale value for a multiple depth intervals along vertical direction. Analysis of low- and high-frequency pore pressure responses also provided a basis to assess hydraulic conductivity anisotropy in field scale without conducting extensive conventional tests.

It should be noted that the two manuscripts included in the Chapters 3 and 5 are based on those initially submitted to the journals. Subsequent corrections and reviews (as demanded by the Reviewers and Editors, and others), before publication in the Journals, are not included here. Thus, the final published papers may differ from the versions appearing in the dissertation.

Chapter 6 gives a summary and discussion for the obtained results, and Chapter 7 presents main results and recommendations for future works.

CHAPTER 2   LITERATURE REVIEW

Pore pressures in aquifer/aquitard systems often respond to natural stresses such as atmospheric pressure fluctuations, Earth and ocean tides, groundwater recharge events, seismic waves, soil moisture storage, and human activities at ground surface. This natural pore pressure response results from the interaction between change in total stress, pore pressure and deformation in a porous medium. This interaction is governed by the mechanical and hydraulic properties of the porous medium. Hydrogeologists have long been interested in taking advantage of these natural pore pressure responses to determine aquifer/aquitard properties (Jacob, 1940; Jacob, 1950; van der Kamp and Gale, 1983; Rojstaczer, 1988a; Timms and Acworth, 2005; Hussein et al., 2013; Smith et al., 2013; Smerdon et al., 2014). However, measuring pore pressures within a clay layer is rarely a straightforward task in both hydrogeology and geotechnical engineering. An appropriate procedure should be selected for piezometer installation in order to measure in-situ pore pressures that are representative of the real clay aquitard condition.

2.1   In-situ pore pressure measurement

Open standpipe piezometers with a sand filter around the piezometer screen have traditionally been used for pore pressure measurement. A smaller inner diameter is essential to have a quick piezometer response (Hvorslev, 1951). In a low permeability formation (e.g., clay layer), the standpipe piezometer response is very slow due to slow pore pressure equalization between the piezometer screen and the formation. This results in a time lag between pressure change within the clay layer and piezometer response. Due to the appreciable response time of open standpipe piezometers, faster diaphragm-type transducers are needed to monitor pore pressures within clay formations (e.g., Hvorslev, 1951). Diaphragm-type piezometers only need a very small volume of water for full scale equalization (McKenna, 1995). A vibrating wire piezometer, VWP, is a kind of quick response diaphragm transducer that needs only 10^{-5} to 10^{-2} cm^3 volume of water for full scale pore pressure equalization. The traditional sand-pack installation method of standpipe piezometers has been adapted for the installation of VWPs by the geotechnical industry (Dunnicliff, 1988). Although the fully grouted or grouted-in method for installation of faster diaphragm-type piezometers was first suggested by Vaughan (1969), the performance of this

installation method is still questioned by some in the geotechnical and hydrogeology communities.

With the conventional method, the VWP is installed within a sand filter at the proper depth within a borehole, and the space above the filter pack is plugged with bentonite chips or pellets. Then, the annular space around the VWP cable in the borehole is backfilled with cement-bentonite grout. With the fully grouted installation method there is no sand filter pack around the piezometer. After having positioned the VWP at the desired depth, the entire borehole is backfilled with low permeability and non-shrinkable cement-bentonite grout (Figure 2.1).
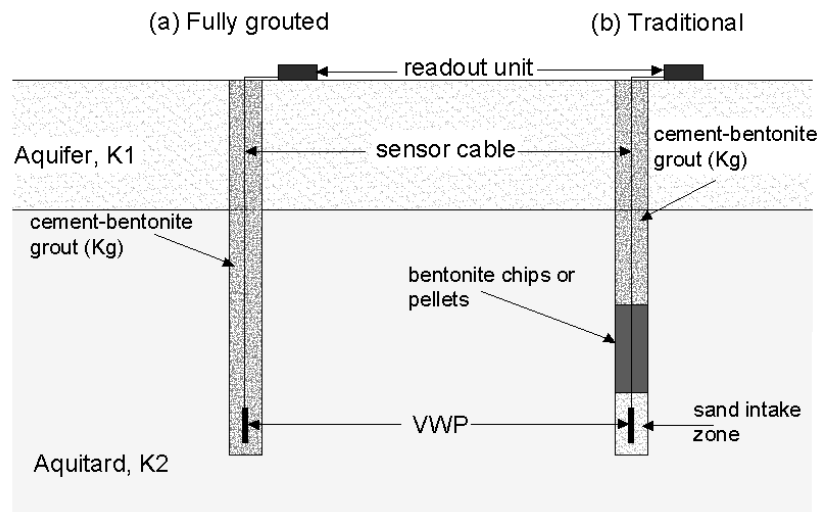
Figure 2.1: Vertical sketch of VWP installation: a) fully grouted method; b) traditional method.

Proponents of the fully grouted method cite several advantages for this method. These advantages include reduced cost, ease of installation, no risk of failure for the sand pack of deep wells, opportunity to install other geotechnical instruments in the same borehole, opportunity to install nested piezometers within the same borehole, and possibility of installing horizontal or inclined piezometers (McKenna, 1995). Recently, a number of investigators have advocated and tried to gain accurate and reliable natural pore pressure measurements for both single and multiple diaphragm-type piezometers installed with the fully grouted method (McKenna, 1995; Simeoni et al., 2011; Contreras et al., 2012; Smith et al., 2013; Smerdon et al., 2014). These

authors demonstrated how fully grouted piezometers were able to monitor natural pore pressure fluctuations within low permeability formations.

Regardless of the installation method, two criteria should be satisfied by each piezometer: 1) the piezometric error should be small, and 2) the time lag should be as short as possible (McKenna, 1995). The conventional installation method satisfies both criteria. First, the bentonite chips or pellets at the top of the sand pack can isolate perfectly the MW's intake zone. The vertical fluid flow along the well axis is thus restricted. Hence, the pressure measured in the intake zone is representative of the real formation conditions. Moreover, the permeable and fairly large intake zone in the conventional installation method quickly equalizes the pressure imbalance between the formation and the well, but there is always a small time lag (Hvorslev, 1951; Chapuis, 2009a). Under specific circumstances, the fully grouted method can also satisfy the two aforementioned criteria. The success of the fully grouted method relies on the fact that this type of transducers only needs 10^{-5} to 10^{-2} cm^3 of water for full scale pore pressure equalization, a small volume which has to travel a short distance in the grout between the surrounding soil and the piezometer tip (McKenna, 1995).

Grout hydraulic conductivity, K_g, is a key factor controlling the piezometric error in the fully grouted method (Vaughan, 1969; McKenna, 1995; Mikkelsen, 2002; Mikkelsen and Green, 2003; Contreras et al., 2008). For steady state seepage, Vaughan (1969) proposed that the error may be negligible for a grout having a permeability up to two orders of magnitude greater than the adjacent formation permeability. Moreover, Contreras et al. (2008), using numerical modelling for steady state seepage condition with SEEP/W, found an error close to zero when the grout had a hydraulic conductivity within 3 orders of magnitude of the surrounding formation. They defined a normalized piezometric error (ε):

$$\varepsilon = \frac{u_g - u}{u} \times 100 \qquad (2.1)$$

where u_g and u are the computed pore water pressure within the fully grouted borehole and in the formation far away from the fully grouted borehole, respectively. The normalized error defined by Eq. (2.1) is biased with regard to the formation pore pressure, or the reference system for the pore pressure measurement (u). Therefore, the piezometric error calculated by Eq. (2.1) cannot be representative of real field conditions. McKenna (1995) compared the accuracy of

piezometers installed with the fully grouted and conventional installation methods. His work resulted in the following important conclusions applicable to various hydrogeological configurations: (1) fully grouted piezometers can provide hydraulic head measurements that are accurate; (2) for most soil conditions, the grout must be less permeable than the surrounding ground in order to reduce the piezometric error.

The response time for modern diaphragm-type piezometers installed within fully grouted boreholes under controlled laboratory conditions has previously been assessed by several investigators. McKenna (1995) conducted some laboratory experiments to describe the response time of fully grouted piezometers. He concluded that for real field conditions with a few centimeters of grout between the borehole wall and the piezometer tip, the response time would be a matter of seconds or minutes. From laboratory testing, Mikkelsen (1999), Bayrd (2011), and Simeoni (2012) found that fully grouted piezometers will equalize after a very short delay for a given pressure change. However with numerical modelling, Zawadzki and Chorley (2014) obtained that the response time for a fully grouted piezometer, installed within a fractured rock and subjected to transient flow, can take hours as compared to the almost instantaneous response of a piezometer installed within a sand filter.

One can clearly see that there are inconsistencies in previous results regarding reliable grout criteria for a successful application of the fully grouted method. The impact of grout hydraulic conductivity and other factors upon the piezometeric error and lag time for the fully grouted method should be studied more thoroughly.

2.2   Effective stress principle

Mechanical surface loading can cause an immediate change in pore water pressure within a saturated soil (Jacob, 1940; Terzaghi and Peck, 1948). The externally applied stress will be distributed between water and solids. Upon the application of a load increment, it is transmitted to the pore water instantaneously. This pore pressure increase is referred to as excess pore pressure. As it dissipates, the load portion carried by the excess pore pressure is progressively transmitted to the soil skeleton (increase in effective stress). Ultimately the excess pore water pressure becomes zero and thus the whole incremental stress is carried by the solid skeleton. This

process is known as consolidation. The difference between the applied total stress, $\boldsymbol{\sigma}$, and pore pressure u_w is known as the effective stress, $\boldsymbol{\sigma}'$. Pore pressure and effective stress in a porous medium after the application of a mechanical loading can be described as follows (Terzaghi, 1936; Holtz et al., 1986):

$$\boldsymbol{\sigma}' = \boldsymbol{\sigma} - u_w \tag{2.2a}$$

where $\boldsymbol{\sigma}$ and $\boldsymbol{\sigma}'$ are the total and effective stress tensors, which can presented in the matrix form as follows:

$$\boldsymbol{\sigma} = \begin{pmatrix} \sigma_{xx} & \tau_{xy} & \tau_{xz} \\ \tau_{yx} & \sigma_{yy} & \tau_{yz} \\ \tau_{zx} & \tau_{zy} & \sigma_{zz} \end{pmatrix} \tag{2.2b}$$

$$\boldsymbol{\sigma}' = \begin{pmatrix} \sigma_{xx} - u_w & \tau_{xy} & \tau_{xz} \\ \tau_{yx} & \sigma_{yy} - u_w & \tau_{yz} \\ \tau_{zx} & \tau_{zy} & \sigma_{zz} - u_w \end{pmatrix} \tag{2.2c}$$

where σ_{xx}, σ_{yy}, and σ_{zz} are total stresses on planes perpendicular to the x, y and z axes, τ_{xy}, τ_{yz}, and τ_{zx} are shear stresses.

In a coarser-grained material, upon loading, the water will be squeezed out of the pores almost instantaneously. Fine grained materials, however, need a long time to dissipate the excess pore water pressure, thus the consolidation of fine grained material is time-dependent. The time needed for consolidation in clay materials can be of the order of months, years or even decades (e.g., Holtz and Kovacs, 1981; Terzaghi et al., 1996). The effective stress principle is applicable for natural stress phenomena (e.g., barometric pressure) as well, that is to say a change in natural stress is shared between pore water and the aquitard skeleton (Anochikwa et al., 2012).

2.3 Stress strain relationship

There are several models describing stress-strain relationship for clays. The linear elastic model has commonly been applied to assess the behaviour of (1) overconsolidated clays (Crooks and Graham, 1976; Burland, 1989; Van der Kamp and Maathuis, 1991; Timms and Acworth, 2005;

Anochikwa et al., 2012; Duhaime, 2012); (2) undrained behaviour of clays (Tavenas et al., 1974; Leroueil et al., 1985); and (3) natural clays for stresses lower than yield (Crooks and Graham, 1976). However, when stresses exceed the yield stress, strains are large and irrecoverable. Then, an elastic-plastic model is required to study the soil plastic behaviour (Wood, 2010). Several elastic-plastic models including Mohr-Coulomb, Cam clay, modified Cam clay, and modified Drucker-Prager/cap models were developed to predict soil plastic behaviours. The modified Cam clay model is a particular elastic-plastic model that is frequently used in geotechnical engineering, especially for soft soils (Helwany, 2007; Wood, 2010). The stress-dependent soil strength, compression, and volume change caused by shearing can be calculated using the modified Cam clay model.

Several authors have used an elastic model to describe the stress and strain induced by natural loading phenomena in a clay layer (van der Kamp and Gale, 1983; Rojstaczer and Agnew, 1989; Van der Kamp and Maathuis, 1991; Timms and Acworth, 2005; Anochikwa et al., 2012). In addition, Duhaime (2012) used a linear elastic model for the interpretation of in-situ permeability tests in Lachenaie clay. For an elastic isotropic behaviour, the generalized Hooke's law can be used and the elastic properties are characterized entirely by the Young's modulus, E, and Poisson's ratio, v, which are independent from orientation (Helwany, 2007; Wood, 2010). The effective stress-strain relationship for a 3D orthogonal coordinate system can be written as:

$$
\begin{Bmatrix} \sigma'_x \\ \sigma'_y \\ \sigma'_z \\ \tau_{xy} \\ \tau_{yz} \\ \tau_{zx} \end{Bmatrix} = \frac{E}{(1+v)(1-2v)} \begin{bmatrix} 1-v & v & v & 0 & 0 & 0 \\ v & 1-v & v & 0 & 0 & 0 \\ v & v & 1-v & 0 & 0 & 0 \\ 0 & 0 & 0 & 1-2v & 0 & 0 \\ 0 & 0 & 0 & 0 & 1-2v & 0 \\ 0 & 0 & 0 & 0 & 0 & 1-2v \end{bmatrix} \times \begin{Bmatrix} \varepsilon_x \\ \varepsilon_y \\ \varepsilon_z \\ \gamma_{xy} \\ \gamma_{yz} \\ \gamma_{zx} \end{Bmatrix} \tag{2.2d}
$$

where σ'_x, σ'_y, and σ'_z are effective stresses on planes perpendicular to the x, y and z axes, ε_x, ε_y, and ε_z are axial strains, and γ_{xy}, γ_{yz}, and γ_{zx} are shear strains. The laterally constrained, M, and shear, G, moduli can be estimated with the following theoretical equations through Poisson's ratio and Young's modulus:

$$
M = \frac{E(1-v)}{(1+v)(1-2v)} \tag{2.3}
$$

$$G = \frac{E}{2(1+v)} \qquad (2.4)$$

A test method may involve three types of stress-strain behaviour for a soil specimen: very small strain $<10^{-3}$ % (e.g., Shibuya et al., 1997; Karray and Lefebvre, 2008), small strain between 0.001 and 0.1 %, and large strain >0.1 % (e.g., Burland, 1989). Dynamic field or laboratory tests considering very small strain provide elastic moduli (e.g., shear modulus) that are significanly greater than those obtained from conventional triaxial tests or in-situ methods assuming linear elastic behaviour (Viggiani and Atkinson, 1995). The shear modulus applicable to very small strain, G_{max}, is required for the analysis of soil dynamic behaviour (Viggiani and Atkinson, 1995; Youd et al., 2001). For example, G_{max} is used to classify sites according to their response to earthquakes (Canadian Geotechnical Society, 2006). Anderson and Richart Jr (1976) with dynamic tests showed that the shear modulus reduces with increasing strain. An analogous reduction in stiffness with strain increment was also found by Jardine et al. (1984) with conventional triaxial tests. Figure 2.2 represents an idealized variation of shear modulus with deformation for a large range of strain levels.
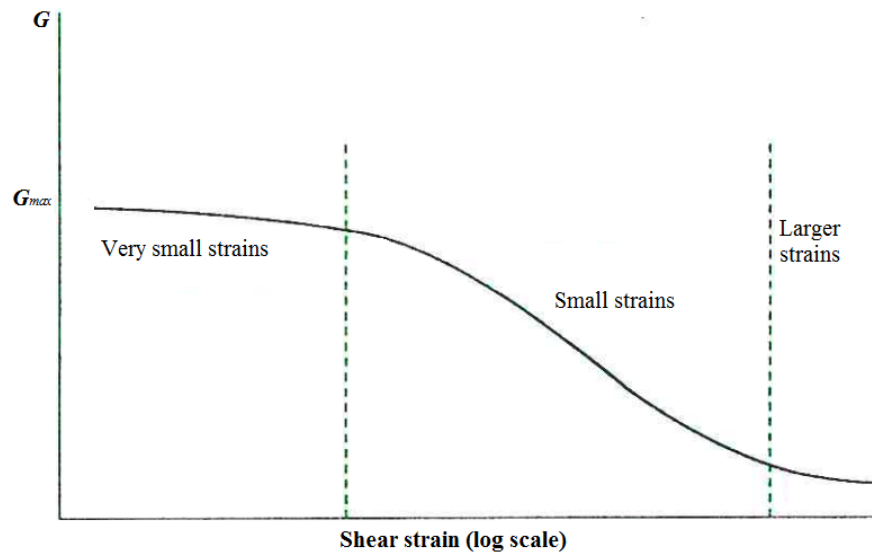
Figure 2.2: idealized variation of soil stiffness versus large range of strain, after Viggiani and Atkinson (1995)

At very small strains, G_{max} reaches a maximum constant value, while in the intermediate small strain range, it declines smoothly with increasing strain (Figure 2.2). The G_{max} value can be obtained utilizing geophysical methods in the field and laboratory methods. For example a field technique considering very small strain is the multi-modal analysis of surface wave (MMASW), in which the deformation properties of the tested material are associated with elastic shear wave velocities. In the laboratory, resonant column tests measures very small strain shear modulus for the shear range from 0.00001% to 1% (Isenhower, 1979). The stiffness values obtained from conventional triaxial tests and self-boring pressuremeter tests involved the intermediate small strain stiffness of a soil.

Strains in the ground due to natural phenomena are assumed to correspond to very small strains (Anochikwa et al., 2012). For the overconsolidated Lachenaie clay, the stresses imposed by natural phenomena are well below the difference between the preconsolidation pressure and the in-situ effective stress. These stress changes should produce very small strains in the clay. At small strains levels, Champlain Sea clay displays anisotropic linear behaviour (e.g., Mitchell, 1970; La Rochelle and Lefebvre, 1971; Tavenas and Leroueil, 1977; Yong and Silvestri, 1979).

2.4 Pore pressure response to natural loading in clay layer

In aquitards pore pressure fluctuations often respond to natural phenomena (Timms and Acworth, 2005; Butler et al., 2011; Anochikwa et al., 2012; Hussein et al., 2013; Smith et al., 2013; Smerdon et al., 2014). Earth tide induced fluctuations in pore pressure are small compared to fluctuations caused by barometric pressure changes (Davis and DeWiest, 1966). For shallow wells, pore pressure fluctuations induced by Earth tides are a matter of mm of water (Smith et al., 2013). The amplitude of barometrically induced fluctuations reaches more than 30 cm for a week and even more for a season. Atmospheric pressure change is the main contributor to natural pore pressure fluctuations for period of times when the groundwater recharge and discharge are limited. The pore pressure fluctuations induced by barometric pressure change may conceal the pore pressure response to a tidal signal (Hsieh et al., 1987; Rojstaczer, 1988b) and disguise lower-frequency fluctuations in water level associated with seasonal change in pore pressure (Furbish, 1991). It can also mask pore pressure response within a clay aquitard to moisture loading (Anochikwa et al., 2012).

For a saturated, isotropic, and linearly elastic porous media, considering small deformations, Biot (1941) and Nur and Byerlee (1971) presented three dimensional constitutive equations for coupled stress-strain and pore-water pressure response. Using the results of Biot (1941) and Nur and Byerlee (1971), Rice and Cleary (1976) presented a relationship for the interactions between stress and pore pressure. This relationship can be considered as the basic constitutive equation for the stress and pore pressure interaction in a homogeneous porous medium. The equations were then extended by van der Kamp and Gale (1983) for laterally extensive surface loading such as barometric pressure change and Earth tide effects. In a laterally extensive and saturated clay formation where the horizontal deformation is negligible, a one-dimensional coupled equation for pore pressure and applied stress can be written as follows for linear elasticity:

$$D_v \frac{\partial^2 u}{\partial z^2} = \frac{\partial u}{\partial t} - LE \frac{\partial \sigma}{\partial t} \tag{2.5}$$

where D_v is vertical hydraulic diffusivity defined as $D_v = K_v/S_s$, where K_v is vertical hydraulic conductivity and S_s is specific storage, z is elevation, u is pore pressure, σ is the total stress applied to the ground surface, t is time, and LE is loading efficiency defined as the ratio between the total pore pressure change and surface loading (van der Kamp and Gale, 1983) or the proportion of a stress increase carried only by pore water. In other words, it is the portion of storage which relates to compressibility of the solid matrix (Timms & Acworth 2005). Specific storage is defined as $S_s = \rho_w g(n\beta_w + m_v)$ by assuming that the solids are incompressible, where ρ_w is fluid density, g is gravitational acceleration, β_w is water compressibility taken as 4.6×10^{-7} kPa^{-1} at 20°C, n is total porosity, m_v is vertical compressibility of aquitards solid matrix. Specific storage in hydrogeology is thus related to m_v in geotechnical engineering.

The LE value is related to aquitard properties. Theoretically it varies between 0 and 1 and practically it can be determined using several methods. For a compressible aquitard, LE is close to 1. This implies that water is much less compressible than the aquitard solid matrix. Thereby pore water bears most of the change in external loading (van der Kamp and Gale, 1983; Spane, 2002; Timms and Acworth, 2005). The loading efficiency is also related to the formation porosity and degree of saturation (Skempton, 1954; Black and Lee, 1973), and the hydraulic and storage properties of the well/aquitard system. Figure 2.3 presents the relationship between loading efficiency and aquitard compressibility for various porosity values.
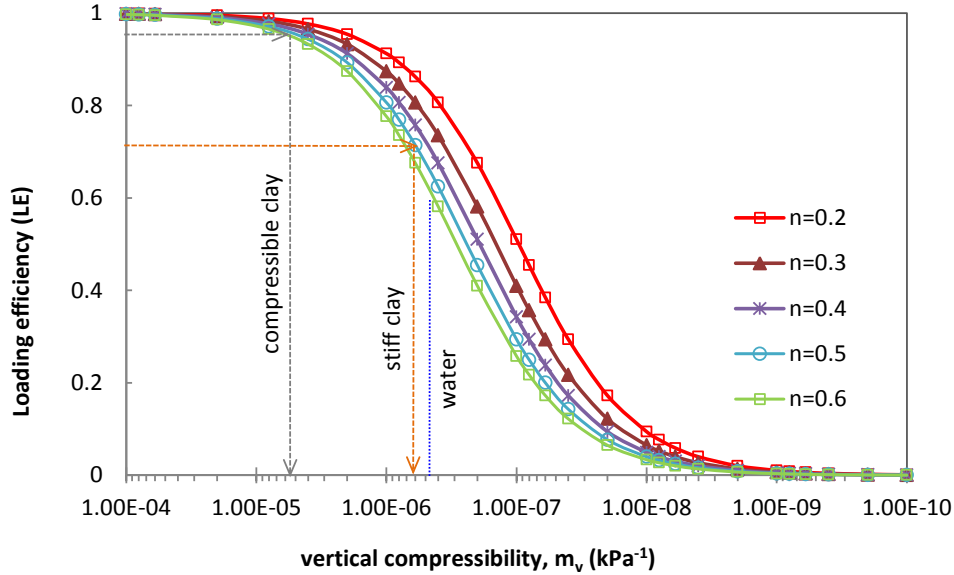
Figure 2.3: Loading efficiency versus vertical compressibility

Similar equations coupling pore pressure and stress were presented by Domenico and Schwartz (1997) and Vuez and Rahal (1993, 1994). Neuzil (2003) derived a more general equation based on force equilibrium and mass conservation. He considered interaction between pore pressure, stress, strain, and temperature:

$$\nabla.\frac{K\rho g}{\mu}\left(\nabla u + \rho g \nabla z\right) = S_S \frac{\partial u}{\partial t} - S_S (LE) \frac{\partial \sigma}{\partial t} - \rho g n \wedge' \frac{\partial T_m}{\partial t} - gJ \tag{2.6}$$

where μ is the fluid dynamic viscosity, z is the elevation above an arbitrary reference, Λ' is the thermal response coefficient for the liquid and solid phases, J is the fluid source or sink, and T_m is the temperature. In the absence of fluid sources, with a constant density and viscosity fluid, and with incompressible solid grains, Eq. (2.6) simplifies to the diffusion-type Eq. (2.5).

2.5 In-situ estimation of clay aquitard elastic properties

Laboratory and in-situ testing methods measure formation elastic properties such as vertical compressibility, specific storage, elastic moduli. Laboratory tests are known to overestimate the vertical compressibility of overconsolidated clays because the clay samples have suffered from

some sampling disturbance and stress change (Klohn, 1965; Clark, 1998; van der Kamp, 2001b). This applies particularly to Champlain clays because of their sensitivity (e.g., La Rochelle and Lefebvre, 1971; Tavenas et al., 1974; La Rochelle et al., 1981; Silvestri and Abou-Samra, 2008). The in-situ clay elastic modulus can be determined either by geotechnical tests (e.g., self-boring pressuremeter tests, vane shear test, and pulse test) or from the natural pore pressure response in the formation.

The natural pore pressure response of aquifers has long been used to estimate their elastic parameters (Jacob, 1940; Jacob, 1950; Bredehoeft, 1967; van der Kamp and Gale, 1983; Rojstaczer, 1988a; Rojstaczer, 1988b; Rojstaczer and Riley, 1990; Evans et al., 1991; Spane, 1999). The pore pressure response of aquitards has also been used to determine their elastic parameters (e.g., Van der Kamp and Maathuis, 1991; Van der Kamp and Schmidt, 1997; Timms and Acworth, 2005; Anochikwa et al., 2012; Smith et al., 2013; Smerdon et al., 2014).

In Eq. (2.5), the term $D_v \partial^2 u/\partial z^2$ represents vertical transient groundwater flow in response to change in pore pressure, while LE $\partial\sigma/\partial t$ represents the undrained pore pressure response to change in surface load (van der Kamp and Gale, 1983). The short-term loading such as barometric pressure change can be assumed to represent undrained conditions. For undrained condition, the fluid flow term on the left-hand side of Eq. (2.5) is equal to zero, and Eq. (2.5) becomes:

$$\frac{\partial u}{\partial \sigma} = \frac{m_v}{m_v + n\beta_w} = LE \tag{2.7}$$

The natural total stress increment $\partial\sigma$ in Eq. (2.5) can have the following components:

$$\frac{\partial \sigma}{\partial t} = \left(\frac{\partial B}{\partial t} + \frac{\partial \varepsilon_T}{\partial t} + \frac{\partial P}{\partial t} + \frac{\partial ET}{\partial t} + \frac{\partial R}{\partial t} \right) \tag{2.8}$$

where $\partial B/\partial t$ represents a barometric pressure change, $\partial \varepsilon_T/\partial t$ represents the Earth tide effect, $\partial P/\partial t$ represents precipitation, $\partial R/\partial t$ represents runoff, and $\partial ET/\partial t$ represents groundwater discharge as evapotranspiration. As expressed before, barometric pressure changes generally produce greater pore pressure changes than Earth tide effects (e.g., Rojstaczer and Agnew, 1989; Schulze et al., 2000). In addition, for shallow wells, pore pressure amplitude induced by Earth tide effects is negligible (Smith et al., 2013). Furthermore, during winter, due to frozen soil

conditions, groundwater recharge and discharge effects are minimized. This yields a high correlation between barometric pressure changes and pore pressure response. Thus under certain circumstances, barometric stress changes can be considered as the major natural stress source that is applied everywhere to the ground surface. For a period between two successive precipitation events Eq. (2.8) reduces to the following expression:

$$\frac{\partial \sigma}{\partial t} = \frac{\partial B}{\partial t} \tag{2.9}$$

After having calculated LE from the pore pressure response to barometric pressure changes using Eq. (2.7), the key elastic parameters can be obtained. Given the standard value for water compressibility, β_w, and the porosity of the tested formation n, the constrained elastic modulus of the soil skeleton is calculated as follows:

$$M = \frac{1 - LE}{LE(n\beta_w)} \tag{2.10}$$

The shear modulus of the tested aquitard can be calculated as follows by assuming a proper value for the Poisson ratio:

$$G = \frac{M(1 - 2v)}{2(1 - v)} \tag{2.11}$$

Specific storage can be calculated as:

$$S_s = \rho_w g n \beta_w \left[1/(1 - LE) \right] \tag{2.12}$$

Previous studies performed by Timms and Acworth (2005) provided S_s values between 3.7×10^{-5} and 6.8×10^{-6} m^{-1} (m_v values between 3.6×10^{-6} and 6.7×10^{-7} kPa^{-1}) for clay aquitard using loading efficiency method in the Liverpool plains of northern New SouthWales, Australia. With the similar LE method, Smerdon et al. (2014) found specific storage values between 1.2×10^{-5} and 4.3×10^{-6} m^{-1} (m_v values between 1.1×10^{-6} and 2.8×10^{-7} kPa^{-1}) for clay aquitard in Great Artesian Basin. Specific storage values between 2.6×10^{-5} and 2.6×10^{-6} m^{-1} (m_v values between 2.4×10^{-6} and 2.5×10^{-7} kPa^{-1}) were calculayed for Saskatchewan clay in Canada by Smith et al. (2013). The obtained specific storage values using LE values are low with respect to the results in the literature for medium to stiff clay obtained from standard hydrologic tests (e.g., Domenico and Schwartz, 1997). van der Kamp (2001) indicated that the in-situ values of specific

storage obtained from LE are several orders of magnitude lower than those obtained from typical laboratory tests.

2.6 Methods for loading efficiency calculation

Loading efficiency is the ratio of change in total head (absolute pressure head) to change in barometric pressure expressed in m of water. It differs from barometric efficiency, BE, which reflects the ratio of change in well water-level to the change in barometric pressure. Loading efficiency is related to barometric efficiency by LE+BE =1 (e.g., Rasmussen and Crawford, 1997; Spane, 2002). The literature presents several methods to calculate loading efficiency including linear regression, the Clark method, visual inspection, and the barometric response function, BRF.

In an ideal confined aquifer, barometric pressure change is transmitted immediately in both the aquifer and to the water surface of an open well. The water column in the well bears all the pressure change. However, it is shared between pore water pressure and the solid grain skeleton in the aquifer. This creates a pressure imbalance between the confined aquifer and the well. In a confined aquifer, the relationship between barometric pressure and well water-level is inverse: an increase in barometric pressure causes a decrease in well water-level and vice versa (Rasmussen and Crawford, 1997). Jacob (1940) was the first to describe BE as a ratio between well water-level and barometric pressure changes within a confined aquifer:

$$BE = \frac{\Delta W}{\Delta B} \tag{2.13}$$

where ΔW is the change in well water-level and ΔB is the change in barometric pressure at the ground surface during the same time step. For an absolute pressure head measurement, the loading efficiency (LE) can be calculated from the slope of the linear fit between changes in absolute pore pressure and barometric pressure as follows:

$$LE = \frac{\Delta u}{\Delta B} \tag{2.14}$$

In a very rigid confined aquifer (e.g., basalt), most of the applied barometric pressure change is borne by the matrix skeleton. Accordingly, total head within the aquifer remains relatively

insensitive to barometric pressure change. Thus, the well water-level has to compensate to maintain a constant total head. This is a direct consequence of the high barometric efficiency (or low loading efficiency) for confined aquifer with a high rigidity (Rasmussen and Crawford, 1997; Spane, 2002).

Clark (1967) presented another method for BE calculations when other phenomena (e.g., distant groundwater withdrawals) influence the pressure head fluctuations. With this method the BE is determined from the slope of a summation plot of incremental change in well-water level versus incremental change in barometric pressure. When the increment signs are the same for both pore pressure and barometric pressure, the pore pressure increment is added to the pore pressure summation. When the increment signs are different, the pore pressure increment is subtracted from the sum.

Loading efficiency can be also determined with "visual inspection method" for an instantaneous pore pressure response (Smith et al., 2013). The LE value can be determined by multiplying the barometric pressure change with a trial LE value between 0 and 1 and then subtracting the result from the raw pore water pressure data in order to obtain a pore pressure time series as smooth as possible.

In an unconfined aquifer with a thick unsaturated zone and a low permeability, or in a borehole with casing storage capacity, the pore pressure response to barometric stress changes is not instantaneous. It is retarded and becomes time-lag or frequency dependent (Weeks, 1979; Furbish, 1991). The aforementioned methods do not take into account a time lag between the barometric and pore pressure changes. Thus they cannot provide a representative loading efficiency values for a low permeability formation. For these cases, the well water-level response to barometric pressure change is described by a barometric response function (BRF). If total head data were utilized instead of well water-level data in the response function calculation, different BRF responses would be revealed which is called barometric head response function (BHRF) in this thesis.

2.7   Barometric response function (BRF/BHRF)

The BRF/BHRF can be determined with either the time domain, i.e., using multiple regression,

(Weeks, 1979; Furbish, 1991; Rasmussen and Crawford, 1997; Spane, 2002) or the frequency domain (e.g., Galloway and Rojstaczer, 1988; Rojstaczer, 1988a; Evans et al., 1991) approaches. For both time and frequency domain solutions, attempts have been made to improve the estimation of the BRF by removing the Earth tide effects (Galloway and Rojstaczer, 1988; Rojstaczer, 1988a; Rasmussen and Mote, 2007; Toll and Rasmussen, 2007), low-frequency background trends (Spane, 2002), and the influence of recharge in water level records (Hussein et al., 2013). Spane (2002) reviewed both the time and frequency domain BRF and concluded that the frequency domain approach involves application of a number of analyses (e.g., frequency spectrum development, cross-correlation examination, and selective filtering of the dominant frequencies) which made this type of analysis not as straightforward as the time domain approach.

The use of a barometric response function in the analysis of well water-level time series was first proposed by Rasmussen and Crawford (1997). In the time domain, the BRF is an impulse response. It describes the well water-level response over time for a step change in barometric pressure, which is a function of BE. For the water-level response of open wells to barometric pressure change, Rasmussen and Crawford (1997) presented three diagnostic models for BRF including an instantaneous and constant response for wells within confined aquifers, a delayed response in unconfined aquifers because of the delayed propagation of barometric pressure changes through the thick unsaturated zone with a low permeability, and a delayed response due to wellbore storage and skin effects. Figure 2.4 represents these three diagnostic models.

For conditions similar to those exhibited in Figure 2.4, Spane (2002) calculated BHRF based on total hydraulic head responses. BHRF describes the time-dependent total head response associated with a unit change in barometric pressure, which is a function of LE = 1-BE.

The pore pressure response to barometric pressure change in confined aquifer was discussed in section (2.6). A brief discussion regarding the BHRF of unconfined aquifers and the borehole storage model is presented given in the next section here.
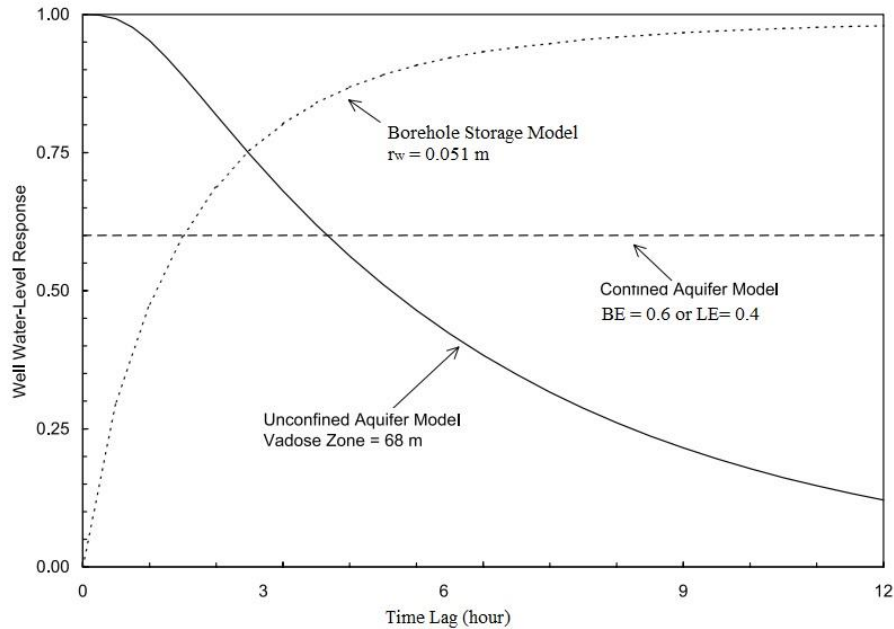
Figure 2.4: Well/aquifer BRF model, adapted from Spane (2002).

2.7.1 Unconfined aquifer model

Wells in unconfined aquifers respond differently from those in confined aquifers. In a deep unconfined aquifer, barometric pressure changes travel through the unsaturated zone from the ground surface down to the groundwater table. The propagation of barometric pressure change is controlled by the thickness of the unsaturated zone and unsaturated soil properties i.e., unsaturated hydraulic conductivity and compressibility of soil gas (Weeks, 1979). Therefore, total head within deep unconfined aquifers is not immediately affected by barometric pressure change. However, in a well deeply penetrating an unconfined aquifer, barometric pressure changes immediately affect the water column in the well casing and the water level. This results in a pressure imbalance between the well screen and the aquifer. Thus, the well water-level has to fluctuate in order to maintain a constant total head. This seemingly results in a high barometric efficiency or a low loading efficiency (Rasmussen and Crawford, 1997). For this type of well, when the well water-level hydrograph is analyzed assuming no time lag (as in section 2.6), it shows a similar behaviour to confined aquifers. Nevertheless, analysis of the well water-level response versus the time lag yields a diagnostic pattern for well water-level response that differs from that of confined aquifers as shown in Figure 2.4 (Spane, 2002).

2.7.2 Borehole storage model

A change in barometric pressure creates a total head (pressure) imbalance between water in the well casing and water in the aquifer, which induces seepage between them. If some time is needed for water to flow between the well and the aquifer, well water-level or pressure head response to barometric pressure change is not immediate (Rasmussen and Crawford, 1997). The time required for total head (energy) equilibration is related to the aquifer hydraulic and elastic properties, and to well skin effects (Furbish, 1991; Rasmussen and Crawford, 1997; Spane, 2002). Furbish (1991) proposed to view an incessantly fluctuating barometric pressure as equivalent to a continuous sequence of bail and slug tests. Thus, the transient flow induced by barometric pressure changes between the well and the aquifer can be modelled using slug test solutions. Previous models (e.g., Furbish, 1991; Rasmussen and Crawford, 1997) used the Hvorslev (1951) slug test solutiom to evaluate the transient flow between borehole and aquifer induced by barometric pressure change. However, because of the restrictive assumption of a perfectly rigid soil skeleton in the Hvorslev (1951) model, Spane (2002) suggested an interpretation based on the Cooper et al. (1967) solution. Nevertheless, the Cooper et al. (1967) solution considers only horizontal flow and ignores the lateral deformation of the borehole cavity. The lateral deformation is significant in compressible clay (Duhaime and Chapuis, 2014; Chapuis, 2015). This will be discussed latter in section (2.10.3).

2.8 Mathematical equations to calculate BRF/BHRF

Based on multiple-regression, the dependent variable (e.g., pore pressure change in this study) is related to independent or explanatory variables (e.g., barometric pressure change). The general model considering k explanatory variables is written as follows (Montgomery and Peck, 1992):

$$\Delta y_i = \delta_0 + \delta_1 \Delta x_{i1} + \delta_2 \Delta x_{i2} + ... + \delta_k \Delta x_{ik} + \varepsilon_i, \quad i = 1,2,...n \tag{2.15}$$

where Δy_i is the change in dependent variable in observation i, δ_0 is the regression intercept, δ_j are the regression coefficients associated with independent variables of Δx_{ij} for $j=1,2,…,k,$, ε is the random distribution of the error. For $j=1$, δ_1 is the change in Δy_i for a unit change in Δx_{i1}, holding the other independent variables at their current values. The multiple regression analysis considers that the variables $\Delta x_1, \Delta x_2, …, \Delta x_n$ are linearly independent which indicates that the

correlation between each Δx_i is small (Montgomery and Peck, 1992; Brown, 2009).

If we extend the Eq. (2.15) between all observations and independent variables, the following vector system is obtained:

$$\Delta \mathbf{Y} = \boldsymbol{\delta} \Delta \mathbf{X} + \boldsymbol{\varepsilon} \tag{2.16}$$

And in matrix notation:

$$
\begin{bmatrix} \Delta y_1 \\ \Delta y_2 \\ . \\ . \\ . \\ \Delta y_n \end{bmatrix} = \begin{bmatrix} 1 & \Delta x_{11} & \cdots & \Delta x_{1k} \\ 1 & \Delta x_{21} & \cdots & \Delta x_{2k} \\ . & . & \cdots & . \\ . & . & \cdots & . \\ . & . & \cdots & . \\ 1 & \Delta x_{n1} & \cdots & \Delta x_{nk} \end{bmatrix} \begin{bmatrix} \delta_1 \\ \delta_2 \\ . \\ . \\ . \\ \delta_n \end{bmatrix} + \begin{bmatrix} \varepsilon_1 \\ \varepsilon_2 \\ . \\ . \\ . \\ \varepsilon_n \end{bmatrix} \tag{2.17}
$$

Ordinary leas squares (OLS) method estimates the regression coefficients. The first step in OLS analysis is to define the least square estimators ($\hat{\delta}_j$) to minimize the residual error between Δy_i and $\Delta \hat{y}_i$. The estimators $\hat{\delta}_j$ deliver the least possible value to sum of the squares difference between Δy_i and $\Delta \hat{y}_i$.

$$\Delta \hat{y}_i = \hat{\delta}_0 + \hat{\delta}_1 \Delta x_{i1} + \hat{\delta}_2 \Delta x_{i2} + \dots + \hat{\delta}_k \Delta x_{ik}, \qquad i = 1,2,\dots,n \tag{2.18}$$

The Eq. (2.18) allows the fitted value of $\Delta \hat{y}_i$ for each Δy_i to be calculated. The error is defined by the difference between an observed value and its corresponding fitted value (i.e., the difference between Δy_i and $\Delta \hat{y}_i$):

$$\hat{\varepsilon}_i = \Delta y_i - \Delta \hat{y}_i = \Delta y_i - \hat{\delta}_0 - \hat{\delta}_1 \Delta x_{i1} - \hat{\delta}_2 \Delta x_{i2} - \dots - \hat{\delta}_k \Delta x_{ik} \tag{2.19}$$

The corresponding vector form for the fitted model and for the residual error can be written as follows (Montgomery and Peck, 1992; Brown, 2009):

$$\Delta \hat{\mathbf{Y}} = \hat{\boldsymbol{\delta}} \Delta \mathbf{X} \tag{2.20}$$

$$\hat{\boldsymbol{\varepsilon}} = \Delta \mathbf{Y} - \Delta \hat{\mathbf{Y}} = \Delta \mathbf{Y} - \hat{\boldsymbol{\delta}} \Delta \mathbf{X} \tag{2.21}$$

The sum of the squared residual error is:

$$Sum = \sum_{i=1}^{n} \hat{\varepsilon}_i^2 = \sum_{i=1}^{n} \left[\Delta y_i - \hat{\delta}_0 - \hat{\delta}_1 \Delta x_{i1} - \hat{\delta}_2 \Delta x_{i2} - \dots - \hat{\delta}_k \Delta x_{ik} \right]^2 \tag{2.22}$$

The first derivative of "*Sum*" should be calculated with respect to each $\hat{\delta}_j$ in order to apply the least squares criterion in the multiple-regression model:

$$\frac{\partial(Sum)}{\partial \hat{\delta}_0} = 2 \sum_{i=1}^{n} \left[\Delta y_i - \hat{\delta}_0 - \hat{\delta}_1 \Delta x_{i1} - \hat{\delta}_2 \Delta x_{i2} - \dots - \hat{\delta}_k \Delta x_{ik} \right] [-1]$$

$$\frac{\partial(Sum)}{\partial \hat{\delta}_1} = 2 \sum_{i=1}^{n} \left[\Delta y_i - \hat{\delta}_0 - \hat{\delta}_1 \Delta x_{i1} - \hat{\delta}_2 \Delta x_{i2} - \dots - \hat{\delta}_k \Delta x_{ik} \right] [-\Delta x_{i1}]$$

$$\frac{\partial(Sum)}{\partial \hat{\delta}_2} = 2 \sum_{i=1}^{n} \left[\Delta y_i - \hat{\delta}_0 - \hat{\delta}_1 \Delta x_{i1} - \hat{\delta}_2 \Delta x_{i2} - \dots - \hat{\delta}_k \Delta x_{ik} \right] [-\Delta x_{i2}] \tag{2.23}$$

$$\dots \quad \dots \quad \quad \dots \quad \quad \dots$$

$$\frac{\partial(Sum)}{\partial \hat{\delta}_k} = 2 \sum_{i=1}^{n} \left[\Delta y_i - \hat{\delta}_0 - \hat{\delta}_1 \Delta x_{i1} - \hat{\delta}_2 \Delta x_{i2} - \dots - \hat{\delta}_k \Delta x_{ik} \right] [-\Delta x_{ik}]$$

Equalling the previous derivatives to 0 provided the least square estimators as follows:

$$\sum_{i=1}^{n} \left[\Delta y_i - \hat{\delta}_0 - \hat{\delta}_1 \Delta x_{i1} - \hat{\delta}_2 \Delta x_{i2} - \dots - \hat{\delta}_k \Delta x_{ik} \right] = 0$$

$$\sum_{i=1}^{n} \left[\Delta y_i - \hat{\delta}_0 - \hat{\delta}_1 \Delta x_{i1} - \hat{\delta}_2 \Delta x_{i2} - \dots - \hat{\delta}_k \Delta x_{ik} \right] \Delta x_{i1} = 0$$

$$\sum_{i=1}^{n} \left[\Delta y_i - \hat{\delta}_0 - \hat{\delta}_1 \Delta x_{i1} - \hat{\delta}_2 \Delta x_{i2} - \dots - \hat{\delta}_k \Delta x_{ik} \right] \Delta x_{i2} = 0 \tag{2.24}$$

$$\dots \quad \dots \quad \quad \dots \quad \quad \dots$$

$$\sum_{i=1}^{n} \left[\Delta y_i - \hat{\delta}_0 - \hat{\delta}_1 \Delta x_{i1} - \hat{\delta}_2 \Delta x_{i2} - \dots - \hat{\delta}_k \Delta x_{ik} \right] \Delta x_{ik} = 0$$

And in the vector form:

$$\Delta \mathbf{X}^{\mathbf{T}} \Delta \mathbf{X} \hat{\boldsymbol{\delta}} = \Delta \mathbf{X}^{\mathbf{T}} \Delta \mathbf{Y} \tag{2.25}$$

The estimators $\hat{\delta}$ can be calculated with following relationship (Montgomery and Peck, 1992):

$$\hat{\boldsymbol{\delta}} = \left[\Delta \mathbf{X}^{\mathbf{T}} \Delta \mathbf{X} \right]^{-1} \Delta \mathbf{X}^{\mathbf{T}} \Delta \mathbf{Y} \tag{2.26}$$

Several mathematical and statistical software packages including Mathematica, MATLAB, Microsoft Excel, and SPSS provide the solution for the Eq. (2.26). In Appendix (A) a MATLAB

script is provided to calculate multiple regression coefficients for pore pressure response to barometric pressure change. While the regression coefficients were calculated, the barometric head response function is constructed by gradually summing up the regression coefficients to k number of the associated time lag.

$$BRF/BHRF = \sum_{j=1}^{k} \delta_j \tag{2.27}$$

2.9 Methods to eliminate barometric pressure effect

Changes in barometric pressure mask the amplitude of pressure head fluctuations induced by other low-frequency natural loading sources, or influence permeability and pumping test data. In low-gradient aquitard conditions where the groundwater table is near-horizontal, influence of barometric pressure change on pore pressure may cause inaccurate estimation of groundwater flow magnitude and direction (Rasmussen and Crawford, 1997; Spane, 2002). Seepage velocities play an important role, for example, in calculations regarding the movement of contaminants in groundwater (Spane, 2002). Thus, barometrically induced pressure head amplitude should be corrected to hydraulic head values that are more precise for the accurate interpretation of in-situ permeability and pumping test data.

2.9.1 Simple linear model

For a perfectly confined aquifer, considering no storage and skin effects, the barometric pressure changes travel almost instantaneously to the aquifer and to the well water surface. The corrected pore pressure data can be obtained as follows:

$$u^* = u - LE \times B \tag{2.28}$$

where u^* and u are the corrected and observed pressure head time series respectively, B is the barometric pressure at the same time step as the pressure head measurement.

2.9.2 Visual inspection method

With the visual inspection method, the corrected pore pressure can be determined as follows (Smith et al., 2013):

$$u^* = (u - B_{ave}) - LE(B - B_{ave}) \tag{2.29}$$

where B_{ave} is the average barometric pressure for the study site. With the visual inspection method, the LE value is adjusted between 0 and 1 to obtain corrected pressure head time series that are as smooth as possible.

2.9.3 Multiple regression method

Multiple regression can be used effectively to correct open/closed well pressure head time series with delayed responses (e.g., confined aquifer/aquitard well with storage effects) (Rasmussen and Crawford, 1997; Spane, 2002). Several authors have used this method to remove successfully the effects of barometric pressure on well water level changes in aquifer/aquitard systems (e.g., Rasmussen and Mote, 2007; Butler et al., 2011). Corrected pore pressure time series can be obtained by subtracting the summation of predicted change in pore water pressure $\Sigma \Delta y_{t-i}$, obtained by Eq. (2.31), from the observed pore pressure response (Spane, 1999; Spane, 2002):

$$u^* = u - \sum_{i=1}^{n} \Delta y_{t-i} \tag{2.30}$$

$$\sum_{i=1}^{n} \Delta y_{t-i} = \Delta y_t + \Delta y_{t-1} + ... + \Delta y_{t-n} \tag{2.31}$$

2.9.4 Frequency-based method

The frequency-based method was developed by Rojstaczer (1988a) based on the periodic nature of barometric pressure changes. The author showed that the frequency of the barometric pressure is the factor controlling the well water response in terms of attenuation and phase lagging. In the frequency based method, the pressure head response is transformed from time domain to

frequency domain through Fourier transformation. Frequency spectrum of the transformed data provides useful information about amplitudes and related frequencies. Correlating pressure head and barometric pressure spectra allows the frequencies associated with barometric pressure changes to be distinguished within the pressure head record. Then, the significant frequencies can be selectively removed from pressure head data using high-low-pass or band-pass filtering applications. However, the application of frequency-based method is not always straightforward. It implies the use of time intensive analysis such as spectral frequency analysis, cross-correlation analysis, and selective filtering applications (Spane, 2002).

2.10   Clay hydraulic conductivity

Hydraulic conductivity is a key parameter to define groundwater recharge, contaminant migration, slope stability problems, consolidation, and seepage through earth dams and around earth structures. Hydraulic conductivity of a saturated soil depends on both fluid (viscosity and density) and porous medium properties (size, shape, and tortuosity of voids) (e.g., Chapuis and Gill, 1989; Chapuis et al., 1989; Chapuis and Aubertin, 2003; Chapuis, 2012). Clay hydraulic conductivity can be determined by small core samples to large scales in-situ tests. These methods include: for core samples laboratory variable-head tests in oedometer or triaxial cells, and for in-situ tests falling- and rising- head tests and pulse test in monitoring wells (MWs), aquifer pumping tests with considering leakage from aquitard, monitoring of cyclic pore pressure fluctuations, analysis of natural pore pressure response to surface loading, and numerical analysis of local and regional groundwater flow (e.g., van der Kamp, 2001a). Clay saturated hydraulic conductivity can also be predicted from basic geotechnical properties.

2.10.1 Prediction of saturated hydraulic conductivity

Kozeny (1927) and Carman (1956) developed predictive methods for the hydraulic conductivity of soils. The resulting equation is well-known as the Kozeny-Carman equation and can be written as follows:

$$K = C_t \frac{g}{\mu \rho_w} \frac{e^3}{S^2 G_s^2 (1+e)} \tag{2.32}$$

where e is void ratio, g is gravitational acceleration, C_t is a factor related to shape and tortuosity of the void network, G_s is specific gravity of solids ($G_s = \rho_s/\rho_w$; ρ_s is density of solids), μ is fluid dynamic viscosity, and S is specific surface of solids (m^2/kg of solids). With Eq. (2.32), permeability is a function of voids size, shape and tortuosity of the flow path. For a given soil, Eq. (2.32) implies a linear relationship between K and $e^3/(1+e)$ (Chapuis and Aubertin, 2003).

The permeability of intact clayey soils at their in-situ void ratio is controlled by void ratio, grain size, plasticity and the clay fabric (Tavenas et al., 1983a). Taylor (1948) noted that the Kozeny-Carman equation is valid just for sand and it cannot be applied for clay. Later, Lambe and Whitman (1969) and Domenico and Schwartz (1997) came to the same conclusion. However, Chapuis and Aubertin (2003) observed that the Kozeny-Carman prediction method can be applied to a wide range of porous materials ranging from clay to gravel. The authors developed a model based on the Kozeny-Carman equation that can be applied to soils with K values ranging from 10^{-1} to 10^{-11} m/s:

$$log \left(K_{predicted}\right) = A + log \left(\frac{e^3}{G_s^2 S^2 (1+e)}\right) \tag{2.33}$$

where A is a constant related to the fluid properties and the tortuosity of the pore network. It varies between 0.29-0.5 for a C_t value between 0.2 and 0.5. For clays with $w_L < 110$ (%), specific surface S, can be evaluated by means of following relationship, where w_L is expressed as a percentage and S is given in m^2/kg.

$$\frac{1}{S} = 1.3513 \left(\frac{1}{w_L}\right) - 0.0089 \tag{2.34}$$

The A value of 0.5 assumed by Chapuis and Aubertin (2003) tends to underestimate the predicted K value for Champlain clays. Duhaime (2012) offered an optimum value of 1.1 for A by means of the K values derived from standard laboratory and field tests for Lachenaie clay and for other localities within the Champlain Sea basin. Mbonimpa et al. (2002) developed an alternative method based on void ratio and liquid limit to predict the hydraulic conductivity of clay as follows:

$$K = 5.6 \frac{g}{\mu} \frac{e^{3+n_l}}{(1+n_l)} \frac{1}{G_s^2 w_L^3} \tag{2.35}$$

where n_l is a function of liquid limit and can be obtained using the following relationship:

$$n_l = 7.7 w_L^{-0.15} - 3 \tag{2.36}$$

Equation (2.35) can be applied for K values ranging from 10^{-12} to 10^{-8} m/s, and for materials with liquid limits between 30 and 120%. For highly plastic materials with very high liquid limit values, n_l tends toward 0. For the Lachenaie clay deposit, n_l varies between 1.43 for $w_L = 40$ and 0.99 for $w_L = 80$. Assuming an average value of 1.21 for n_l, the hydraulic conductivity of Lachenaie clay can be predicted using following equation:

$$K = 5.6 \frac{g}{\mu} \frac{e^{4.21}}{2.21} \frac{1}{G_s^2 w_L^3} \tag{2.37}$$

2.10.2 Laboratory tests

The most common types of laboratory tests to measure clayey soils hydraulic conductivity are the variable-head tests in oedometer or triaxial cells (e.g., Tavenas et al., 1983a; Tavenas et al., 1983b; Duhaime, 2012; Duhaime et al., 2013). ASTM D2435 and D-5084 provides details for these tests respectively.

Laboratory tests shows a linear relationship between $\log(K)$ and $\log(e)$ for very compressible materials with wide range of void ratio (Mesri and Olson, 1971). A log-linear relationship between e and $\log(K)$ has been reported by some authors (Taylor, 1948; Lambe and Whitman, 1969). For the strain range encountered in engineering practice (less than 20%), the relationship between e and $\log(K)$ is linear in natural soft Champlain clays. While, for larger strains (> 20%), the shape of the e versus $\log(K)$ relationship shows a definite curvature (Tavenas et al., 1983a). The plasticity index and clay-size fraction are the important factors to determine K and the shape of the e versus $\log(K)$ relationship. For high plasticity indices and high clay size fractions, the shape of the e versus $\log(K)$ relation is curved (Tavenas et al., 1983a). From standard variable-head tests in oedometer or triaxial cells, Tavenas et al (1983) obtained K values ranging between 5×10^{-10} and 5×10^{-9} m/s for samples taken from the Champlain Sea basin (Figure 2.5).
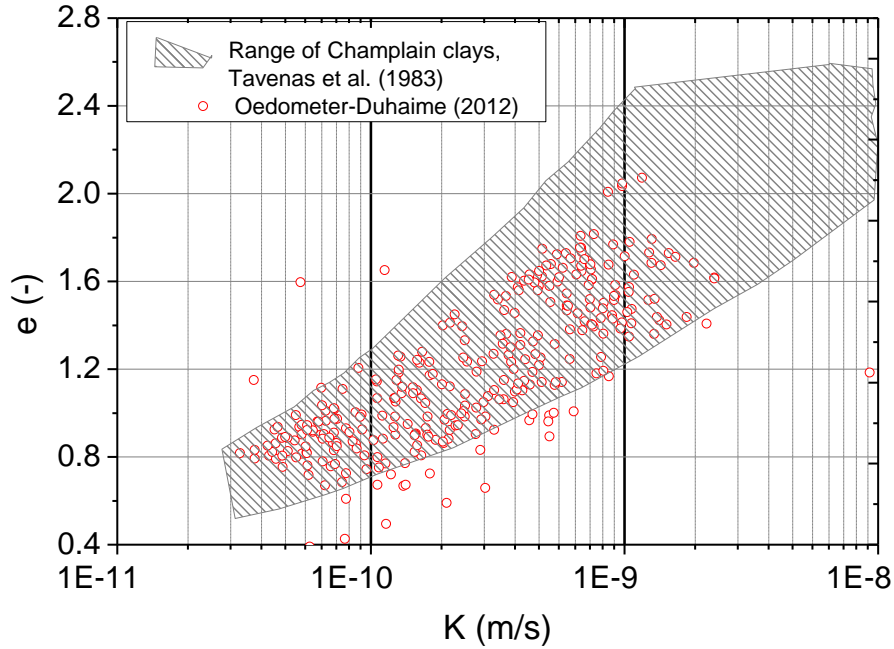
Figure 2.5: Typical *e*- log(*K*) relationship for Champlain clay.

2.10.3 Conventional field tests

Laboratory tests provide small-scale permeability due to the small specimen size which may not be perfectly representative of large-scale field conditions. Field tests to determine clay *K* values are recommended (Benson et al., 1994; Benson et al., 1997; van der Kamp, 2001a; Chapuis, 2002; Duhaime, 2012).

The usual method to measure *K* in clay is the variable-head tests in observation wells. These tests are initiated by applying a hydraulic head difference (*H*) in a monitoring well within a short time. The following hydraulic head equalization between well and surrounding clay are then recorded versus time. The clay *K* value can be derived from two interpretation methods: velocity graph method and Hvorslev (1951) method.

The velocity graph method has the advantages to measure the systematic error (H_0), explore some phenomena during the test (e.g., clay consolidation), and no assumption of hydraulic head at the beginning of the test. The classical equations for a variable-head test simply write that the flow rate in the soil (Q_{soil}) is equal to the flow rate into the pipe (Q_{inj}):

$$Q_{inj} = Q_{soil} = cKH \tag{2.38}$$

where c is the test shape factor. The riser pipe, of inner diameter d, has an internal cross section area $S_{inj} = \pi d^2/4$ and the water velocity in the riser pipe is dH/dt. Thus the injected flow rate is:

$$Q_{inj} = -S_{inj}\frac{dH}{dt} \tag{2.39}$$

Combining Eqs. (2.38) and (2.39) yields:

$$\frac{dH}{dt} = -\frac{cKH}{S_{inj}} \tag{2.40}$$

Hvorslev's solution is derived from integrating of Eq. (2.40):

$$ln\left(\frac{H_1}{H_2}\right) = -\frac{cK}{S_{inj}}(t_1 - t_2) \tag{2.41}$$

where H_1 and H_2 are the total head differences at times t_1 and t_2. In the semi log graph (Hvorslev's solution) the test data are plotted as ln (H) on the y-axis and time t on the x-axis. Equation (2.41) gives a straight-line in theory and its slope P gives K as follow:

$$K = \frac{PS_{inj}}{c} \tag{2.42}$$

The velocity graph method uses directly Eq. (2.40). It estimates the real piezometric level (PL) and the hydraulic conductivity K (Chapuis et al. 1981; Chapuis 1998, 2001, 2015) from a graph of the water level velocity $\Delta H/\Delta t$ in the pipe versus the mean value of the assumed difference in hydraulic head:

$$H_m = -\frac{S_{inj}}{cK}\frac{dH}{dt} + H_0 \tag{2.43}$$

Thus K is calculated from slope P of a straight line from Eq. (2.43) as follows:

$$K = \frac{S_{inj}}{cP} \tag{2.44}$$

For the field permeability tests performed with monitoring wells in the Lachenaie clay deposit with a range of $5.8 \leq L_{Cavity}/D_{Cavity} \leq 12$, the shape factor is given by (Duhaime et al., 2013):

$$c = \frac{2.2\pi L_{Cavity}}{Ln\left(\frac{L_{Cavity}}{D_{cavity}} + \sqrt{1 + \frac{L^2_{Cavity}}{D^2_{Cavity}}}\right)} \tag{2.45}$$

In situ variable-head tests in clay last a long time. For Lachenaie clay a typical variable-head test conducted in the monitoring well riser pipe lasted more than one month. Previous study performed by Duhaime (2012) used two methods to shorten the test duration: smaller inner section for the injected pipe and pulse test. Whit the pulse test, an inflatable packer seals the interval of formation to be tested (in case of Lachenaie, packer isolates the sand filter). The test initiates by injecting a known volume of water or rod into the isolated interval to increase the pressure of the isolated cavity. The increased pressure dissipates versus time as the water flows from the sealed cavity into the soil (Duhaime, 2012).

Pressure dissipation versus time generated by pulse tests can be interpreted with two groups of solution. The group 1 is the solution proposed by Bredehoeft and Papadopulos (1980) method, similar to that of Cooper et al. (1967) for the slug test. The group 2 is the method developed by Chapuis and Cazaux (2002), which considers perfectly elastic soil skeleton. With this method, volume of injected water (ΔV_{inj}) into isolated cavity and the initial pressure increase (Δp) provide a virtual pipe cross section, and also the clay modulus. The provided virtual pipe cross section allows the interpretation of the test data with the velocity graph method with Eq. (2.43). A virtual S_{inj} is calculated as follow:

$$S_{inj} = \frac{\gamma_w \Delta V_{inj}}{\Delta p} \tag{2.46}$$

The group 1 interpretation method was derived for fully saturated and linearly elastic formation. The hydraulic head is considered as a function of radial distance r and time $h=h(r,t)$. The water balance equation provided analytical solution as follows:

$$\frac{\partial^2 h}{\partial r^2} + (1/r)\frac{\partial h}{\partial r} = \frac{S_s}{K}\left(\frac{\partial h}{\partial t}\right) \tag{2.47}$$

In Eq. (2.47) specific storage (S_s) is proportional to formation compressibility (m_v). Thus, this analytical solution theoretically takes into account the deformation of the tested soil skeleton. The final analytical solution of Eq. (2.47), after several initial and boundary conditions led to the

dimensionless α and β parameters as follows (Cooper et al., 1967):

$$\alpha = \frac{\pi r_w^2 S}{V_m \beta_w \gamma_w}$$

(2.48)

and

$$\beta = \frac{\pi K T}{V_m \beta_w \gamma_w}$$

(2.49)

For $\alpha < 0.1$, the experimental semi log plot of $H/H(t=0)$ versus t is superimposed to the analytical type curves of $H/H(t=0)$ versus β shown on Figure 2.6. Equation (2.49) provides K value from the x-axis translation and the best match for experimental data on type curve. The best match also gives α value which when applied to the Eq. (2.48) yields elastic parameters of the tested formation (S_s and m_v).
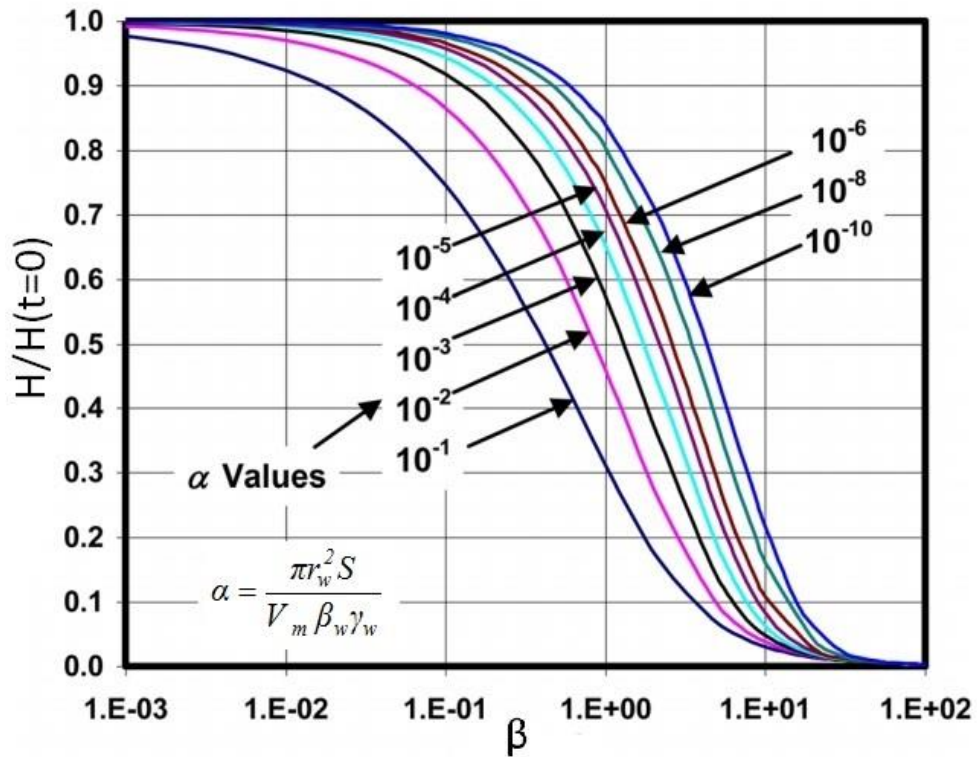
Figure 2.6: Graph of type curves as proposed by Cooper et al. (1967) and Bredehoeft and Papadopulos (1980), adapted from Chapuis (2015).

The group 1 solution does not assure approximate equilibrium of equal hydraulic head in the well and formation at the beginning of the test. Moreover, the compressibility of water used in this solution is lesser than that for the complete test system which provides small hydraulic conductivity and storage coefficient for the tested formation. Neuzil (1982) proposed that the compressibility of the complete test system (packer, pipe, measurement equipment) should be replaced for that of water in the group 1 solution.

In soft clay, the cavity expansion is the significant component on the relationship between the pressure change and the injected water. The compressibility of water and the testing equipment is small with respect to the cavity expansion under saturated conditions (Duhaime and Chapuis, 2014). For such a case, Eq. (2.47) is inaccurate as it does not consider the variation of total stress and displacement field in the clay. For interpretation of pulse test in soft Lachenaie clay, Duhaime and Chapuis (2014) used a linear elastic displacement-pressure relationship based on Biot (1941) model. The proposed displacement-pressure solution significantly limited the range of type curves compared with the Bredehoeft and Papadopulos (1980) solution. For the elastic clay, the isolated cavity expansion is linearly related to the cavity pressure change through shear modulus as follow (Duhaime and Chapuis, 2014):

$$\Delta p = G\left(\frac{\Delta V_{cavity}}{V_{cavity}}\right) \tag{2.50}$$

In Lachenaie clay, the hydraulic conductivity has little variation. Previous field tests (variable-head and pulse tests in monitoring wells) provide K values between 3.9×10^{-10} and 8.8×10^{-9} m/s for the intact clay (GSI Environnement, 2001; Benabdallah, 2006; Duhaime, 2012). Table (2.1) summarizes the K values available in the literature for Champlain clays.

Table 2.1: Typical *K* values in Champlain clay. Laboratory tests include triaxial and oedometer tests.

Location	Description of test	Range of K (m/s)	Reference
Lachenaie	Laboratory tests	$3.9 \times 10^{-10} - 6.3 \times 10^{-9}$	Benabdallah (2006) GSI Env. (2001)
Lachenaie	variable-head tests in MW	$6.7 \times 10{-}10 - 8.8 \times 10{-}9$	GSI Env. (2001)
Lachenaie	variable-head tests in MW	$1.2 \times 10^{-9} - 5.7 \times 10^{-9}$	Benabdallah (2006)
Lachenaie	variable-head tests in MW	$4.0 \times 10^{-10} - 7.0 \times 10^{-9}$	Duhaime (2012)
Lachenaie	Pulse Test	$5.21 \times 10^{-10} - 7.8 \times 10^{-9}$	Duhaime (2012)
Louiseville	SBPT	$4.9 \times 10^{-10} - 1.5 \times 10^{-9}$	Tavenas et al. (1983, 1986, 1990)
Ottawa region	variable-head tests in piezometer	$8.2 \times 10{-}10 - 1.4 \times 10{-}9$	O'Shaugnessy and Garga (1994)
Champlain clay	Laboratory tests	$5 \times 10^{-10} - 5 \times 10^{-9}$	Tavenas et al. (1983)
Varenne	Pushed piezometer	$7.5 \times 10^{-11} - 4.9 \times 10^{-10}$	Desaulniers and Cherry (1989)

2.10.4 Natural pore pressure analysis to estimate clay hydraulic conductivity

A number of researchers have used the pore pressure response to high-frequency barometric pressure change, BRF, in both time (Butler et al., 2011) and frequency domains to estimate the vertical hydraulic diffusivity of aquifers and confining layers (Rojstaczer, 1988a; Evans et al., 1991; Ritzi et al., 1991; Hussein et al., 2013). Previous studies performed by Butler et al. (2011) and Hussein et al. (2013) fitted the BRF given by a confined aquifer with an analytical model to determine the vertical hydraulic diffusivity for the overlying confining layer/clay aquitard

system. This model considers two important flow problems associated with barometric pressure change: vertical flow within the confining layer and horizontal flow between the aquifer and the borehole (Rojstaczer, 1988a; Hussein et al., 2013). Curve fitting between BRF and the analytical model, when assuming a value for the confined aquifer transmissivity, provide vertical hydraulic diffusivity for the confining layer. However, pressure responses to barometric pressure change obtained from partially penetrating wells within the clay aquitard was never analyzed in previous studies. The BRF analysis for partially penetrating wells within a clay aquitard provides the clay horizontal hydraulic properties.

Using a frequency domain BRF analysis, Hussein et al. (2013) found confining layer transmissivity values that were too low by up to two orders of magnitude with respect to pumping test results for the Chalk Aquifer in East Yorkshire, UK. The authors noted that the discrepancies between BRF and pumping test results are likely related to the presence of skin effects due to the precipitation of calcium carbonate in the wells. The very small pressure head difference induced by barometric pressure changes would not overcome the skin effect.

Butler et al. (2011) derived an analytical solution from a one-dimensional vertical simple model of an aquitard and underlying confined aquifer based on the couple pore pressure-stress equation proposed by van der Kamp and Gale (1983). By fitting the BRF derived from multiple-regression with an analytical solution, Butler et al. (2011) were able to calculate the aquitard hydraulic diffusivity, the ratio between aquifer and aquitard hydraulic conductivity and the aquitard loading efficiency. They found a hydraulic diffusivity of 1.97×10^{-3} m^2/s for an aquitard. This obtained hydraulic diffusivity value is much greater than that obtained by Keller et al. (1989) and Timms and Acworth (2005) respectively for Saskatchewan clay and smectitic clay in Australia based on analysis of annual groundwater recharge cycle.

Ferris (1952) provided an analytical model for describing the propagation of a uniform river-stage fluctuations to neighboring well response patterns for the purpose of assessing aquifer transmissivity/storativity conditions. A similar approach was applied to calculate clay aquitard hydraulic diffusivity from analysis of downward propagation of groundwater recharge cycles through a clay layer (Keller et al., 1989). Downward propagation of a pressure head cycle through an underlying clay aquitard is mainly controlled by the vertical hydraulic diffusivity of the clay aquitard (Keller et al., 1989; Neuman and Gardner, 1989) and the frequency of the

surficial pressure head cycle (Van der Kamp and Maathuis, 1991). For a sinusoidal fluctuation (e.g., annual groundwater cycle), the vertical hydraulic diffusivity can be obtained using following relationship (Keller et al., 1989):

$$D_v = \frac{z^2 \pi}{T_p} \left[ln \left(\frac{a_z}{a_s} \right) \right]^{-2}$$
(2.51)

where T_p is the fluctuation period, α_s and α_z are respectively the amplitude of the pore pressure cycle at top of the clay aquitard and the attenuated amplitude at depth z. Keller et al. (1989) proposed to take half of the vertical distance from sequential trough and peak in each hydrograph for the amplitude of the annual pore pressure fluctuations. Using the downward propagation of low-frequency pore pressure cycles, Keller et al. (1989) found a hydraulic diffusivity D_v on the order of 1×10^{-6} m^2/s for a dense clayey till in Saskatchewan. Timms and Acworth (2005) obtained D_v values between 3.7×10^{-5} and 7.6×10^{-5} m^2/s from observed amplitudes of pressure head within clay aquitard for smectitic clay on the Liverpool Plains, Australia.

The previously proposed graphical method by Keller et al. (1989) for the amplitude calculation is inaccurate. Its accuracy depends upon the scale of the hydrographs and visual appreciation. More precise amplitude of the annual pore pressure fluctuations at each measurement location can be calculated with spectral frequency analysis through the Fourier Transformation with conjunction of filtering theory.

2.11   Simple spectral frequency analysis and filtering

A time series (e.g., barometric pressure changes and Earth tides) can be approximated by the composite sum of various components which are periodic in the nature. Spectral frequency analysis is a tool to evaluate the periodic time series properties through converting them from time domain to frequency domain by the Fourier Transform (e.g., Shih et al., 2000). The Fourier Transform decomposes a time series into sinusoids wave components (Figure 2.7). It identifies the different frequency components and their respective amplitudes. The Fourier Transform of a random variable in the time domain $f(t)$ is (Brigham, 1988; Bendat and Piersol, 1991):

$$F(\omega) = \int_{-\infty}^{\infty} f(t) e^{-2\pi \omega t i} dt$$
(2.52)

where *f* is a time domain variable, *t* is the elapsed time, ω is cyclical frequency, *F* is the complex Fourier components in the frequency domain, and *i* is $\sqrt{-1}$.
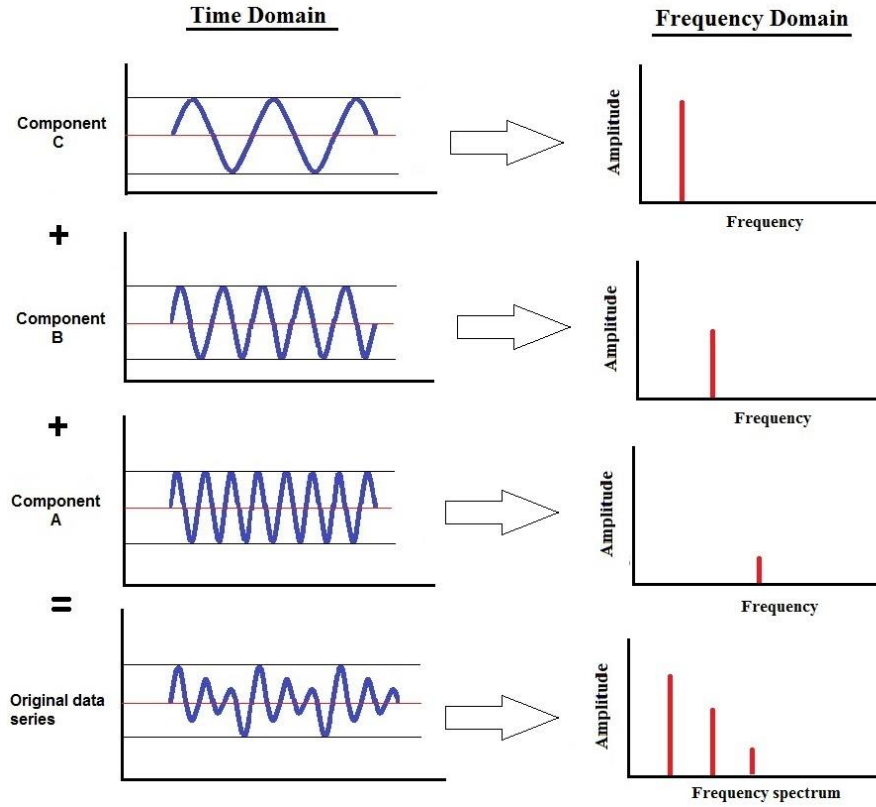
Figure 2.7: Schematic representation of Fourier transform

For a practical applications, finite record length (T_d) can be assumed. Thus, the transformed component *F* becomes a function of frequency and finite time length (Bendat and Piersol, 1991; Shih et al., 2008):

$$F(\omega, T_d) = \int_0^{T_d} f(t)e^{-2\pi\omega ti}dt \tag{2.53}$$

Two-sided autospectral density function can be estimated as (Bendat and Piersol, 1991):

$$S_{xx} = \frac{1}{T_s}|F(\omega, T_s)|^2 \tag{2.54}$$

where T_s is the ratio of total length of time series (T_d) to the continuous segments of n_d. For a

sampling interval of Δt in time domain, the discrete frequency is (Bendat and Piersol, 1991):

$$\omega_k = \frac{k}{T_s} = \frac{k}{N\Delta t} \quad k = 0, 1, 2, \dots, N - 1 \tag{2.55}$$

where N is the length of the segments. The smoothed, one-side autospectral density can be written as (Bendat and Piersol, 1991):

$$G_{xx} = \frac{2}{n_d N\Delta t} \sum_{i=1}^{n_d} |F_i(\omega_k)|^2 \quad k = 0, 1, 2, \dots, \frac{N}{2} \tag{2.56}$$

Frequency spectrum of a time series can be computed by MATLAB's FFT function or other mathematical programs. In Appendix B, a MATLAB script provides the spectral frequency for natural pore pressure response time series.

Filtering is a process to isolate and manipulate one or more of the components of the frequency spectrum. While a specified frequency within the record is identified from the frequency spectrum, the noises above and below the specified frequency can be filtered. Two methods can be applied: bandpass or high-lowpass filters. Bandpass filtering provides a "window" for a specified frequency to be isolated within the observed record. The high-lowpass filters and the bandpass filter (Figure 2.8) are similar except that the window is infinite on one side in high-lowpass filters (Hydrotechnique Associates, 1984).
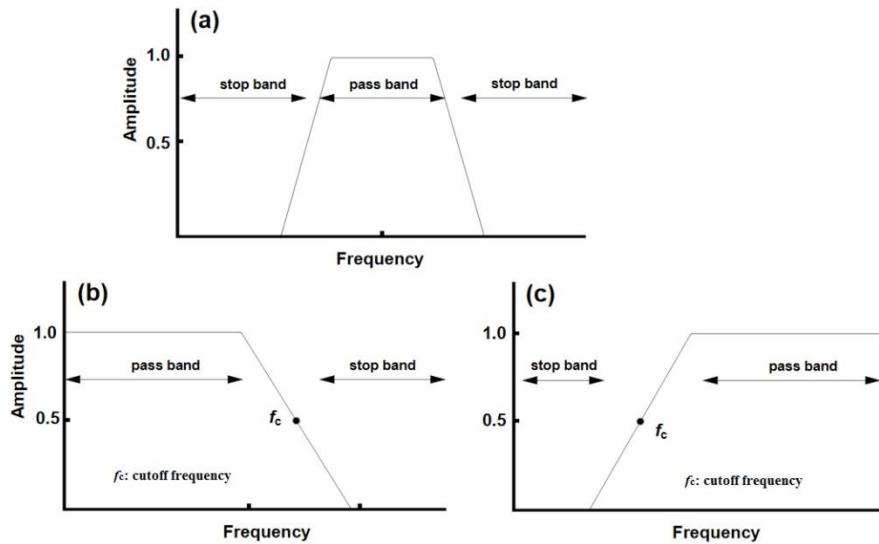
Figure 2.8: Schematic representation data filtering: a) bandpass filter, b) lowpass filter, and c) highpass filter.

2.12 Hydraulic conductivity anisotropy

Natural, even homogenous, soils are known to develop some hydraulic conductivity anisotropy during deposition and densification (e.g., Chan and Kenney, 1973; Olson and Daniel, 1981; Tavenas et al., 1983a; Al-Tabbaa and Wood, 1987; Chapuis and Gill, 1989; Leroueil et al., 1990; Bolton et al., 2000; Scholes et al., 2007; Chapuis, 2012). Hydraulic conductivity anisotropy is an important parameter for the analysis and design of earth dams and dykes, settlement rates of consolidating clays, contaminant migration, drainage systems, and oil or water well fields (e.g., Chapuis and Gill, 1989). Laboratory assessments of the hydraulic conductivity anisotropy for granular and cohesive soils are well documented in the literature (e.g., Chan and Kenney, 1973; Olson and Daniel, 1981; Zimmie et al., 1981; Tavenas et al., 1983a; Al-Tabbaa and Wood, 1987; Chapuis and Gill, 1989; Chapuis et al., 1989; Leroueil et al., 1990; Kiyama et al., 1996; Scholes et al., 2007).

Chapuis and Gill (1989) summarized some published anisotropy ratios for natural clays from the literature. The anisotropy ratio ranges from 0.7 to 4 from most experimental results of homogenous clays. For Champlain clays, within the strain range encountered in engineering applications (i.e., up to 25%), permeability anisotropy is small, e.g. 1.35 according to small-scale laboratory tests (Tavenas et al., 1983a; Leroueil et al., 1990), and that of the Lachenaie clay was found to be insignificant (Duhaime, 2012).

Assessing the in-situ hydraulic conductivity anisotropy is rarely a straightforward task. A few in-situ methods can be used to assess the hydraulic conductivity anisotropy. These methods include the comparison of results for piezometers with different injection zone lengths (Hvorslev, 1951), the interpretation of pumping test results (Arnold et al., 1962; Mansur and Dietrich, 1965; Hantush, 1966; Dagan, 1967; Hsieh and Neuman, 1985), and fitting the results of a predicted numerical model with an experimental flow net (Chan and Kenney, 1973).

2.13 Champlain clay

Champlain clays were deposited in the Champlain Sea approximately from 12000 to 8500 BP (before present), during the late Quaternary Period (La Rochelle et al., 1970; Quigley, 1980). They cover the southern lowland of Quebec (St. Lawrence River and Ottawa River lowlands) in

eastern Canada (Figure 2.9). The clay thickness reaches up to 100 m in the middle of the basin. The hydraulic conductivity of Champlain clays are discussed in section (2.11). This section presents some mechanical properties of the clay related to this thesis. Champlain clay mechanical properties are strongly affected by sampling and test methods (Crawford and Burn, 1963; La Rochelle and Lefebvre, 1971; La Rochelle et al., 1981; Leroueil et al., 1983; Silvestri and Abou-Samra, 2008). The important mechanical properties of Champlain clay in the current study are the preconsolidation pressure (σ'_P), compressibility (m_v), elastic moduli, and Poisson's ratio (v).
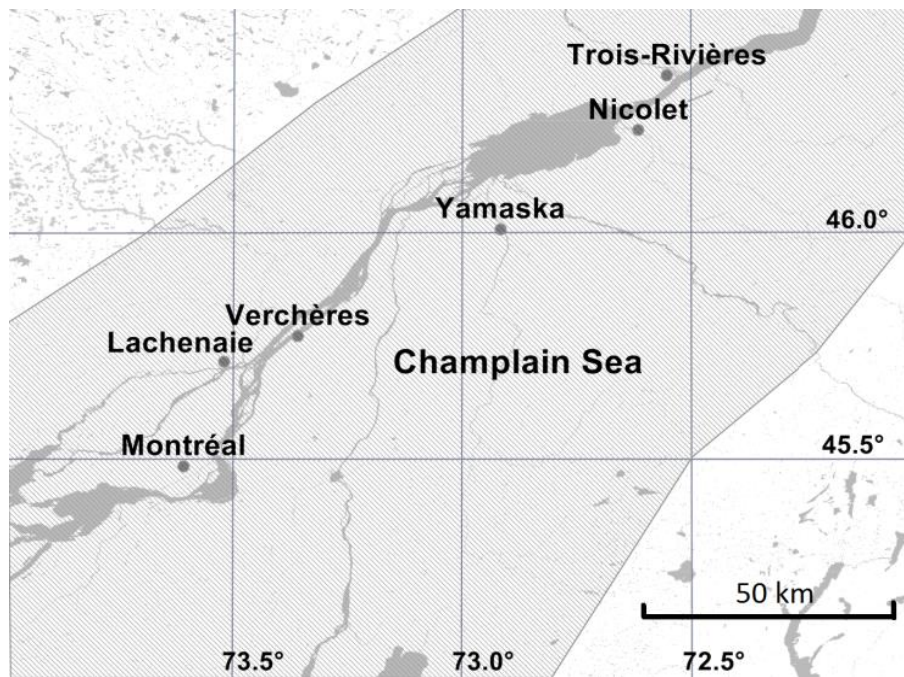
Figure 2.9: Maximum area covered by the Champlain Sea in southern Quebec, adapted from Duhaime (2012)

2.13.1 Preconsolidation pressure

Preconsolidation pressure, σ'_p, provides yield stress for a clay sample. Below the yield stress, the strain is small and recoverable governed by the theory of elasticity (e.g., Mitchell, 1970). This section reviews σ'_p for Champlain clay deposit. In general, the preconsolidation pressure is often described as the maximum effective vertical overburden pressure that a specific soil sample has sustained in the past (Holtz and Kovacs, 1981).

Preconsolidation pressure can be determined commonly consolidation curve from conventional oedometer tests on intact soil samples. It can also be found by an isotropic compression test (Helwany, 2007; Wood, 2010). The preconsolidation pressure can be thought as the yield point of the soil. For a stress level lower than the preconsolidation pressure, the soil response is approximately elastic (Wood, 2010).

There are some difficulties regarding the determination of σ'_p: different methods do not provide a unique preconsolidation pressure for certain clays (Crawford, 1964). Soil disturbance during sampling and testing has an influence on σ'_p (La Rochelle and Lefebvre, 1971; Lefebvre and Poulin, 1979; La Rochelle et al., 1981). Furthermore, the σ'_p value obtained from laboratory and in-situ tests are not always in agreement.

The σ'_p values for Champlain clays generally vary between 50 and 600 kPa. In the Saguenay River valley, Demers and Leroueil (2002) reported much higher σ'_p values of up to 1000 kPa and OCR values of up to 25. For the Champlain clay deposit in Lachenaie, σ'_p vary between 180 and 580 kPa with an OCR between 1.8 and 11 (Duhaime, 2012; Duhaime et al., 2013). The high OCR values in the Lachenaie deposit can be explained by the erosion of a layer of sediment that covered the clay deposits (Bouchard et al., 1983; Duhaime et al., 2013). Table (2.2) represents some published σ'_p values for Champlain clays.

2.13.2 Clay stiffness parameters

Parameters describing clay stiffness, for example clay compressibility (m_v), are required to estimate the volume change of the clay layer. Clay compressibility can usually be obtained from a stress-strain relationship (e.g., void ratio, e, versus vertical effective stress, σ'_v). There are a large number of tests in geotechnical engineering that provide stress-strain relationship for a soil sample (e.g., oedometer test and triaxial test in the laboratory or a self-boring pressuremeter test in the field). The m_v value of clay depends on stress path, strain rate, disturbance level, and temperature (Leroueil, 1996). In general, the compressibility decreases with an increase in the strain rate and a decrease in temperature, while it increases with sample disturbance due to stress change during sample collection (Clark, 1998).

Sensitive clays tend to be affected by mechanical disturbance to a high degree during sampling,

handling and testing (La Rochelle and Lefebvre, 1971; Lefebvre and Poulin, 1979; La Rochelle et al., 1981). Thus, it is difficult to obtain truly undisturbed samples. Because of this unavoidable disturbance, the laboratory e-log(σ'_v) may differ from field conditions. A typical e-log(σ'_v) for undisturbed sensitive clay with respect to its remoulded state is shown in Figure 2.10.
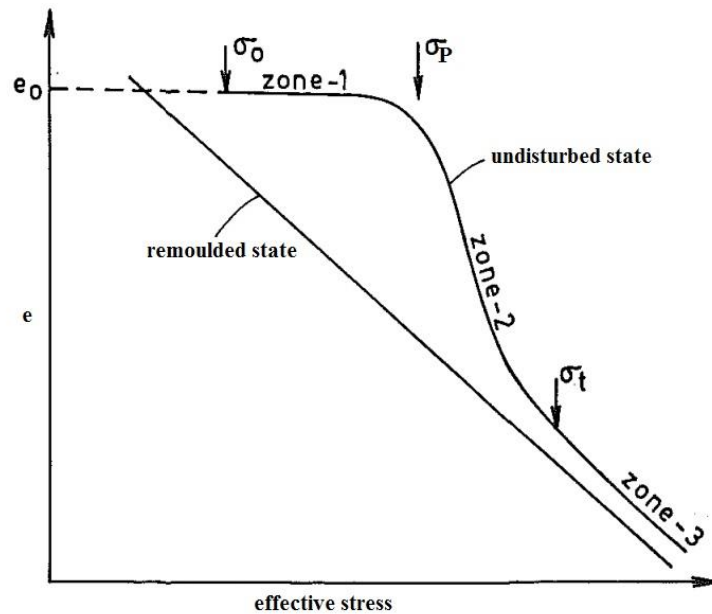
Figure 2.10: Typical stress-strain curve for a sensitive clay, after Nagaraj et al. (1990)

For the undisturbed clay sample, up to a given stress level, the compression is very small (zone 1). In zone 1, the soil displays a rigid response due to the inherent cementation bonding (Nagaraj et al., 1990). Beyond σ'_p, there is a relatively steep break and high compression in zone 2 results in widespread failure of the soil skeleton and high compression indices (Hamilton and Crawford, 1960). In zone 2, the soil tends toward the remoulded state. In zone 3, the slope of compression curve decreases, the cementation bonds are completely broken and the clay behaves as remoulded soil (Nagaraj et al., 1990). For Lachenaie clay, similar e-log(σ'_v) relationships with sharp breaks at σ'_p have only been found for the upper sublayer of the intact clay (Duhaime et al., 2013). The m_v values for Lachenaie clay were obtained from both in-situ pulse tests and laboratory oedometer tests. In-situ pulse tests provided a compressibility value on the order of 1×10^{-5} kPa^{-1} for the Lachenaie clay. With respect to pulse tests, laboratory oedometer tests

overestimate the clay compressibility by one order of magnitude (Duhaime, 2012).

Sample disturbance influences clay compressibility, e-log(σ'_v) relationship and clay elastic moduli (La Rochelle and Lefebvre, 1971; Holtz et al., 1986; Nagaraj et al., 1990). An increase in disturbance degree decreases the magnitude of experimentally determined preconsolidation pressure (Figure 2.11). The thin-walled tube sampling causes a decrease by 50 to 60 % in the elastic moduli when compared with block samples according to La Rochelle and Lefebvre (1971) who claimed that even for a perfect sample of cemented Champlain clay, the stress release due to sampling might break cementation bonds thereby leading to sample disturbance.
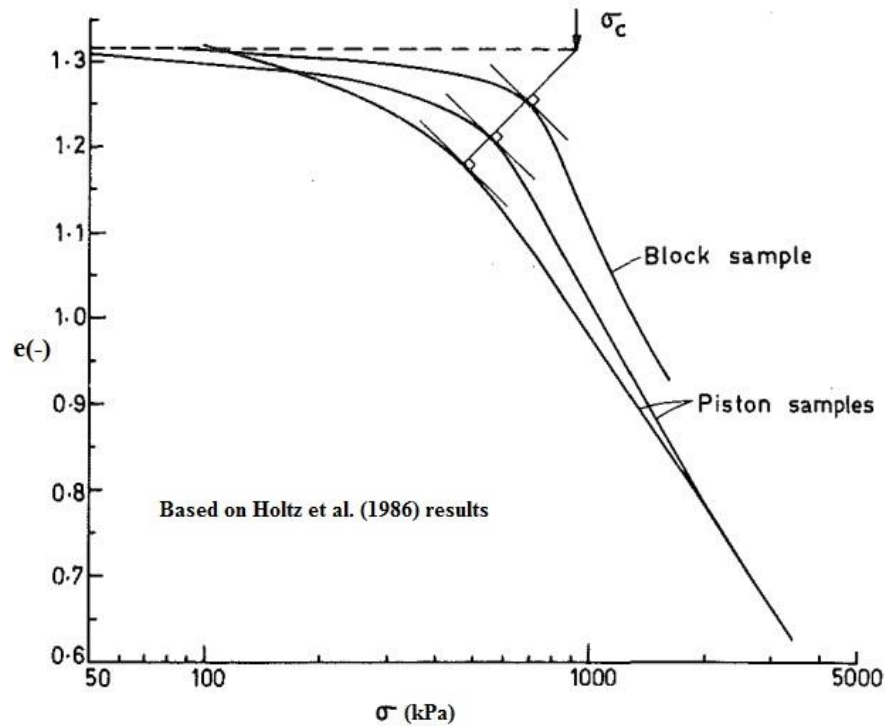
Figure 2.11: Effect of sample disturbance in a sensitive clay, adapted from Nagaraj et al. (1990)

The m_v values can be calculated from the consolidation curve using the following equation (Bardet, 1997):

$$m_v = \frac{0.435}{1+e} \frac{C_x}{\sigma'_v} \qquad (2.57)$$

where C_x can be replaced with the recompression index (C_r), the compression index (C_c), and the swelling index (C_s). The plot of axial strain ε_z versus vertical effective stress σ'_z presented by Janbu (1969), can provide a simpler method to determine m_v from its slope.

For Champlain clays, some stiffness parameters are available in the literature (Leroueil et al. 1983). The self-boring pressure meter (SBPM) test allows determining G_0 values for low strain in-situ conditions. The G_0 value is obtained from the slope of pressure–expansion curves in the unloading step. Several authors (e.g., Hamouche, 1995; Silvestri, 2003; Silvestri and Abou-Samra, 2008) performed SBPM tests in diverse locations of the Champlain Sea basin. Silvestri (2003) determined G_0 values between 6 and 15 MPa and G values between 1 and 4 MPa from the pressure–expansion curves, for depths between 6 and 14 m below ground surface, utilizing data for SBPM tests performed by Hamouche (1995) in Louiseville clay. In addition, Silvestri and Abou-Samra (2008) obtained G_0 values between 8 and 14 MPa for Mascouche clay (near Lachenaie) performing SBPM tests. For Lachenaie clay Duhaime (2012) determined a G_0 value between 8 and 17 MPa from in-situ pulse tests.

Soil stiffness parameters (e.g., G_{max}) can be determined from very small strain field dynamic tests (e.g., multi-modal analysis of surface wave method, MMASW). With this technique, G_{max} is related to the shear wave velocity as follows (e.g., Lefebvre et al., 1994):

$$G_{max} = \rho V_s^2 \tag{2.58}$$

where ρ is soil density and V_s is the shear wave velocity. From surface wave analysis, Lefebvre et al. (1994) obtained G_{max} values between 14 and 130 MPa for depths of 1 to 11 m below ground surface for the Champlain clay deposit in Saint Alban. Furthermore, for a series of profiles close to the Lachenaie study area, Karray and Lefebvre (2001) used the MMASW method to determine G_{max}. Values of G_{max} between 13 and 64 MPa were obtained for depths of 0.5 and 23.5 m respectively. A comparison between shear modulus obtained for Champlain clay from field dynamic test and other in-situ methods (e.g., SBPM, pulse test) shows that the very small strain tests provide greater G values for the shear modulus.

There are high uncertainties in the determination of an appropriate value for Poisson's ratio, v, in Champlain clay. A v value of 0.5 was defined theoretically by several authors for saturated clay when considering undrained conditions (D'Appolonia et al., 1971; Bjerrum, 1972). For

Champlain clays however, a value lower than 0.5 has been reported by some authors for undrained conditions. Bozozuk (1963) and Crawford and Burn (1963) have proposed v values on the order of 0.4 for cemented clay. Karray and Lefebvre (2001) considered a value of 0.499 for saturated Lachenaie clay to determine the small-strain shear modulus using MMASW. Tavenas et al. (1974) used a value of $v = 0.3$ to investigate the immediate settlement of Champlain clay under embankments. A drained value of $v = 0.3$ was used by Duhaime (2012) to model in-situ permeability tests in the Lachenaie clay deposit. Table (2.2) presents some published values of the mechanical properties of the Champlain clay.

Table 2.2: Some published mechanical properties for Champlain clay. Where σ'_p is preconsolidation pressure, C_c and C_r are virgin compression and recompression indexes, OCR is overconsolidation ratio, G_S is specific gravity of solids, G_0, G_{max}, and G are small strain, very small strain and secant shear modulus respectively, HFT is hydraulic fracture test, SBPT is self-boring pressuremeter test, PMT is prebored pressuremeter test, ISCT is instrumented sharp cone test, FC is fall cone test, PPT is probed pressuremeter test, PMT is pushed

Property	σ'_p (kPa)									
Value	105-200	40-300	47-270	60-310	175-300	240-320	Up to 580	38-940	267-410	180-584
Place	Lachute-Quebec	8 sites in Champlain Sea basin	11 sites in Champlain Sea basin	five sites in St. Lawrence Valley	Montreal (City Hall)	Montreal Island	Lachenaie	31 sites in Quebec	Mascouche (B)	Lachenaie
Reference	Silvestri (1980)	Tavenas et al. (1983)	Leroueil et al. (1983)	Lefebvre et al. (1991)	Silvestri et al. (1992)	Silvestri (2000)	GSI Env. (2001)	Demers and Leroueil (2002)	Silvestri and Abou-Samra (2008)	Duhaime (2012)

Property	OCR								Gs	
Value	1.5-4.0	1.3-7.9	1.6-4.8	1.1-8.9	1.0-28	2.4-11	5.1-6.4	1.8-11	2.70-2.80	2.63-2.78
Place	Champlain clay	15 sites in Champlain Sea basin	five sites in St. Lawrence Valley	Montreal Island	31 sites in Quebec	Montreal Island	Mascouche (B)	Lachenaie	Champlain Sea basin	Lachenaie
Reference	Leroueil et al. (1979)	Leroueil et al. (1983)	Lefebvre et al. (1991)	Silvestri et al. (1992)	Demers and Leroueil (2002)	Silvestri (2000)	Silvestri and Abou-Samra (2008)	Duhaime (2012)	Leroueil et al (1983)	Duhaime (2012)

Table 2.3: Some published mechanical properties for Champlain clay. Where σ'_p is preconsolidation pressure, C_c and C_r are virgin compression and recompression indexes, OCR is overconsolidation ratio, G_S is specific gravity of solids, G_0, G_{max}, and G are small strain, very small strain and secant shear modulus respectively, HFT is hydraulic fracture test, SBPT is self-boring pressuremeter test, PMT is prebored pressuremeter test, ISCT is instrumented sharp cone test, FC is fall cone test, PPT is probed pressuremeter test, PMT is pushed (continued).

Property	Cc				Cr	v			G (MPa)	
Value	1.2-2.3	1.2-6.0	0.32-1.88	0.43-2.08	0.03-0.08	0.4	0.3	0.499	4.54	4.04
Place	Saint-Alban	8 sites in Champlain clay	Montreal Island	Lachenaie	Montreal Island	Champlain clay	Saint-Alban	Lachenaie	Mascouche A-(PMT)	Mascouche A (ISCT)
Reference	Tavenas et al. (1974)	Tavenas et al. (1983)	Silvestri et al. (1992)	Duhaime (2012)	Silvestri et al. (1992)	Bozozuk (1963)	Tavenas et al. (1974)	Karray and Lefebvre (2001)	Silvestri and Abou-Samra (2008)	Silvestri and Abou-Samra (2008)

Property	G0 (MPa)				Gmax (MPa)				G (MPa)	
Value	6-15	8.3-14.4	1.5-6.9	8-17	15-26	30	14-130	13-64	1-4	1-5.1
Place	Louiseville (SBPT)	Mascouche (B)- (SBPT)	Mascouche (A)- (PMT)	Lachenaie (Pulse test)	Louiseville (Cross-hole)	Louiseville (Bender elements)	Saint Alban (Shear wave)	Lachenaie (Shear wave)	Louiseville (SBPT)	Mascouche A-(PMT)
Reference	Silvestri (2003)	Silvestri and Abou-Samra (2008)	Silvestri and Abou-Samra (2008)	Duhaime (2012)	Leroueil et al. (2003)	Shibuya (2000)	Lefebvre et al. (1994)	Karray and Lefebvre (2001)	Silvestri (2003)	Silvestri and Abou-Samra (2008)

CHAPTER 3   ARTICLE 1 : FULLY GROUTED PIEZOMETERS: IMPLICATIONS FOR PORE PRESSURE MONITORING IN CLAY LAYERS

Vahid Marefat[1*], François Duhaime[2], Robert P. Chapuis[1]

Submitted to *Engineering Geology*, September 2015.

[1] Department of Civil, Geological and Mining Engineering, Ecole Polytechnique, P.O. Box 6079, Stn CV, Montreal, Quebec, Canada, H3C 3A7

[2] Laboratory for Geotechnical and Geoenvironmental Engineering (LG2), École de technologie supérieure, 1100 Notre-Dame Ouest, Montreal, QC, Canada, H3C 1K3

[*] Corresponding author: Phone +1-438-931-9797; fax +1-514-340-4477-Email:vahid.marefat@polymtl.ca

Abstract

Piezometers can be installed in clay layers or aquitards using the fully grouted method. This method is said to have the following advantages: reduced cost, no risk of failure for the sand pack, and ease of installation, especially for nested piezometers. The success of the fully grouted method depends on three parameters: the permeability ratio (ratio of grout permeability to surrounding aquitard permeability), the natural vertical hydraulic gradient within the aquitard, and the borehole depth within the aquitard. Each installation has a piezometric error which may or may not be small. This paper gives a new analytical solution for the piezometric error in steady-state natural flow conditions. The solution was assessed using finite element studies. For most field conditions (vertical hydraulic gradient of less than 1), it was found that the grout permeability can exceed that of the tested aquitard by up to one order of magnitude without producing a significant piezometric error. For a lower permeability ratio (i.e.,10) and for almost all borehole depths, the piezometric error does not change significantly with borehole depth, while for higher permeability ratios (greater than 100*)*, the error increases with borehole depth. As a general conclusion, to avoid significant piezometric errors with the fully grouted method, the permeability ratio should be lower than 10, particularly for field conditions with a significant vertical hydraulic gradient.

Keywords: Fully grouted piezometer, piezometric error, hydraulic head, clay layer, aquitard.

3.1 Introduction

The fully grouted method to install piezometers entails lowering a pressure transducer in a borehole which is backfilled with grout, without using a filter pack. The method has been used since the 1970s for several geotechnical and mining applications. Proponents of the fully grouted method appreciate its advantages: reduced cost, shorter installation time, ease in installing, no risk of failure for the sand pack, ease in using nested piezometers in a single borehole, ease to use the same borehole for other instruments, and the possibility of adapting the method for installing horizontal or inclined piezometers. The fully grouted installation method can be 15% less expensive than the traditional installation method with a filter pack and it can save around 75% of the installation cost when a borehole is shared with other geotechnical instruments (McKenna, 1995).

The fully grouted technique of installing vibrating wire pressure transducers (VWP) has recently received much interest in the field of mining, geotechnical engineering, and hydrogeology. In mining engineering, VWP installed with the fully grouted technique are commonly used to monitor hydraulic head fluctuations caused by underground mining activities (Yungwirth et al., 2013; Zawadzki and Chorley, 2014). In geotechnical engineering, they are installed within clay layers to monitor the consolidation caused by earth structures such as embankments, dikes, and earth dams. Similarly, they are installed to monitor slope stability for natural river banks (Simeoni et al., 2011) or for excavations in urban areas (e.g., de Rienzo et al., 2008; Xu et al., 2009; Jurado et al., 2012; Pujades et al., 2012; Pujades et al., 2014). In hydrogeology they are deployed in clay aquitards to assess natural pore pressure fluctuations and to estimate in situ large-scale clay elastic and hydraulic properties (Smith et al., 2013; Smerdon et al., 2014).

Even if the fully grouted installation method has spread throughout the world, the performance of this installation technique is still questioned, particularly when it is used to register pore pressure change in low permeability soil. A piezometer performance can be defined by its time lag and measurement accuracy (McKenna, 1995). Time-lag represents the time taken by a piezometer to reach its equilibrium pressure following a pore pressure change in the area surrounding the sensor (Hvorslev, 1951). Deviation of the measured pore pressure from the real pore pressure of the natural soil before drilling can be called piezometric error. This deviation may be due to several factors, especially grout permeability.

Assessments of the response time for modern diaphragm-type piezometers installed within fully grouted boreholes have previously been presented in the literature. Earlier laboratory results have concluded that the response time for a fully grouted piezometer is on the order of seconds or minutes (McKenna, 1995; Mikkelsen, 1999; Bayrd, 2011; Contreras et al., 2012; Simeoni, 2012). On the other hand, with numerical modelling, Zawadzki and Chorley (2014) calculated that the response time for a fully grouted piezometer, installed within fractured bedrock and subjected to transient flow, can be on the order of hours compared to the almost instantaneous response of a piezometer installed within a sand filter.

Several authors have noted that the grout permeability, K_g, is the most crucial factor influencing the piezometric error (Vaughan, 1969; McKenna, 1995; Mikkelsen and Green, 2003; Contreras et al., 2008). A few authors have tried to prove that a grout more permeable than the target formation can induce a small error (e.g., Vaughan, 1969; Mikkelsen and Green, 2003; Contreras et al., 2008). However, field measurements led McKenna (1995) to conclude that for most soil conditions the grout must be less permeable than the formation to reduce the piezometric error.

The grout hydraulic conductivity is not the sole factor influencing the piezometric error. Errors can be influenced by other factors, like the natural vertical hydraulic gradient in the clay formation and the piezometer embedment depth in the clay layer. The natural hydraulic gradient may have significant impact on piezometer performance since it changes with seasons or any variation in the groundwater table. For example, during an excavation project, the hydraulic gradient within the excavated formation can change notably due to pumping of water from the underlying aquifer. Moreover, the authors have witnessed changes in hydraulic gradient within deposits of soft Champlain clay of around two orders of magnitude for one year of pore pressure monitoring (Marefat et al., 2015c). The effects of such factors on piezometric error were not explored in previous works. The respective influence of grout permeability, vertical hydraulic gradient, and borehole depth on piezometric error have yet to be studied systematically.

Knowing the piezometric error induced by the grout hydraulic conductivity for varying geometries and vertical hydraulic gradients would help to evaluate the capacity of the fully grouted method to obtain precise pore water pressure measurements in diverse settings. The main objective of this paper is to determine the accuracy of the fully grouted installation method when pore water pressures are measured within a clay layer. The influence on piezometric error of

grout hydraulic conductivity, grouted borehole length, and the vertical hydraulic gradient in the clay formation penetrated by the borehole has been investigated with both numerical and analytical solutions. This paper also briefly discusses cement-bentonite grout properties and development of fast response vibrating wire piezometers, VWPs.

3.2   Grout properties

There are several types of commercially available bentonite in North America and elsewhere. They include granulates, powder, chips, and pellets of sodium bentonite. Moreover, calcium bentonite and opalite are also used (Mikkelsen, 2002). Bentonite chips or pellets are commonly used to seal the borehole above the sand pack in monitoring wells and standpipe piezometers. They can also be used to seal the intake zone of a VWP when following the traditional (sand pack) installation procedure. In the sand pack procedure, the permeability of the seals is low enough to isolate the sand pack. For both the traditional and fully grouted installation methods, the borehole above the chips or pellets is backfilled with a bentonite slurry or cement-bentonite grout produced from powdered sodium bentonite.

There are typically two types of grouts for piezometer installation: bentonite and cement-bentonite grouts. Bentonite grout is made by mixing water and bentonite powder. Bentonite grouts may be volumetrically unstable, and the hydration process is suspected to produce local excess pore water pressure. Moreover, this type of grout is difficult to pump down the borehole with small diameter tremie pipes (Mikkelsen, 2002). Adding cement into hydrated bentonite results in a much more stable grout which is called self-hardening grout. The mechanical properties of these grouts can be controlled. They are time-dependent, and evolve from a liquid grout and gradually set to become a clay-like material (Chapuis et al., 1984). Moreover, adding cement provides the ability to produce a grout mix which is initially less viscous and easier to pump than bentonite grout (Mikkelsen, 2002).

Grout permeability is a key factor in a successful fully grouted transducer installation (Vaughan, 1969; McKenna, 1995). The grout permeability is inversely related to the quantity of bentonite. Adding more bentonite yields a more plastic grout with a lower permeability (Gustin et al., 2007), which increases the time lag for the VWP response. On the other hand, the grout strength

depends on the water-cement ratio. It can be increased by decreasing the water-cement ratio (Portland Cement Association, 1984; Mikkelsen, 2002; Contreras et al., 2008). While adding more cement results in a rigid grout, it may also result in grout cracking and macro permeability during ground movements. Additionally, the water-cement ratio controls the void ratio of the mix and thus also influences the permeability (Contreras et al., 2008). One can see that determining the recipe and producing a grout with appropriate permeability and stiffness may be the most complicated task in a fully grouted installation.

Unfortunately, there are not enough data in the literature on the hydraulic and mechanical properties of cement-bentonite grout mixes. The available data mostly concern the properties of cement-bentonite mixes that include sand, soil, or other materials for specific geotechnical applications such as cut-off walls, clay liners and so forth. A review of previous published data of K_g provides some useful preliminary information for users who are interested in using the fully grouted method for pressure transducer installation. Table (3.1) presents some published K_g values for several types of bentonite and cement-bentonite grouts.

Table 3.1: Some published values of hydraulic conductivity for net cement, bentonite slurry, bentonite chips, and cement-bentonite grout.

Grout type	Characteristics	K (cm/s)	Reference
Neat cement	W:C =0.53-0.89	10^{-5} to 10^{-7}	Baroid, taken from Mikkelsen (2002)
Sodium-Bentinte slurry	-	10^{-11} to 10^{-12}	Pusch (1992)
Bentinte slurry	6% solid	1×10^{-5}	Baroid, taken from Mikkelsen (2002)
Bentinte slurry	20% solid	1×10^{-8}	Baroid, taken from Mikkelse (2002)
Bentinte chips	-	1×10^{-9}	Filho (1976)
Bentinte chips	Hydrated	1×10^{-8}	Baroid, taken from Mikkelsen (2002)
Cement-bentonite	water/solids= 4 to 1	1×10^{-6}	Vaughan (1969)
Cement-bentonite	4:01:01	5×10^{-8}	Vaughan (1973), taken from Mikkelsen (2002)
Cement-bentonite	0.2:1:0.03	1×10^{-7}	Chapuis et al. (1984)
Cement-bentonite	0.8:1:0.025	1×10^{-8}	McKenna (1995)
Cement-bentonite	2.5:1:0.35	1×10^{-6}	Contreras et al. (2008)
Cement-bentonite	6.55:1:0.4	6.5×10^{-6}	Contreras et al. (2008)
Cement-bentonite	3.99:1:0.67	2×10^{-6}	Contreras et al. (2008)
Cement-bentonite	2.0:1:0.36	1×10^{-7}	Contreras et al. (2008)
Cement-bentonite	2.49:1:0.41	5×10^{-7}	Contreras et al. (2008)
Cement-bentonite	6.64:1:1.19	4×10^{-6}	Contreras et al. (2008)
Cement-bentonite	2.66:1:0.27	2×10^{-6}	Contreras et al. (2008)

3.3   Development of VWP, error sources, and limitations

With the traditional method in groundwater investigation, an open standpipe and a sand filter around the piezometer tip (Figure 3.1a) are essential to hasten the pressure equalization between the soil and the piezometer. A smaller inner diameter results in a quicker piezometer response. In low permeability clay aquitards, the standpipe piezometers equalize slowly with change in pore pressure within the surrounding clay formation. This is because a finite volume of water must flow into or out of the standpipe to equalize the pore pressure imbalance between the piezometer and the clay layer. This leads to time lag between piezometer equalization and pore pressure change in the clay formation (Hvorslev, 1951).

The development of VWPs in the 1980s and 1990s was a significant step in overcoming time lag problems for pore pressure measurement within low permeability clay layers. Only a very small volume of water (10^{-2} to 10^{-5} cm^3) is needed for full scale equalization with a VWP (McKenna, 1995). For decades, a procedure adapted from the traditional sand-pack installation method (Figure 3.1b) was used by the geotechnical and mining industry for the installation of VWPs (Dunnicliff, 1988). However, pouring the sand filter with the conventional method is not only time-consuming and prone to failure (Mikkelsen and Green, 2003), but the sand can also contain air bubbles which can increase the piezometer response time (van der Kamp, 2001b; Simeoni, 2012) or interfere with permeability tests (Chapuis, 2009b; Duhaime and Chapuis, 2014).

In the fully grouted installation method, once the borehole is drilled, the VWP is attached to a sacrificial grout pipe, which is lowered in the borehole to the chosen depth. The sacrificial pipe supports installation weight and allows the borehole to be grouted from the bottom up. The VWP is connected to a datalogger through a cable which is attached to the grout pipe (Yungwirth et al., 2013). After having positioned the piezometer, the borehole is directly backfilled with low permeability and non-shrinking cement-bentonite grout (Figure 3.1c). Grouting the borehole from the bottom up to surface is desired to assure the absence of voids or separation in the grout (Yungwirth et al., 2013). The mixing and backfilling procedures of the grout have been discussed in detail by Mikkelsen (2002) and Contreras et al. (2008). In a fully grouted VWP, pore pressure is registered by the VWP diaphragm. This provides an opportunity for fully grouted VWP to register hydraulic head at a specific point. Contrary to a fully grouted VWP, a VWP installed with the sand pack procedure typically measures a pore pressure corresponding to

the average hydraulic head along the sand filter zones. For example, it allows isolated fracture zones to be targeted in bedrock, or measurements to be taken in soil and lithology with complex stratigraphy where the hydraulic head may vary across short distances. An appropriate knowledge of stratigraphy is required prior to piezometer installation when fully grouted piezometers are considered for the measurement of accurate pore pressure at multiple points along a borehole. This is possible for boreholes with core samples or with reliable geophysics results (Yungwirth et al., 2013).
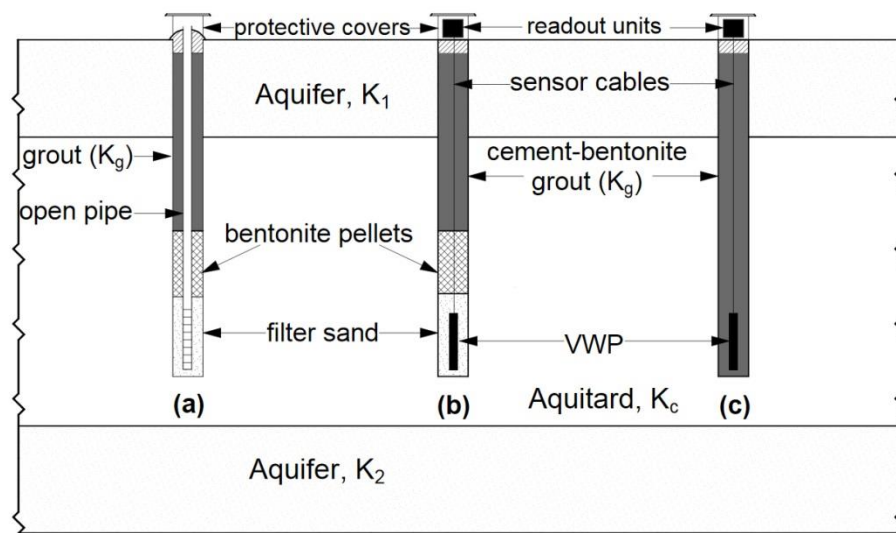
Figure 3.1: Vertical sketch of piezometer installation within a clay deposit:
a) standpipe piezometer; b) VWP with sand pocket; and c) fully grouted VWP.

A successful piezometer installation method should satisfy two criteria: 1) the piezometric error should be small, and 2) the time lag should be as short as possible (McKenna, 1995). The traditional installation method satisfies both criteria. First, the bentonite chips or pellets at the top of the sand pack can isolate perfectly the borehole's intake zone. The vertical fluid flow along the standpipe is thus restricted. Hence the pressure measured in the intake zone is representative of the pressure in the formation. Secondly, the permeable and fairly large intake zone in the traditional installation quickly equalizes the pressure imbalance between the formation and the well thereby decreasing the time lag (Hvorslev, 1951). For modern diaphragm-type piezometers,

the fully grouted method can also satisfy the two aforementioned criteria. The grout permeability should be low enough to restrict the vertical flow along the borehole axis and reading cables in order to maintain accurate measurements. The grout is able to transmit a sufficient volume of water within a short distance under a reasonable time for full scale equalization of the VWP (McKenna, 1995).

The principal sources of error for standpipe piezometers and transducers installed with the fully grouted method have respectively been documented by Hvorslev (1951) and McKenna (1995). For a diaphragm-type piezometer installed with the fully grouted method, piezometric error can be related to (1) random and systematic errors in the calibration, readings and measurements; (2) time lag imposed by grout; (3) systematic error due to improper placement of the piezometer; (4) systematic error related to improper sealing, or hydraulic short circuiting due to preferential flow along the grouted borehole and/or high contrast between formation and grout hydraulic properties; (5) chemical and thermal induced degradation and evolution of the grout; and (6) upward and downward seepage along the piezometer wires, especially if several transducers are installed in the same borehole.

Limitations of the fully grouted method have already been discussed by McKenna (1995). The some of most important limitations and difficulties regarding the fully grouted technique are summarized herein: (1) Preparing a grout with proper permeability is not a straightforward task. The grout permeability may vary with time due to cement and bentonite hydration. (2) In contaminated sites the grout mechanical and hydraulic properties may be influenced by the grout chemical degradation. (3) Groundwater sampling with this method is not possible. (4) The grout may crack due to ground movement in a seismic event which could create a higher permeability associated with macropores or hydraulic short-circuting. As a result, fully grouted piezometers might not provide accurate measurements for applications involving post-seismic pore pressure measurements or measurement in soils undergoing large deformation. (5) The VWP porous stone can becomes sealed with grout. (6) Improperly mixed grout yields measurements that are not representative. (7) The grout must be designed to prevent cracking while curing in order to preclude hydraulic short circuiting between the overlying aquifer and the piezometer tip.

The following sections explain the analytical and numerical models used to determine the error induced by the contrast between formation and grout hydraulic conductivities, borehole

geometry, and aquitard properties. The results explain the role played by the permeability of the grout, vertical hydraulic gradient, and borehole depth on the piezometric error.

3.4 Methodology

Consider a horizontal clay layer of constant thickness b between two aquifers. The natural hydraulic head profile for either downward or upward seepage is schematized in Figure 3.2. Flow condition is assumed to be entirely saturated and steady-state. If the clay layer is homogeneous, the downward or upward seepage is vertical with a linear hydraulic head distribution within the clay. As a consequence, the vertical hydraulic gradient is constant through the clay formation (Cherry et al., 2004). The natural hydraulic head for a given location at depth L within the clay formation before a piezometer installation can be calculated as follows:

$$i_{AB} = i_{BC} = i^* \tag{3.1}$$

$$i^* = \frac{h_1 - h_2}{z_1 - z_2} \tag{3.2}$$

where i_{AB} and i_{BC} are the vertical hydraulic gradients between levels A and B and between levels B and C, i^* is the vertical hydraulic gradient in the clay before installing a piezometer. The hydraulic head in the upper and lower aquifers are h_1 and h_2 respectively, and z_1 and z_2 are the elevations of the top and bottom of the clay layer with respect to the datum. The hydraulic head in upper and lower aquifers can be measured using perfectly sealed standpipe piezometers. These hydraulic heads can be determined as follows:

$$h_1 = h_2 + bi^* \tag{3.3a}$$

$$h_2 = h_1 - bi^* \tag{3.3b}$$

The natural hydraulic head to be measured by a piezometer perfectly installed at a depth L in the clay layer can be calculated with Eq. (3.4):

$$h^* = h_2 + (b - L)i^* = h_1 - Li^* \tag{3.4}$$

In the case of improper sealing of the borehole, or if the grout has a higher permeability than the surrounding soil, the borehole axis is a pathway for vertical seepage (McKenna, 1995), which

induces a hydraulic short-circuit. There is preferential seepage between the upper aquifer and the piezometer tip. Hydraulic short-circuiting occurs if the grout is more permeable than the surrounding formation ($K_g >> K_c$, where K_g and K_c are respectively the hydraulic conductivity of the grout and surrounding soil). A hydraulic short-circuit can also be produced outside of the sealing material due to hydraulic damage or internal erosion of the natural soil during borehole drilling (Chapuis and Sabourin, 1989).
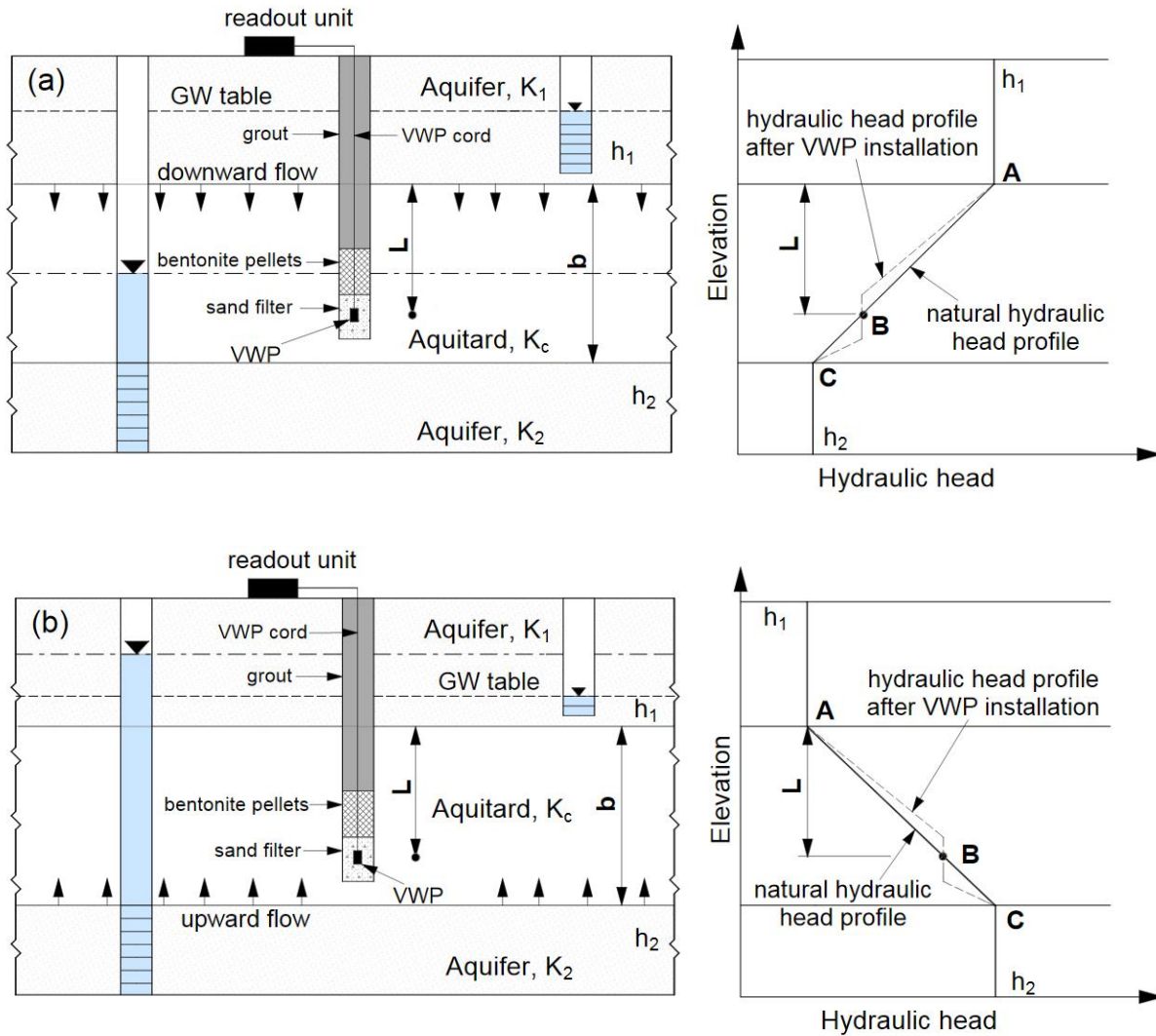
Figure 3. 2: Hydraulic head profiles within a homogenous clay formation before and after VWP installation with sand pocket: a) downward flow; b) upward flow.

If the clay hydraulic conductivity varies vertically, this causes variation in the vertical gradient within the clay layer (Cherry et al., 2004). As a consequence, for vertical seepage along the borehole axis, the hydraulic head profile will not be represented by a single straight line. In this case, the hydraulic head profile along the borehole axis, as shown in Figure 3.3, changes to two lines with different slopes. In Figure 3.3, these two lines are simply considered to be straight lines.
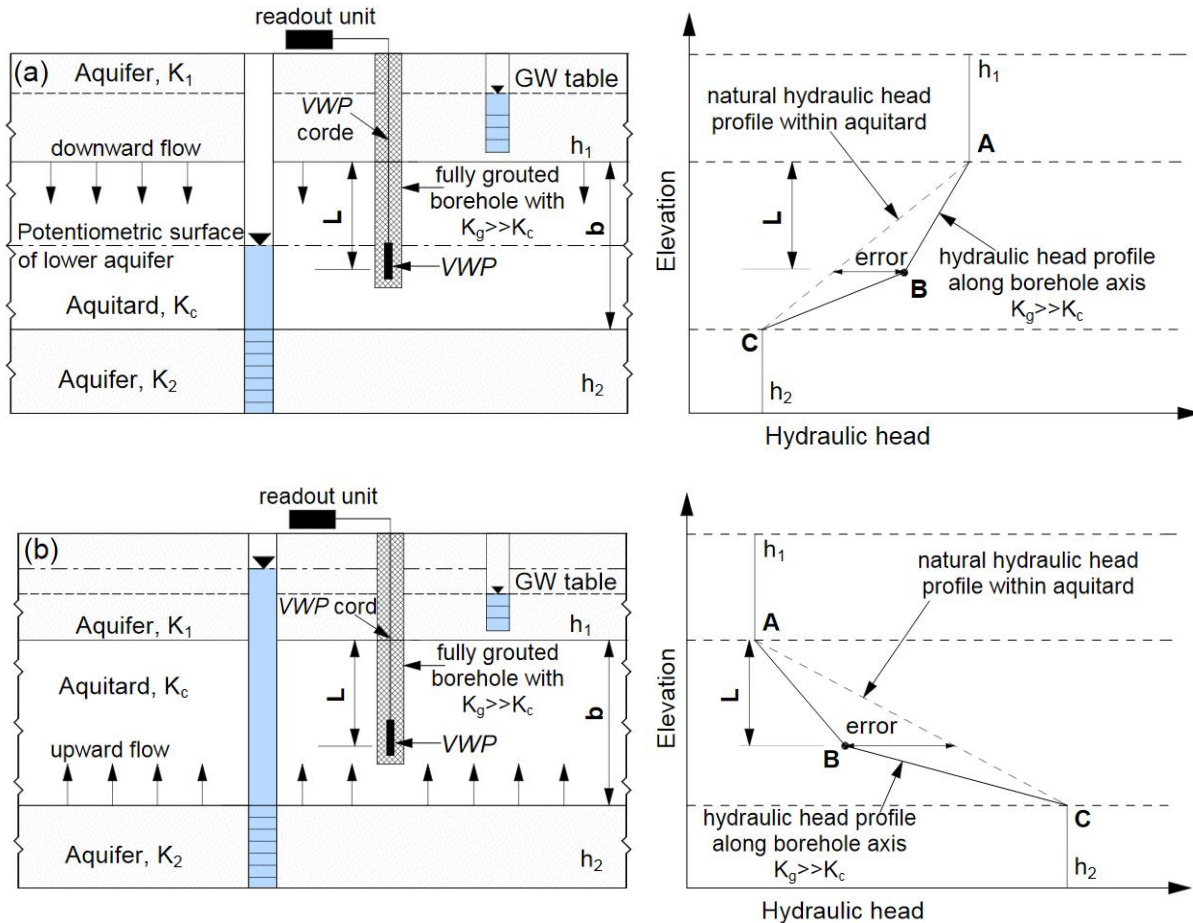
Figure 3.3: Hydraulic head profile within a clay layer with a fully grouted installation with $K_g \gg K_c$: a) downward flow; b) upward flow.

For $K_g \gg K_c$, due to hydraulic short-circuiting, the hydraulic head given by the piezometer is not equal to the natural hydraulic head before the piezometer installation. Therefore a piezometric error due to a poor choice of cement-bentonite permeability or improper sealing would occur. As

shown in Figure 3.3, the error can be defined as the difference between h_p, the hydraulic head measured with the piezometer, and the natural hydraulic head h^* at the same elevation. The h_p value can be estimated with numerical and analytical models. As h^* is determined from Eq. (3.4), the piezometric error can be determined as follows:

$$\varepsilon = h_p - h^*$$
(3.5)

If a low permeability grout minimizes the piezometric error, one might ask why practitioners would choose a grout that is more permeable than the surrounding formation. It is important to understand that if the grout is less permeable than the surrounding soil, the grout will induce an additional time-lag. Moreover, it is difficult to produce pumpable cement-bentonite grout with permeability values that are much lower than 5×10^{-8} cm/s (Vaughan, 1969). Therefore, in low permeability formations, producing a pumpable low permeability grout would be difficult. An objective of this paper is to determine the grout permeability threshold to get correct readings with a fully grouted VWP. For steady-state and saturated seepage conditions, analytical solution has been developed to directly determine the piezometric error. With numerical model once the hydraulic head measured by the VWP is calculated, the piezometric error can be obtained via Eq. (3.5).

3.5 Analytical solution

Analytical solutions are needed for upward and downward seepage (Figure 3.3). The analytical solutions consider that the flow rate injected from the borehole sidewall to the clay formation varies linearly along the borehole axis. This hypothesis will be discussed in light of the numerical results later in the paper. The different parameters that appear in the solution are illustrated in Figures. 3.4a and 3.4b.

3.5.1 Downward seepage

For steady-state downward seepage, it can be assumed that the flow rate Q_0 coming from the upper aquifer to the borehole (Figure 3. 4a) is completely injected in the clay formation through the borehole sidewall (Q_1). This can be written as the following flow rate conservation equation:

$$Q_0 = Q_1 = \int_{b-L}^{b} q\,dz \tag{3.6}$$

where q is the injected flow rate per unit length of borehole which is defined in detail later in this paper. To estimate the piezometric error for different conditions, the analytical solution considers that the flow rate injected directly from the bottom of the borehole (Q_2 in Figures 3.4a and 3.4b) into the clay layer is assumed to be negligible before the laterally injected flow rate. The unit flow rate injected from the borehole sidewall can be estimated using the general flow rate definition that forms the basis of the Hvorslev (1951) family of interpretation methods for variable-head permeability tests, $Q=CKH$, where C is a geometric shape factor for the injection zone (Chapuis, 1989), K is the isotropic hydraulic conductivity, and H is the hydraulic head difference between the soil under natural conditions and the borehole. This equation stems from the solution to Laplace's equation for different well geometries.
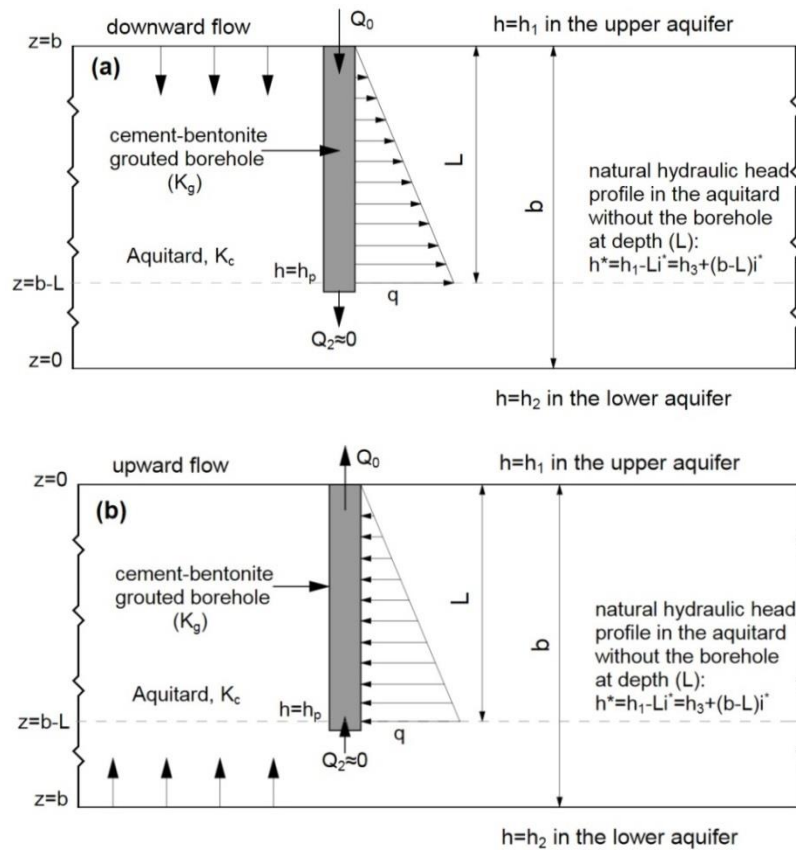
Figure 3.4: Schematic representation of the analytical study for a fully grouted borehole within a clay formation with ($K_g \gg K_c$): a) downward flow; b) upward flow.

For downward seepage, it can be assumed that the unit flow rate injected from the borehole sidewall is related to the following flow rate Q:

$$Q = C_I . \alpha_I . K_c . \left[h_p - h^* \right]$$ (3.7)

where C_I is a shape factor for an ideal geometry (Hvorslev, 1951) and α_1 is a correction coefficient which is obtained numerically (finite element method). For a cylindrical borehole, C_1 can be given the following definition:

$$C_I = 2\pi\pi / ln\left(r_0 / r_w\right)$$ (3.8)

where r_0 and r_w are respectively the radius of influence and the borehole radius. Chapuis (1999) suggested a value of 5 for $ln\ (r_0/r_w)$. This shape factor definition is usually applied to fully penetrating wells. The expression of $[h_p-h^*]$ in Eq. (3.7) can be replaced by ε according to Eq. (3.5). By substituting Eq. (3.8) in Eq. (3.7), Eq. (3.9) is obtained:

$$Q = \frac{2\pi L}{5} \alpha_I K_c \left[\varepsilon \right]$$ (3.9)

The injected flow rate q per unit length of borehole is assumed to be:

$$q = az + c$$ (3.10)

where z is any elevation in the borehole within the clay layer (Figure 3.4), and a, c are constants. If $a=0$, q is equally distributed along the borehole sidewall, if not it varies linearly with elevation. The a and c coefficients can be obtained by specifying unit flow rate values at the top and bottom of the fully grouted borehole. At the interface of the clay formation with the upper aquifer ($z=b$), q can be assumed to be negligible. According to Eq. (3.10), this implies that $a=-c/b$. At the bottom of the borehole ($z=b-L$), q is assumed to be equal to Q/L, where Q is the flow rate injected into the clay layer as defined by Eq. (3.9). Hence the unit flow rate q at $z=b-L$ can be obtained as follows:

$$q = \frac{2\pi}{5} \alpha_I K_c \left[\varepsilon \right]$$ (3.11)

The c coefficient of Eq. (3.10) can be found by substituting Eq. (3.11) in Eq. (3.10):

$$c = \frac{2\pi}{5} . \frac{b}{L} \alpha_I K_c \left[\varepsilon \right]$$ (3.12)

From there, q can be obtained by substituting the a and c coefficients into Eq. (3.10):

$$q = \frac{2\pi}{5L}\alpha_1 K_c [\varepsilon](b - z)$$ (3.13)

Integrating Eq. (3.13) from the bottom of the borehole ($z = b\text{-}L$) to $z=b$ provides the lateral flow rate injected from the sidewall of the borehole (Q_1). This indicates that the lateral flow rate is identical to $Q/2$ if a linear flow rate along the borehole axis is considered.

The flow rate along the borehole at elevation z can be obtained by integrating q from the bottom of the borehole ($z = b\text{-}L$) to z. The head loss between the upper aquifer and the bottom of the borehole can be obtained by integrating Darcy's law between these two boundaries:

$$h_1 - h_p = \frac{4}{\pi D^2 K_g} \int_{b-L}^{b} \left(\int_{b-L}^{z} q dz \right) dz$$ (3.14)

Integration of Eq. (3.14) provides the following equation:

$$h_1 - h_p = \frac{8\alpha_1}{15} \left(\frac{L}{D} \right)^2 \frac{K_c}{K_g} [\varepsilon]$$ (3.15)

In Eq. (3.15) the expression ($8\alpha_1.L^2.K_c/15.D^2.K_g$) can be named α_2. The hydraulic head of h_1 can be substituted by h^* via Eq. (3.4). Rearranging of Eq. (3.15) provides piezometric error as follows:

$$\varepsilon = \frac{L}{1 + \alpha_2} i^*$$ (3.16)

3.5.2 Upward seepage

For upward seepage, similar parameters and assumptions have been considered (Figure 3.4b). An equation identical to Eq. (3.16) is obtained but the sign of the gradient is different. This indicates that the upward and downward seepage solutions are symmetric.

3.6   Numerical simulation

More than 300 numerical simulations were completed to assess the ε value for fully grouted piezometers within a clay layer subjected to either downward or upward seepage conditions. Different values of grout permeability and piezometer depth were used for the simulations.

Problems of axial symmetry such as ground water flow around a monitoring well can be solved using the finite element method (Chapuis, 1998; Chapuis and Chenaf, 2002; Chapuis, 2005; Chapuis, 2009a; Chapuis et al., 2012; Duhaime, 2012). The finite element code Seep/W, a computer code developed by GEO-Slope International, was used for the analysis of steady-state seepage around a fully grouted borehole. This code solves Darcy's law for seepage and Richards' (1931) equation for mass conservation of water as follows:

$$\mathbf{V} = -\mathbf{K}grad(h) \tag{3.17}$$

$$div[\mathbf{K}grad(h)] + Q = \frac{\partial \theta}{\partial t} \tag{3.18}$$

where $\mathbf{V}$ is Darcy's velocity vector, $\mathbf{K}$ the hydraulic conductivity matrix, h the hydraulic head, θ the volumetric water content, Q a local well or source term, and t the time. For saturated and steady state seepage, Eq. (3.18) in a vertical plane (z, r) becomes:

$$k_r \left(\frac{\partial^2 h}{\partial r^2} + \frac{1}{r} \frac{\partial h}{\partial r} \right) + k_z \frac{\partial^2 h}{\partial z^2} + Q = 0 \tag{3.19}$$

For the numerical simulations in this paper, the horizontal clay deposit was assumed to be homogeneous with a constant thickness of 4 m between elevations of 2 and 6 m. The clay layer lies between two sandy aquifers (Figure 3.5). The upper and lower aquifers are 2 m thick. The axisymmetric model with a 20 m radius consists of a fully grouted well with a radius of 10 cm which penetrates within the clay layer over a depth L. The two aquifers were defined to be sandy aquifers with a hydraulic conductivity of 10^{-4} m/s. The hydraulic conductivity for the clay formation was assumed to be 10^{-11} m/s.

With the finite element method, the obtained solutions must be independent of the mesh size (Chapuis, 2010). A refined mesh was required to compute the hydraulic head accurately in the vicinity of the borehole. The refined mesh has smaller elements of 1 cm around the borehole and coarser elements of 25 cm away from the borehole. On average, the final simulations were

conducted with meshes that comprised 66655 nodes and 66597 elements.
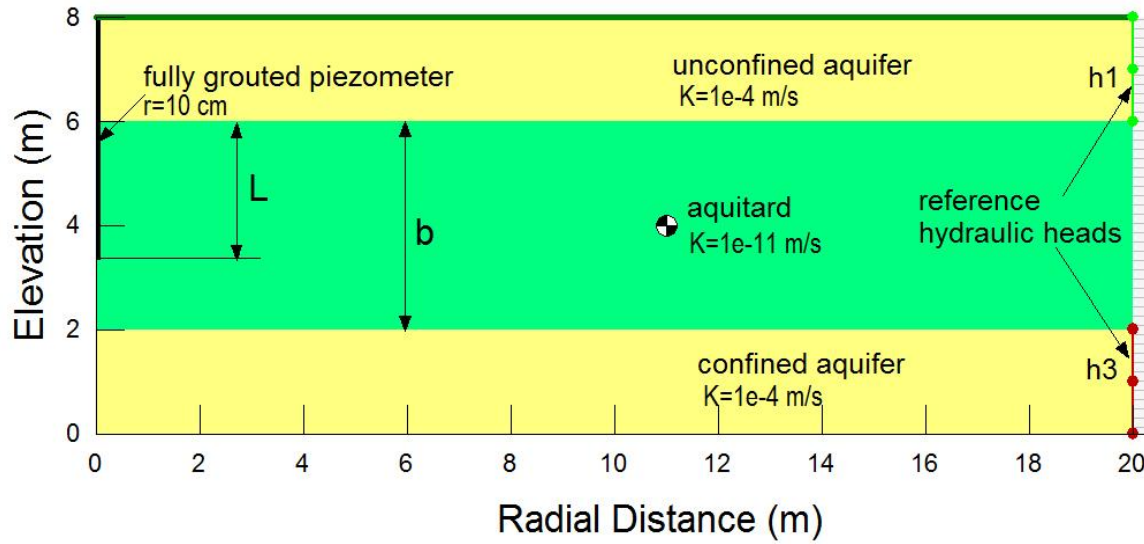
Figure 3.5: Cross section of a fully grouted borehole within a clay layer for numerical study.

Many cases were investigated by varying different parameters. The studied parameters were the grout hydraulic conductivity, K_g, the hydraulic head in the bottom and top aquifers, h_2, for downward and upward natural seepage, and the length of the borehole within the clay deposit, L. The L value was varied between 0.8 and 3.6 m and the K_g value was varied between 10^{-7} and 10^{-11} m/s. To establish a downward seepage, the hydraulic head within the upper aquifer was considered to be constant at 8 m, while the lower aquifer's hydraulic head was varied from 4 to 7.8 m. Upward seepage was induced using a similar method. The lower layer's hydraulic head was varied from 8.2 to 12 m. In the numerical simulations, the measured hydraulic head h_p is the hydraulic head within the borehole at depth L and the natural hydraulic head is the hydraulic head at the same depth, but at a radial distance of 20 m away from the borehole. For each simulation, the numerical piezometric error was calculated using Eq. (3.5).

3.7 Results and discussion

Dimensionless numbers were defined with the parameters in order to compare their influence on the ε value that arises from the cement-bentonite grout permeability, vertical hydraulic gradient, and borehole depth. The dimensionless parameters are the permeability ratio (K_g/K_c), the ratio of borehole depth within the clay layer to total clay layer thickness (L/b), and the vertical hydraulic gradient [$i^* = (h_1-h_2)/b$] across the clay layer. The set of values that were used for the dimensionless parameters in this study is listed in Table 3.2. For upward and downward seepage, K_g/K_c varies between 1 and 10^4, L/b between 0.2 to 0.9, and i^* between -1 and 1.

Table 3.2: Dimensionless variables considered in the numerical and analytical calculations.

Dimensionless variables	Span of variation
K_g/K_c	1, 10, 100, 1000, and 10000
$i^*=(h_1-h_2)/b$	-1, -0.7, -0.5, -0.3, -0.1, 0.1, 0.3, 0.5, 0.7, and 1
L/b	0.2, 0.4, 0.5, 0.67, 0.75, and 0.9

Figure 3.6 shows the equipotential and flow lines around the fully grouted borehole for various values of L/b and K_g/K_c. They were obtained for downward seepage with a vertical hydraulic gradient of 0.5. The hydraulic head distribution around the borehole for $L/b = 0.5$ and $K_g/K_c = 10$ and 1000 are presented in Figures 3.6a and 3.6b. The hydraulic head distribution changes around the borehole if there is a high contrast between grout and formation permeability. As shown in Figure 3.6b, the hydraulic head around the bottom of the borehole, at the *VWP* elevation, is similar to that obtained for the upper portion of the clay layer and sandy aquifer. This is a consequence of the hydraulic short-circuiting between the borehole and the upper aquifer. The hydraulic short-circuiting can also be seen for deeper piezometers if the contrast between K_g and K_c is high, particularly for large vertical hydraulic gradients. The numerical results for the hydraulic head distribution around the borehole show that the flow rate along the borehole side wall is not equally distributed along the borehole.

For the deepest simulated borehole (i.e., *L/b=0.9*), Figure 3.7 represents the hydraulic head profiles in the radial direction at an elevation corresponding to the bottom of the borehole for vertical hydraulic gradients of 0.5 and 1. For a vertical gradient of 0.5, if the ratio between grout

and formation permeability increases by two orders of magnitude, the hydraulic head within the borehole increases from 6.3 to 7.5 m (Figure 3.7a). For a vertical gradient of 1, an even larger increase in hydraulic head is obtained (Figure 3.7b). For both cases illustrated in Figure 3.7, approximately 85 percent of the radial head loss occurs within 0.5 m of the borehole sidewall. This radial gradient is responsible for the flow rate between the borehole and clay layer that is modeled with Eqs. (3.9) and (3.13) with the analytical solutions. The hydraulic head distribution in the radial direction for a lower permeability ratio ($K_g/K_c=10$) shows that the hydraulic head remains much closer to the natural hydraulic head before the piezometer installation. For a permeability ratio of 10, changes in hydraulic head of respectively 0.10 and 0.16 m were obtained at the bottom of the borehole for vertical gradients of 0.5 and 1. These changes in hydraulic head correspond to 1.6% and 3.6% of the natural hydraulic head in the clay layer (6.2 and 4.4 m), an error which is acceptable for most geotechnical applications.
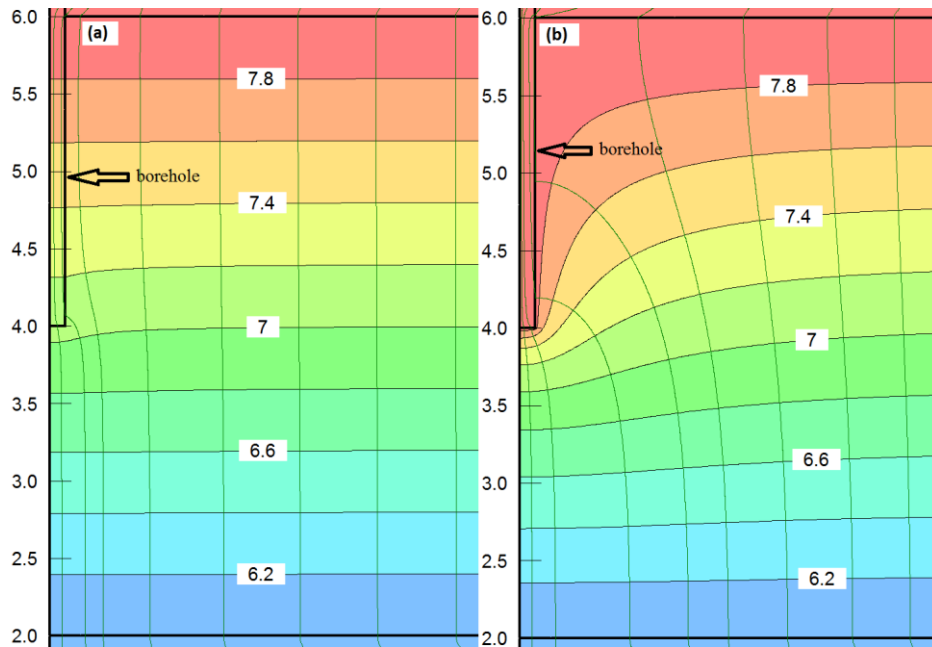
Figure 3.6: Equipotential and flow lines around fully grouted borehole for $i^* = 0.5$: a) $L/b = 0.5$ and $K_g/K_c = 10$, and b) $L/b = 0.5$ and $K_g/K_c = 1000$, c) $L/b = 0.2$ and $K_g/K_c = 1000$, d) $L/b = 0.9$ and $K_g/K_c = 1000$, e) $L/b = 0.2$ and $K_g/K_c = 10$, f) $L/b = 0.9$ and $K_g/K_c = 10$.
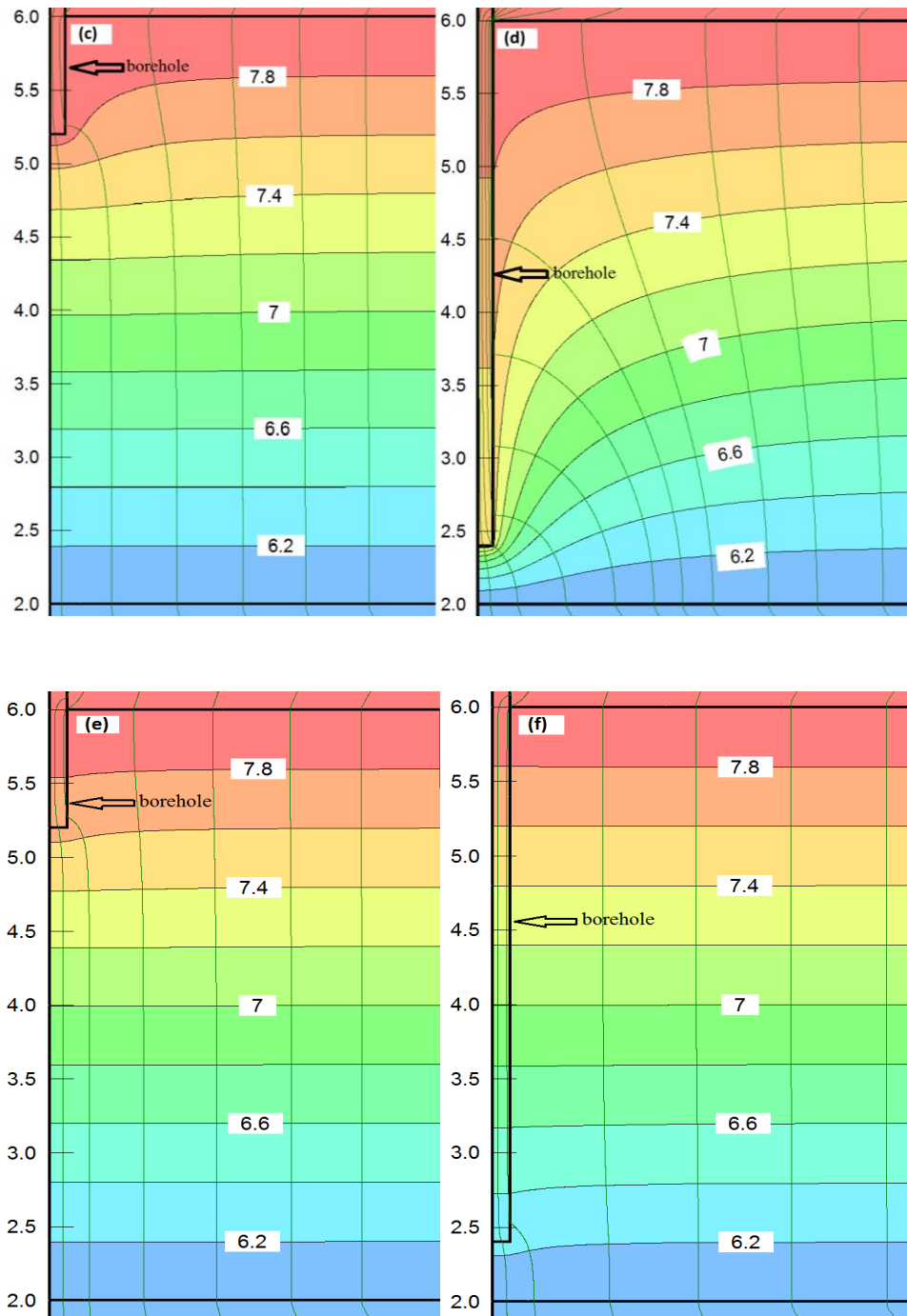
Figure 3.6: Equipotential and flow lines around fully grouted borehole for $i^* = 0.5$: a) $L/b = 0.5$ and $K_g/K_c = 10$, and b) $L/b = 0.5$ and $K_g/K_c = 1000$, c) $L/b = 0.2$ and $K_g/K_c = 1000$, d) $L/b = 0.9$ and $K_g/K_c = 1000$, e) $L/b = 0.2$ and $K_g/K_c = 10$, f) $L/b = 0.9$ and $K_g/K_c = 10$ (continued).
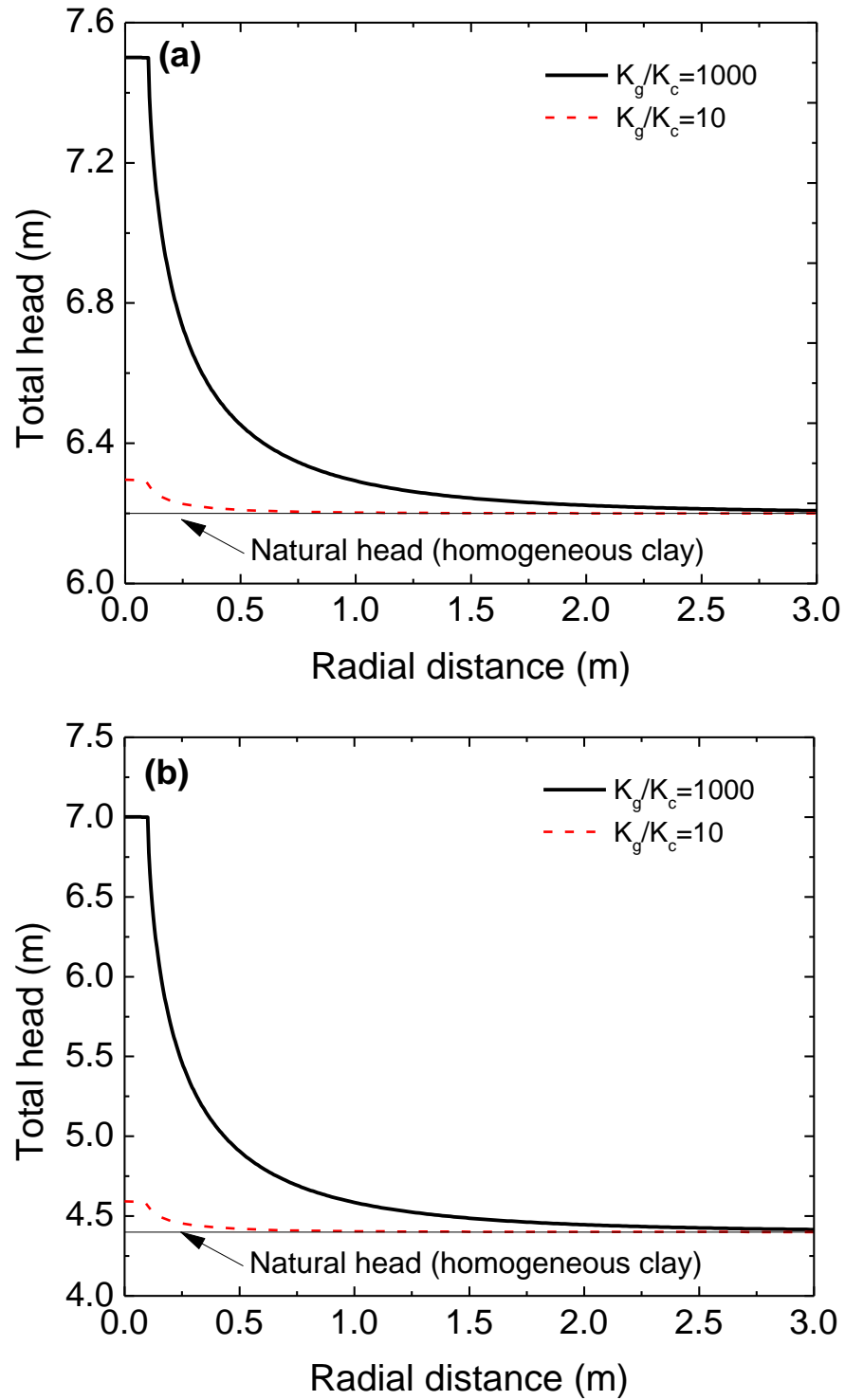
Figure 3.7: Hydraulic head profile in the radial direction at an elevation corresponding to the bottom of the borehole for $L/b = 0.9$: a) $i^* = 0.5$ and b) $i^* = 1$.

The flow nets obtained from the numerical simulation indicate how flow can be established around the borehole if there is a high contrast between the formation and grout permeability (Figures 3.6b and 3.6d). The influence of borehole depth on hydraulic head distribution around the borehole is presented in Figures 3.6c–3.6f. When K_g is much higher than K_c, the equipotentials around the borehole are disturbed by the installation of a deep piezometer (Figure 3.6d). However, for a lower permeability ratio, the hydraulic head contours around the borehole are comparable to those obtained for natural conditions before the piezometer installation (Figures 3.6a and 3.6f). The numerical results indicate that the borehole depth has no significant effect on the hydraulic head distribution around the borehole for lower values of the permeability ratio ($K_g/K_c=10$) (Figures 3.6a, 3.6e and 3.6f).

For high values of K_g/K_c, the hydraulic head loss around the borehole particularly in the vicinity of the borehole bottom provides a large radial hydraulic gradient (Figure 3.8). Figure 3.8 represents the radial hydraulic gradient versus borehole depth. For high K_g/K_c values, the radial hydraulic gradient increases with depth. The variation of the radial gradient with depth is approximately linear for most of the borehole length. This justifies our hypothesis for the analytical model of a unit flow rate at the borehole sidewall that increases linearly with depth [Eq. (3.10)], especially for higher values of the permeability ratio. The change in radial hydraulic gradient at the borehole sidewall results in a variable flow rate between the clay formation and borehole. Near the bottom of the borehole, the radial hydraulic gradient increases abruptly. For downward seepage, at the upper portion of the borehole, just a few centimetres below the upper sandy aquifers, the radial hydraulic gradient is negative, particularly for low values of permeability ratio. It shows that some water flows from the clay layer into the borehole near the top of the clay layer.

Examples of numerical hydraulic head profiles along the borehole axis are shown in Figure 3.9. Within the homogeneous clay layer, the slope of hydraulic head profile along the borehole axis changes due to the different permeability of the grout in the borehole. Figure 3.9 displays how the hydraulic head distribution can change in the vertical direction for various permeability ratios. The numerical model results for the hydraulic head profile along the borehole axis validate the conceptual model in Figure 3.3 for the hydraulic head distribution along the vertical axis of a borehole with improper sealing.
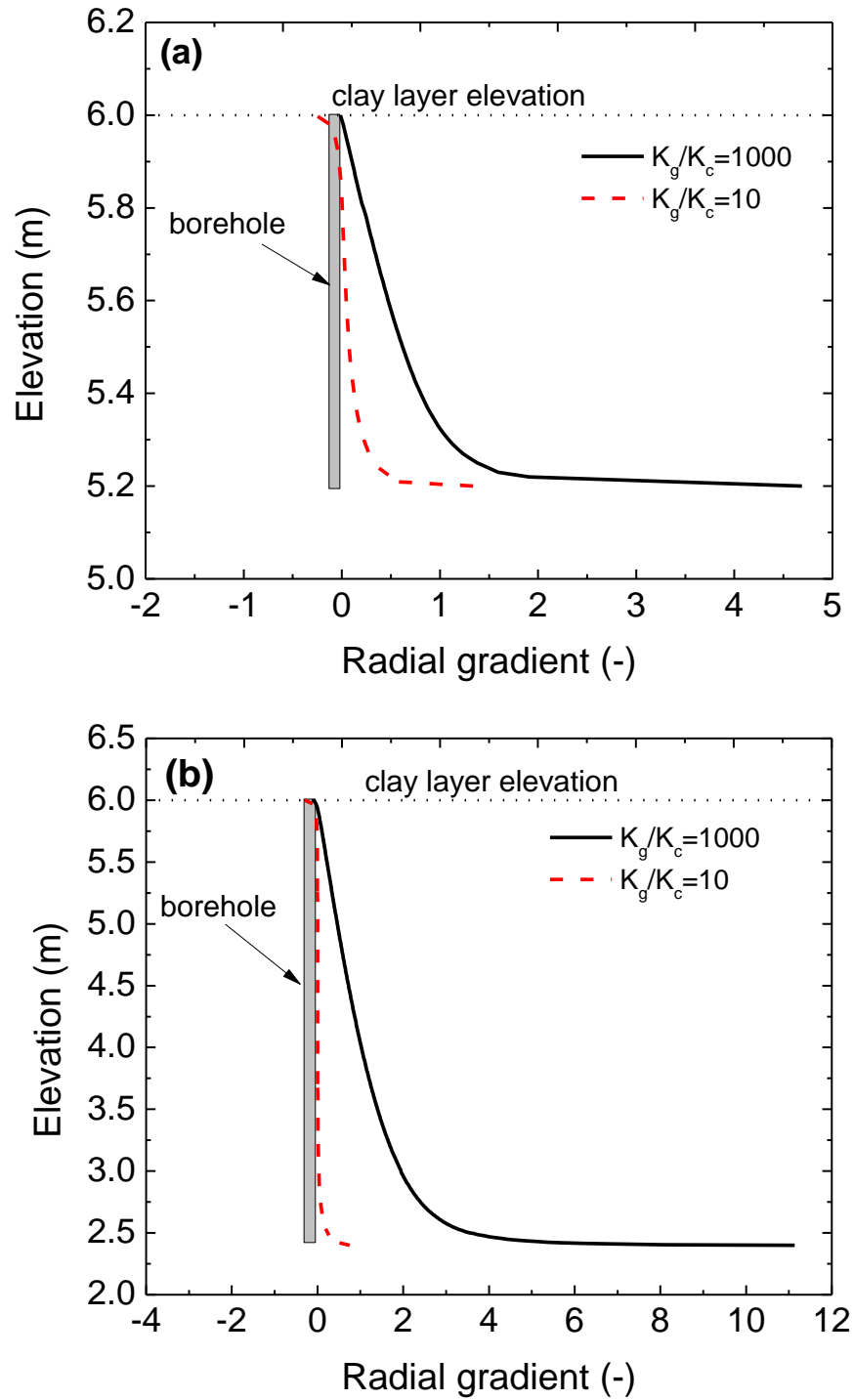
Figure 3.8: Variation of the radial hydraulic gradient at the borehole sidewall versus elevation for $i^* = 0.5$: a) $L/b = 0.2$ and b) $L/b = 0.9$.

The numerical and analytical results were compared to obtain best-fit values for α_1. The

analytical values for the piezometric error were calculated with Eq. (3.16). The numerical simulations provided values for h_p and h^* for various borehole geometries and the ε values were estimated using Eq. (3.5). For each value of L/b ratio, and various combinations of K_g/K_c and i^* (Table 3.2) the α_1 coefficient was determined in order to obtain a best fit between analytical and numerical results. We found that the best-fit α_1 coefficient varies linearly with borehole depth as shown in Fig. 3.10 with the following linear relationship:

$$\alpha_1 = -2.48(L/b) + 3.84 \tag{3.20}$$

For a given value of L/b, once the α_1 coefficient is calculated with Eq. (3.20), the analytical value of the piezometric error can be calculated with Eq. (3.16).

The following section provides an insight on how the permeability ratio, vertical hydraulic gradient, and borehole depth influence the ε value, using the analytical and numerical results.
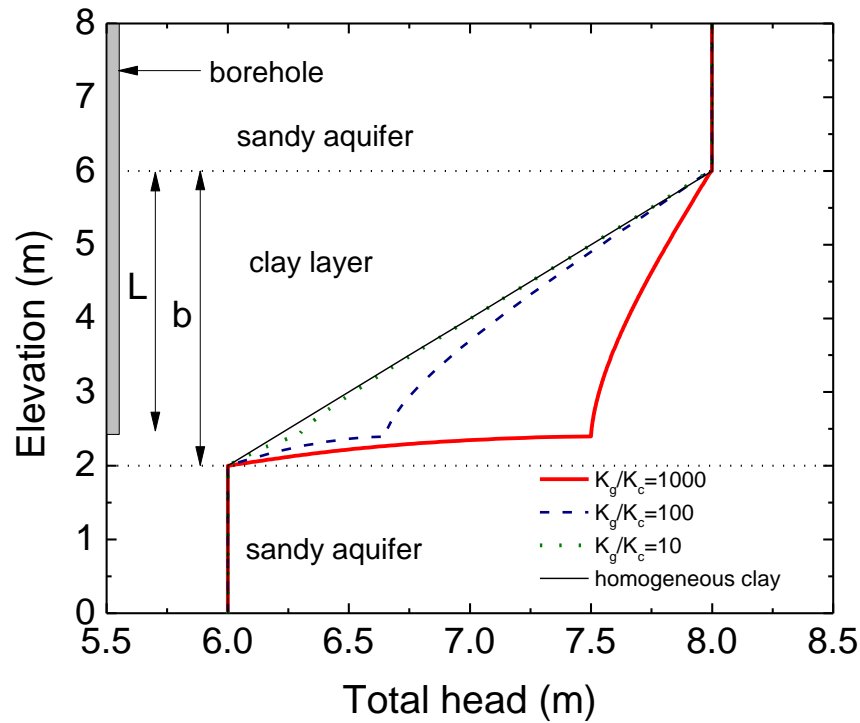
Figure 3.9: Hydraulic head profile along borehole axis (Seep/W) for $i^* = 0.5$ and $L/b = 0.9$.
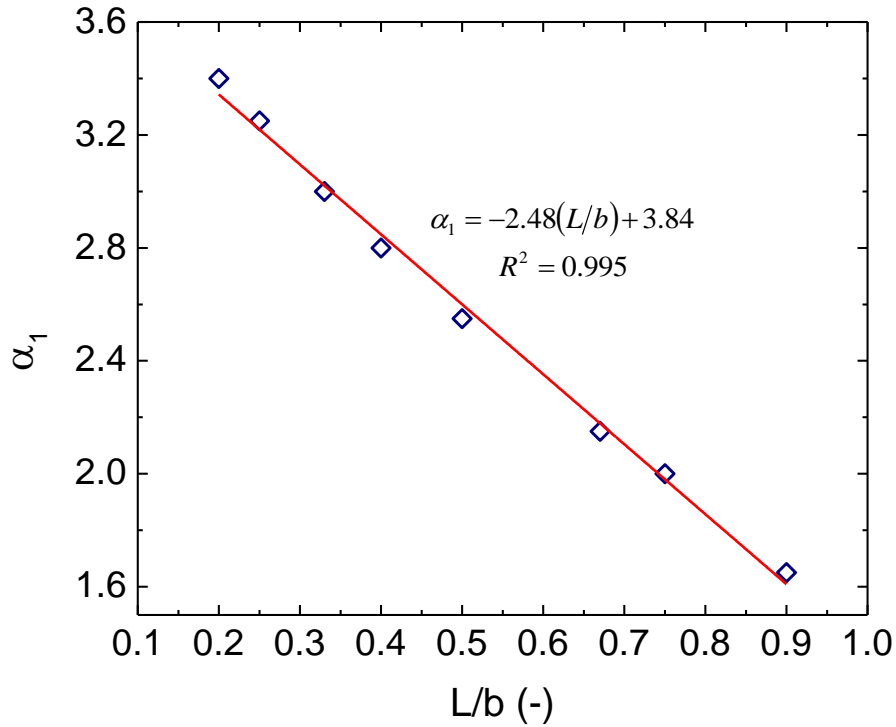
Figure 3.10: Best-fit α_1 coefficient for the analytical solution versus the L/b ratio.

3.7.1 Piezometric error versus permeability ratio (K_g/K_c)

For each L/b ratio, the ε value was calculated with Eqs. (3.5) and (3.16), respectively, for numerical and analytical models for vertical hydraulic gradients from -1 to 1, and presented with respect to the permeability ratio. For L/b = 0.2, 0.5, and 0.9, the variation of the error versus K_g/K_c for vertical hydraulic gradients of -1. -0.5, -0.1, 0.1, 0.5 and 1 is presented in Figure 3.11. The error is seen to increase with the permeability ratio for a given vertical hydraulic gradient. The ε value increases rapidly for higher values of vertical hydraulic gradient, particularly for permeability ratios of 10 to 1000. A very good fit was obtained between numerical and analytical results. For all L/b ratios (not all results are shown here), similar trends of ε versus permeability ratio have been obtained. For the upward seepage condition, similar trends for ε versus permeability ratio were obtained (Figures 3.11d - 3.11f). The numerical results also show that the piezometric error for upward seepage is symmetric with respect to that obtained for downward seepage. Figures 3.11a - 3.11c display the results when the distributed unit flow rate along

borehole sidewall is assumed to be uniform: it appears that the best fit between analytical and numerical results is good only when the ratio L/b equals 0.5.
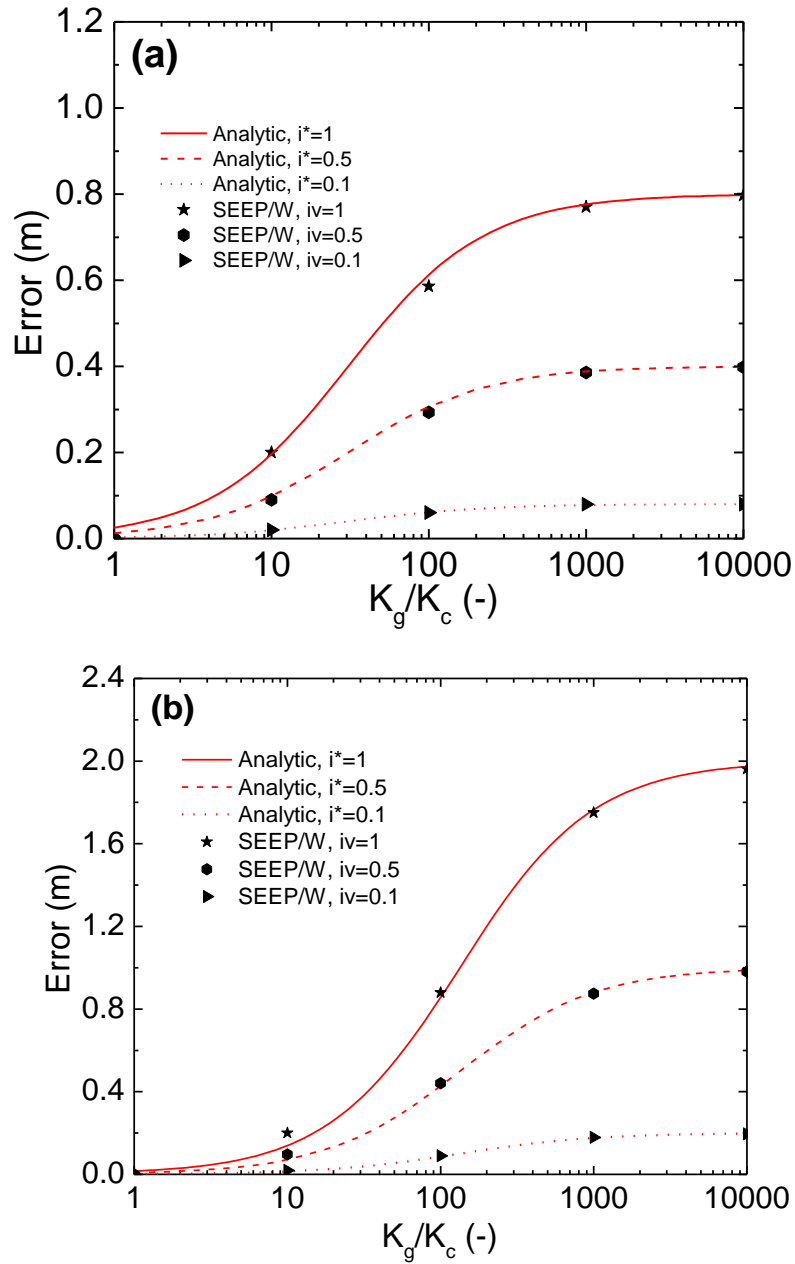
Figure 3.11: Piezometric error versus K_g/K_c: a) $L/b = 0.2$ downward flow; b) $L/b = 0.5$ downward flow; c) $L/b = 0.9$ downward flow; d) $L/b = 0.2$ upward flow; e) $L/b = 0.5$ upward flow; and f) $L/b = 0.9$ upward flow.
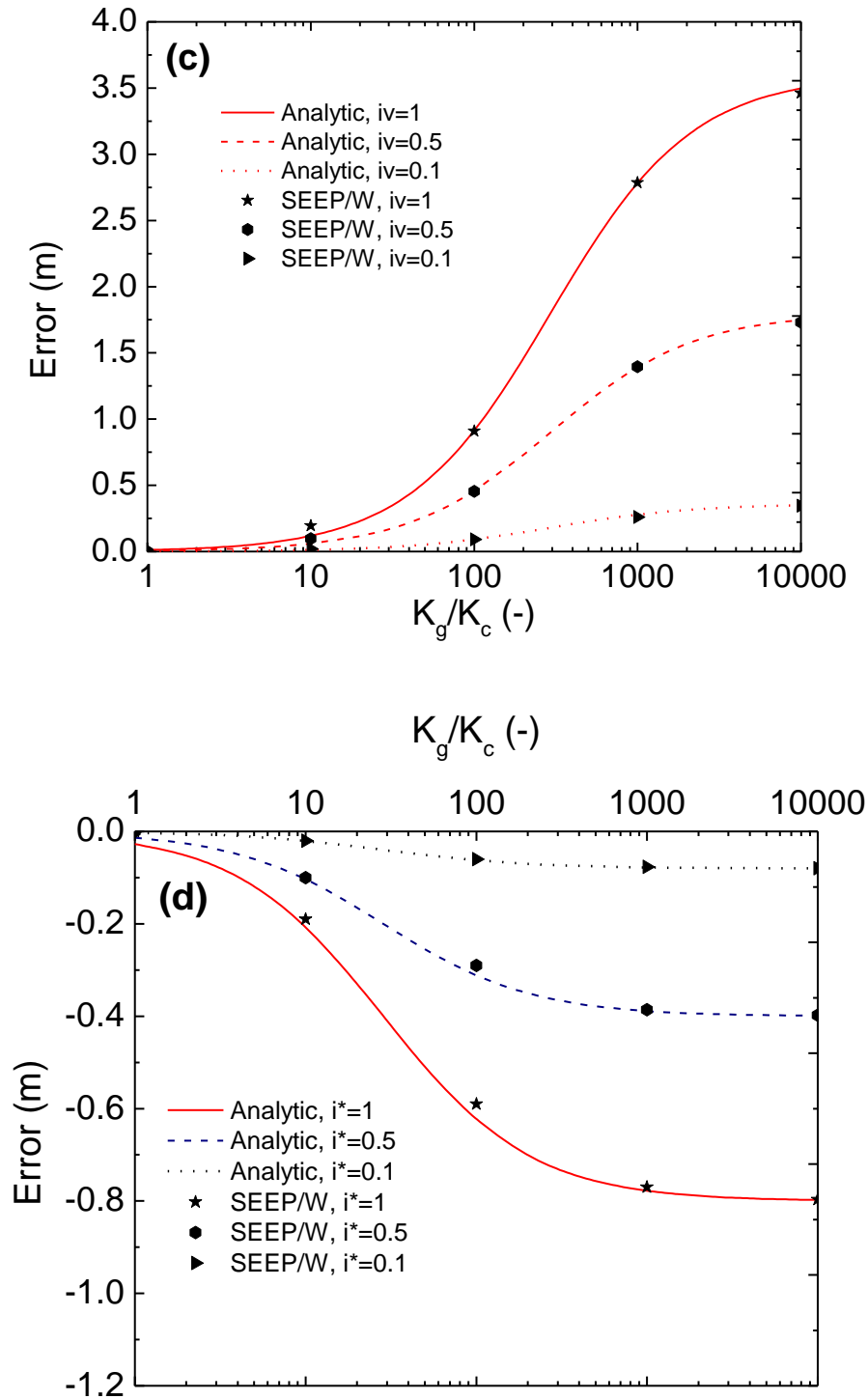
Figure 3.11: Piezometric error versus K_g/K_c: a) $L/b = 0.2$ downward flow; b) $L/b = 0.5$ downward flow; c) $L/b = 0.9$ downward flow; d) $L/b = 0.2$ upward flow; e) $L/b = 0.5$ upward flow; and f) $L/b = 0.9$ upward flow (continued).
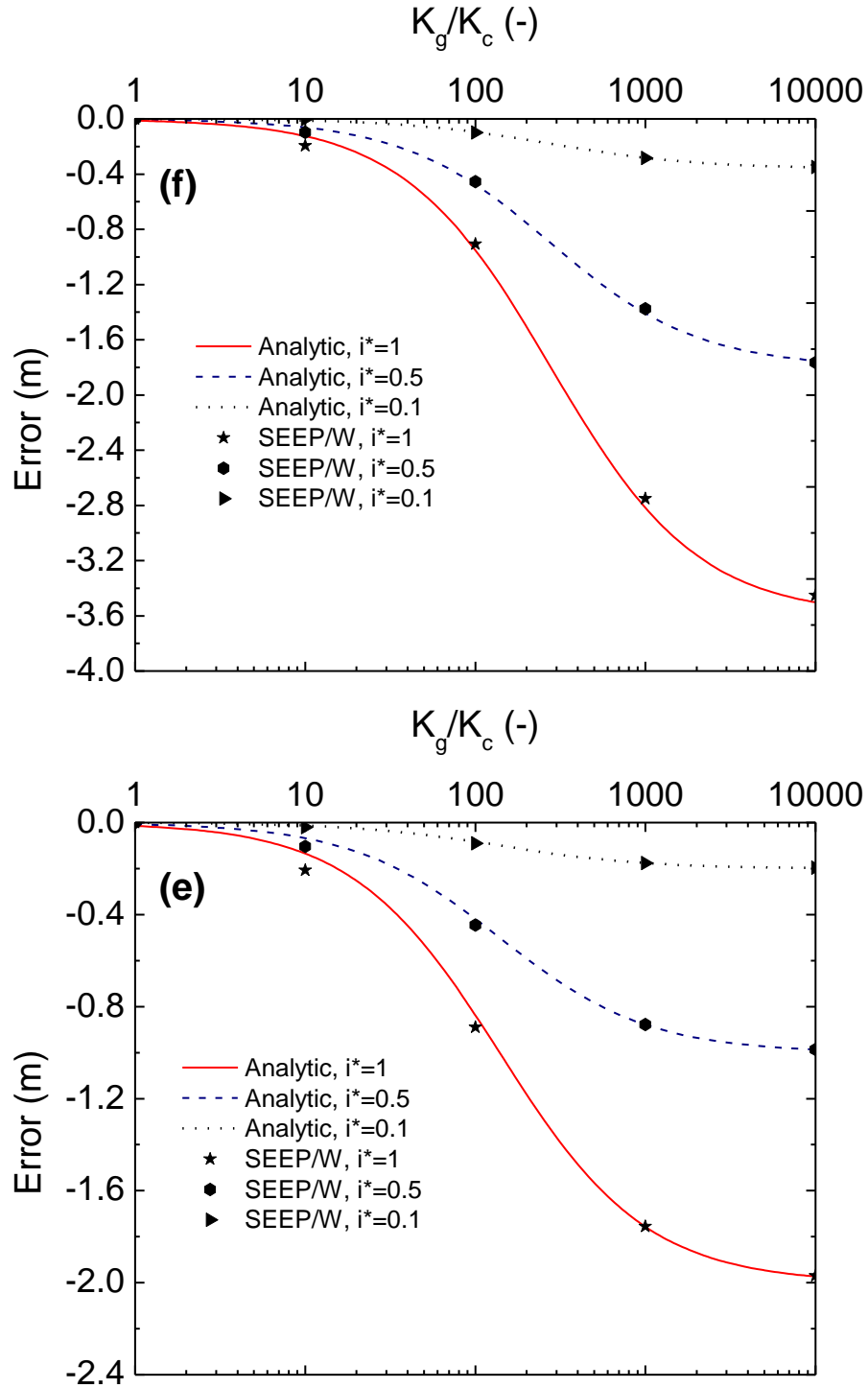
Figure 3.11: Piezometric error versus K_g/K_c: a) $L/b = 0.2$ downward flow; b) $L/b = 0.5$ downward flow; c) $L/b = 0.9$ downward flow; d) $L/b = 0.2$ upward flow; e) $L/b = 0.5$ upward flow; and f) $L/b = 0.9$ upward flow (continued).

The analytical solution of Vaughan (1969) indicated that the grout could be two orders of magnitude more permeable than the surrounding formation without inducing an appreciable ε. The numerical simulations of Contreras et al. (2008) showed that the normalized error was zero up to a permeability ratio of 1000. Our results show, however, that this claim might only be true for a small hydraulic gradient (i.e., $i^* \approx 0.1$). Figure 3.11 shows that in all cases the ε value increases with $K_g/K_c > 1$. For various values of L/b, the error for $K_g/K_c = 100$ is substantial for a high vertical hydraulic gradient across the clay layer. For instance, for $K_g/K_c = 100$ as shown in Figure 3.11b (*L/b = 0.5*), piezometric errors of 0.08, 0.44, and 0.88 m were respectively obtained for vertical hydraulic gradients of 0.1, 0.5 and 1. These errors respectively amount to 1, 7, and 17 percent of the pre-installation hydraulic head values (respectively 7.8, 7.0, and 6.0 m).

3.7.2 Piezometric error versus vertical hydraulic gradient

For a ratio L/b of 0.5, the relationship between ε and the vertical hydraulic gradient is shown in Figure 3.12. For a given permeability ratio, the ε value increases linearly with the vertical hydraulic gradient. The same result is obtained with the analytical solution [Eq. (3.16)].

Due to preferential seepage along the borehole axis, the ε value can be greatly increased for higher permeability ratios when the hydraulic gradient is large. Therefore the measured pore water pressure is not representative of the natural pore water pressure in the clay layer before the piezometer installation. For instance, with $L/b = 0.5$ at $K_g/K_c = 1000$, the ε value is increased from 0.18 to 1.75 m for an increase in i^* from 0.1 to 1. Figure 3.12 shows that for a given vertical hydraulic gradient, the ε value is strongly related to the permeability ratio. Moreover, Figure 3.12 indicates that for a given permeability ratio, the ε value is also related to the vertical hydraulic gradient, particularly for a permeability ratio greater than 10.

According to our results, to obtain an accurate hydraulic head reading with fully grouted piezometers, for most field conditions with a vertical hydraulic gradient of less than 1, the grout permeability must be similar or one order of magnitude greater than the surrounding formation permeability. This is consistent with the conclusion of McKenna (1995). For a pore pressure measurement at the base of an aquitard immediately above a high pressure aquifer where the gradients may be much greater than 1, the grout permeability should be at least equal or less than

the surrounding formation permeability to reduce piezometric error. The infuence of vertical hydraulic gradient on ε was not taken into account by Vaughan (1969) and Contreras et al. (2008). However our results have shown that the vertical natural hydraulic gradient within the clay layer has a fundamental impact on ε, particularly for high permeability cement-bentonite.
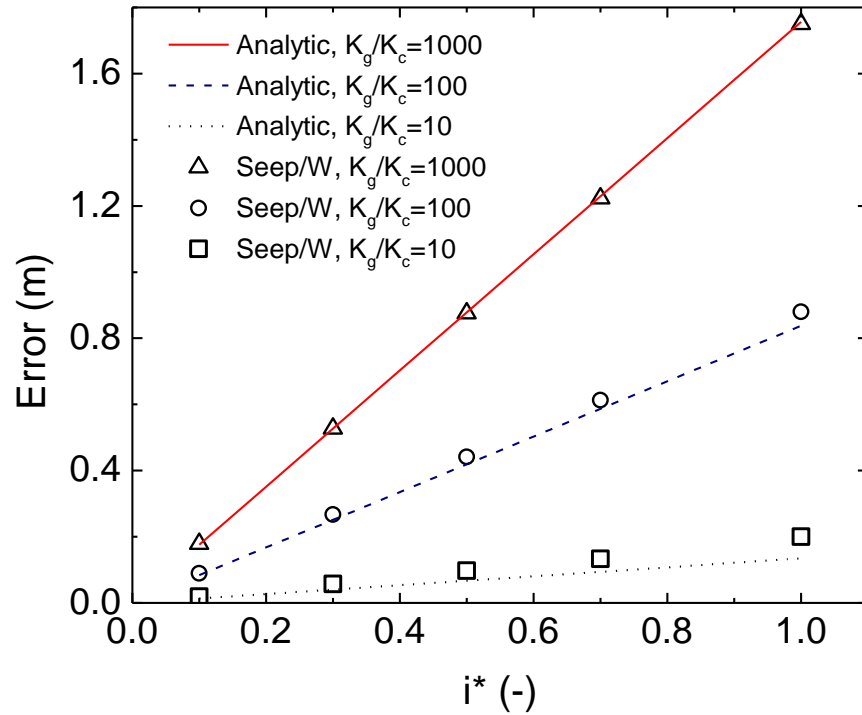
Figure 3.12: Piezometric error versus vertical hydraulic gradient for *L/b = 0.5* (downward flow).

3.7.3 Piezometric error versus L/b ratio

The variation of the ε versus *L/b* for permeability ratios of 10, 100, and 1000 is shown in Figure 3.13. For higher permeability ratios (e.g., 100 and 1000), the analytical and numerical results are almost identical. For these high permeability ratios, the ε value increases with borehole depth, especially for increased hydraulic gradients (Figure 3.13c). For a permeability ratio of 100 (Figure 3.13b), the ε value increases up to *L/b* of 0.5, then it remains approximately constant and decreases slightly for deeper piezometers (*L/b* > 0.8). For a small permeability ratio, the results show that the borehole depth has no significant influence on ε. For example, with a permeability

ratio of 10 (Figure 3.13a), the ε value is not significantly influenced by borehole depth. The numerical results reveal that for this permeability ratio, the ε value is roughly constant for all L/b ratios. For a K_g/K_c ratio of 10, the numerical and analytical results do not match perfectly, particularly at vertical hydraulic gradients of 0.5 and 1.
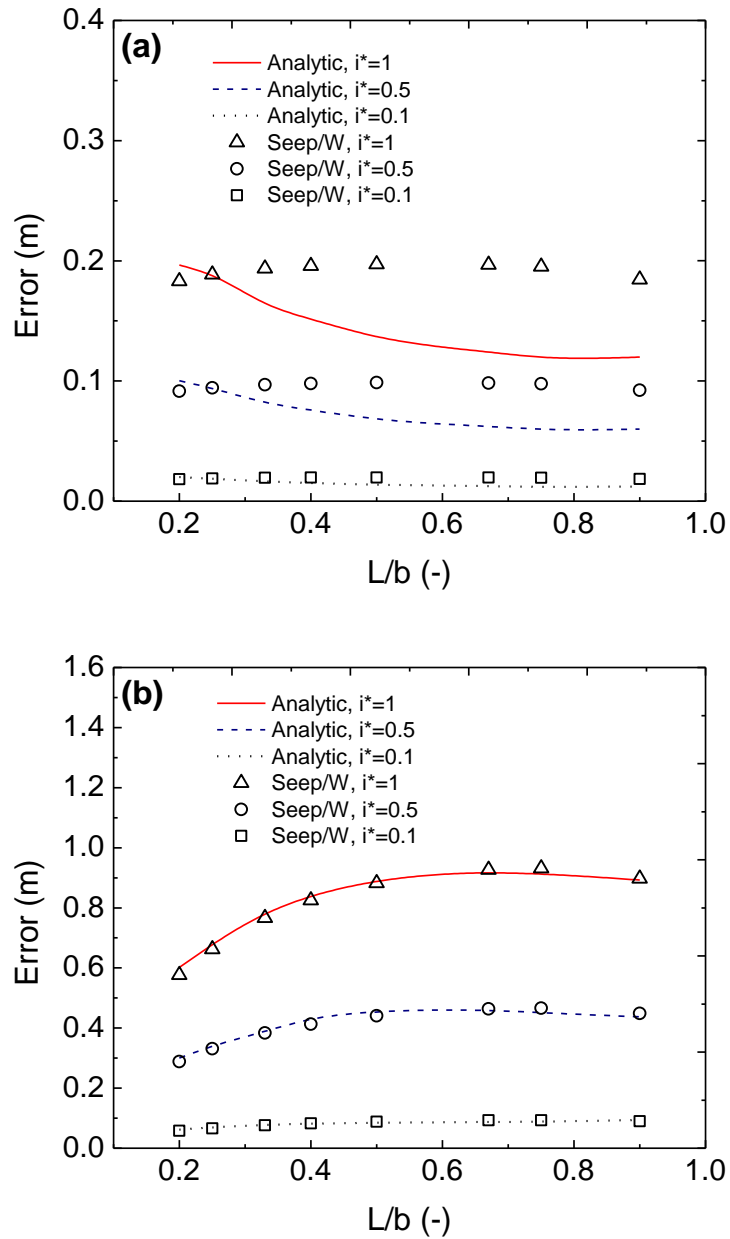
Figure 3.13: Piezometric error versus L/b ratio for downward flow: a) $K_g/K_c = 10$; b) $K_g/K_c = 100$, c) $K_g/K_c = 1000$.
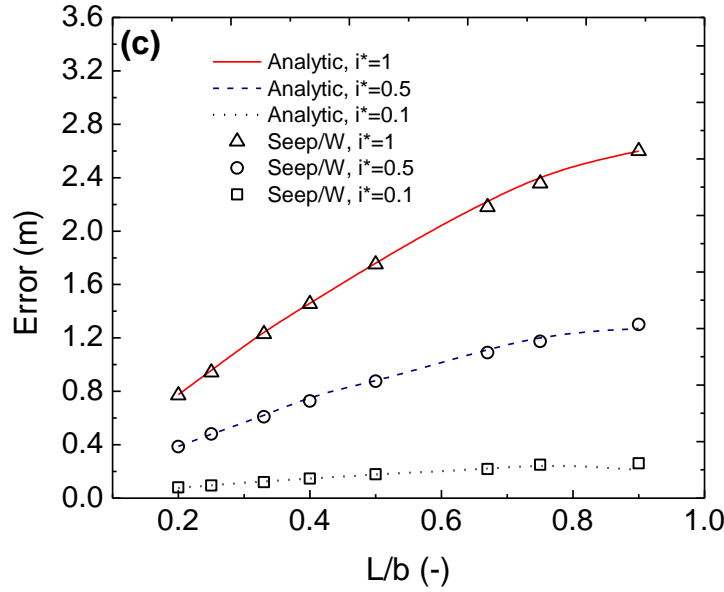
Figure 3.13: Piezometric error versus L/b ratio for downward flow: a) $K_g/K_c = 10$; b) $K_g/K_c = 100$, c) $K_g/K_c = 1000$ (continued).

The ε value is underestimated by the analytical solution for this permeability ratio. It might be related to the assumption of a unit flow rate at the borehole sidewall that varies linearly with depth for all conditions in our analytical model. As shown in Figure 3.8b, the radial hydraulic gradient remains constant and very small for most of the borehole length with deeper boreholes ($L/b = 0.9$) and when a permeability ratio of 10 is considered. The unit flow rate only increases near the bottom of the borehole. As shown in Figure 3.6f, the hydraulic head contours for a deep piezometer with similar grout permeability ratio and vertical hydraulic gradient (i.e., $K_g/K_c=10$ and $i^*=0.5$) are horizontal around the borehole. Consequently the flow direction within the borehole is vertical similar to the flow direction for homogenous clay layer. As a result, for a deep piezometer our analytical model cannot provide an appropriate estimation of the ε value for a low value of the permeability ratio (e.g., 10). For a surficial piezometer ($L/b = 0.2$) the radial hydraulic gradient for a permeability ratio of 10 is also small (Figure 3.8a), but it increases with depth. Therefore for the surficial piezometers (Figure 3.13a), the analytical model produces a good estimate for the ε value.

3.8 Conclusion

The fully grouted technique has many advantages. It reduces the installation costs, saves installation time, eliminates the risk of failure for the sand pack of deep wells, and makes piezometer installation easier. In this paper, numerical and analytical solutions have been developped to investigate the influence of different parameters on piezometric error for steady state seepage conditions. The results indicate that the ε magnitude is strongly related to the permeability ratio and vertical hydraulic gradient. Producing a grout which is suitable for given field conditions is an essential concern with the fully grouted technique. As long as the criteria are met, the fully grouted method can be a substitute for the conventional installation method.

For most field conditions ($i^*<1$), the numerical and analytical results showed that the grout permeability can be greater than the surrounding formation permeability by up to one order of magnitude without producing a significant error. For field conditions with a very low vertical hydraulic gradient ($i^* \approx 0.1$), the ε value is small but the maximum theoretical error is also small. For a low permeability ratio of $K_g/K_c = 10$ for almost all borehole depths, the flow condition around the borehole was comparable with that obtained for natural homogenous clay layer. Therefore the ε value does not change significantly with borehole depth, while for higher permeability ratios (e.g., $K_g/K_c \geq 100$), the ε value increases with borehole depth.

3.9 Acknowledgements

3.10 References

Bayrd, G. 2011. Evaluating Practices for Installation of Vibrating Wire Piezometers Geotech. News. **27(4),** 26-29.

Chapuis, R. 2009a. Monitoring a well in a clay layer: revisiting the time lag problem. Bull. Eng. Geol. Environ. **68**, 387-395, doi: 10.1007/s10064-009-0210-5.

Chapuis, R., Duhaime, F., Benabdallah, E. 2012. Monitoring wells in clay: the apparently static water level and its influence during variable-head permeability tests. Bull. Eng. Geol. Environ. **71**, 663-678, doi: 10.1007/s10064-012-0433-8.

Chapuis, R.P. 1989. Shape Factors for Permeability Tests in Boreholes and Piezometers. GroundWater. **27**, 647-654, doi: 10.1111/j.1745-6584.1989.tb00478.x.

Chapuis, R.P. 1998. Overdamped slug test in monitoring wells: review of interpretation methods with mathematical, physical, and numerical analysis of storativity influence. Can. Geotech. J. **35**, 697-719, doi: 10.1139/Cgj-35-5-697.

Chapuis, R.P. 2005. Numerical modeling of rising-head permeability tests in monitoring wells after lowering the water level down to the screen. Can. Geotech. J. **42**, 705-715, doi: 10.1139/t05-003.

Chapuis, R.P. 2009b. Field variable-head test in low-permeability materials: Assessing the effects of trapped gas pocket and cavity expansion. Can. Geotech. J. **46**, 81-92, doi: 10.1139/T08-106.

Chapuis, R.P. 2010. Influence of Element Size in Numerical Studies of Seepage: 1. Large-Scale of Regional Studies. Geotech. News. **28**, 31-34.

Chapuis, R.P., Chenaf, D. 2002. Slug tests in a confined aquifer: experimental results in a large soil tank and numerical modeling. Can. Geotech. J. **39**, 14-21, doi: 10.1139/t01-070.

Chapuis, R.P., Paré, J.-J., Loiselle, A.A. 1984. Laboratory test results on self-hardening grouts for flexible cutoffs. Can. Geotech. J. **21**, 185-191.

Chapuis, R.P., Sabourin, L. 1989. Effects of installation of piezometers and wells on groundwater characteristics and measurements. Can. Geotech. J. **26**, 604-613, doi: 10.1139/t89-073.

Cherry, J., Parker, B., Bradbury, K., Eaton, T., Gotkowitz, M., Hart, D., Borchardt, M. 2004. *Role of* aquitards *in the protection of aquifers from contamination: a "state of the science" report*.

Contreras, I.A., Grosser, A.T., Ver Strate, R.H. 2012. Update of the fully-grouted method for piezometer installation. Geotech. News. **30**, 20-25.

Contreras, I.A., Grosser, A.T., VerStrate, R.H. 2008. The use of the fully-grouted method for piezometer installation. Geotech. News. **26**, 30-37.

De Rienzo, F., Oreste, P., Pelizza, S. 2008. Subsurface geological-geotechnical modelling to sustain underground civil planning. Eng. Geol. J. **96**, 187-204, doi: 10.1016/j.enggeo.2007.11.002.

Duhaime, F. 2012. *Mesure de la conductivité hydraulique du dépôt d'argile Champlain de Lachenaie, Québec: théorie et applications.* Ph.D. thesis, École Polytechnique de Montréal.

Duhaime, F., Chapuis, R.P. 2014. A coupled analysis of cavity and pore volume changes for pulse tests conducted in soft clay deposits. Int. J. Numer. Anal. Method. Geomech. **38**, 903-924, doi: 10.1002/nag.2238.

Dunnicliff, J. 1988. Geotechnical Instrumentation for Measuring Field Performance. J.Wiley, New York.

Geo-Slope, 2008. Seepage Modeling with SEEP/W 2007. Calgary, Canada: Geo-Slope International Ltd.

Gustin, E.J.G., Karim, U.F.A., Brouwers, H.J.H. 2007. Bleeding characteristics for viscous cement and cement-bentonite grouts. Geotech. **57**, 391-395, doi: 10.1680/geot.2007.57.4.391.

Hvorslev, M.J. 1951. *Time lag and soil permeability in ground-water observations*. Bulletin No. 36, Waterways Experiment Station, US Corps of Engineers, Vicksburg, Mississippi.

Jurado, A., De Gaspari, F., Vilarrasa, V., Bolster, D., Sánchez-Vila, X., Fernàndez-Garcia, D., Tartakovsky, D.M. 2012. Probabilistic analysis of groundwater-related risks at subsurface excavation sites. Eng. Geol. J. **125**, 35-44, doi: 10.1016/j.enggeo.2011.10.015.

Marefat, V., Duhaime, F., Chapuis, R.P. 2015. Pore pressure response to barometric pressure change in Champlain clay: prediction of the clay elastic properties Eng. Geol. J. **Accepted**.

McKenna, G.T. 1995. Grouted-in installation of piezometers in boreholes. Can. Geotech. J. **32**, 355-363.

Mikkelsen, P., Green, G.E. 2003. Piezometers in fully grouted boreholes. FMGM-Field Measurements in Geomechanics, Oslo, Norway.

Mikkelsen, P.E. 2002. Cement-bentonite grout backfill for borehole instruments. Geotech. News. **20**, 38-42.

Mikkelsen, P.E., Slope Indicator Co. 2000. Grouting-in Piezometers. Technical Note at www.slope.com, 2 pages.

Portland Cement Association. 1984. Cement-Bentonite Slurry Trench Cutoff Walls, USA.

Pujades, E., Carrera, J., Vázquez-Suñé, E., Jurado, A., Vilarrasa, V., Mascuñano-Salvador, E. 2012. Hydraulic characterization of diaphragm walls for cut and cover tunnelling. Eng. Geol. J. **125**, 1-10, doi: 10.1016/j.enggeo.2011.10.012.

Pujades, E., Vázquez-Suñé, E., Carrera, J., Vilarrasa, V., De Simone, S., Jurado, A., Ledesma, A., Ramos, G., Lloret, A. 2014. Deep enclosures versus pumping to reduce settlements during shaft excavations. Eng. Geol. J. **169**, 100-111, doi: 10.1016/j.enggeo.2013.11.017.

Simeoni, L. 2012. Laboratory tests for measuring the time-lag of fully grouted piezometers. J. Hydrol. **438-439**, 215-222, doi: 10.1016/j.jhydrol.2012.03.025.

Simeoni, L., De Polo, F., Caloni, G., Pezzetti, G. 2011. Field performance of fully grouted piezometers. *Proceedings of the FMGM Congress*.

Smerdon, B.D., Smith, L.A., Harrington, G.A., Gardner, W.P., Delle Piane, C., Sarout, J. 2014. Estimating the hydraulic properties of an aquitard from in situ pore pressure measurements. Hydrogeol. J. **22**, 1875-1887, doi: 10.1007/s10040-014-1161-x.

Smith, L.A., Van Der Kamp, G., Jim Hendry, M. 2013. A new technique for obtaining high-resolution pore pressure records in thick claystone aquitards and its use to determine in situ compressibility. Water Resour. Res. **49**, 732-743, doi: 10.1002/wrcr.20084.

van der Kamp, G. 2001. Methods for determining the in situ hydraulic conductivity of shallow aquitards – an overview. Hydrogeol. J. **9**, 5-16, doi: 10.1007/s100400000118.

Vaughan, P.R. 1969. A Note on Sealing Piezometers in Boreholes. Geotechnique, **19**, 405-413, doi: 10.1680/geot.1969.19.3.405.

Xu, Y.-S., Shen, S.-L., Du, Y.-J. 2009. Geological and hydrogeological environment in Shanghai with geohazards to construction and maintenance of infrastructures. Eng. Geol. J. **109**, 241-254, doi: 10.1016/j.enggeo.2009.08.009.

Yungwirth, G., Preene, M., Dobr, M., Forero Garcia, F. 2013. Practical Application and Design Considerations for Fully Grouted Vibrating Wire Piezometers in Mine Water Investigations. *Annual International Mine Water Association Conference – Reliable Mine Water Technology*, Golden, Colorado, USA, 229 – 237.

Zawadzki, W., Chorley, D. 2014. Grouted-in Pressure Transducers: Implications for Hydrogeological Testing and Monitoring in Bedrock. Mine Water Environ. **33**, 289-292, doi: 10.1007/s10230-014-0261-0.

CHAPTER 4   ARTICLE 2 : PORE PRESSURE RESPONSE TO BAROMETRIC PRESSURE CHANGE IN CHAMPLAIN CLAY: PREDICTION OF THE CLAY ELASTIC PROPERTIES

Vahid Marefat[1*], François Duhaime[2], Robert P. Chapuis[1]

Published in *Engineering Geology*, Vol.198, 16-29. doi: 10.1016/j.enggeo.2015.

[1] Department of Civil, Geological and Mining Engineering, Ecole Polytechnique, P.O. Box 6079, Stn CV, Montreal, Quebec, Canada, H3C 3A7

[2] Laboratory for Geotechnical and Geoenvironmental Engineering (LG2), École de technologie supérieure, 1100 Notre-Dame Ouest, Montreal, QC, Canada, H3C 1K3

[*] Corresponding author: Phone +1-438-931-9797; fax +1-514-340-4477-Email:vahid.marefat@polymtl.ca

Abstract

Champlain Sea clay deposits play a crucial role in limiting contaminant migration to underlying aquifers in the Saint Lawrence River Valley. Champlain Sea clays are well known as being prone to landslide and sample disturbance. Estimation of their elastic properties using their in situ loading efficiency would provide mechanical properties for the soil dynamic analyses and immediate settlement calculations encountered in geotechnical projects. Determination of loading efficiency can be envisioned as a very small strain test. In this paper we describe a detailed monitoring program for 10 vibrating wire piezometers installed within sealed boreholes on 5 study sites near Montreal in Quebec, Canada. The pore pressure response to barometric pressure variation was analyzed with three methods: linear regression, visual inspection, and multiple regression, which gave loading efficiencies between 0.7 and 0.95. These values were then used to estimate the elastic properties of the clay formation. Vertical compressibility and specific storage on the order of 1×10^{-6} kPa^{-1} and 1×10^{-5} m^{-1} were respectively obtained for most of the monitoring sites. A comparison of compressibility values derived from the in situ loading efficiency method, with those obtained with pressuremeter, oedometer, and pulse tests confirmed that clay compressibility is strain dependent. The pore pressures measured on the study sites have been corrected by applying the multiple regression and visual inspection

methods. For most piezometers, both methods provided nearly identical results. However, for deep piezometers, the multiple regression method provided smoother pore pressure time series than the visual inspection method. The vertical hydraulic gradient obtained with corrected pressure data was shown to change significantly on some test sites during the monitoring period.

Keywords: pore pressure, barometric pressure, Champlain Sea clay, loading efficiency, elastic properties, vertical hydraulic gradient.

4.1 Introduction

Aquitards play a crucial role in defining groundwater regimes. Aquitards are often poorly understood components of groundwater systems. Yet they control recharge and prevent contaminated surface sources to reach underlying aquifers (Cherry et al., 2004). Aquitards can host and isolate hazardous waste (Smith et al., 2013). Groundwater management and determination of groundwater flow regime require precise values of geometric conditions, boundary conditions, specific storage, hydraulic head, hydraulic conductivity, and an assessment of aquitard integrity, and scale effects if any (e.g., Cherry et al., 2004; Smith et al., 2013; Timms and Acworth, 2005).

From a geotechnical standpoint, representative values of the clay elastic parameters for very small-strain deformation are needed to understand the dynamic behavior of clay deposits (e.g., Lefebvre et al., 1994; Youd et al., 2001). For example, the small-strain shear modulus allows sites to be classified according to their response to earthquakes (Canadian Geotechnical Society, 2006).

Poor estimation of hydraulic head, particularly in formations with low hydraulic gradients, can lead to inaccurate calculations of groundwater flow properties (Rasmussen and Crawford, 1997; Spane, 2002). These properties play an important role, for example, in assessing the movement of contaminants in groundwater. Piezometric levels in confined or unconfined aquifers fluctuate in response to externally induced stress changes (barometric pressure change, Earth tide). These water level fluctuations are extensively discussed in the literature (e.g., Ferris et al., 1962; Jacob, 1940; Rasmussen and Crawford, 1997; Spane, 2002; Weeks, 1979). The diurnal groundwater

level change caused by a variation in barometric pressure is around 3 to 12 cm. It can reach 30 cm during a week and even larger values for a season (Merritt, 2004). While they may disguise the water level/pore water pressure change imposed by other natural phenomena or aquifer tests; hydraulic head changes caused by external stress changes are often ignored (Hare and Morse, 1997; Toll and Rasmussen, 2007). In this paper, the term "pore pressure" implies positive pore water pressure within a saturated soil. An understanding of the influence of barometric pressure on pore pressure and the elimination of that effect provide an enhanced characterization of groundwater flow properties (Rasmussen and Crawford, 1997; Spane, 2002).

Because of the potential benefits associated with precise hydraulic head values, many documents deal with well water response to barometric pressure change in aquifers. For an ideal confined aquifer, the well and aquifer responses to barometric stress change are instantaneous (e.g., Ferris et al., 1962; Jacob, 1940). Therefore, practitioners have traditionally used a simple linear relationship to analyze well response and eliminate barometric effect from well records. On the other hand, for an unconfined aquifer with a thick unsaturated zone of low hydraulic conductivity, the well response becomes delayed and frequency dependent (Furbish, 1991; Weeks, 1979). For such a case, two methods may be used, the time domain method (Furbish, 1991; Rasmussen and Crawford, 1997; Weeks, 1979) and the frequency domain method (Evans et al., 1991; Galloway and Rojstaczer, 1988).

For a confining layer or aquitard, several methods have been used to analyze the water level and/or pore pressure response to barometric pressure change. Timms and Acworth (2005) simply used a linear regression to estimate the barometric or loading efficiency (BE or LE) of a clay aquitard. Other authors (e.g., Anochikwa et al., 2012; Smerdon et al., 2014; Smith et al., 2013) have used a visual inspection method to select representative LE values for clay aquitards. The barometric response function, BRF, obtained with multiple regression and frequency domain solution were respectively used by Butler et al. (2011) and Hussein et al. (2013) to analyze the open well water level response to change in barometric stress within aquitards.

Some elastic properties (e.g., vertical compressibility, specific storage, elastic modulus) and vertical hydraulic conductivity can be estimated with laboratory and in situ testing methods. Laboratory tests are known to overestimate the compressibility of geological materials (Clark, 1998; Klohn, 1965; van der Kamp, 2001). Laboratory tests, due to sample disturbance and stress

change in clay samples (Clark, 1998), often yield elastic properties that are not reliable: this is the case of sensitive Champlain Sea clays (e.g., La Rochelle and Lefebvre, 1971; LaRochelle et al., 1981; Tavenas et al., 1974). For instance, thin-walled tube sampling affects both the undrained and drained parameters of Champlain Sea clay. This sampling method causes a decrease by 50 to 60 % in the elastic modulus when compared with block samples according to La Rochelle and Lefebvre (1971) who claimed that even for a perfect sample of cemented Champlain clay, the stress release due to sampling might break cementation bonds thereby leading to sample disturbance.

Analysis of in situ pore pressure response to change in barometric pressure is one of the most reliable methods to estimate elastic formation properties (e.g., van der Kamp, 2001). Several authors have recently used this technique to estimate the in situ elastic parameters of clay aquitards across the world (e.g., Butler et al., 2011; Hussein et al., 2013; Smerdon et al., 2014; Smith et al., 2013; Timms and Acworth, 2005).

The lowlands of the Saint Lawrence River valley in Quebec, in eastern Canada, are covered with sensitive soft marine clay (referred to as Champlain Sea clay) which plays an essential role in protecting underlying aquifers from contamination sources at the surface. An extensive program of pore pressure monitoring within a Champlain Sea clay layer in the Lachenaie area near Montreal, Quebec, provided an opportunity to observe the long-term variation of vertical hydraulic gradient and to estimate the elastic properties of Champlain Sea clay when subjected to very small-strain deformations. This study reports a monitoring program during which 10 vibrating wire piezometers, VWPs were installed and monitored for about two years. The 10 VWPs were installed on 5 study sites in Lachenaie. The study sites cover an area of around 50 km^2. The objectives of this paper were to estimate the in situ vertical compressibility, m_v, specific storage, S_s, and constrained modulus, M, of Champlain Sea clay from the loading efficiency, LE, values obtained with three methods: linear regression, visual inspection and BRF. The visual inspection and BRF methods were then used to correct pore pressure data for barometric response to calculate precise vertical hydraulic gradients through the clay layer.

To the authors' knowledge, this is the first estimation of the in situ elastic parameters of sensitive Champlain Sea clay from the pore pressure response to barometric pressure change. The in situ

elastic parameters estimated from very small-strain deformation provide a better evaluation of the dynamic soil response and of immediate settlement in Champlain Sea clay deposits.

4.2 Theoretical undrained response to barometric pressure change

An increment in total stress of $\Delta\sigma$ causes a transient pore pressure, Δu_w, in excess of the hydrostatic pressure, u_w, and an increase in effective stress, $\Delta\sigma'$, which can be written using the concept of effective stress as follows (Holtz and Kovacs, 1981; Terzaghi et al., 1996):

$$\sigma + \Delta\sigma = \left(\sigma'_v + \Delta\sigma'\right) + \left(u_w + \Delta u_w\right) \tag{4.1}$$

where σ'_v is the vertical effective stress or the portion of the vertical stress born by the soil skeleton which tends to compress the porous matrix, and σ is the total applied stress. The same principle is applicable for barometric loading as well, that is to say a change in barometric stress is shared between pore water and the aquitard skeleton (Anochikwa et al., 2012). In horizontally extensive aquitards, vertical deformation is essentially due to natural loading components such as barometric stress change (van der Kamp and Gale, 1983). Thus a one-dimensional coupled equation for pore pressure and stress can be written as follows (van der Kamp and Gale, 1983; Domenico and Schwartz, 1997):

$$K_z \frac{\partial^2 \Delta u_w}{\partial z^2} = \rho_w g \left(n\beta_w + m_v\right) \frac{\partial \Delta u_w}{\partial t} - \left(\rho_w g m_v\right) \frac{\partial \sigma}{\partial t} \tag{4.2}$$

where K_z is the vertical component of the hydraulic conductivity, $\rho_w g$ is the unit weight of water, n is the formation porosity, β_w is the compressibility of water taken as 4.6×10^{-7} kPa^{-1} at $20\,^{\circ}$C, and m_v is the compressibility of the formation in the vertical direction. Clay compressibility varies with stress level (e.g., Bardet, 1997). However, below the yield stress, when the clay is overconsolidated, the strain is small and recoverable (e.g., Mitchell, 1970). Dividing Eq. (4.2) by the specific storage, S_s, which is given by the expression $\rho_w g(n\beta_w + m_v)$, provides the following equation (Timms and Acworth, 2005):

$$D \frac{\partial^2 \Delta u_w}{\partial z^2} = \frac{\partial \Delta u_w}{\partial t} - \left(LE\right) \frac{\partial \sigma}{\partial t} \tag{4.3}$$

where D is the hydraulic diffusivity, K/S_s, and LE is the loading efficiency defined as $m_v / (m_v + n\beta_w)$ by assuming incompressible solid grains. The loading efficiency is the fraction of the applied load carried by pore water itself (van der Kamp and Gale, 1983) and thus, the ratio of change in total pressure or hydraulic head to the change in barometric pressure. It differs from barometric efficiency which reflects the ratio of change in well water elevation to the change in barometric pressure. Loading efficiency is related to barometric efficiency by LE= 1–BE (e.g., Rasmussen and Crawford, 1997 and Spane, 2002).

Tidal and barometric pressure changes are assumed to be quick loading phenomena which are treated as undrained condition (Domenico and Schwartz, 1997 and van der Kamp and Gale, 1983). Consequently, if the fluid flow term on the left-hand side of Eq. (4.2) is equal to zero, Eq. (4.4) is obtained:

$$\frac{\partial u_w}{\partial \sigma} = \frac{m_v}{m_v + n\beta_w} = LE \tag{4.4}$$

If the barometric pressure change is assumed to be the sole cause of pore pressure change, for undrained conditions, LE can be obtained from the slope of the linear relationship between pore pressure response and barometric pressure change. Thus, rearranging Eq. (4.4) provides an equation to estimate the vertical compressibility of the formation as follows:

$$m_v = \frac{LE(n\beta_w)}{1 - LE} \tag{4.5}$$

Once the compressibility of the formation is derived, the constrained modulus can be obtained by:

$$M = \frac{1}{m_v} \tag{4.6}$$

When a pore pressure response to barometric stress change is not immediate (unconfined aquifer with thick unsaturated zone, semi-confined aquifer, and compressible clay layer), the barometric/loading efficiency cannot be estimated from a linear relationship. It becomes retarded and frequency dependent (Weeks, 1979). This is briefly explained in Section 4.4.2.

4.3 Geological setting of the study area

Champlain Sea clay is the name given to marine clays found in the lowlands of Quebec (Figure 4.1). There is an extensive body of literature dealing with Champlain Sea clay geology (e.g., Dyke et al., 2003, Karrow, 1961, Occhietti, 1989 and Parent and Occhietti, 1988). Champlain Sea clays were deposited in the Champlain Sea from approximately 12,000 to 8500 BP (before present) during the late Quaternary Period. The Champlain Sea covered the Saint Lawrence River lowlands and it extended up to the Lake Saint-Jean region as the Laflamme Sea (La Rochelle et al., 1970 and Leroueil et al., 1983).
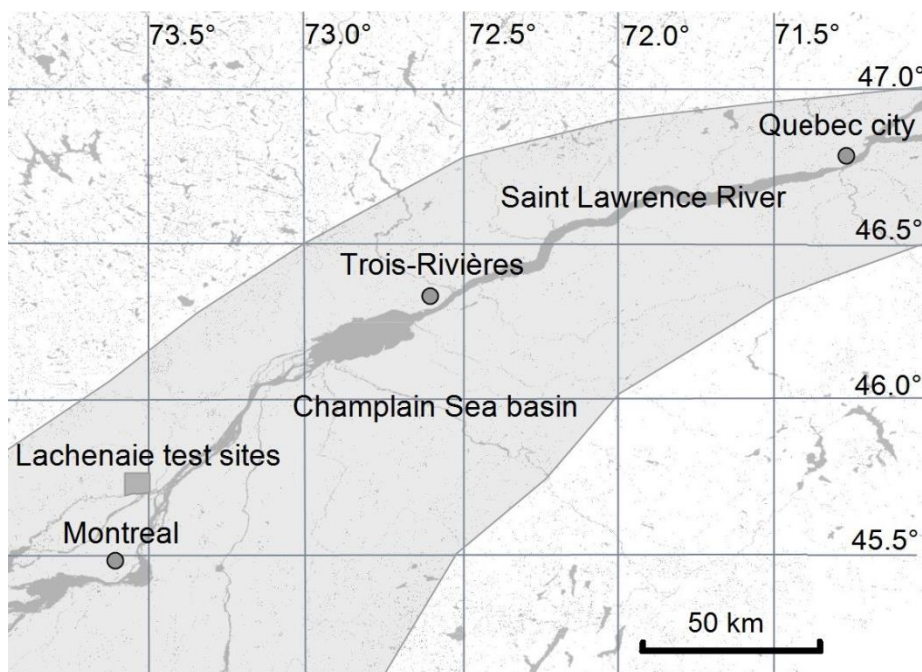
Figure 4.1: Maximum area covered by the Champlain Sea in southern Quebec, adapted from Duhaime et al. (2013a).

On the nine (9) Lachenaie test sites described by Duhaime et al. (2013a), the Champlain Sea clay deposit is located under eolian and alluvial sands, and organic material. In the top portion, the clay is sometimes oxidized and fractured, and called the crust. The crust thickness may reach up to 5 m. The crust is underlain by two layers of unoxidized and massive gray silty clay. The thickness of the unoxidized clay is up to 25 m on the test sites. The erosion of part of the clay

profile, aging, chemistry change, GWL changes, etc. have caused the underlying clay to have a relatively high degree of overconsolidation for a Champlain Sea clay deposit. The intact clay deposit is underlain by a till layer up to 7 m thick and a shale bedrock which is thoroughly fractured at the interface with the till.

4.4   Material and methods

4.4.1   Piezometer installation

Figure 4. 2 presents the location of the test sites. The test sites are placed north of the Mille-Îles River, west of Highway 40 and the L'Assomption River, and on the east side of the Mascouche River. The sites are situated on both sides of Highway 640.
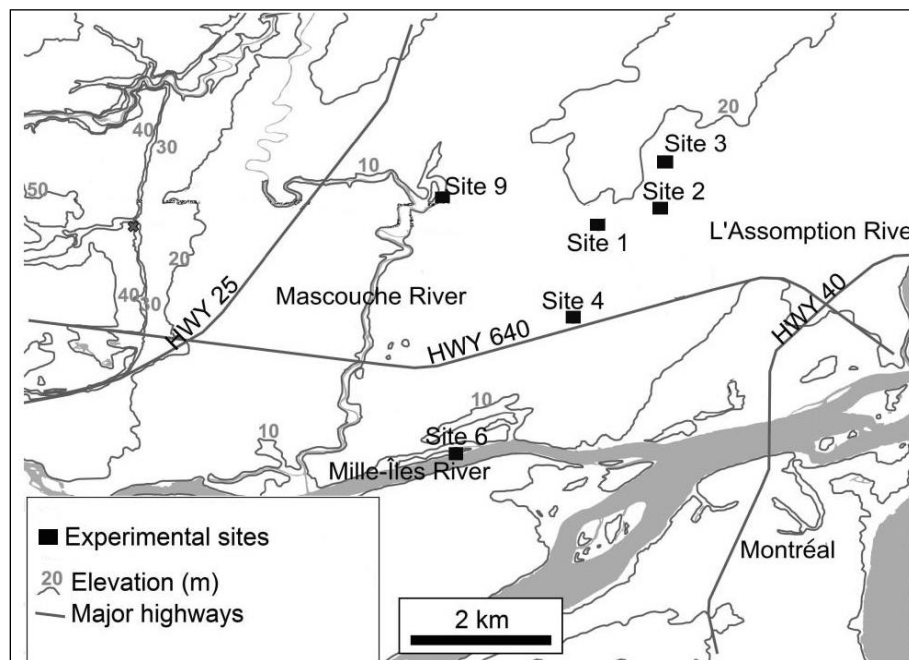
Figure 4.2: Locations and identification of the study area, adapted from Duhaime et al. (2013a).

This paper deals with the installation of VWP and the monitoring program on sites 2, 3, 4, 6, and 9, a subset of the Lachenaie test sites (Duhaime et al., 2013a). Figure 4.3 summarizes the

stratigraphy of the study sites. Three monitoring wells, MWs, identified as AH, AB, and R were installed on each site between 2006 and 2008. The AH and AB wells were respectively installed at the upper and lower third of the clay layer. The third well (i.e., R) was installed in the fractured bedrock (Duhaime, 2012 and Duhaime et al., 2013a).

Although pressure transducers installed in fully grouted boreholes can provide accurate pore pressure measurements if they are installed properly (McKenna, 1995), the traditional installation method for piezometers was selected for this project. With this method, a sand filter is installed around the pressure transducer. This method was selected because the VWPs were installed within pre-existing MWs with a sand filter around the well screen. The VWP installation was conducted in October 2012 for site 2 and between July and October 2013 on sites 3, 4, 6 and 9. The pre-existing AB and AH monitoring wells on each study site were instrumented with absolute (not vented) RST-VW2100-0.35 pressure transducers. These VWPs have a full scale reading range of 350 kPa and a resolution of 1 mm of water. Each VWP was connected to a programmable single channel data logger. The VWPs were fitted with high air entrance value ceramic filters which were saturated according to the manufacturer instructions in the laboratory, and then kept in deaired water until their installation.
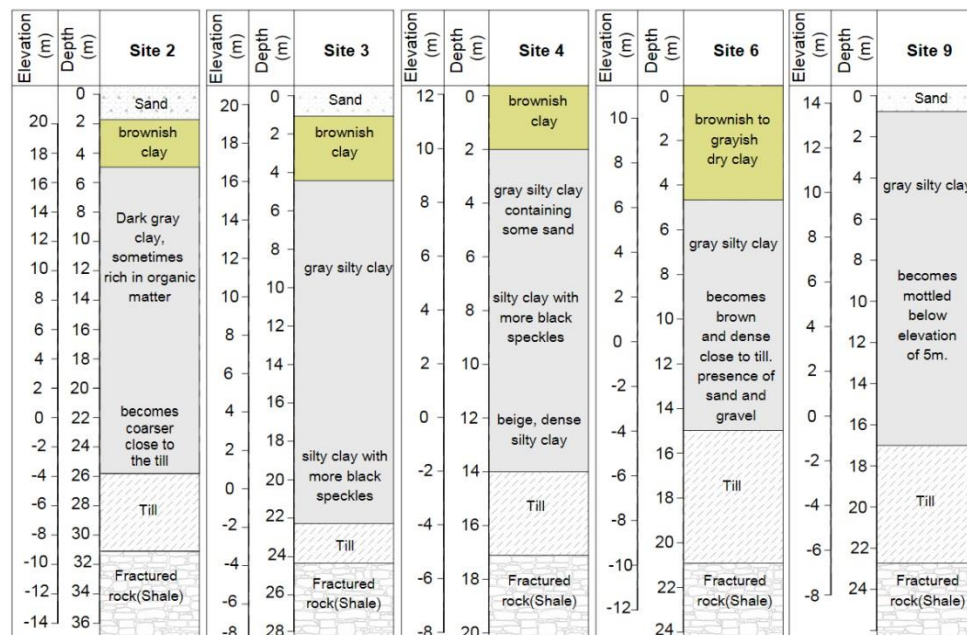
Figure 4.3: Summarized stratigraphy of study sites (adapted from Duhaime, 2012).

The pressure transducers, PT, are absolute: they measure the sum of water and atmospheric pressures. The atmospheric pressure transducers, APT, measure the atmospheric pressure. The pressure transducers typically have a zero offset. That is to say, when both APT and PT measure the atmospheric pressure at the same location, time and altitude; the difference PT−APT is not zero. In practice, a pressure difference between −10 and +10 cm of water is usually found. That is because the PT and APT were not calibrated as the same time in the plant (Chapuis, 2009b). This was confirmed by Sorensen and Butcher (2011) and Von Asmuth et al. (2008). Therefore, PTs should be calibrated before installation in order to provide absolute pore pressure measurements that are precise. In this study the PTs were calibrated with respect to APT.

A schematic view of the VWP installation is presented in Figure 4.4. The PVC riser pipe of the existing MW has an inside diameter of 52.5 mm. The height and diameter of the MWs screen are respectively 53 cm and 31.75 mm. Each VWP was placed in a roughly 1.00 to 1.30 m long filter of saturated fine sand.

The presence of gas bubbles in the MW intake zone induces an additional time lag due to gas compressibility (Duhaime and Chapuis, 2008). Gas bubbles can enter the intake zone when the water level is lowered to the well screen or when the sand filter is poured into the filter cavity. Pore pressure change results in volume change for the bubbles, thereby slowing the equalization of the pressure imbalance. Bubbles can cause a piezometric error and lead to an increase in time lag (Simeoni, 2012). They influence also field permeability tests results (Chapuis, 2009a). Therefore, air should be extracted from the well before the installation. To extract air bubbles from the intake zone, a vacuum of 30 kPa was applied on the MW for a 24 h period before the installation. First, the PVC riser pipe of the MW was isolated using an inflatable packer. Then a 30 kPa vacuum was applied into the well. The change in water pressure causes an expansion of the gas bubbles and degassing of the water. The vacuum was applied in the field using two reservoirs. After 20 cm of saturated sand was poured with water into the sand cavity, the suction was reapplied to the MW for approximately 2 h. The VWP was thereafter lowered into the MW screen. A 1.5 m long stainless steel rod was attached to the VWP and cable to keep them straight and ease the placement of the transducer into the well screen.

Once the VWP was placed into the MW screen, a further layer of saturated fine sand was poured with water into the borehole above the VWP. This layer of saturated sand was poured into the

borehole through a funnel which was attached to a 2.5 m long pipe and a controlling valve. The water level within the PVC riser pipe was first increased. The funnel was then filled with saturated sand mixed with deaired water. The saturated sand within the funnel was fed into the well water by opening the valve. After having installed the saturated sand filter, the VWP was plugged with approximately 90–110 cm of coated bentonite pellets. Coated bentonite pellets were selected because they can easily reach the top of the sand filter when they are poured in the PVC riser pipe without clogging it. The VWP installation was ended by backfilling the borehole to the top of the PVC riser pipe with bentonite–cement grouting. The bentonite–cement mix was pumped into the borehole from the bottom up. The mix recipe was selected in the laboratory before the installation to have proper consistency and permeability. The selected bentonite–water and cement–water ratios were respectively 6% and 30% (wt.%). The bentonite–cement grout was carried out using deaired and distilled water in order to decrease the presence of air in the mix. The grout was prepared by mixing the bentonite with the water first (24 h in advance). The cement was added in the field a few minutes before grouting. This procedure results in a grout with better volumetric stability, in other words in a grout that shrinks less with aging (Chapuis et al., 1984).
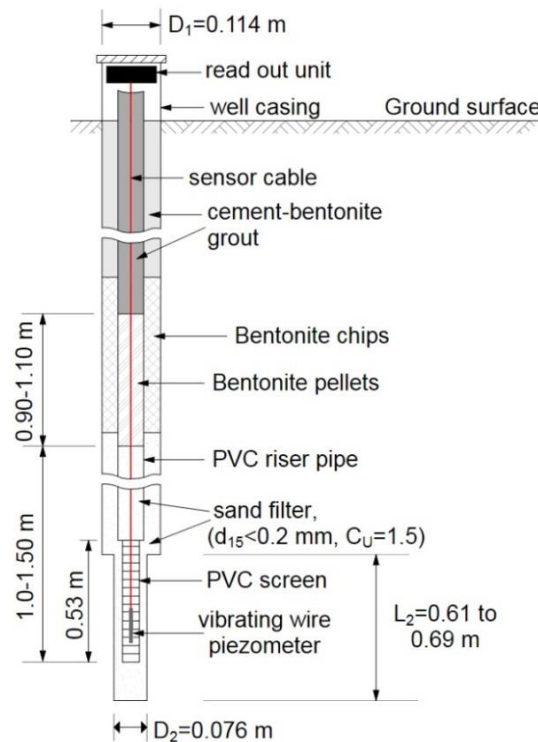
Figure 4.4: Detail of the VWP installation in MW.

Hydraulic head fluctuations in the crust and in the lower confined aquifer were measured with two absolute pressure transducers with a full scale of 10 m of water, and with resolution and accuracy of 2 and 1 mm of water respectively. To measure the hydraulic head in the surficial layer, a standpipe piezometer with a 20 mm diameter and with a 40 cm long slotted tip was installed in a borehole that had been augered below the ground water table. The atmospheric pressure change was recorded separately on each site using an APT with a full scale of 15 kPa, and with resolution and accuracy of respectively 1 mm and 5 mm of water.

4.4.2 Assessment of loading efficiency

Pore pressure measured by an absolute pressure transducer provides an opportunity to directly estimate a value for loading efficiency. The LE value is related to formation properties. It theoretically varies between 0 and 1 and it can be determined using several methods. Relatively soft clay formations like the Lachenaie clay deposit have LE values that are close to 1. This implies that water is much less compressible than the formation solid matrix. Thereby most of the change in external loading is carried by pore water (e.g., Spane, 2002, Timms and Acworth, 2005 and van der Kamp and Gale, 1983). The loading efficiency is also related to the degree of saturation of the formation (Black and Lee, 1973 and Skempton, 1954) and the hydraulic and storage properties of the well/formation system. Accordingly, assuming a saturated formation and a well with a negligible time lag, the magnitude of LE should be related to the hydraulic/storage properties of the formation (Smith et al., 2013).

Three methods were used to assess the pore pressure response to barometric pressure change of the wells that had been sealed in the Lachenaie clay deposit: linear regression, visual inspection, and BRF. A brief explanation will now be presented for each method.

For an instantaneous pore pressure response governed by Eq. (4.4), the linear regression method provides a LE value from the slope of the linear fit between changes in barometric pressure and pore pressure. However, the impact of other natural phenomena, such as tidal force and groundwater recharge and discharge, can be superimposed on the linear relationship between pore water and barometric pressures (Seo, 1999 and Timms and Acworth, 2005). In Lachenaie, the surficial soil layer is frozen during winter, thus restricting ground water recharge and

discharge. As a result, if tidal pore pressure changes are small, barometric pressure should be the main control on pore pressure. Hence for winter in Lachenaie, the relationship between barometric and pore pressure variations should be close to a straight line that allows a representative estimation of loading efficiency.

The visual inspection method was recently applied by several authors (e.g., Anochikwa et al., 2012, Smerdon et al., 2014 and Smith et al., 2013) to remove the barometric pressure change effects on pore pressure measured within clay aquitards. This method was used in this study to predict values of LE for Lachenaie clay as well. With the visual inspection method, the LE value is adjusted so that the corrected pore pressure time series are as smooth as possible. Loading efficiency can be determined by multiplying the barometric pressure change with a trial LE value between 0 and 1 and then subtracting the result from the raw pore water pressure in order to obtain a pore pressure time series as smooth as possible (Smith et al., 2013).

The use of a BRF in the analysis of pore pressure time series was first proposed by Rasmussen and Crawford (1997). It is a robust tool to analyze the pore pressure response to change in natural loads if a delay occurs between stress change and pore pressure response. The barometric response function is defined as the pore pressure response through time to a unit change in barometric pressure. Several authors used BRF to analyze well water response to changes in barometric pressure and to successfully remove the effects of barometric pressure on well water level changes in aquifer/aquitard systems (e.g., Butler et al., 2011, Rasmussen and Mote, 2007, Spane, 2002 and Spane and Mackley, 2011). Furthermore BRF can be a useful tool to investigate formation integrity (Butler et al., 2011) and distinguish different response patterns for various well/aquifer systems (Rasmussen and Crawford, 1997). The exact shape of the BRF is dictated by the well and formation characteristics (see also Rasmussen and Crawford, 1997 and Spane, 2002). For instance, for a given well with significant well-bore storage, the BRF plot typically has a concave downward curve over time.

In statistics, the current value of a dependent variable can be predicted based on both the current and lagged values of an explanatory variable using multiple regression models (Judge et al., 1988). A linear set of multiple regression equations can be written between pore pressure change (dependent variable) and barometric pressure change (explanatory variable) as follows (e.g., Rasmussen and Crawford, 1997 and Spane, 2002):

$$\Delta u_t = \alpha_0 + \delta_0 (\Delta B)_t + \delta_1 (\Delta B)_{t-1} + \delta_2 (\Delta B)_{t-2} + ... + \delta_n (\Delta B)_{t-m} + \varepsilon \tag{4.7}$$

where Δu_t is the change in pore water pressure $u_t - u_{t-1}$, $(\Delta B)_t$ is the change in barometric pressure $B_t - B_{t-1}$, $(\Delta B)_{t-1}$ is the change in barometric pressure for the previous time step, $(\Delta B)_{t-m}$ is the change in barometric pressure for the mth previous time step, α_0 is the regression intercept, $\delta_0 ... \delta_n$ are the regression coefficients corresponding to time lags of 0 to m, ε is the residual error term, and m is the maximum lag. The barometric response function is constructed by gradually summing up the regression coefficients to m number of the associated time lag.

$$BRF = \sum_{i=0}^{i=m} \delta_i \tag{4.8}$$

For instance, the BRF time-lag value is equal to δ_0 for a time lag of 0, and it is equal to $\delta_0 + \delta_1 + \delta_2 + \delta_3 + \delta_4$ for a time lag of 4 time steps (Toll and Rasmussen, 2007; Spane and Mackley, 2011).

The regression coefficients can be determined by ordinary least squares (Toll and Rasmussen, 2007; Spane and Mackley, 2011). Microsoft Excel spreadsheets or typical statistical software (e.g., Statistical Package for the Social Sciences, SPSS) can be used to assess the *BRF*. Some Excel spreadsheets and computer utilities (Multiple Regression in Excel, MRCX, Kansas Geological Survey Barometric response function, KGS-BRF, and Barometric and earth Tide Response Correction, BETCO) have been developed to automatically calculate the *BRF* and eliminate the barometric pressure effects on pore pressure response using the multiple regression deconvolution technique.

4.4.3 Correcting pore pressure time series

In this study, the visual inspection and multiple regression methods were used to correct the pore pressure time series measured by 10 sealed VWPs installed on the 5 Lachenaie test sites. With the visual inspection method, the corrected pore pressure can be determined as follows (Smith et al., 2013):

$$u^* = (u_t - B_{ave}) - LE(B_t - B_{ave}) \tag{4.9}$$

where u^* is the corrected relative pore water pressure, u_t is the observed absolute pore pressure, B_t is the observed barometric pressure, and B_{ave} is the average barometric pressure for the study site. For a period when the pore pressure fluctuations follow the barometric pressure changes (i.e., a period between two precipitation events), representative values for *LE* can be determined. For a case of delayed response however, corrected pore pressure time series can be obtained by subtracting the summation of predicted change in pore water pressure $\Sigma\Delta u_t$ [Δu_t is obtained by Eq. (4.7)] from the observed pore pressure response (Rasmussen and Crawford, 1997 and Spane, 2002):

$$u^* = u_t - \sum \Delta u_t \qquad (4.10)$$

4.5   Results and discussion

To assess the pore pressure response to barometric pressure change within the Lachenaie clay deposit, barometric and pore pressures were automatically logged at intervals of 15 min between November 2012 and November 2014 on site 2 and between July 2013 to November 2014 on the other test sites (i.e., 3, 4, 6, and 9). To simplify the comparison of pore pressure response with a change in barometric pressure, all measurements are expressed as equivalent height of water. The maximum range of barometric pressure variation on the test sites was around 0.62 m between July 2013 and November 2014. On site 2, a maximum range for barometric pressure of 0.68 m was recorded between November 2012 and May 2013. For the period between July 2013 and November 2014, fluctuations of the barometric pressure on each site were plotted against each other. Figure 4.5 presents the fluctuations of barometric pressure for sites 2 and 9. Very good correlations with high values of R2 (i.e., 0.997) were found for sites 2, 4, 6, and 9. The linear fit for barometric pressure variations between site 3 and the other sites was not as good as those obtained between sites 2, 4, 6 and 9. The good correlation between the barometric pressure measurements in our study area shows that the barometric pressure change was almost uniform over the whole study area (50 km^2).

Water level and pore pressure fluctuate in response to lunar and solar gravity, (i.e., Earth tide) (Bredehoeft, 1967). To investigate the pore pressure fluctuations induced by Earth tides, the

theoretical earth tide gravitational acceleration obtained by TSoft (Van Camp and Vauterin, 2005), a freely accessible software package for the analysis of Time Series and Earth Tides, was used. A visual comparison of pore pressure data for several piezometers with synthetic Earth tide has shown that there is no obvious Earth tide signal in our pore pressure data. This matches the conclusion of Smith et al. (2013) for shallow piezometers (i.e., 1 mm of variation in pore pressure due to Earth tide stress for piezometers at a depth of less than 25 m). Since the deepest piezometer on the test sites was around 15 m below ground surface, the Earth tide effect on pore pressure fluctuations can be expected to be smaller than 1 mm. This is negligible with respect to barometric effects which were more than 100 mm.
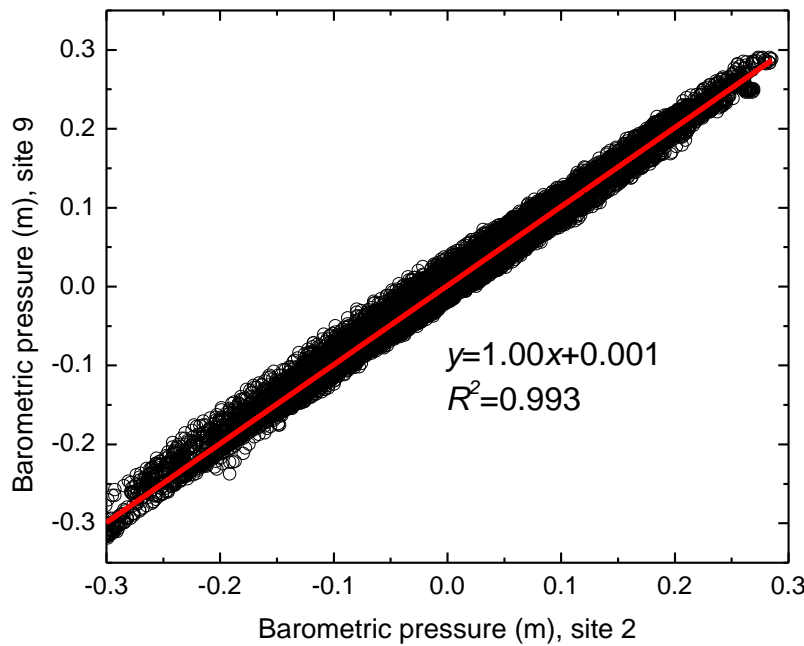
Figure 4.5: Observed change in barometric stress, site 2 versus site 9
from Jul. 2013 to Nov. 2014.

4.5.1 Estimation of loading efficiency

Figure 4.6 shows the observed barometric pressure and uncorrected pore pressure responses based on measurements taken every 15 min between November 2012 and November 2014 on

site 2 (Figure 4.6a), and between November 2013 and November 2014 on piezometers 6AB and 9AB (Figure 4.6b). The VWPs used in this study were calibrated with respect to average barometric pressure at sea level (B_{sea}). The VWPs measure pore pressure (static and transient components) and the barometric pressure transducers measure change in air pressure with respect to B_{sea}. In this paper, pore pressure refers to the difference between total pressure measured by the VWPs and B_{sea}. Figure 4.6a displays how pore pressure fluctuations in the upper and lower portions of the clay layer are similar for site 2. For the other sites (3, 4, and 9) the same visual similarity of pore pressure fluctuations between the upper and lower portions of the clay layer was obtained. The similar trend of long-term pore pressure fluctuations through the clay layer in the study area is a preliminary evidence of clay layer integrity. It indicates that there is no hydraulic connection between the measuring locations and the upper or lower aquifers (e.g., Hare and Morse, 1997).

To obtain representative values for LE, pore pressure data were analyzed for winter measurements with no significant background trend in pore pressure (i.e., a period with a correlation between barometric and pore pressure changes). As mentioned earlier, in the pore pressure data, the Earth tide effect on pore pressure oscillations appears to be negligible. Therefore the main cause of pore pressure variations during winter would be barometric pressure change. Two hourly based subdatasets for site 2 (winter 2013 and winter 2014) and one for each of the other sites (winter 2014) were selected as target datasets to analyze the pore pressure response to barometric loading and to obtain LE values (highlighted slices on Figure 4.6). The subdataset of winter 2014 running from January 1st to April 1st was used in this study to determine LE for all piezometers. It will hereafter be referred to as the selected period.

The barometric and pore pressures time series for piezometers 2AH, 2AB, 6AB and 9AB appear on Figure 4.7 for the selected period. Figure 4.7a shows an obvious correlation between the barometric and pore water pressure response through the clay formation in piezometers 2AH and 2AB. In other words, the pore pressure changes almost instantly follow the barometric pressure change. However, Figure 4.7b presents a poor visual correlation between the barometric and pore pressure response for piezometer 6AB. For piezometer 9AB, even though the long-term trend of pore pressure follows barometric pressure fluctuations, there are rapid oscillations of pore pressure data. As shown in Figure 4.7, there are background trends on pore pressure data in the piezometers. The trend is significant for the piezometer 6AB. Before performing any analysis to

estimate LE, these background trends were simply detrended using a linear regression as proposed by Spane (2002).

Table 4.1 presents estimated values for loading efficiency obtained from hourly based sub datasets. The three methods to estimate LE used detrended data for all piezometers. The linear regression method gave good correlations, particularly for shallower piezometers which follow closely the relationship of Eq. (4.4). By providing a stabilized value for LE, the BRF method was particularly useful for piezometers deeper in the clay profile (e.g., 2AB) because this method takes into account a lagging pore pressure response. The visual inspection method was not very sensitive to LE since the smoothed pore pressure time series for all piezometers were not significantly changed when LE was changed by 0.05 from the optimal value. Nevertheless the three approaches provided values for LE that differed by less than 10%.

Table 4.1: Calculated values for LE with various methods, Lachenaie study area.

site	piezometer	Depth (m)	Loading efficiency (LE)		
			Linear regression	BRF	Visual inspection
2	2AH	8.70	0.95	0.91	0.92
	2AB	15.17	0.76	0.82	0.78
3	3AH	7.80	-	0.35-0.5	0.50
	3AB	14.85	0.87	0.80	0.82
4	4AH	5.40	0.92	0.90	0.92
	4AB	9.05	0.88	0.88	0.90
6	6AH	4.80	0.90	0.89	0.92
	6AB	9.40	-	0.60-0.65	0.75
9	9AH	5.40	0.94	0.91	0.92
	9AB	11.50	0.88	0.80-0.90	0.90

Even though the deepest piezometer was only about 15 m below ground surface, the results show that the LE values decline slightly with depth. This is consistent with previous findings (e.g., Smerdon et al., 2014 and Smith et al., 2013). All methods provided high values for LE (i.e., 0.70–0.95) which indicates that most of the external natural loading is born by pore water. This shows that Lachenaie clay layer is more compressible than water, similar to most shallow clayey aquitards (Smith et al., 2013). For a few piezometers (3AH, 6AB, and 9AB), some methods could not provide proper values for LE as explained later in this paper.
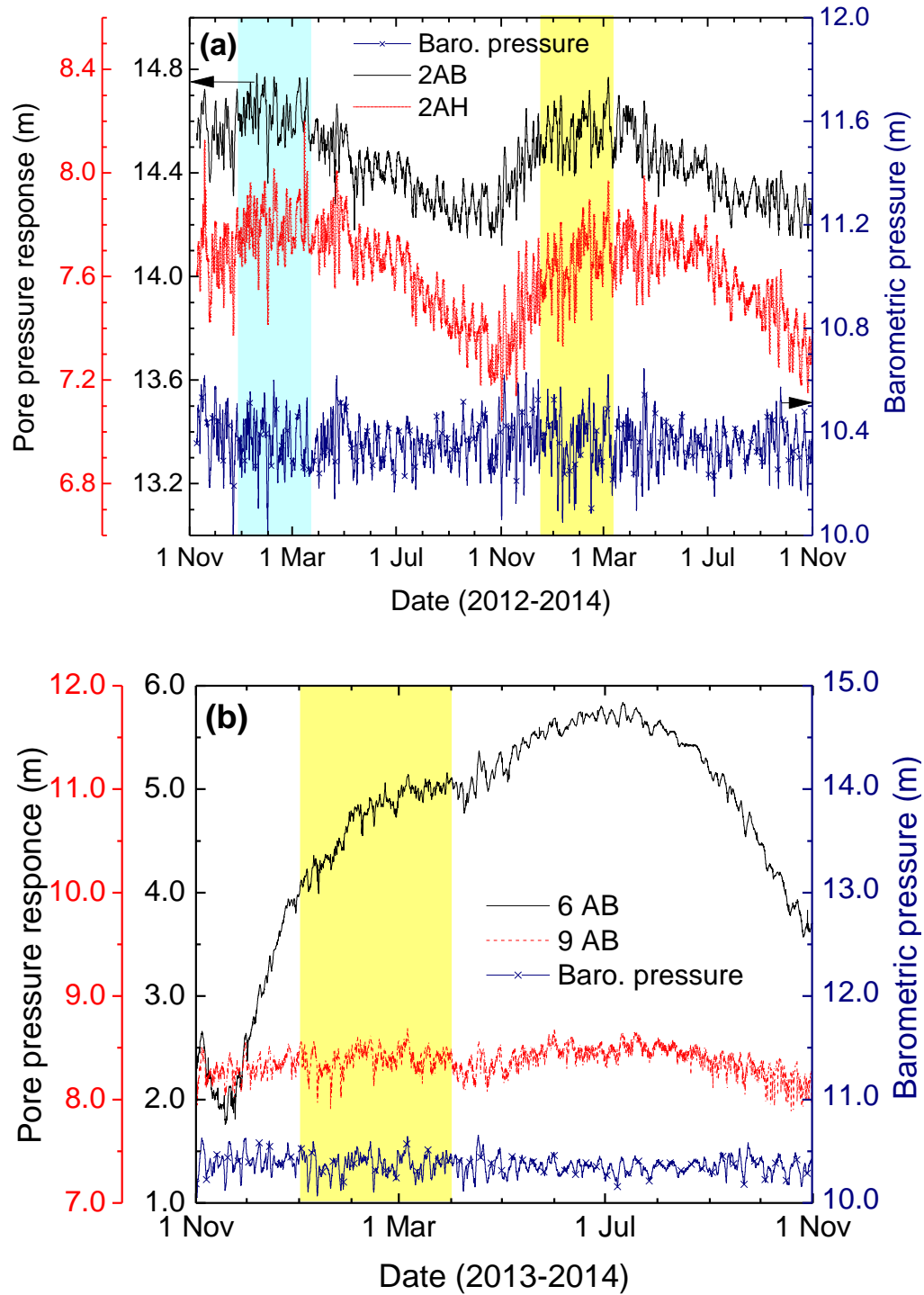
Figure 4.6: Observed pore pressure and barometric pressure measurements, Lachenaie: a) piezometers 2AH and 2AB from Nov. 2012 to Nov. 2014; b) piezometers 6AB and 9AB from Nov. 2013 to Nov. 2014.

Since the groundwater table is high in the Lachenaie area (1–2 m below ground), the unsaturated portion of the crust is very thin. Therefore the barometric pressure change is quickly transferred to the groundwater table. Figure 4.8 represents the linear relationships between changes in barometric and pore pressures for the piezometers 2AH and 6AB. As shown in Figure 4.8a, piezometer 2AH exhibits best-fit responses that are linear. For piezometer 6AB (Figure 4.8b) the linear fit is poor. For piezometer 3AH similarly a poor linear fit is obtained (result not shown). On site 9, piezometer 9AH shows a good correlation, but the fit was poor for piezometer 9AB installed at a depth of 11.3 m within the clay. The R^2 for piezometer 9AB was around 0.81 (results not shown).

Figure 4.9 shows the hourly based plots of BRF obtained for the selected period. As said before, according to the Rasmussen and Crawford (1997) diagnostic models, within low permeability and compressible formations, the total head (absolute pressure) BRF plots should have a concave downward pattern. Accordingly, for all piezometers in the Lachenaie clay deposit, concave downward patterns for BRF plots were obtained. The shallowest wells (located in the upper portion of clay layer) exhibit a quickly increasing BRF with a low time lag. The pressure imbalance between the formation and piezometer is equalized rapidly for piezometer 2AH. However, it is delayed for the lower piezometer (2AB). As shown in Figure 4.9, approximately 91 and 80% of the unit change in barometric pressure has been transferred to the pore pressure in wells 2AH and 2AB after roughly 5 and 45 h of delay. These stabilized values of the pore pressure response for a unit change in barometric pressure have been used to define a stabilized value for loading efficiency.

On most test sites, the BRF manifested a smooth concave downward curve that increased at an early time then reached its maximum value and is stabilized over time. For piezometers 3AH, 6AB, and 9AB as shown in Figure 4.9, the smooth concave downward shape for the BRF was not obtained. The barometric response function stabilized to some extent for piezometers 6AB and 9AB, but it kept oscillating around 0.8–0.9 and 0.60–0.65 respectively. For piezometer 3AH, the BRF fluctuated around a low LE value of 0.35–0.50, a LE value that is much lower than those obtained for a similar depth. It should be noted here that the BRF plots for all piezometers were slightly smoothed with a three point moving average.
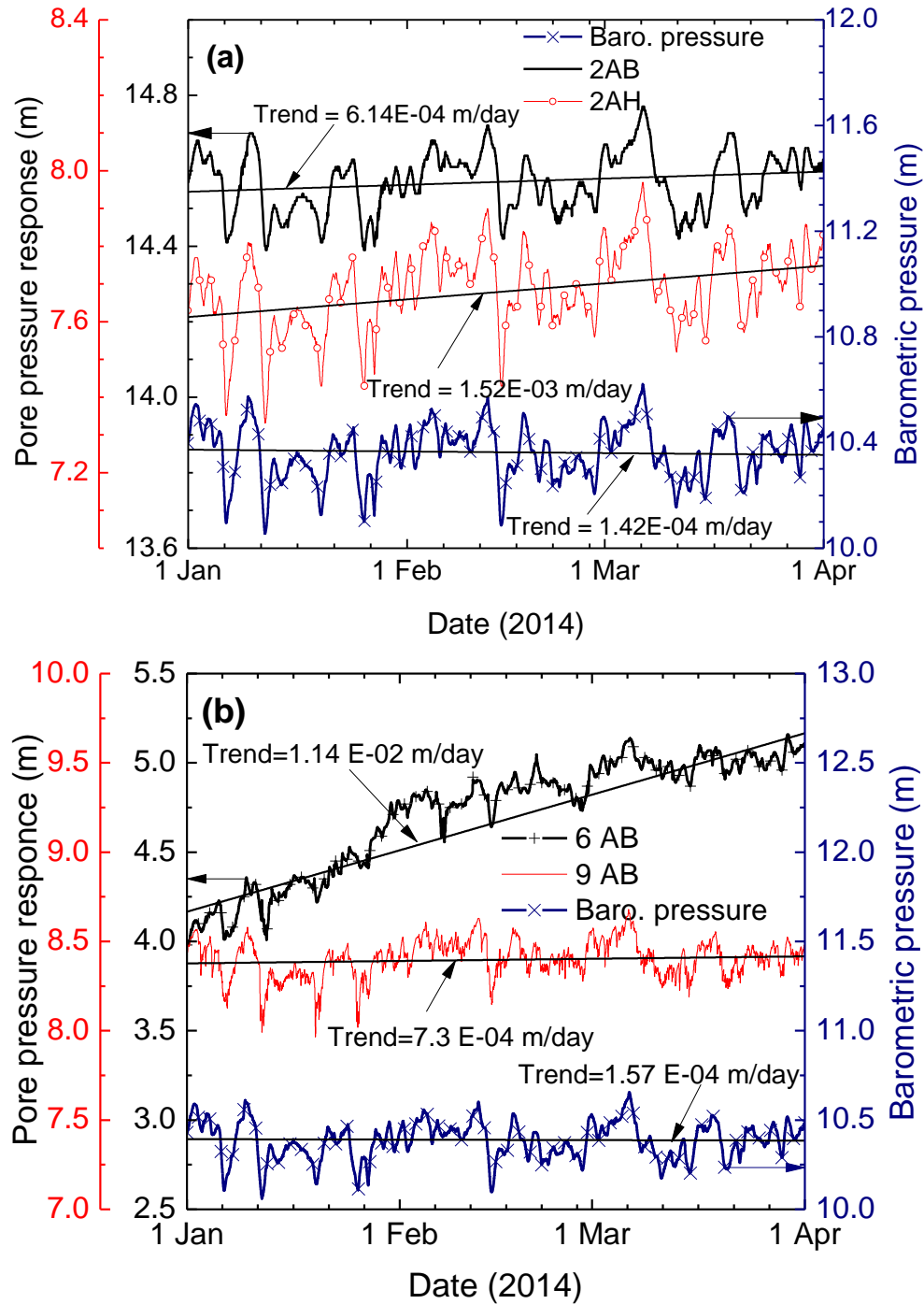
Figure 4.7: Observed pore pressure and barometric pressure changes, Lachenaie from Jan. 2014 to Apr. 2014 (selected period): a) 2AH and 2AB; b) 6AB and 9AB.
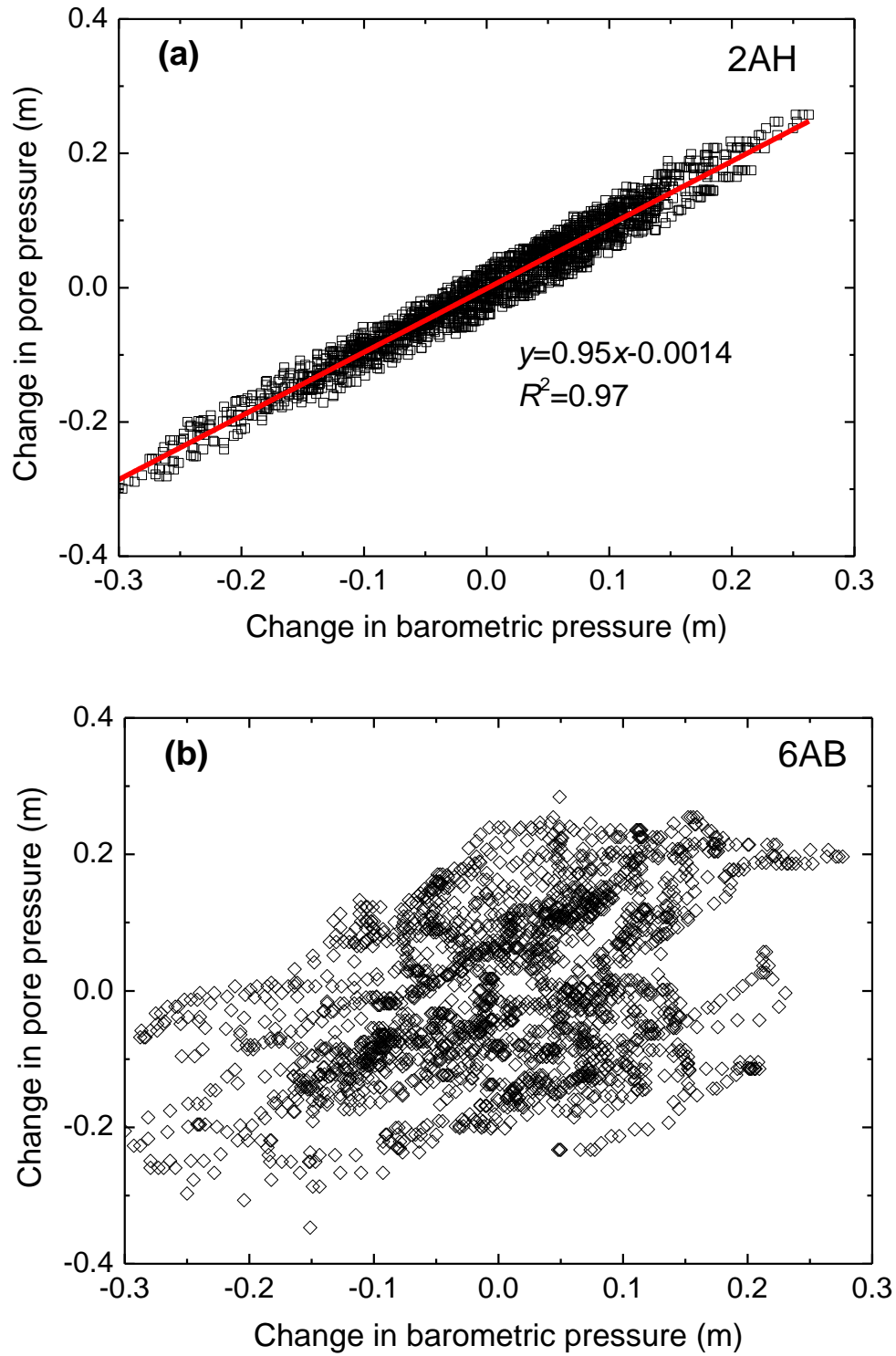
Figure 4.8: Examples of pore pressure variation versus barometric pressure change for Jan. 2014 to Apr. 2014: a) piezometer 2AH; b) piezometer 6AB.
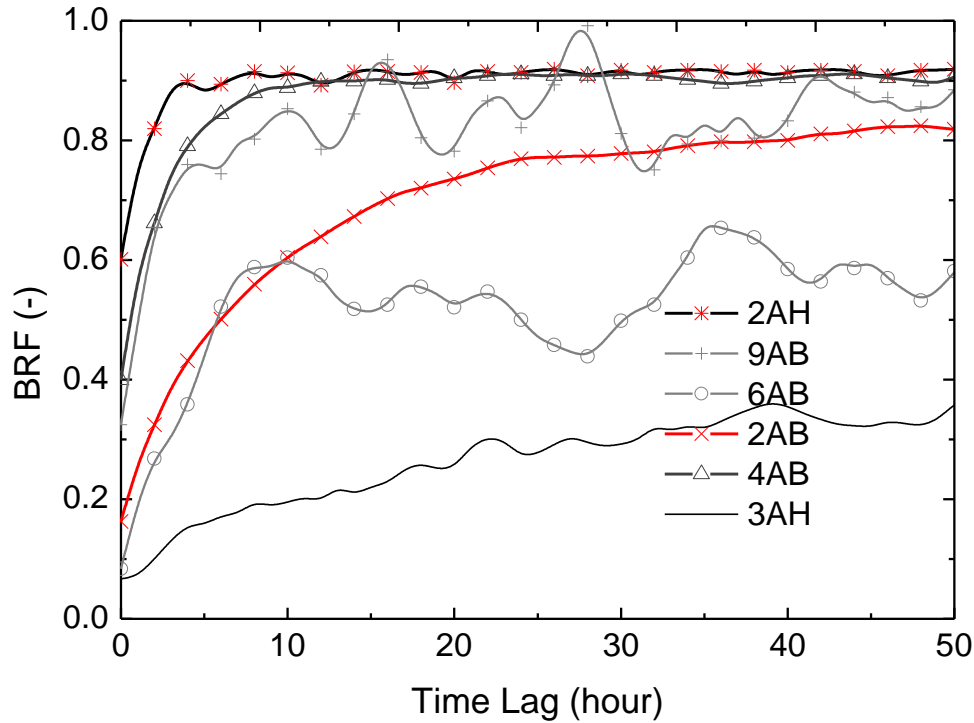
Figure 4.9: Barometric response functions for Jan. 2014 to Apr. 2014.

As noted with Figure 4.8b, the linear regression method could not yield an acceptable LE value for piezometer 6AB. Furthermore, as shown in Figure 4.9, for piezometers 3AH, 6AB, and 9AB the BRF could not yield a stabilized value for LE. This may be due to some unknown phenomena or externally imposed stress in the vicinity of these test sites. Piezometers 3AH, 6AB, and 9AB would be located within the zone of influence for this major stress. It is important to note that sites 6 and 9 are respectively located near the Mille-Îles River and Cabane-Ronde road respectively. In piezometer 6AB, the pore pressure response to change in barometric stress might be influenced by the contribution of the river stage. Likewise for piezometer 9AB where the road traffic likely affects the pore pressure fluctuations. Site 3 is located in the vicinity of a landfill cell which is presently being filled. It is possible that landfill activities disturb the pore pressure response to change in barometric pressure. However, the low LE value for this piezometer (≈ 0.35–0.50) is not fully understood. It is possible that the transducer installed in piezometer 3AH may have malfunctioned.

The presence of gas bubble generation on some study sites in Lachenaie is probably partly responsible for abnormal pore pressure responses. On the Lachenaie test sites, some wells installed in the bedrock are degassing. The high organic matter content at an elevation of around 5 m within the clay layer and the underlying methane gas-producing Utica shale could both be responsible for the degassing (Duhaime, 2012, Duhaime et al., 2013b and Duhaime and Chapuis, 2014). For instance, a continuous stream of gas bubbles could be seen at the water surface in artesian well 3R during the VWP installation and when collecting the data. Well 3R is tapping the fractured bedrock layer on site 3. Furthermore, previous studies regarding the Lachenaie clay aquitard indicated that pulse tests, a type of rapid permeability test, could not yield reliable results for some test sites probably because of the presence of gas bubbles (Duhaime, 2012 and Duhaime and Chapuis, 2014).

The unusual shape of the BRF plots for piezometers 3AH, 6AB, and 9AB (Figure 4.9) implies the contribution of other phenomena (gas bubble generation or external stress). The influence of river stage (site 6) and dynamic traffic load (site 9) have dissimilar amplitude and frequency. Accordingly, these externally imposed stresses lead to different BRF shapes. As shown in Figure 4.9, because the frequency of dynamic traffic load is higher than river stage load, the resulting BRF oscillation is also faster. If the properties (frequency and amplitude) of the externally imposed stresses are known, they can be filtered or eliminated from pore pressure data, but this is not part of the paper scope. For example the river stage or dynamic traffic loads can be identified and filtered using Fast Fourier Transformation (FFT) or signal processing techniques. Likewise, the river stage data could be used to eliminate the influence of river stage on pore pressure data as proposed by Spane and Mackley (2011) with the multiple regression method.

4.5.2 Pore pressure correction

The effect of barometric pressure change on pore pressure data measured with sealed VWPs can be removed using the methods described in Section 4.4.3. With the visual inspection method, the smoothed pore pressure time series and the LE values are obtained simultaneously. Smith et al. (2013) have proposed to analyze pore pressure data measured between two rainfall events in order to obtain a representative value for LE. Figure 4.10 presents corrected pore pressure datasets for piezometer 2AB calculated with both the visual inspection and multiple regression

methods. To provide high resolution pore pressure time series, two datasets were corrected and compared: 1) data between two precipitation events (from January 15th to 25th, 2014) within the selected period and 2) full data for the selected period (from January 1st to April 1st, 2014). Precipitation data were collected by our onsite weather station and the nearby Environment Canada meteorological station. Both datasets provided roughly identical results for corrected pore pressure time series. Therefore the results obtained for the selected period (from January 1st to April 1st) are presented in this paper (Figure 4.10). The results for this selected period were used as reference data for subsequent pore pressure corrections.

Figure 4.10 shows that the two methods are able to remove the barometric pressure effects from the raw pore pressure data. For a clearer plot, the corrected pore pressure values were offset by −0.4 and −0.6 m for the multiple regression and visual inspection methods respectively. Figure 4.10 indicates that the visual inspection method leaves more noise in the corrected results for deeper piezometers (e.g., 2AB), while the multiple regression method provides smoother corrected pore pressure values. Hence, as discussed by Toll and Rasmussen (2007), the transient nature of the delayed response function allows barometric pressure change effects to be eliminated more effectively. However, for shallower piezometers, both methods provide roughly identical corrected results. Even though the main source of pore pressure fluctuation during the selected time has been removed, some minor pore pressure oscillations are still visible. They could be related to the effect on pore pressure of Earth tide or other natural loading phenomena.

Figure 4.11 represents the corrected pore pressure data for site 2 for the monitoring period between Nov. 2012 and Nov. 2014. The results were corrected with the multiple regression technique. The corrected results for piezometers 2AB and 2AH were shifted down by 0.4 m in the plot. The corrected pore pressure time series display significant seasonal variations in both the upper and lower piezometers. The long-term pore pressure trend on site 2 displays a decrease in pore pressure of around 0.42 m in the lower piezometer (2AB) from April 2013 to October 2013. From October 2013 to January 2014, the pore pressure increased by about 0.35 m. It remained roughly constant from January 2014 to April 2014. It seems that there is some yearly pore pressure cycle within the clay formation for the study period. A similar pattern of long-term pore pressure fluctuations is evident for the upper piezometer of this site. For most test sites, nearly parallel profiles of long-term corrected pore pressure were observed for the upper and lower portions of the clay formation. A longer period of pore pressure measurement would be

helpful to investigate the impact of climate change on some hydrogeology and geotechnical issues; for example, groundwater recharge and discharge, groundwater contamination, and the stability of natural slopes.
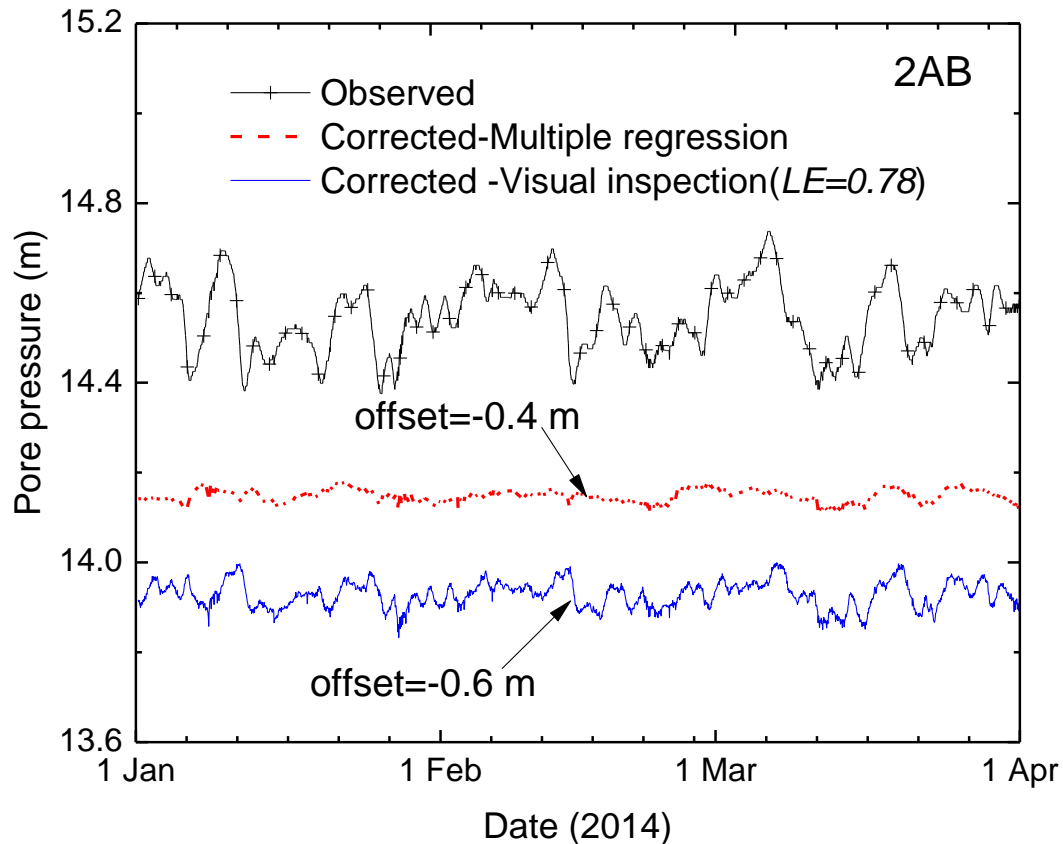
Figure 4.10: Corrected pore pressure time series, piezometer 2AB from Jan. 2014 to Apr. 2014.

4.5.3 Estimation of clay elastic parameters

A test method may involve three strain levels: very small strain, $< 10^{-3}\%$ (e.g., Karray and Lefebvre, 2008 and Shibuya et al., 1997), small strain between 0.001 and 0.1%, and large strain, $> 0.1\%$ (e.g., Burland, 1989). Laboratory and in situ tests involving strain below those associated with yield provide elastic properties that are between the values obtained for very small and large strains (Viggiani and Atkinson, 1995). At small strains Champlain Sea clay locally shows linear elastic behavior while, for stresses in the range beyond yield stress, the clay strain is large and

mostly irrecoverable (e.g., Mitchell, 1970,Tavenas and Leroueil, 1977 and Tavenas et al., 1974). A linear elastic relationship has been assumed by Anochikwa et al. (2012) for barometrically induced strain for glacial clay-till. However for Champlain Sea clay, the relationship between elastic parameters for very small strain is not clearly understood. Nevertheless, for a case of Rayleigh wave testing (strains less than 10^{-3}%), a linear elastic behavior has been assumed by Karray and Lefebvre (2009). Moreover, at stress below preconsolidation pressure, the Champlain Sea clay shows a significant anisotropic behavior (Delage and Lefebvre, 1984, La Rochelle and Lefebvre, 1971, Mitchell, 1970 and Yong and Silvestri, 1979).
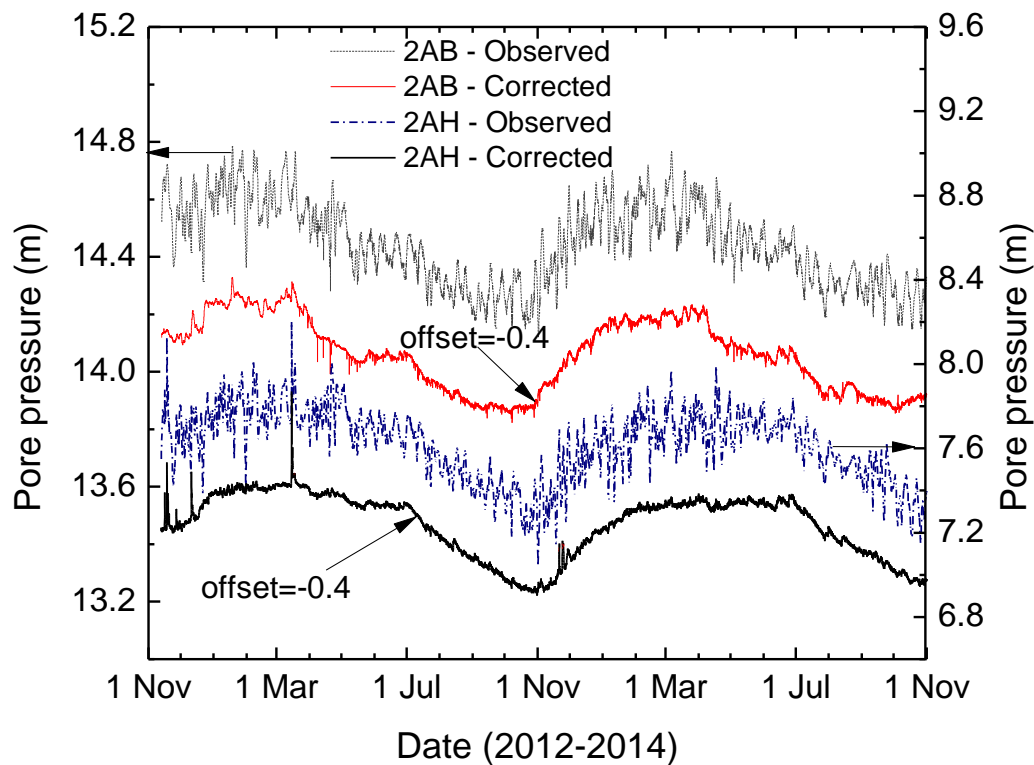
Figure 4.11: Corrected pore pressure time series using multiple regression technique from Nov. 2012 to Nov.2014, Lachenaie, site 2.

The Lachenaie clay deposit is lightly to moderately overconsolidated with a vertical preconsolidation pressure, σ'_p, varying between 180 and 580 kPa and an overconsolidation ratio, OCR, between 1.8 and 11 (Duhaime, 2012 and Duhaime et al., 2013a). In the study area, the

maximum barometric pressure change was around 7 kPa (0.7 m of water) between 2012 and 2014. This is well below the difference between the in situ stress conditions and the preconsolidation pressure σ'_p. Therefore the barometrically induced strain can be categorized as a very small strain governed by the theory of elasticity. Thus the values obtained for m_v, S_s, and M in this paper, using the in situ LE method, correspond to the elastic and very small strain properties of the Lachenaie clay. As a consequence, these results should be comparable with those of other in situ tests involving very small strain as well (e.g., shear wave velocity tests).

Several authors have performed self-boring pressuremeter tests, SBPM, on various locations in the Champlain Sea basin. For instance, Hamouche (1995); Silvestri (2003), and Silvestri and Abou-Samra (2008) have presented shear strain modulus, G, values for Champlain clay based on SBPM tests. Considering the initial phase of cavity expansion, Silvestri (2003) measured values for the small-strain shear modulus, G_0, of around 6–15 MPa for depths between 6 and 14 m below ground surface. The G values which are obtained with the SBPM or laboratory tests are typically smaller than those obtained with in situ LE method in this study, since the soil deformation in the SBPM test (even for the initial cavity expansion), is greater than that induced by barometric stress change.

As stated above, other in situ tests which investigate the very small strain rigidity of soils are the different shear wave velocity tests. Several authors have used this type of test in order to investigate G_{max}, the low-strain elastic modulus, E_{max}, and the Poisson ratio, v, for Champlain Sea clay. These parameters play a key role in dynamic analyses of soil behavior (e.g., Karray and Lefebvre, 2008, Lefebvre et al., 1994 and Youd et al., 2001). For a series of profiles close to sites 2 and 3 in Lachenaie, Karray and Lefebvre (2001) used the modal analysis of surface wave method (MASW) to determine G_{max}. Values of G_{max} between 13 and 64 MPa were obtained for depths of 0.5 and 23.5 m respectively.

Elastic properties of Champlain Sea clay that were estimated from the in situ LE method are presented in Table 4.2. Vertical compressibility m_v, specific storage S_s, and constrained modulus M for the Lachenaie clay were estimated with Eqs (4.5) and (4.6). Porosity values for each study site were calculated using $e/(1 + e)$ where e is void ratio which can be defined by wG_s for saturated clay, where G_s is the average specific gravity of the soil particles and w is the natural gravimetric water content of the saturated clay. The natural water content and specific

gravity data of the clay layer were presented by Duhaime (2012) and Duhaime et al. (2013a). Table 4.2 similarly presents values of the in situ vertical effective stress, values at the depth of the piezometers. The slightly decreasing values for m_v with depth did not come as a surprise. According to Duhaime (2012) and Duhaime et al. (2013a), the lower portion of the clay layer is less compressible than its upper portion, because the effective stresses and the preconsolidation pressure increase with depth. Values of m_v on the order of $1.0 \times 10^{-6} \, kPa^{-1}$ were found for most study sites based on the LE values obtained with the three methods presented in Section 4.4.2.

The m_v values presented in Table 4.2 are approximately one order of magnitude lower than previous results obtained with pulse tests, and approximately two orders of magnitude lower than those obtained with oedometer tests (Duhaime, 2012 and Duhaime and Chapuis, 2014). Oedometer test results also yield m_v values that are decreasing with depth. In their case studies, Timms and Acworth (2005) and Smith et al. (2013) also reported in situ m_v values (obtained with LE method) that were quite low with respect to laboratory testing results. The low values obtained for m_v using the in situ loading efficiency methods is related to the very small strain and very low clay disturbance induced by barometric pressure change.

For most Lachenaie test sites, fairly low values of specific storage were estimated (Table 4.2, on the order of $1.0 \times 10^{-5} \, m^{-1}$) if compared with results in the literature for medium to stiff clay (e.g., Domenico and Schwartz, 1997). The estimated values for S_s in this study support the previous finding by Timms and Acworth (2005) who calculated a S_s on the same order for slightly overconsolidated fluvial clay deposits in the Liverpool plains of northern New South Wales, Australia with the in situ LE method. Moreover results obtained for S_s support a claim by van der Kamp (2001) who indicated that the in situ values of specific storage obtained from LE were several orders of magnitude lower than those obtained from typical laboratory tests. Using the specific storage of the Lachenaie clay estimated here and taking a value for hydraulic conductivity from the literature on the order of $1.0 \times 10^{-9} \, m/s$ (Duhaime et al., 2013a), a value for hydraulic diffusivity on the order of $1.0 \times 10^{-4} \, m^2/s$ can be estimated.

Values of the *M* modulus for Lachenaie clay based on in situ LE values were obtained using Eq. (4.6). These values are presented in Table 4.2. Figure 4.12 shows a comparison between the constrained modulus obtained in this study and those obtained previously using other in situ and

laboratory methods. Laboratory values of M for Lachenaie clay have been derived directly from values of mv obtained by consolidation tests completed on samples obtained using thin-walled samplers during borehole drilling on the Lachenaie test sites. In contrast, SBPM and shear wave velocity tests provide G values. In this case, the M modulus can be calculated considering a proper value for v and the following equation:

$$M = \frac{2G(1+v)}{1-2v}$$

$$(4.11)$$
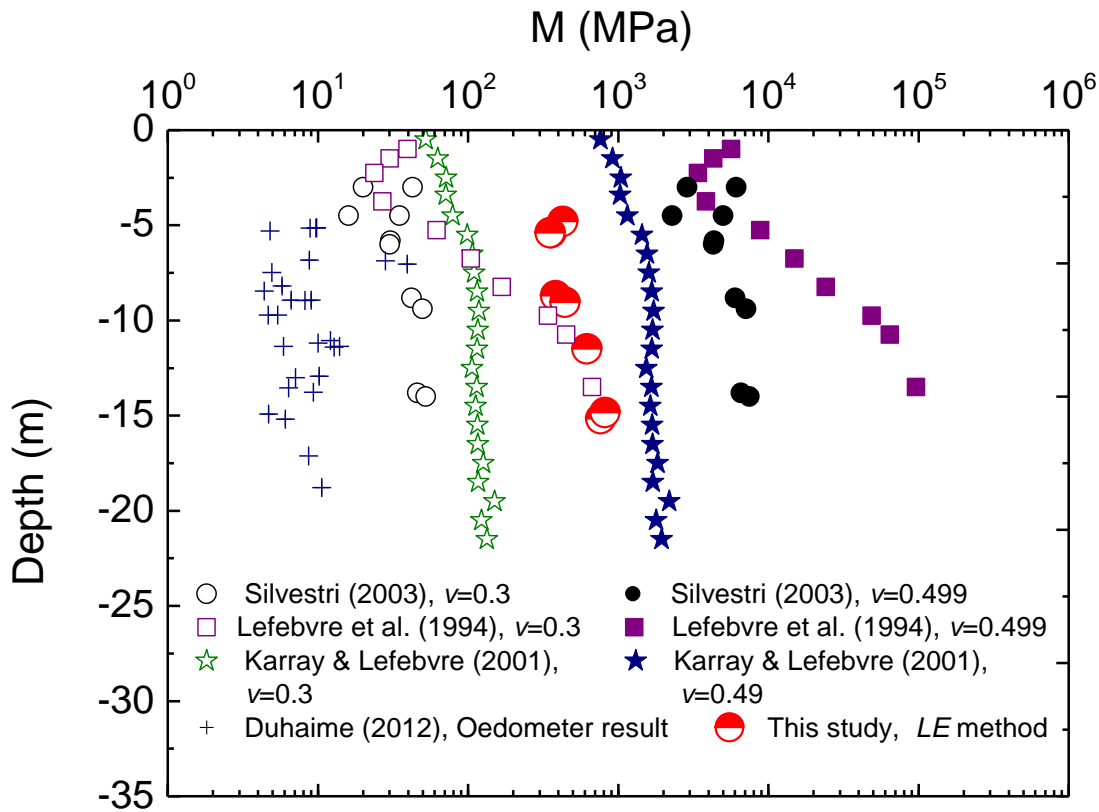
Figure 4.12: Constrained modulus of M obtained from various methods for diverse locations in the Champlain sea basin.

Table 4.2: Estimated values for the elastic properties of Lachenaie clay deposit.

Piezometer	in-situ σ'_v (kPa)	n	m_v (kPa^{-1})			S_s (m^{-1}) (BRF)	M (MPa) (BRF)
			linear regression	BRF	Visual inspection		
2AH	67	0.63	5.5×10^{-6}	$2.6E\times10^{-6}$	3.3×10^{-6}	2.8×10^{-5}	3.8×10^{2}
2AB	110	0.65	1.0×10^{-6}	1.3×10^{-6}	1.0×10^{-6}	1.6×10^{-5}	7.6×10^{2}
3AH	59	0.65	-	2.55×10^{-7}	3.0×10^{-7}	5.3×10^{-6}	4.0×10^{3}
3AB	102	0.66	2.1×10^{-6}	1.2×10^{-6}	1.4×10^{-6}	1.5×10^{-5}	8.2×10^{2}
4AH	34	0.60	3.2×10^{-6}	2.8×10^{-6}	3.2×10^{-6}	3.0×10^{-5}	3.5×10^{2}
4AB	62	0.61	2.1×10^{-6}	2.3×10^{-6}	2.5×10^{-6}	2.5×10^{-5}	4.4×10^{2}
6AH	75	0.63	2.6×10^{-6}	2.3×10^{-6}	3.3×10^{-6}	2.6×10^{-5}	4.3×10^{2}
6AB	120	0.54	-	4.25×10^{-7}	7.5×10^{-7}	6.62×10^{-6}	2.3×10^{3}
9AH	58	0.61	4.4×10^{-6}	2.8×10^{-6}	3.2×10^{-6}	3.1×10^{-5}	3.5×10^{2}
9AB	99	0.62	2.1×10^{-6}	1.6×10^{-6}	2.6×10^{-6}	1.9×10^{-5}	6.2×10^{2}

A v value of 0.5 was defined theoretically by several authors (e.g., Bjerrum, 1972 and D'Appolonia et al., 1971) for saturated clay when considering undrained conditions essentially saying the water component is incompressible. However some studies have shown that v might be lower for cemented Champlain Sea clay deposits, even for undrained conditions. It may be linked to the anisotropic elasticity of Champlain Sea clay (Mitchell, 1970 and Yong and Silvestri, 1979). Bozozuk (1963) and Crawford and Burn (1963) have proposed v values on the order of 0.4 for cemented clay. Tavenas et al. (1974) have found a value of $v = 0.3$ for immediate settlement at the end of construction for cemented Champlain Sea clay. Karray and Lefebvre (2001) considered a value of 0.499 for saturated Lachenaie clay to determine the small-strain shear modulus using MASW. One can see that there are high uncertainties in the determination of an appropriate value for v in Champlain Sea clay. On the other hand, the M modulus is highly sensitive to v when M is indirectly calculated from the G values obtained with MASW and SBPM test methods. In this study we considered values between 0.300 to 0.499 for v in order to calculate and compare the M modulus obtained with various methods. Figure 4.12 shows the wide ranges of M values that can be estimated for various test methods. The constrained modulus calculated from SBPM and MASW varies over two orders of magnitudes for a change of v from 0.3 to 0.499. The M values calculated from MASW coincide with those obtained in this study when a value of 0.47 for v is considered for the clay.

4.5.4 Hydraulic heads and vertical gradient in the study area

In previous studies regarding the Lachenaie test sites, groundwater flow direction and velocity were typically estimated from uncorrected water level measurements. Monitoring the pore pressure change over 2 years on site 2 and approximately 1 year on the other test sites provided an opportunity to assess the long-term variation in hydraulic head within the clay layer. Hydraulic heads and vertical gradient were calculated using the corrected pore pressure data. A comparison of the total head values for piezometers AB and AH indicated that groundwater was flowing upward on sites 2, 3, and 4. In contrast, it was flowing downward on sites 6 and 9 during most of the monitoring time. The same flow directions were also deduced from the water levels measured in the wells before the VWP installation. It might be related to the location of sites 6 and 9 which are completed on the top of the sloping ground. Figure 4.13 illustrates short-term

and seasonal variations in the hydraulic head and vertical hydraulic gradient on the study sites. Long-term variation of the hydraulic head through the clay layer is essential for assessing the vertical hydraulic gradient variation over time. This variation plays a crucial role in assessing the migration of contaminant and other chemical species through the clay aquitard (Duhaime et al., 2013b).
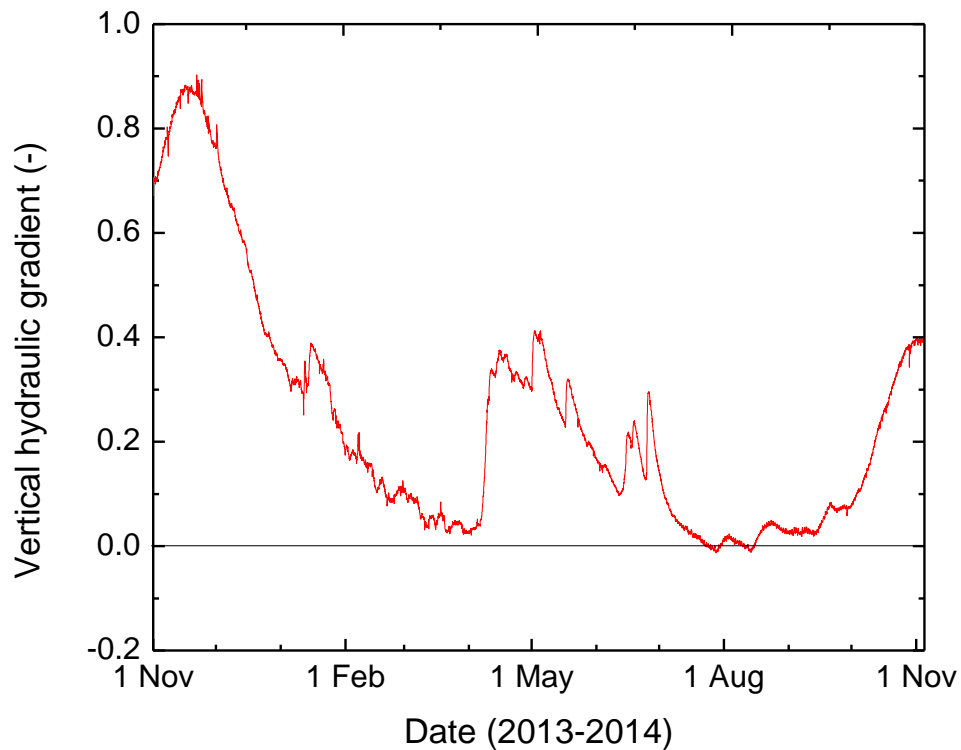
Figure 4.13: Variation of vertical hydraulic gradient from Nov. 2013 to Nov.2014, site 6.

According to our results, the vertical gradient varied between −0.02 and −0.07 on site 2 and between −0.005 and −0.076 on site 4 from July 2013 to November 2014 (a negative gradient implies an upward flow direction). On site 3, a higher vertical gradient of around −0.11 due to the infilling of a nearby landfill cell was observed. However the vertical hydraulic gradient in sites 6 and 9 stayed positive for most of the monitoring period. On site 6, during December 2013 and January 2014, since the Mille-Îles River water level was quite low, a higher vertical gradient close to 1 was observed. The gradient then decreased gradually through winter until a sudden

increase was observed in April 2014, during spring thaw. This gradient decreased and became negative sometime during August and September 2014 (Figure 4.13). The influence of the river stage on the gradient within the clay layer is caused by a change in hydraulic head within the underlying aquifer (fractured shale), which is directly connected to the nearby River. Likewise on site 9, the groundwater flow direction was reversed between 20 July and 20 September 2014.

4.6   Conclusion

This paper describes a comprehensive monitoring program involving the installation of 10 VWPs in a series of sealed boreholes covering an area of around 50 km2 in the Lachenaie region, Quebec. Three methods (linear regression, visual inspection, and multiple regression) provided values for LE within a 10% range. Values for m_v and S_s on the order of 1.0×10^{-6} kPa^{-1} and 1.0×10^{-5} m^{-1} were respectively obtained. The values of m_v obtained in this study are one order of magnitude lower than previous results obtained with pulse tests, and approximately two orders of magnitude lower than those obtained with oedometer tests. The values correspond to compressibility in the range of very small strains. The in situ LE method highlights some practical implications regarding the elastic parameters of the Lachenaie clay associated with a very small strain deformation.

When a pore pressure response is examined, the multiple-regression method has the capacity to distinguish more phenomena than the visual inspection method. For most piezometers, both the multiple regression and the visual inspection methods provided similar corrected pore pressure time series. However, for deep piezometers, the multiple regression technique provided smoother pore pressure time series than the visual inspection method.

The long-term pore pressure monitoring provided an opportunity to recalculate the seasonal variation in hydraulic heads throughout the clay layer. This has allowed monitoring of the long-term variation in vertical hydraulic gradient and vertical flow direction of groundwater. On a yearly basis, the vertical hydraulic gradient changed significantly on some of the Lachenaie study sites, particularly for site 6 in the vicinity of the Mille-Îles River.

4.7 Acknowledgements

4.8 References

Anochikwa, C.I., van der Kamp, G., Barbour, S.L. 2012. Interpreting pore-water pressure changes induced by water table fluctuations and mechanical loading due to soil moisture changes. Can. Geotech. J. **49**, 357-366.

Bardet, J.-P. 1997. Experimental soil mechanics. Prentice Hall Upper Saddle River, NJ.

Bjerrum, L. 1972. Embankments on soft ground. State-of-the-art paper. Proc. A.S.C.E. Conf. Performance Earth and Earth Supported Struct., Purdue Univ., Lafayette, Ind. 2, 1-54.

Black, D.K., Lee, K.L. 1973. Saturated laboratory samples by back pressure. A.S.C.E. J.Soil Mech. Found.Div. **99**, 75-93.

Bozozuk, M. 1963. The Modulus of Elasticity of Leda Clay from Field Measurements. Can. Geotech. J. **1**, 43-51. http://dx.doi.org/10.1139/t63-005.

Bredehoeft, J.D. 1967. Response of well-aquifer systems in earth tides. J. Geophys. Res. **72**, 3075-3087.

Burland, J.B. 1989. Ninth Laurits Bjerrum Memorial Lecture: "Small is beautiful"—the stiffness of soils at small strains. Can. Geotech. J. **26**, 499-516. http://dx.doi.org/10.1139/t89-064.

Butler, J.J., Jr., Jin, W., Mohammed, G.A., Reboulet, E.C. 2011. New insights from well responses to fluctuations in barometric pressure. Groundwater, **49**, 525-533. http://dx.doi.org/10.1111/j.1745-6584.2010.00768.x.

Canadian Geotechnical Society. 2006. Canadian Foundation Engineering Manual. 4th ed. BiTech Publisher, Richmond, BC.

Chapuis, R.P. 2009a. Field variable-head test in low-permeability materials: Assessing the effects of trapped gas pocket and cavity expansion. Can. Geotech. J. **46**, 81-92. http://dx.doi.org/10.1139/T08-106.

Chapuis, R.P. 2009b. Interpreting slug tests with large data sets. Geotech. Testing J. **32**, 139-146.

Chapuis, R.P., Paré, J.J., Loiselle, A.A. 1984. Laboratory test results on self-hardening grouts for flexible cutoffs. Can. Geotech. J. **21**, 185-191. http://dx.doi.org/10.1139/t84-016.

Cherry, J., Parker, B., Bradbury, K., Eaton, T., Gotkowitz, M., Hart, D., Borchardt, M. 2004. *Role of aquitards in the protection of aquifers from contamination: a "state of the science" report*. Waterloo, Ontario: AWWA Res. Found.

Clark, J.I. 1998. The settlement and bearing capacity of very large foundations on strong soils: 1996 R.M. Hardy keynote address. Can. Geotech. J. **35**, 131-145. http://dx.doi.org/10.1139/t97-070.

Crawford, C.B., Burn, K.N. 1963. Discussion of Settlement studies of the Mount Sinai Hospital, Toronto. Eng. Geol. J. **46**, 31-37.

D'Appolonia, D.J., Poulos, H.G., Ladd, C.C. 1971. Initial settlement of structures on clay. ASCE, J. Soil Mech. Found. Div. **97**(SM10), 1359-1377.

Delage, P., Lefebvre, G. 1984. Study of the structure of a sensitive Champlain clay and of its evolution during consolidation. Can. Geotech. J. **21**, 21-35. http://dx.doi.org/10.1139/t84-003.

Domenico, P.A., Schwartz, F.W. 1997. Physical and chemical hydrogeology. 2nd ed. John Wiley, New York.

Duhaime, F. 2012. *Mesure de la conductivité hydraulique du dépôt d'argile Champlain de Lachenaie, Québec: théorie et applications.* Ph.D., École Polytechnique de Montréal.

Duhaime, F., Benabdallah, E.M., Chapuis, R.P. 2013a. The Lachenaie clay deposit: some geochemical and geotechnical properties in relation to the salt-leaching process. Can. Geotech. J. **50**, 311-325. http://dx.doi.org/10.1139/cgj-2012-0079.

Duhaime, F., Benabdallah, E.M., Chapuis, R.P. 2013b. Pore water geochemistry for the Lachenaie clay deposit, Québec. *66th Canadian Geotechnical Conference*, Montréal, Canada.

Duhaime, F., Chapuis, R.P. 2008. Evaluating the effects of clay and gas compressibility during field permeability tests. *61th Canadian Geotechnical Conference and 9th Joint IAH-CNC-CGS Conference*, Edmonton, Canada, 1459-1465.

Duhaime, F., Chapuis, R.P. 2014. A coupled analysis of cavity and pore volume changes for pulse tests conducted in soft clay deposits. Int. J. Numer. Anal. Meth. Geomech. **38**, 903-924. http://dx.doi.org/10.1002/nag.2238.

Dyke, A.S., Moore, A., Robertson, L. 2003. Deglaciation of North America. Geological Survey of Canada Ottawa, ON.

Environment Canada,http://climate.weather.gc.ca/climateData/dailydata_e.html. StationID=5237.

Evans, K., Beavan, J., Simpson, D., Mousa, S. 1991. Estimating aquifer parameters from analysis of forced fluctuations in well level: An example from the Nubian Formation near Aswan, Egypt: 3. Diffusivity estimates for saturated and unsaturated zones. J. Geophys. Res. **96**, 12161-12191.

Ferris, J.G., Knowles, D., Brown, R., Stallman, R.W. 1962. Theory of aquifer tests. U. S. Geological Survey Water-Supply.

Furbish, D.J. 1991. The response of water level in a well to a time series of atmospheric loading under confined conditions. Water Resour. Res. **27**, 557-568. http://dx.doi.org/10.1029/90WR02775.

Galloway, D., Rojstaczer, S. 1988. Analysis of the frequency response of water levels in wells to earth tides and atmospheric loading. Proc.4th Canadian/American Conference on Hydrogeology. Fluid Flow, Heat Transfer and Mass Transport in Fractured Rocks, Dublin, Ohio. 4, 100-113.

Hamouche, K.K. 1995. *Comportement des argiles Champlain sollicitées horizontalement.* Ph.D. thesis, Département de génie civil, Université Laval, Sainte-Foy, Que.

Hare, P.W., Morse, R.E. 1997. Water-Level Fluctuations Due to Barometric Pressure Changes in an Isolated Portion of an Unconfined Aquifer. Groundwater, **35**, 667-671. http://dx.doi.org/10.1111/j.1745-6584.1997.tb00132.x.

Holtz, R.D., Kovacs, W.D. 1981. An introduction to geotechnical engineering. Prentice Hall, Englewood Cliffs, N.J.

Hussein, M.E., Odling, N.E., Clark, R.A. 2013. Borehole water level response to barometric pressure as an indicator of aquifer vulnerability. Water Resour. Res. **49**, 7102-7119. http://dx.doi.org/10.1002/2013wr014134.

Jacob, C.E. 1940. On the flow of water in an elastic artesian aquifer. EOS Trans. AGU. **21**, 574-586. http://dx.doi.org/10.1029/TR021i002p00574.

Judge, G.G., Hill, R.C., Griffiths, W., Lutkepohl, H., Lee, T.C. 1988. Introduction to the Theory and Practice of Econometrics. John Wiley, New York.

Karray, M., Lefebvre, G. 2001. *Étude parasismique pour l'agrandissement du secteur nord-BFI usine de triage Lachenaie LTEE.* Report **GEO-01-07**. Varennes, Québec.

Karray, M., Lefebvre, G. 2008. Significance and evaluation of Poisson's ratio in Rayleigh wave testing. Can. Geotech. J. **45**, 624-635. http://dx.doi.org/10.1139/T08-016.

Karray, M., Lefebvre, G. 2009. Techniques for mode separation in Rayleigh wave testing. Soil Dyn. Earthq. Eng. **29**, 607-619. http://dx.doi.org/10.1016/j.soildyn.2008.07.005.

Karrow, P. 1961. The Champlain Sea and its sediments. *Soils in Canada, Geological Pedological and Engineering Studies*, 97-108.

Klohn, E.J. 1965. The Elastic Properties of a Dense Glacial Till Deposit. Can. Geotech. J. **2**, 116-128. http://dx.doi.org/10.1139/t65-014.

La Rochelle, P., Chagnon, J.Y., Lefebvre, G. 1970. Regional geology and landslides in the marine clay deposits of eastern Canada. Can. Geotech. J. **7**, 145-156. http://dx.doi.org/10.1139/t70-018.

La Rochelle, P., Lefebvre, G. 1971. Sampling disturbance in Champlain clays. *sampleing og soil and rock.* ASTM. STP. **483**, 43-163.

La Rochelle, P., Sarrailh, J., Tavenas, F., Roy, M., Leroueil, S. 1981. Causes of sampling disturbance and design of a new sampler for sensitive soils. Can. Geotech. J. **18**, 52-66. http://dx.doi.org/10.1139/t81-006.

Lefebvre, G., Leboeuf, D., Rahhal, M.E., Lacroix, A., Warde, J., Stokoe Ii, K.H. 1994. Laboratory and field determinations of small-strain shear modulus for a structured Champlain clay. Can. Geotech. J. **31**, 61-70. http://dx.doi.org/10.1139/t94-007.

Leroueil, S., Tavenas, F., Samson, L., Morin, P. 1983. Preconsolidation pressure of Champlain clays. Part II. Laboratory determination. Can. Geotech. J. **20**, 803-816. http://dx.doi.org/10.1139/t83-084.

Marefat, V., Duhaime, F., Chapuis, R.P. 2015. Fully grouted piezometers: Implications for pore pressure measurement in clay layers. Eng. Geol. J. **(submitted)**.

McKenna, G.T. 1995. Grouted-in installation of piezometers in boreholes. Can. Geotech. J. **32**, 355-363.

Merritt, M.L. 2004. Estimating hydraulic properties of the Floridan aquifer system by analysis of earth-tide, ocean-tide, and barometric effects, Collier and Hendry Counties, Florida. U. S. U.S. Geol. Surv. Water Resour. Invest. Rep. 03-4267, 4203–4267.

Mitchell, R.J. 1970. On the yielding and mechanical strength of Leda clays. Can. Geotech. J. **7**, 297-312. http://dx.doi.org/10.1139/t70-036.

Occhietti, S. 1989. Quaternary geology of St. Lawrence Valley and adjacent Appalachian subregion. In Quaternary geology of Canada and Greenland. Edited by R.J. Fulton. Geological Survey of Canada, Ottawa, Ont. 319–388.

Parent, M., Occhietti, S. 1988. Late Wisconsinan deglaciation and Champlain sea invasion in the St. Lawrence valley, Québec. Géographie physique et Quaternaire, **42**, 215-246.

Rasmussen, T.C., Crawford, L.A. 1997. Identifying and removing barometric pressure effects in confined and unconfined aquifers. Groundwater, **35**, 502-511.

Rasmussen, T.C., Mote, T.L. 2007. Monitoring Surface and Subsurface Water Storage Using Confined Aquifer Water Levels at the Savannah River Site, USA. Vadose Zone J. **6**, 327-335. http://dx.doi.org/10.2136/vzj2006.0049.

Seo, H.H. 1999. *Modeling the response of ground-water levels in wells to changes in barometric pressure.* Ph.D., Iowa State University.

Shibuya, S., Hwang, S.C., Mitachi, T. 1997. Elastic shear modulus of soft clays from shear wave velocity measurement. Geotechnique, **47**, 593-601.

Silvestri, V. 2003. Assessment of self-boring pressuremeter tests in sensitive clay. Can. Geotech. J. **40**, 365-387. http://dx.doi.org/10.1139/t02-121.

Silvestri, V., Abou-Samra, G. 2008. Analysis of instrumented sharp cone and pressuremeter tests in stiff sensitive clay. Can. Geotech. J. **45**, 957-972. http://dx.doi.org/10.1139/T08-028.

Simeoni, L. 2012. Laboratory tests for measuring the time-lag of fully grouted piezometers. J. Hydrol.**438-439**, 215-222. http://dx.doi.org/10.1016/j.jhydrol.2012.03.025.

Skempton, A. 1954. The pore-pressure coefficients A and B. Geotechnique, **4**, 143-147.

Smerdon, B.D., Smith, L.A., Harrington, G.A., Gardner, W.P., Delle Piane, C., Sarout, J. 2014. Estimating the hydraulic properties of an aquitard from in situ pore pressure measurements. Hydrogeol. J. **22**, 1875-1887. http://dx.doi.org/10.1007/s10040-014-1161-x.

Smith, L.A., Van Der Kamp, G., Jim Hendry, M. 2013. A new technique for obtaining high-resolution pore pressure records in thick claystone aquitards and its use to determine in situ compressibility. Water Resour. Res. **49**, 732-743. http://dx.doi.org/10.1002/wrcr.20084.

Sorensen, J.P.R., Butcher, A.S. 2011. Water Level Monitoring Pressure Transducers—A Need for Industry-Wide Standards. Ground Water Monit. R. 31, 56-62. http://dx.doi.org/10.1111/j.1745-6592.2011.01346.x.

Spane, F.A. 2002. Considering barometric pressure in groundwater flow investigations. Water Resour. Res. **38**, 14-11-14-18.

Spane, F.A., Mackley, R.D. 2011. Removal of River-Stage Fluctuations from Well Response Using Multiple Regression. Groundwater, **49**, 794-807.

Tavenas, F., Leroueil, S. 1977. The effect of stresses and time on yielding of clays. *9th International Conference Soil Mechanics and Foundation Engineering*, Tokyo, 319-326.

Tavenas, F.A., Chapeau, C., Rochelle, P.L., Roy, M. 1974. Immediate Settlements of Three Test Embankments on Champlain Clay. Can. Geotech. J. **11**, 109-141. http://dx.doi.org/10.1139/t74-008.

Terzaghi, K., Peck, R., Mesri, G. 1996. Soil mechanics in engineering practice, 3rd ed. John Wiley, New York.

Timms, W.A., Acworth, R.I. 2005. Propagation of pressure change through thick clay sequences: an example from Liverpool Plains, NSW, Australia. Hydrogeol. J. **13**, 858-870. http://dx.doi.org/10.1007/s10040-005-0436-7.

Toll, N.J., Rasmussen, T.C. 2007. Removal of barometric pressure effects and earth tides from observed water levels. Groundwater, **45**, 101-105.

van Camp, M., Vauterin, P. 2005. Tsoft: graphical and interactive software for the analysis of time series and Earth tides. Comput. Geosci. **31**, 631-640.

van der Kamp, G. 2001. Methods for determining the in situ hydraulic conductivity of shallow aquitards – an overview. Hydrogeol. J. **9**, 5-16.

van der Kamp, G., Gale, J.E. 1983. Theory of Earth tide and barometric effects in porous formations with compressible grains. Water Resour. Res. **19**, 538-544.

Viggiani, G., Atkinson, J.H. 1995. Stiffness of fine-grained soil at very small strains. Geotechnique, **45**, 249-265.

Von Asmuth, J.R., Maas, K., Bakker, M., Petersen, J. 2008. Modeling Time Series of Ground Water Head Fluctuations Subjected to Multiple Stresses. GroundWater, **46**, 30-40. http://dx.doi.org/10.1111/j.1745-6584.2007.00382.x.

Weeks, E.P. 1979. Barometric fluctuations in wells tapping deep unconfined aquifers. Water Resour. Res. **15**, 1167-1176.

Yong, R.N., Silvestri, V. 1979. Anisotropic behaviour of a sensitive clay. Can. Geotech. J. **16**, 335-350. http://dx.doi.org/10.1139/t79-033.

Youd, T.L., Idriss, I.M., Andrus, R.D., Arango, I., Castro, G., Christian, J.T., Dobry, R., Finn, W.D.L., Harder, L.F., Hynes, M.E., Ishihara, K., Koester, J.P., Liao, S.S.C., Marcuson, W.F., Martin, G.R., Mitchell, J.K., Moriwaki, Y., Power, M.S., Robertson, P.K., Seed, R.B., Stokoe, K.H. 2001. Liquefaction Resistance of Soils: Summary Report from the 1996 NCEER and 1998 NCEER/NSF Workshops on Evaluation of Liquefaction Resistance of Soils. J. Geotech. Geoenviron. Eng. **127**, 817-833.

CHAPTER 5   ARTICLE 3 : ESTIMATES OF IN-SITU VERTICAL AND HORIZONTAL HYDRAULIC DIFFUSIVITY AND CONDUCTIVITY FOR A SHALLOW CLAY AQUITARD, USING A COMBINED NATURAL RECHARGE AND BAROMETRIC PRESSURE RESPONSE APPROACH

Vahid Marefat[1*], François Duhaime[2], Robert P. Chapuis[1] and Frank A. Spane[3]

Submitted to *Journal of Hydrology*, January 2015.

[1] Department of Civil, Geological and Mining Engineering, Ecole Polytechnique, P.O. Box 6079, Stn CV, Montreal, Quebec, Canada, H3C 3A7

[2] Laboratory for Geotechnical and Geoenvironmental Engineering (LG2), École de technologie supérieure, 1100 Notre-Dame Ouest, Montreal, QC, Canada, H3C 1K3

[3] Environmental Systems/Earth Systems Science Division, Pacific Northwest National Laboratory, Richland, Washington 99352.

[*]Corresponding author: Phone +1-438-931-9797; fax +1-514-340-4477-Email:vahid.marefat@polymtl.ca

Abstract

The hydrologic response of open and closed wells to barometric pressure changes and cyclic groundwater flow recharge events in a shallow aquifer/aquitard system can be used to determine the composite vertical and horizontal hydraulic diffusivity and conductivity for the intervening clay aquitard. The assessment of aquitard hydraulic properties is important to appraise the vulnerability of drinking water supplies in shallow confined aquifers from surficial contamination. This paper presents a novel analysis approach combining low- and high-frequency well water-level/pressure head to characterise shallow clay aquitard hydraulic properties and permeability anisotropy. Spectral frequency analysis of long-term cyclic groundwater flow recharge events were applied for assessing the in-situ vertical hydraulic diffusivity. Loading efficiencies determined from barometric head response function (BHRF) analysis provided the basis for direct determination of in-situ specific storage which, when applied to the vertical hydraulic diffusivity calculation, yields an in-situ vertical hydraulic conductivity for the clay aquitard. In addition, BHRF analysis of the associated pore pressure

response obtained from time-domain, multiple-regression was used to determine horizontal hydraulic conductivity of the clay aquitard. This combined analytical approach (i.e., spectral analysis of long-term natural recharge events and short-term barometric loading analysis) allows the determination of vertical and horizontal clay aquitard hydraulic property information without conducting extensive hydrologic field characterization tests.

Keywords: Champlain clay, Barometric response function, groundwater recharge cycle, Hydraulic diffusivity, Hydraulic conductivity, Anisotropy, Numerical modeling.

5.1 Introduction

Vertical hydraulic conductivity, K_v, of clay aquitards is a fundamental parameter in controlling surface and near-surface recharge and contaminant migration to underlying aquifers (e.g., Cherry et al., 2004; Bradbury et al., 2006). When permeability anisotropy is present, horizontal hydraulic conductivity, K_h, is also important for contaminant migration, settlement rates of consolidated clays, design of a drainage system, and optimum design of water well fields (e.g., Chapuis and Gill, 1989). This paper demonstrates a novel combined analysis approach utilizing aquifer/aquitard natural response to barometric pressure fluctuations and cyclic groundwater flow/recharge events, which can be used for assessing in-situ horizontal and vertical hydraulic diffusivity and conductivity of the clay aquitard systems.

When an aquitard is heterogeneous, in-situ measurements are expected to yield *K* values that are more representative of large-scale in-situ conditions than laboratory core results (Bradbury and Muldoon, 1990; Bredehoeft et al., 2008). Due to their inherent small size, core samples commonly used in laboratory tests often provide small-scale, matrix permeability estimates, which may not adequately represent large-scale aquitard conditions. In addition, soft or sensitive aquitard samples, such as Champlain clay sample, can be easily disturbed by the core-sampling process, which may then yield non-representative results for actual in-situ conditions. Because of this potential bias in laboratory core test results, in-situ tests to determine *K* values are preferable for most engineering/hydrologic characterization applications (Benson et al., 1994; Benson et al., 1997; van der Kamp, 2001b; Chapuis, 2002; Duhaime, 2012).

Natural clays are known to develop some hydraulic conductivity anisotropy during deposition

and densification processes (e.g., Chan and Kenney, 1973; Al-Tabbaa and Wood, 1987; Chapuis and Gill, 1989; Scholes et al., 2007). In clay-rich sediments, the permeability anisotropy is caused by changes in grain-particle orientation, pore size and shape distribution (Neuzil, 1994). Laboratory assessments of the permeability anisotropy are well documented in the literature for granular soils (e.g., Witt and Brauns, 1983; Chapuis and Gill, 1989; Chapuis et al., 1989) and for clays (Mitchell, 1956; Al-Tabbaa and Wood, 1987; Scholes et al., 2007). For large-scale field condition, clay aquitard anisotropy is traditionally assessed based on combined hydrologic tests of partially penetrating slug tests (Hvorslev, 1951) and aquifer pumping tests with leakage from clay aquitard (Hantush, 1956). These field test methods however, may not be adaptable for a wide-range of field test conditions. This paper proves that the analysis of low to high-frequency natural pore pressure response of associated well/piezometer can be used alone for the in-situ assessment of permeability and its anisotropy.

As it is widely recognized for aquifers, well water-level/pore pressure in low permeability clay aquitards also responds to various natural stress changes including barometric pressure change, Earth and ocean-tide fluctuations, precipitation and groundwater recharge/discharge events (e.g., Anochikwa et al., 2012; Hussein et al., 2013; Smith et al., 2013; Marefat et al., 2015b). Among the variety of natural stress sources with varying frequency, short-term barometric stress loading and long-term groundwater recharge/discharge events deserve more attention. Hydrogeologists have long been interested in opportunistically taking advantage of these natural stress responses in monitoring wells for determination of aquifer/aquitard properties (e.g., van der Kamp and Gale, 1983; Rojstaczer, 1988a; Keller et al., 1989; Neuman and Gardner, 1989; Timms and Acworth, 2005; Butler et al., 2011; Hussein et al., 2013; Smith et al., 2013; Smerdon et al., 2014). This opportunistic approach is particularly useful where groundwater is contaminated and conventional in-situ tests may be limited (Furbish, 1991).

In a perfectly confined aquifer of moderate permeability, well water-level responses associated with barometric stress changes are considered to be instantaneous (Jacob, 1940; Ferris et al., 1962). The ratio of the associated well water-level response to the barometric pressure change is referred to as the barometric efficiency, BE, of the well/aquifer system (Jacob, 1940; Rojstaczer, 1988a; Rasmussen and Crawford, 1997; Spane, 2002). BE represents that portion of the barometric stress borne by the rigidity of the aquifer solid matrix. Parameter BE differs from loading efficiency, LE, which reflects the ratio of change in aquifer total head (absolute pressure)

to the change in barometric stress (i.e., that portion of the barometric stress borne by aquifer pore fluid). As noted in the classic hydrologic papers by Jacob (1940) and Ferris et al. (1962), loading efficiency is related to the barometric efficiency by the relationship LE + BE= 1 (note: loading efficiency is referred to as "tidal efficiency" in these early classical papers). By contrast, when a well-water level/pressure head response to barometric stress change is not instantaneous (e.g., unconfined aquifer with thick unsaturated zone or confined aquifer with borehole storage and skin effects), the pore pressure response is delayed and the barometric/loading efficiency becomes time-lag dependent (Weeks, 1979; Furbish, 1991). In this case LE is described by a barometric head response function, BHRF, which can be analyzed using the time-domain multiple regression method as described in Spane (1999, 2002).

The barometric response function (BRF) and the BHRF represent two sets of complementary functions. BRF describes the time-dependent response of a well water-level to a unit change in barometric pressure, which is a function of BE. On the other hand, BHRF describes the time-dependent total head response associated with a unit change in barometric pressure, which is a function of LE = 1-BE (Spane, 2002).

Analysis of long-term, low-frequency groundwater recharge cycles for an aquifer/aquitard system can be used to determine the in-situ vertical hydraulic diffusivity, D_v of the overlying clay aquitard interval (where $D_v = K_v/S_s$; and S_s is specific storage, and K_v is vertical hydraulic conductivity for the clay aquitard) (Keller et al., 1989; Neuman and Gardner, 1989). The amplitude of the groundwater recharge cycle imposed by the surficial aquifer is attenuated and lagged while propagating downward within the clay aquitard. The associated attenuation in the amplitude response for a given signal period is required for vertical hydraulic diffusivity calculation. Keller et al. (1989) simply subtracted the associated well hydrographs to calculate the attenuation in the groundwater recharge amplitude. This paper, however, utilizes spectral frequency analysis using Fast Fourier Transform, FFT, to refine the amplitude and frequency content analysis for major annual groundwater recharge cycles.

This paper discusses a novel approach based on a combined analysis to assess in-situ hydraulic properties and permeability anisotropy for shallow aquitard formations. The results obtained from an extensive baseline monitoring program of natural pore pressure response of a shallow aquifer/aquitard system near Montreal, Quebec, Canada, are presented. Two significant

hydrologic phenomena are identifiable at the observation sites: 1) an immediate short-term, high-frequency, pressure head response associated with barometric pressure fluctuations and 2) a long-term, low-frequency, downward propagation of cyclic groundwater flow/recharge events within the clay aquitard to the underlying confined aquifer. The first objective of the combined analysis approach as presented in this paper is to estimate the in-situ vertical hydraulic diffusivity. The D_v was obtained from frequency analysis of the associated annual recharge pressure head amplitude for various clay aquitard locations. Loading efficiencies determined from BHRF analysis provided the basis for direct determination of in-situ specific storage which, when applied to the vertical hydraulic diffusivity calculation, yields an in-situ vertical hydraulic conductivity, K_v for the clay aquitard. The second objective was to determine the horizontal hydraulic conductivity, K_h, for the clay aquitard by fitting the observed BHRF response based on time-domain, multiple-regression relationships with numerical results for groundwater flow around the well intake zones. To the authors' knowledge, this is the first assessment of the in-situ values for composite vertical and horizontal hydraulic diffusivity-conductivity for a compressible clay aquitard formation using a multi-timescale analysis of naturally occurring groundwater/pressure head fluctuations with varying frequencies.

5.2   Material and methods

5.2.1   Study site description and piezometer installation

The study area is described in Duhaime et al. (2013) and includes nine (9) monitoring sites with a combined area of around 50 km^2 in Lachenaie near Montreal, Canada. Five sites (i.e., sites 2, 3, 4, 6, and 9) identified in Figure 5.1 are undergoing long-term monitoring of baseline pore pressure. The monitoring sites are bounded to the east by the Mascouche River and to the south by the Mille-Iles River.

The clay within the study area is typical, albeit relatively stiff, Champlain clay. It is bounded by two layers above and below that are several orders of magnitude more permeable. The top layer is composed of sand of alluvial or eolian origin and up to 5 m of fissured and oxidized clay. The altered part of the clay layer is often referred to as the crust in geotechnical engineering. Under the crust, the unoxidized part of the clay deposit has a thickness varying between 11 and 25 m

depending on the study site. The degree of overconsolidation is relatively high for a Champlain clay deposit. This is due to the erosion of part of the clay profile (Duhaime et al. 2013). Below the intact clay is a till layer and the fractured upper portion of the shale bedrock. Their combined thickness varies between 6 and 10 m.
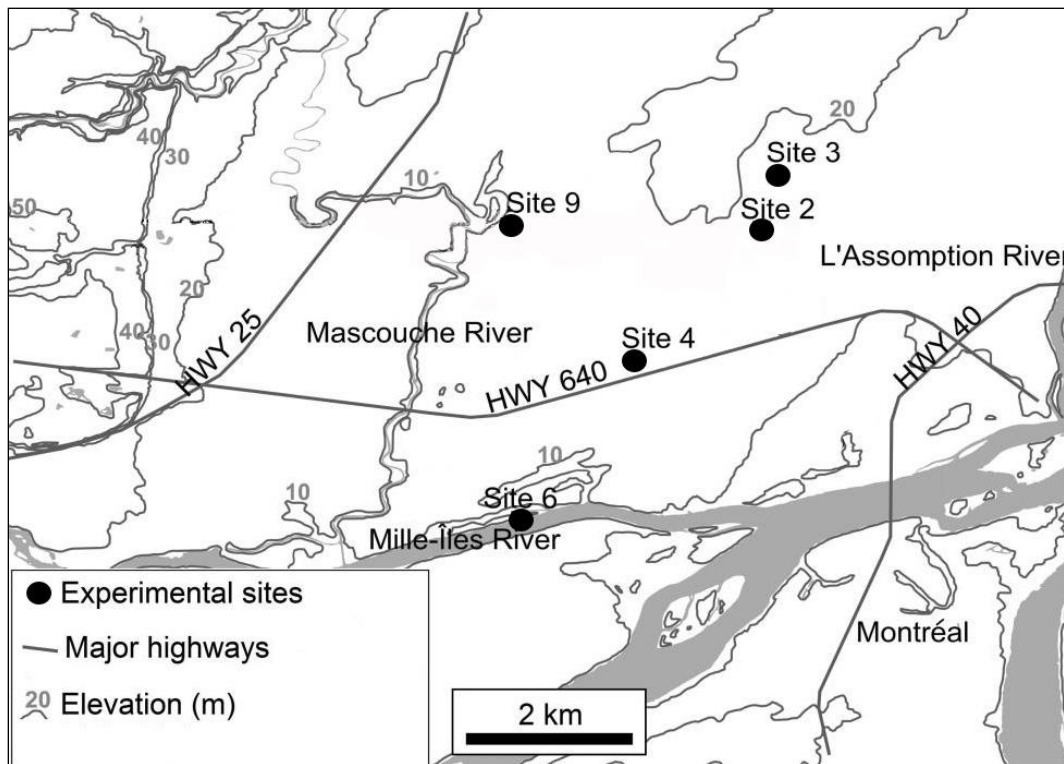
Figure 5.1: Location and identification of the test sites, adapted from Duhaime et al., (2013).

Pore pressures have been monitored since November 2012 at site 2 and October 2013 at the other observation sites (Figure 5.1). Figure 5.2 shows a schematic representation of the monitoring well and pressure transducer installations. Three monitoring wells (MWs) labelled AH, AB, and R were completed on each observation site. Drilling was conducted using a wash-boring technique (Duhaime et al. 2013). In the clay layer, the intake zone of each MW was "carved" using a thin-walled tube sampler to minimize clay disturbance. Two vibrating wire absolute pressure transducers (VWPs) were sealed at the upper and lower thirds of the clay layer. The VWPs were sealed in pre-existing MWs with 2-inch PVC riser pipes. The VWPs have a full-

scale range of 350 kPa and a resolution of 0.01 kPa (1 mm of water). To assess the surficial hydraulic head perturbation at the top of the aquitard/aquifer system, standpipe piezometers, labelled S, with a 20 mm diameter and a 40 cm long slotted tip were completed on each site within shallow boreholes that reached immediately below the ground water table. Commercial filter sand 000 with $C_U=2.0$ and $d_{10}<0.2$ were used in this study, where $C_U = d_{60}/d_{10}$ is the coefficient of uniformity, and d_{10} and d_{60} are the grain diameters at which 10 and 60 % of the solid mass is finer.
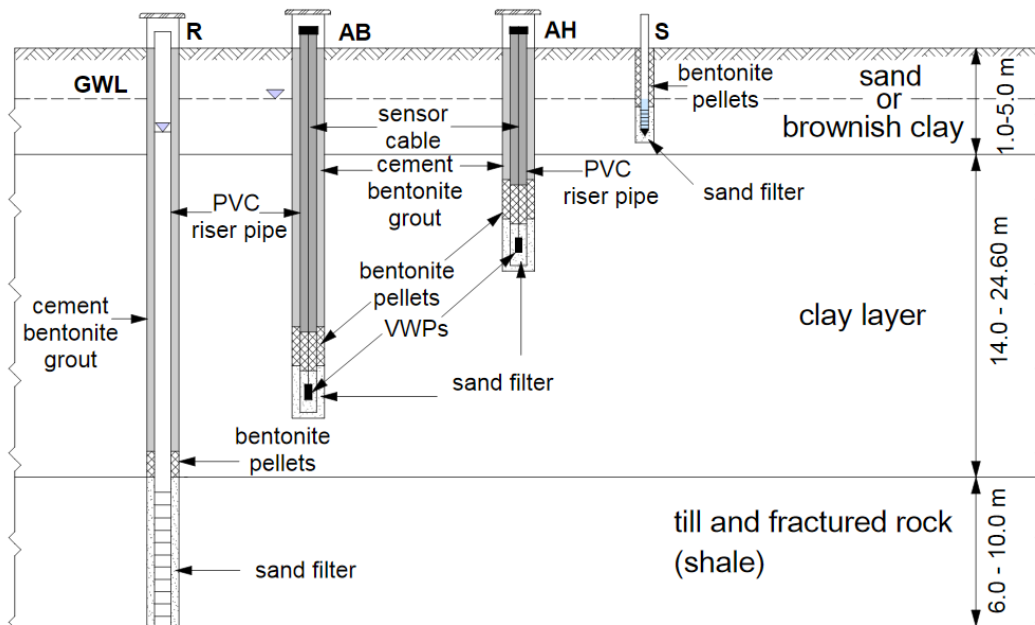
Figure 5.2: Vertical view of MWs and VWPs installation.

Water-level fluctuations within well R and piezometer S were recorded using two absolute pressure transducers with full scale range of 100 kPa, and with resolution and accuracy of 0.02 and 0.1 kPa (0.2 and 1 cm of water) respectively. It should be noted that, unlike differential gauge pressure transducers, absolute pressure transducers measure the sum of water and atmospheric pressures rather than the pressure due to the water column above the sensor for an open well. For a closed well, an absolute VWP measures pore pressure (static and transient components) plus the difference between barometric pressures at the monitoring site, B, and the mean barometric pressure at sea level (B_{sea}). Changes in atmospheric pressure were recorded at

each monitoring site using an atmospheric pressure transducer attached in the well protectors. These atmospheric pressure transducers have a full scale range of 15 kPa, with accuracy and resolution of respectively 0.05 and 0.01 kPa (5 and 1 mm of water). The transducers for the barometric pressure, absolute pressure in wells, and VWPs within the clay aquitard were synchronized and data were recorded electronically every 15 minutes.

VWPs can be installed according to the fully grouted or conventional sand pack methods (McKenna, 1995; Marefat et al., 2015a). In this study, the conventional method with a sand filter around the VWP in the well cavity was used for the VWP installations. The installation was completed in three steps. Special care had to be taken to avoid trapping air bubbles into the sand filters. The presence of entrapped air in sand packs may slow the pore pressure response and influence the results of field permeability tests (van der Kamp, 2001b; Chapuis, 2009b). The first step was the degassing of the MWs. To do so, a 30 kPa vacuum was applied on each MW for around 24 hours in order to extract as much gas as possible from the MWs sand cavity before the installation. For the second step, the VWPs were placed in 1.0 to 1.3 m long saturated sand filters at the depth of the pre-existing monitoring wells screens. A 20 cm thick layer of saturated sand was first poured with water into the MWs riser pipe. After having positioned the VWPs at the proper depth, an extra layer of saturated sand of 0.80 to 1.10 m thickness was poured with water into the MW. The final step was plugging the PVC riser pipe with sealing material. Hence, the sand filter was plugged with 0.90 m of coated bentonite pellets and the remaining part of the MW riser pipe was backfilled with cement-bentonite grout from the bottom to the ground surface. More detail on VWP installation can be found in Marefat et al. (2015b).

5.2.2 Estimation of in-situ vertical hydraulic conductivity-diffusivity

As noted previously, the downward propagation of a surficial/boundary pressure head cycle through an underlying clay layer is primarily controlled by the vertical hydraulic diffusivity of the clay aquitard (Keller et al., 1989; Neuman and Gardner, 1989) and the frequency of the surficial/boundary pressure head cycle (Van der Kamp and Maathuis, 1991). Keller et al. (1989) utilized a model based on the water conservation equation for transient vertical flow to estimate the D_v for clay aquitards. It should be noted that the same analytical model was derived previously by Ferris (1952) for describing the propagation of uniform river-stage fluctuations to

a neighboring well for the purpose of assessing aquifer transmissivity/storativity conditions. The obtained D_v values can be used to characterize the potential for contaminant migration through the clay aquitard to the aquifer (e.g., Hussein et al., 2013; Odling et al., 2015). Hydraulic diffusivity is calculated from the amplitude and period of the cyclic pressure wave with depth. For a sinusoidal fluctuation (e.g., annual pore pressure cycle in a clay formation), the amplitude of the attenuated pressure head (α_z) at depth z can be calculated using the following relationship (Ferris, 1952; Keller et al., 1989):

$$\alpha_z = \alpha_s \, exp[-z\pi/C] \tag{5.1}$$

where α_s and a_z are the pressure head amplitude at the top of the aquitard and at depth z respectively, and C is the relative penetration depth which can be calculated as follows (Keller et al., 1989):

$$C = \sqrt{\pi D_v T_P} \tag{5.2}$$

where T_P is the period of the fluctuation. The calculation of the pressure head amplitude ratio (i.e., α_z/α_s) allows D_v to be determined as described in Keller et al. (1989) using the following equation:

$$D_v = \frac{z^2 \pi}{T_P} \left[ln\left(\frac{\alpha_z}{\alpha_s}\right) \right]^{-2} \tag{5.3}$$

Vertical hydraulic diffusivity, D_v, is a function of both vertical hydraulic conductivity and storage properties of the media. The vertical hydraulic conductivity for the clay aquitard can be calculated using its in-situ S_s value ($K_v = D_v \times S_s$). The in-situ specific storage values can be calculated from the in-situ loading efficiency BHRF, the total pressure head response to barometric pressure change registered by the piezometers. As noted originally by Jacob (1940, 1950), S_s can be determined from LE using the following relationship:

$$S_s = \rho_w g n \beta_w \left[1/(1-LE) \right] \tag{5.4}$$

where ρ_w is the water density for the monitored test interval, g the gravity acceleration, n the test interval porosity, and β_w the compressibility of the test interval water taken as 4.6×10^{-7} kPa^{-1} at $20°$C. The LE value can be calculated with several techniques, for example using a multiple regression (Spane, 1999; Spane, 2002; Marefat et al., 2015b).

5.2.3 Time-domain barometric head response function (BHRF)

Atmospheric pressure fluctuations can be considered as areal, extensive stresses applied directly to both the land and water surface in open wells (Spane, 2002). The groundwater flow between well and formation caused by barometric pressure changes is governed by the loading efficiency, LE, which is fully expressed after the pressure imbalance between the well and the formation is completely equilibrated. Rasmussen and Crawford (1997) proposed the BRF concept to describe the well water-level response over time for a step change in barometric pressure. With the time domain approach, the BRF is an impulse response function. It is obtained by performing a multiple regression. Spane (2002) found an inverse response function (1-BE) using aquifer total head response instead of well water-level response in BRF calculation. This is the case of the current study because absolute pressure transducers were used for pressure head measurement. When the total head response is used instead of the water-level response, the impulse function becomes the BHRF.

A linear set of multiple-regression equations can be written between absolute pore pressure changes and barometric stress changes as follows (e.g., Rasmussen and Crawford, 1997; Spane, 2002):

$$\Delta u_t = \alpha_0 + \delta_0 (\Delta B)_t + \delta_1 (\Delta B)_{t-1} + ... + \delta_n (\Delta B)_{t-m} + \varepsilon \tag{5.5}$$

where Δu_t is the absolute pore pressure change $u_t - u_{t-1}$, $(\Delta B)_t = B_{t+1} - B_t$ is the atmospheric pressure change, $(\Delta B)_{t-1} = B_t - B_{t-1}$ is the atmospheric pressure change for the previous time step, $(\Delta B)_{t-m}$ is the atmospheric pressure change for the mth previous time step, α_0 is the regression intercept, δ_0 $...\delta_n$ are the regression coefficients associated with time lags of 0 to M, and ε is the residual error term. The regression coefficients can be determined by ordinary least squares (OLS).

Similarly to the BRF, a BHRF can also be constructed by gradually summing up the regression coefficients to M number of the associated time lag. For example, the BHRF time-lag value is equal to δ_0 for a time lag of 0, and it is equal to $\delta_0 + \delta_1 + \delta_2 + \delta_3$ for a time-lag of 3 time steps:

$$\mathrm{BHRF} = \sum_{i=0}^{i=M} \delta_i \tag{5.6}$$

5.2.4 Estimation of in-situ horizontal hydraulic conductivity

Barometric response and BRF analysis have commonly been presented in a type-curve format (in both time and frequency domains) to determine hydraulic properties for various aquifer/aquitard system relationships (Weeks, 1979; Rojstaczer, 1988a; Evans et al., 1991; Furbish, 1991; Butler et al., 2011; Hussein et al., 2013). Of pertinence to this paper, previous studies performed by Butler et al. (2011) and Hussein et al. (2013) fitted BRF from a confined aquifer responses with an analytical model to determine the vertical hydraulic diffusivity for the overlying confining layer/clay aquitard system. These previous studies however, did not analyze actual aquitard pressure responses obtained from partially penetrating wells within clay aquitard as a basis for estimating in-situ clay aquitard hydraulic properties (i.e., both vertical and horizontal).

For a closed well that is partially penetrating the Lachenaie clay deposit, the absolute pore pressure response to barometric pressure change is delayed due to pressure imbalance between the borehole and the surrounding clay layer and due to the low permeability of the clay (Marefat et al., 2015b). The delayed response is due to the time required for pressure in the borehole to equilibrate with the surrounding media. This time-lag depends upon the formation properties and well bore storage and skin conditions (Furbish, 1991; Spane, 2002). The resulting pressure imbalance implies transient groundwater flow between the piezometer and the formation. This groundwater flow is essentially horizontal. As shown in Figure 5.3, for absolute pressure measurements in the Lachenaie clay aquitard, a concave downward pattern for BHRF was calculated by Marefat et al. (2015b) using the time-domain multiple regression method as described in Spane (1999, 2000). The general shape of the BHRF response pattern shown in Fig. 6.3 appears to conform to the pressure behavior of a highly compressible (i.e., LE = 0.81), composite confined aquifer system with wellbore storage as proposed by Spane (1999, 2002).

Furbish (1991) noted that the early-time, wellbore-storage dominated, pressure imbalance between borehole and formation associated with barometric stress changes can be treated as an individual step change in pressure (i.e., $\Delta BP \times LE$) which is imposed to the well/aquifer system. The imposed atmospheric load step can be considered as a specific well slug (for open wells) or a pressurized slug/pulse test (for closed well conditions). These can be used to estimate the permeability of the geological units that immediately surround the well (Spane, 2002). Rasmussen and Crawford (1997) adapted the Hvorslev (1951) slug test model to describe the

pressure imbalance between borehole and formation, due to a unit change in barometric pressure, and its relationship with BRF. However, because of limiting assumptions in the Hvorslev (1951) model with respect to wellbore storage and aquifer storativity/elasticity, Spane (2002) suggested that an interpretation based on the Cooper et al. (1967) solution could be more effective to describe the delayed response of a borehole/test interval to barometric pressure change.
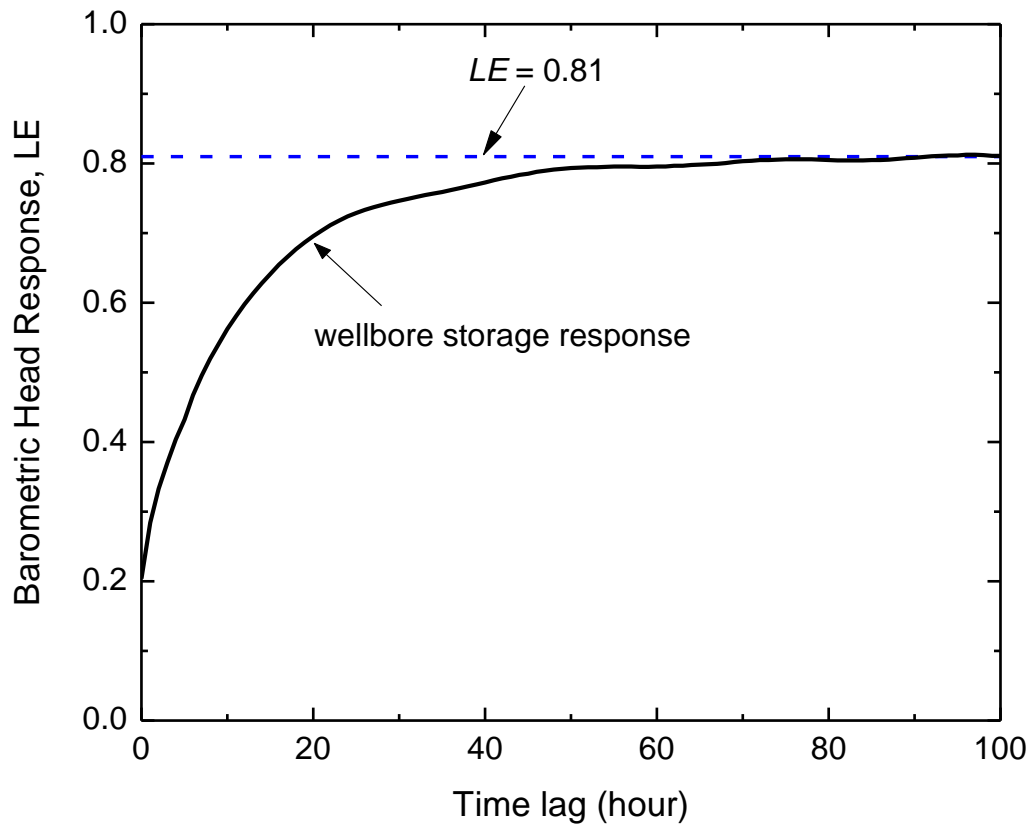
Figure 5.3: Typical BHRF of absolute pressure head for closed piezometers completed within Lachenaie clay, modified from Marefat et al. (2015a).

Since numerical approaches provide greater latitude (e.g., aquitard heterogeneities and layering) that are not easily addressed with analytical methods, the finite-element code SEEP/W (Krahn, 2004), a computer code developed by GEO-SLOPE International, was used for modeling transient seepage between the closed-piezometer system and the clay aquitard. The horizontal

hydraulic conductivity of the Lachenaie clay was determined by fitting the observed BHRFs to the predicted numerical model type-curves.

5.2.5 Numerical modeling

The loading and unloading associated with barometric pressure is equivalent to a continuous series of slug/bail tests for an undrained loading condition (Furbish, 1991). In this study, a numerical model was used to predict the pressure head equalization in a closed-piezometer system following an instantaneous pressure change in the clay aquitard. The pressure head equilibration following a unit change in barometric pressure was modeled as a slug/pulse test, an analog to the well response associated with a unit change in barometric pressure as defined by the BHRF.

Type curves for BHRF curve fitting were defined from the numerical results to determine the aquitard horizontal hydraulic conductivity. Because the pressure change is applied in the piezometer in the numerical model instead of in the aquitard as it is the case with barometric loading, the raw numerical type curves are a mirror image of the observed BHRF. For direct comparison with the BHRF, the numerical type curves were inverted. For curve fitting, the *x*-axis of the type curves is the time variable from the numerical simulations and the *y*-axis is *(1-H(t)/H(t=0))×LE,* where *H(t=0)* and *H(t)* are respectively the initial and subsequent differences in hydraulic head within the well cavity during the simulation.

Slug tests and seepage around boreholes can be simulated numerically with finite element code SEEP/W (Chapuis, 1998; Chapuis and Chenaf, 2002; Chapuis, 2005; Chapuis, 2009a; Duhaime, 2012). This software package solves steady state and transient flow problems for saturated and unsaturated soils. It solves the complete Richards' (1931) equation for mass conservation of water and Darcy's law for seepage.

Figure 5.4 shows a vertical view of the numerical model used in this study. The axisymmetric model has a 10 m radius and includes a borehole similar to the AB and AH MWs which are completed on each site. Its height of 24.6 m is representative of the thickness of the saturated clay layer for site 2.

The numerical simulations were carried out in three steps. The first step was to model a steady-

state condition which was used as an initial condition for the subsequent transient simulation. The initial condition was set by applying an arbitrary constant total head of 25.0 m as a boundary condition to the model. The second step was to model a first transient condition which corresponds to a sudden increase of 10.20 cm in hydraulic head (i.e., a 1 kPa pressure increase) within the sealed sand cavity. To do so, a total head versus time boundary condition, $H(t)$, was applied to the interface between the well/piezometer sand pack and the clay layer. The total head was increased from 25.000m to 25.102 m in 1 second. The main purpose of this transient change in boundary condition is to avoid numerical oscillation of the primary variable, here the hydraulic head, that can be observed when an instantaneous change in boundary conditions is applied on a model (Zienkiewicz et al., 2005). The final step was to model the dissipation through time of the hydraulic head difference between the sand cavity and the clay formation. This step was initiated with a new boundary condition relating the hydraulic head versus the water volume outflow, $H(V)$. It was applied to the interface between the well/piezometer sand pack and the clay layer.

The slope of the $H(V)$ boundary condition can be calculated from the relationship between changes in cavity volume and cavity pressure. During hydraulic head equilibration between the sand pack and clay formation, the volume of water leaving the cavity is equal to an initial cavity expansion. For pulse tests conducted in clay, assuming linear elasticity, the volume change of an isolated cavity is linearly related to the change in cavity pressure (Δp) through the shear modulus, G, as follows (Duhaime and Chapuis, 2014):

$$\Delta p = G\left(\frac{\Delta V_{cavity}}{V_{cavity}}\right) \tag{6.7}$$

where ΔV_{cavity} is the cavity volume change and $V_{cavity} = \pi d^2 L/4$ is the cavity volume. Because of the linear relationship between ΔV_{cavity} and Δp, the relationship between the dimensionless head change from the numerical simulations (i.e., $H(t)/H(t=0)$) and time is unique for a given G value for the surrounding clay. It does not depend on the initial Δp value. This was verified for Δp values of 1, 5, and 10 kPa. Thus an initial cavity pressure change of 1 kPa was considered in the numerical simulations (i.e., step 2). Duhaime and Chapuis (2014) obtained G values for the same series of monitoring wells with pulse tests. In the numerical model, ΔV_{cavity} is divided by 2π because the SEEP/W code considers only a one radian sector for axisymmetric geometries.
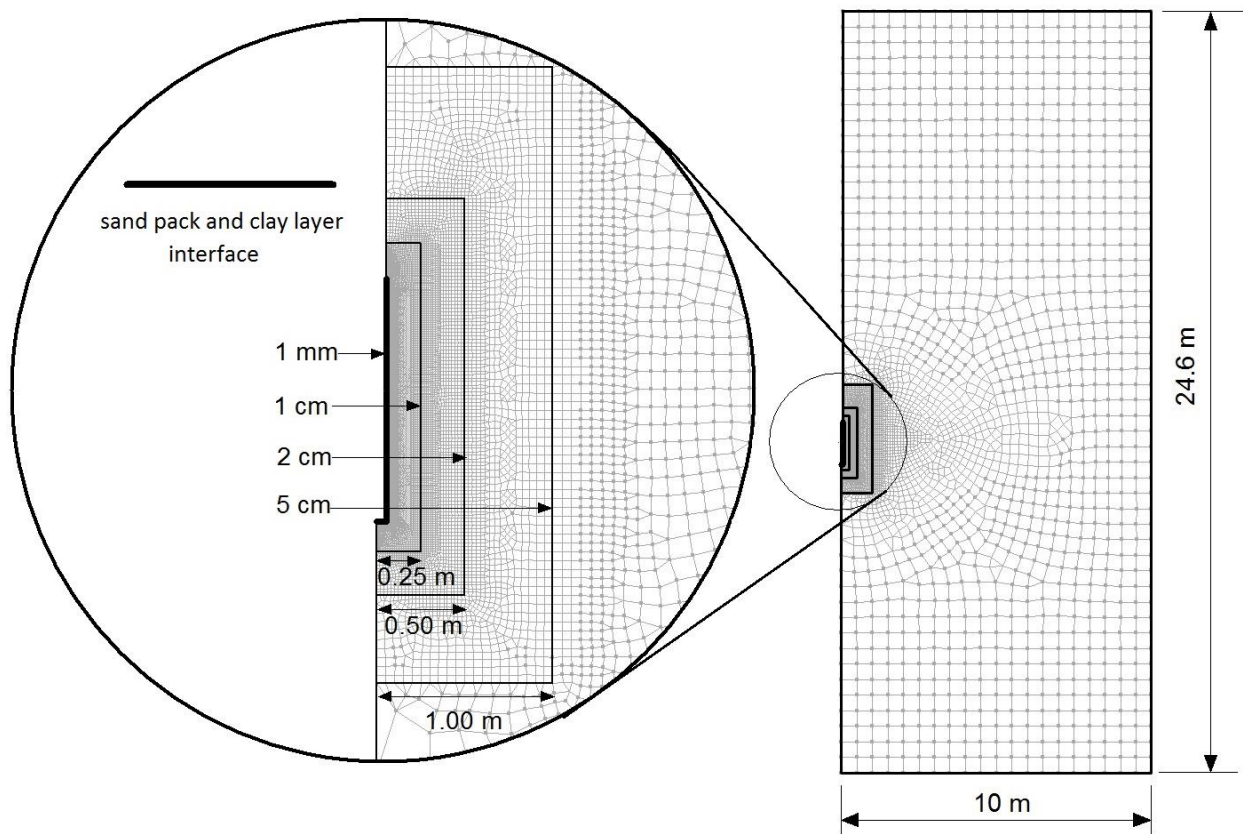
Figure 5.4: Detail of the refined mesh used for the numerical simulation with SEEP/W.

The solutions obtained numerically for transient flow must be independent from the mesh size and time-step increments (Chapuis, 2010; Duhaime, 2012). Figure 5.4 shows the refined mesh around the sand pack. In order to obtain independent results for total head decline within the injection zone, several mesh sizes, time-step increments and duration of the initial pressure step were tested. The final simulations were conducted with: 1) a refined mesh with small elements of 1 mm at the sand-clay interface, and coarse elements of 50 cm far away from the sand pack, 2) time steps that increase exponentially starting from 0.01 s, and 3) a mesh comprising 37872 nodes and 38048 elements.

5.3   Results and discussion

Figure 5.5 presents the change in barometric pressure, *B*, with respect to its long-term mean value at site 2 for the study period (2012-2015). The long-term barometric pressure mean value during the study period was equivalent to 10.37 m of water, with a fluctuation range around the mean value of between -0.43 and +0.30 m (i.e., a total variation of 0.79 m). This fluctuation range represents the maximum limit of barometric induced well water-level change and aquifer head response for BRF and BHRF analyses, respectively. The barometric pressure change was uniform within the study area (Marefat et al., 2015b). The largest fluctuations in barometric pressure were registered during winter from November to April, which appear to be related to greater temperature-induced fluctuations and passage of major storm weather events.
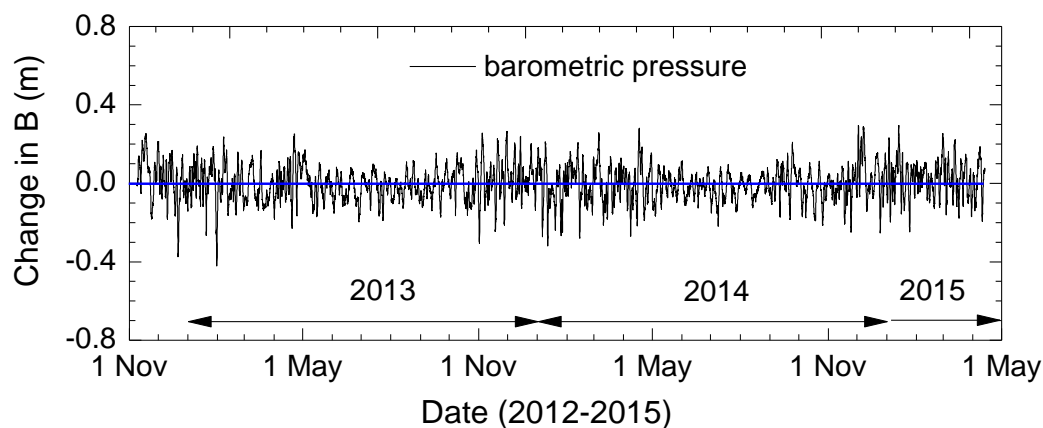
Figure 5.5: Change in barometric pressure (*B*), Lachenaie area, near Montreal, Quebec, Canada.

The observed pressure head hydrographs for open wells 2R and 2S, and closed- piezometers 2AB and 2AH shown in Figure 5.6 represent the composite responses from various hydrogeological factors/events, each with varying periods (frequencies) of stress application (e.g., aquifer loading due to barometric stress change/precipitation events, and surficial groundwater recharge or discharge events). To visually examine longer-term hydrologic effects within the record, short-term loading effects associated with barometric pressure change were removed from the observed well/piezometer head response (Figure 5.6). Although short-term noise is considerably reduced, some longer-term noise and variation are still there in the

barometric-corrected response. This indicates that several stress and groundwater flow effects of varying periods/frequencies are still embedded in the corrected head response patterns.
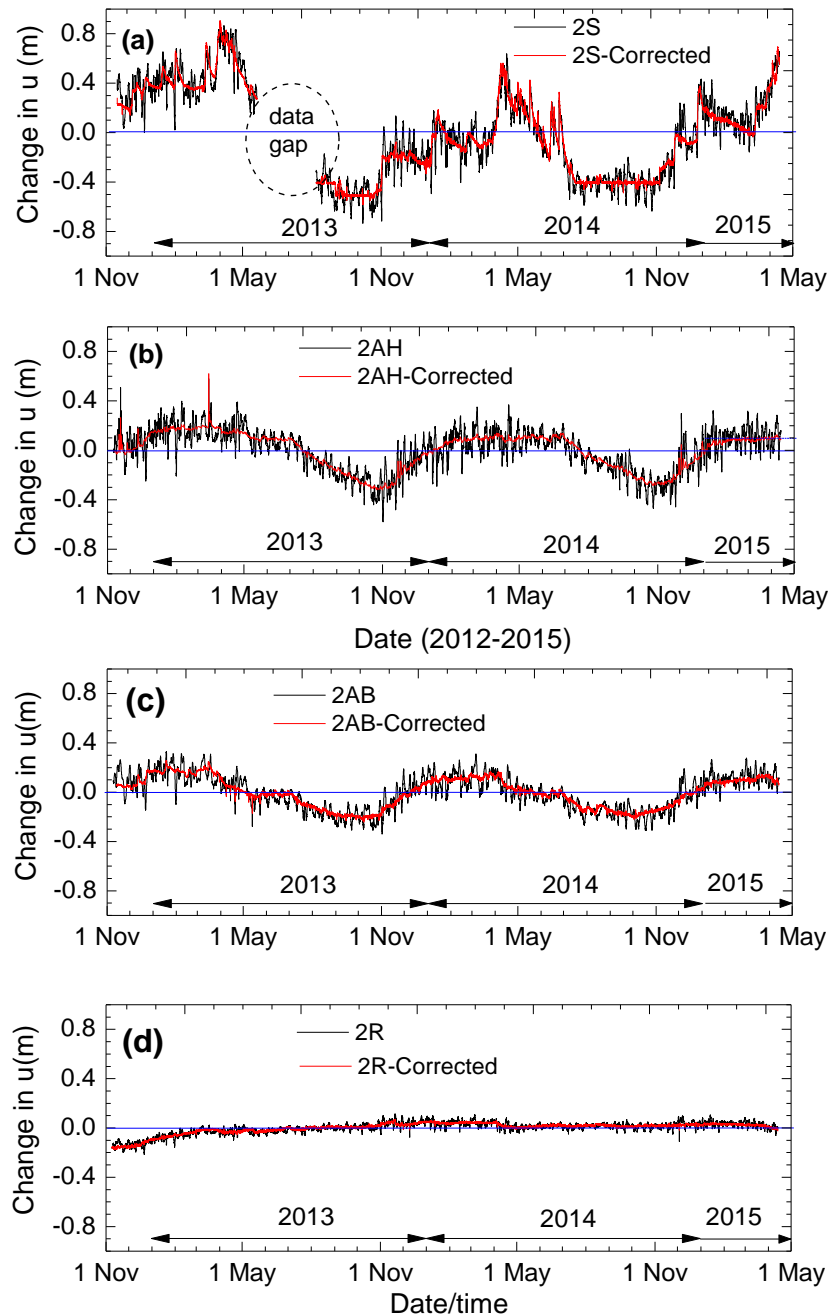
Figure 5.6: Observed absolute pressure head (*u*), Lachenaie site 2 from Nov. 2012 to Apr.2015; a) 2S; b) 2AH; c) 2AB; and d) 2R.

All hydrographs shown in Figure 5.6 present the change in absolute pressure head, u, with respect to their respective mean values observed during the study period. A number of hydrologic patterns are exhibited in Figure 5.6. First, during the monitoring period, the absolute pressure head in the surficial aquifer and within the clay aquitard directly respond to the observed barometric pressure changes (Figures 5.6a, 5.6b, and 5.6c). The absolute pressure head within the confined aquifer, however, was much less sensitive to changes in barometric pressure (Figure 5.6d, piezometer 2R). Second, the amplitude of the observed annual pore pressure cycle differed for each piezometer. Piezometers 2S, 2AH, and 2AB clearly reflected the seasonal difference between groundwater recharge and discharge events i.e., precipitation events and evapotranspiration (Figures 5.6a, 5.6b, and 5.6c). An irregular local and seasonal fluctuation in hydraulic head was observed in the shallow aquifer (i.e., 2S). These fluctuations in the total head changes within the shallow aquifer are related to specific precipitation events and evapotranspiration (e.g., rainy day or hot summer day). In comparison, for the underlying confined aquifer (Figure 5.6d), the observed seasonal fluctuations were very small.

5.3.1 Vertical hydraulic diffusivity-conductivity of the clay

Because the annual groundwater flow/recharge cycle is clearly expressed in the background of the clay aquitard piezometers response (i.e., 2AH and 2AB), efforts were focused on isolating the well and piezometer responses for frequencies that are close to an annual cycle (i.e., 365 day period = 2.74×10^{-3} day^{-1} frequency). The amplitude of the annual recharge/groundwater-flow cycle imposed by the surficial aquifer attenuates and lags as it propagates vertically through the underlying clay aquitard to the confined aquifer. To visually evaluate the attenuation of the response amplitude, band-pass filtering was applied to isolate the embedded annual head cycles for each monitored depth interval. General filtering theory, along with spectral frequency analysis was applied. With general filtering theory, it is assumed that the well/piezometer pressure head time series can be approximated by the sum of a finite-number of periodic components that are defined on the basis of frequency. Band-pass filtering provides a "window" for head responses with specified periods/frequencies. Hence, for a selected bandwidth (range), a window allows only those components of observed head response with specified frequency to pass through. Figure 5.7 shows the filtered daily head responses, expressed as in Figure 5.6, as a

difference from the observed mean for the various well/piezometer records. The observed daily head data was first de-trended prior to applying the band-pass filtering to remove any minor background, low-frequency effects. The band-pass filtered responses shown in Figure 5.7 were developed using the FILTER software program as described in Hydrotechnique Associates (1984), using a band-pass filter frequency range of 0.0024 to 0.00328 day^{-1} (i.e., periods of 425 to 305 days) to fully capture the annual hydrologic components within the time-series records.
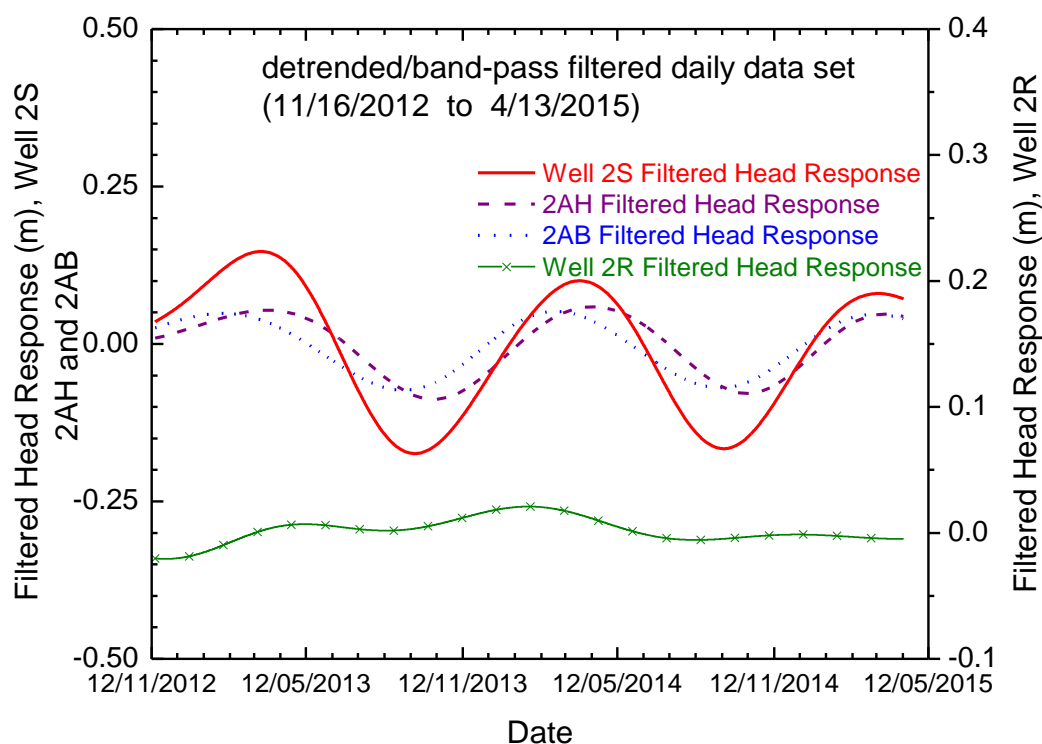
Figure 5.7: Well/piezometer band-pass filtered daily head responses from mean values, Lachenaie site 2, time interval: 11/16/2012 to 04/13/2015.

As indicated in Figure 5.7, the filtered annual head cycle imposed by the surficial aquifer (well 2S) is clearly expressed in the piezometer records for the underlying clay aquitard (2AH and 2AB). However, the cycle is greatly attenuated in the filtered head response within the deeper confined aquifer (well 2R). The reason for this correspondence is that the band-pass frequency window utilized for the filtering, effectively removes the higher-frequency dependent barometric signal from the observed head response. It should also be noted that the filtered response for

piezometer 2AB appears to be out-of-phase with the surficial aquifer (i.e., well 2S) head signal. The cause for this phase discrepancy is not currently known, however, the causes for high-frequency, time-lag differences for this piezometer (in comparison to the other monitor well/piezometer facilities) is briefly discussed in Section 5.3.3.

To facilitate calculation of the vertical hydraulic diffusivity, D_v, for the clay aquitard based on the annual recharge events as expressed in Eq.(5.3), spectral frequency analysis was performed on the daily, band-passed filtered well/piezometer records shown in Figure 5.7. The spectral frequency analysis allowed the pressure head amplitudes to be calculated for each well/piezometer. Figures 5.8A-5.8C show a comparison of the spectral frequency density function for head amplitudes for the clay aquitard piezometers (2AH and 2AB) and the deeper confined aquifer (well 2R) with head amplitudes for the surficial aquifer (well 2S). The spectral frequency spectrums shown were developed using the ETFFT software program, as described in Hydrotechnique Associates (1984) and summarized in Chien et al. (1986). The ETFFT program is based on standard Fourier analysis theory, which is presented in standard statistical textbooks such as Bendat and Piersol (1991). Similar spectral frequency plots (as well as frequency filtering applications) were also obtained using MATLAB^{TM} (2010).

The spectral response comparisons shown in Figures 5.8A – 5.8C were "tapered" to reduce the noise and impact of abrupt changes in head amplitudes across the frequency spectra. The use of tapering, however, does cause some minimal pollution of the frequency spectra immediately outside the band-pass filter window frequency range of 0.00224 to 0.00328 day^{-1}. As indicated in Figures 5.8A and 5.8B, piezometers 2AH and 2AB exhibit visually correlated, but attenuated amplitude profile in comparison to the well 2S signal. This similarity in spectral response patterns for the clay aquitard piezometers in comparison to the overlying surficial aquifer response suggests that their response characteristics are largely influenced by the annual vertical/recharge cycle. In contrast, the underlying confined aquifer spectral frequency pattern shown in Figure 5.8C, does not exhibit this high degree of correspondence. The distinct spectral frequency for well 2R also suggests that hydrologic phenomena other than vertical annual recharge may be included in the annual confined aquifer response pattern (e.g., areal/lateral groundwater flow/recharge).
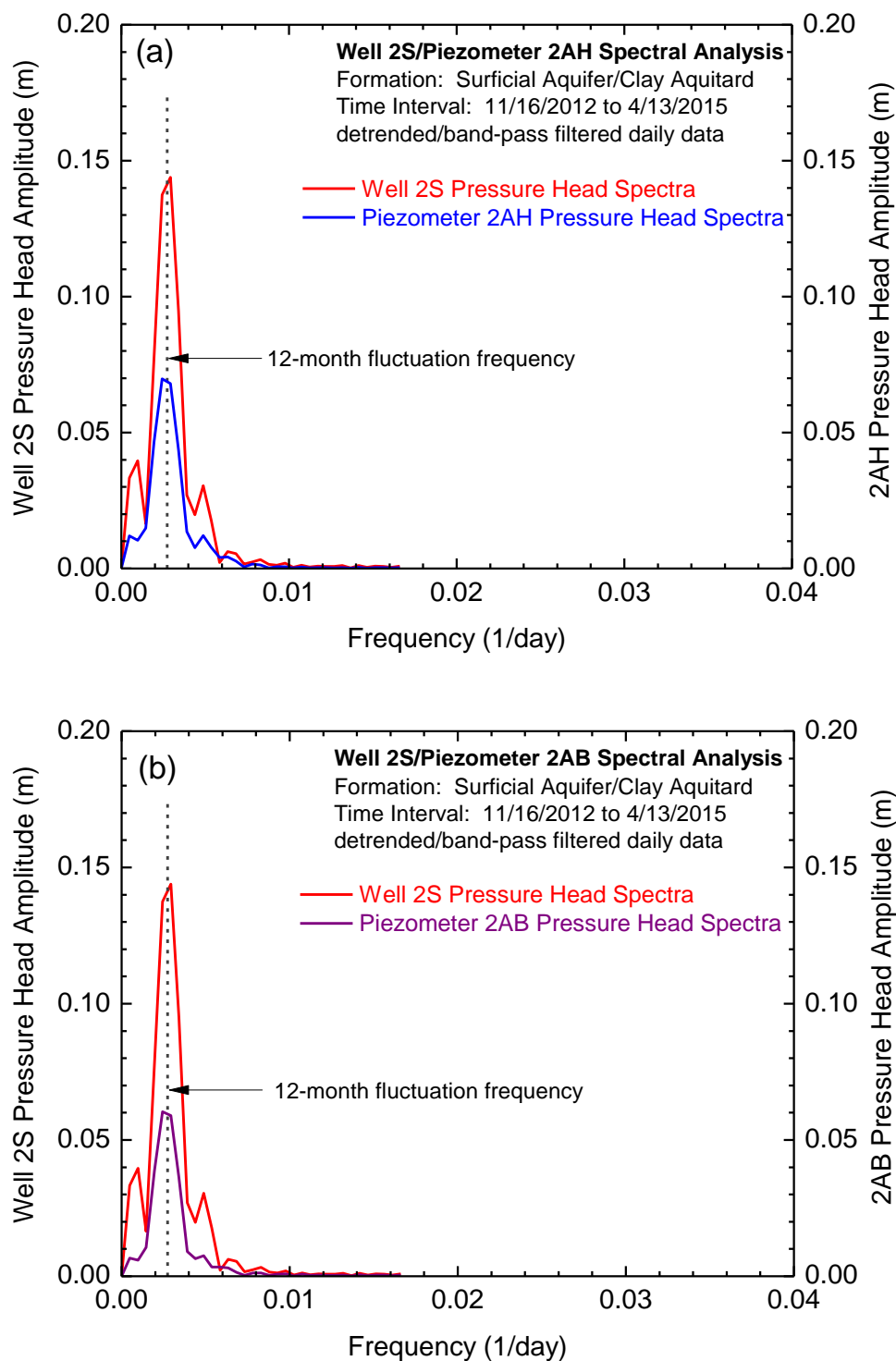
Figure 5.8: Spectral frequency analysis comparison: a) Well 2S and Piezometer 2AH; b) Well 2S and Piezometer 2AB; and c) Well 2S and Well 2R.
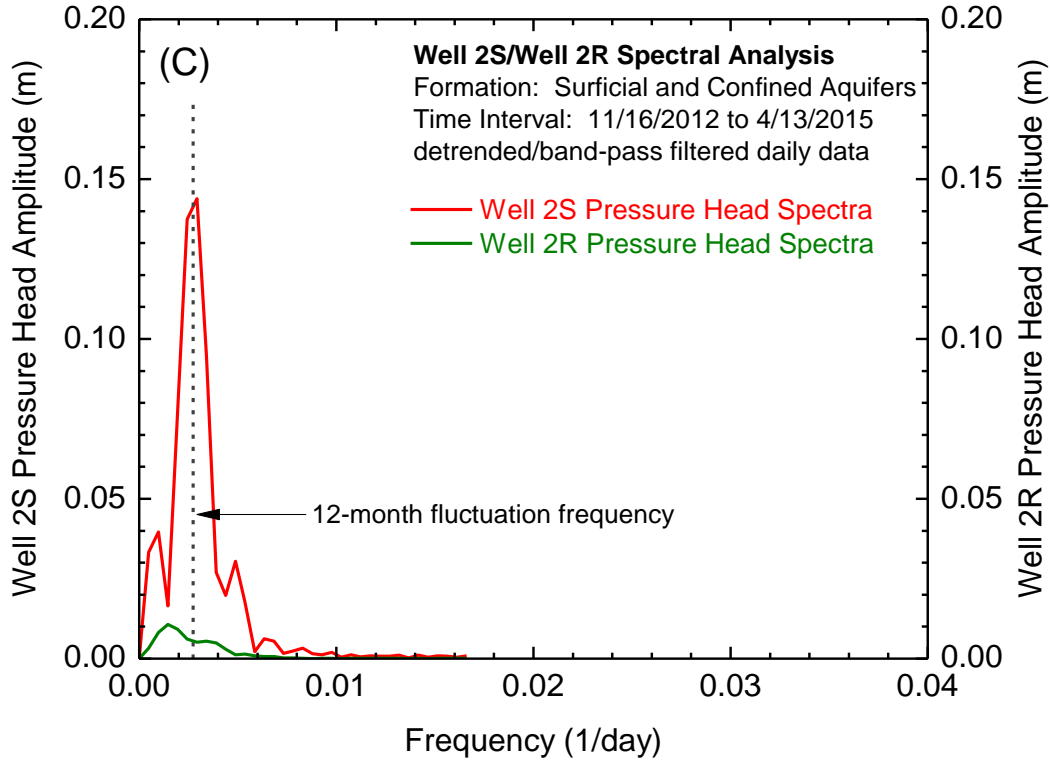
Figure 5.8: Spectral frequency analysis comparison: a) Well 2S and Piezometer 2AH; b) Well 2S and Piezometer 2AB; and c) Well 2S and Well 2R (continued).

To assess the vertical hydraulic diffusivity for the clay aquitard, pressure head amplitudes for piezometers 2AH and 2AB and well 2R were compared to the amplitudes calculated for well 2S, for the annual-encompassing, band-pass filtered signal (i.e., 0.00224 to 0.00328 day^{-1}), based on the spectral frequency analysis results presented in Figures 5.8A through 5.8C. The amplitude ratios (i.e., α_z/α_s) that were calculated from this comparison were then utilized in Eq. (5.3) to calculate a composite vertical hydraulic diffusivity for the clay aquitard over the depth measurement distance. It should be noted that the ETFFT software program does not allow for calculation of specific frequency amplitudes (e.g., 1 year gives 0.00274 day^{-1}), but calculates the frequency spectra plot based on a set frequency offset/separation of 4.88×10^{-4} day^{-1}. The closest bounding frequencies available for an annual cycle were frequencies of 0.00244 and 0.00293 day^{-1} (periods of 410 to 341 days).

Figure 5.9 shows a comparison of the calculated amplitude ratios for the two clay aquitard piezometers 2AH and 2AB based on the surficial aquifer well 2S response. In addition, amplitude ratios for the underlying confined aquifer (well 2R) are also shown based on surficial aquifer (well 2S) response, as well as based on 2AH. As indicated in Figure 5.9, the two amplitude ratio calculations for the two frequencies bounding an annual period of 365 days generally exhibit a slightly decreasing amplitude ratio with increasing spectra frequency (i.e. with decreasing period).
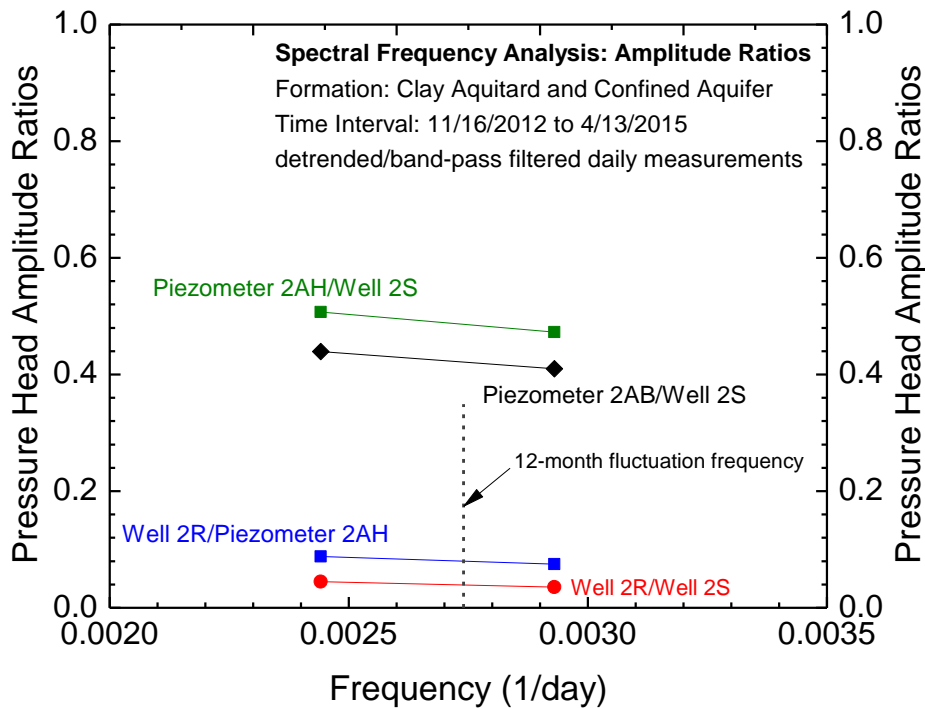
Figure 5.9: Spectral frequency analysis: amplitude ratio comparison.

Figure 5.10 shows the calculated clay aquitard vertical hydraulic diffusivities for the two bounding annual frequencies based on the associated amplitude ratios presented in Figure 5.9 and the depth from the top of the clay aquitard to the top of the monitored test interval as specified in Eq. (5.3). Nearly identical vertical hydraulic diffusivities were derived for each of the clay aquitard piezometer locations (Table 5.1). When using the amplitude change with respect to well 2S, the D_v values for piezometer 2AH vary between 9.98×10^{-6} and 1.01×10^{-5} m^2/s

whereas they vary between 2.32×10^{-5} and 2.37×10^{-5} m^2/s for piezometer 2AB. If it is assumed that amplitude ratios determined for the underlying confined aquifer response reflect primarily the vertical transmission of the surficial aquifer signal through the clay aquitard and are not unduly impacted by other lateral aquifer response characteristics, then the following calculated vertical hydraulic diffusivities are obtained: Well 2R/Well 2S, $D_v = 5.55 \times 10^{-6}$ to 5.78×10^{-6} m^2/s, and Well 2R/Piezometer 2AH, $D_v = 4.05 \times 10^{-6}$ to 4.29×10^{-6} m^2/s.
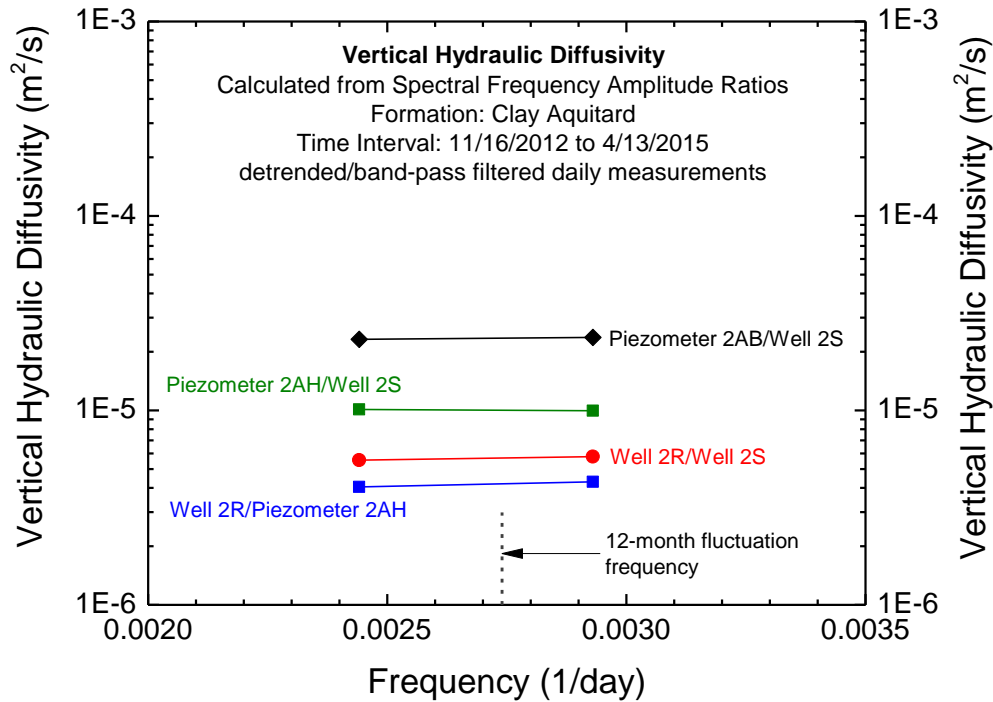
Figure 5.10: Vertical hydraulic diffusivity calculated from spectral frequency analysis.

For comparison, a hydraulic diffusivity on the order of 1×10^{-6} m^2/s was also obtained for a dense clayey till in Saskatchewan from the analysis of cyclic pressure head recharge event fluctuations (Keller et al. 1989). Applying this value of hydraulic diffusivity in Eq. (5.2) yields a relative penetration depth of around 10 m for the annual pressure head cycle. This relative penetration depth was observed and verified by Van der Kamp and Maathuis (1991) for the same test site. The slightly higher D_v in Lachenaie with respect to that obtained by Keller et al. (1989) is supported by the fact that groundwater recharge cycle in Lachenaie could propogate through 24.6

m of clay to the confined aquifer (for example on site 2). This implies a higher hydraulic diffusivity for Lachenaie clay.

Because vertical hydraulic diffusivity is a function of both vertical hydraulic conductivity and storativity (or elasticity) of the formation, it is not possible to directly determine whether the high and low D_v values registered for piezometer 2AB and well 2R, respectively, can be attributed to changes in hydraulic conductivity or storativity within the clay aquitard over their respective monitoring depth intervals. To distinguish between changes in K_v and S_s, the S_s values based on loading efficiency (Eq. 5.4) for piezometer 2AH and 2AB can be used to solve for K_v from the D_v definition. Given the standard values of freshwater density and compressibility, the test interval porosity values of 0.63 (2AH) and 0.65 (2AB) obtained from laboratory core analyses, and LE values of 0.90 (2AH) and 0.82 (2AB) obtained from BHRF multiple-regression analysis, S_s values of 3.15×10^{-5} m^{-1} and 1.60×10^{-5} m^{-1} can be obtained for the intervals monitored by piezometers 2AH and 2AB, respectively. These calculated S_s values fall within the range of shallow consolidated claystone formations and slightly overconsolidated fluvial clay deposits as reported previously in Smith et al. (2013) and Timms and Acworth (2005) repectively, based on similar in-situ, LE response analysis methods.

Figure 5.11 shows the calculated K_v values for the clay aquitard for the two bounding annual frequencies based on the associated D_v values indicated in Figure 5.10 multiplied by the S_s values obtained from in-situ loading efficiency as described above. As indicated in the figure, nearly identical vertical hydraulic conductivities were derived for the two bounding frequencies for each of the clay aquitard piezometer locations: $K_v = 3.15\times10^{-10}$ to 3.19×10^{-10} m/s for piezometer 2AH and $K_v = 3.72\times10^{-10}$ to 3.80×10^{-10} m/s for piezometer 2AB. The fact that these K_v values are nearly identical while representing two different aquitard depths indicates a high degree of uniformity in the clay aquitard down to the composite depth monitored by piezometer 2AB. It also indicates that the differences indicated in Figure 5.10 for D_v for 2AH and 2AB mainly depend on differences in S_s. The associated values regarding vertical hydraulic diffusivity-conductivity estimation and specific storage calculation are summarised in Table (5.1).

For comparison purposes, Figure 5.11 also shows the calculated K_v for the entire composite clay aquitard based on the D_v values for well 2R indicated in Figure 5.10, and the average S_s values determined for 2AH and 2AB. As shown, a lower composite clay aquitard vertical permeability

is indicated for the well 2R responses: well 2R/well 2S, $K_v = 1.18 \times 10^{-10}$ to 1.23×10^{-10} m/s with mean $S_s = 2.12 \times 10^{-5}$ m^{-1}; well 2R/piezometer 2AH, $K_v = 8.58 \times 10^{-11}$ to 9.09×10^{-11} m/s with mean $S_s = 3.15 \times 10^{-5}$ m^{-1}. The overall lower vertical hydraulic conductivity estimate for the entire composite aquitard can be either explained by a significantly lower permeability within the lower clay aquitard section or by extraneous, attenuating hydrologic effects imposed by the confined aquifer system on the annual surficial aquifer recharge signal that propagates vertically. It is currently not known which of these causes may be responsible for the apparently lower composite clay aquitard vertical hydraulic conductivity, based on the analysis of the confined aquifer/well 2R response.
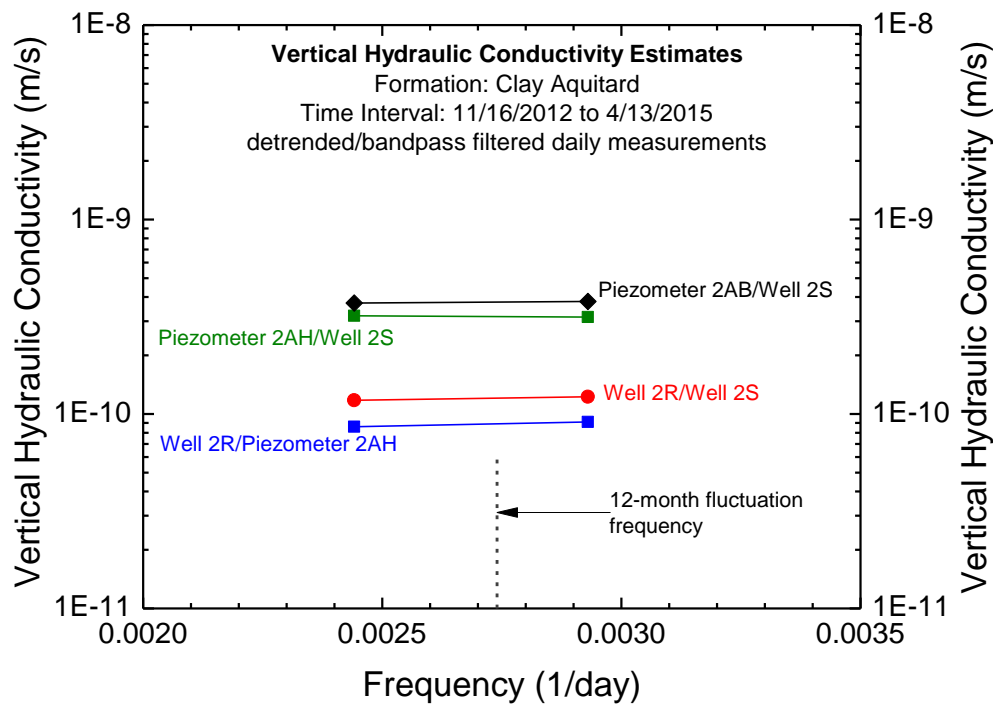
Figure 5.11: Vertical hydraulic conductivity estimates.

The annual groundwater flow cycle is also visible in the background of the responses for the clay aquitard piezometers on site 4 (i.e., 4AH and 4AB). The same method of analysis (filtering and spectral frequency) was applied for the pressure head responses registered on this site to determine the in-situ vertical hydraulic diffusivity and conductivity for each monitored depth

interval. A good correspondence was obtained for the spectral frequency analysis of the daily filtered head response for surficial aquifer (well 4S) and the underlying clay aquitard, piezometers 4AH and 4AB, (result not shown here). It should be noted that on site 4, the pressure head time series for the confined aquifer (i.e., well 4R) was not long enough to be appropriate for spectral frequency analysis. This was due to a malfunctioning of the data-logger installed in this monitoring well. For the two bounding annual frequencies (0.00244 to 0.00293 day^{-1}) the pressure head amplitudes were calculated for the clay aquitard and surficial aquifer piezometers. For frequencies of 0.00244 to 0.00293 day^{-1}, amplitude ratios (α_z/α_s) of 0.784 to 0.759 and 0.574 to 0.558 were respectively obtained for each set of aquitard piezometers (4AH and 4AB) based on a comparison with the amplitude of the surficial aquifer response (4S). Nearly identical vertical hydraulic diffusivities were derived for each piezometer from the amplitude ratios and the associated depths from the top of the clay aquitard to the top of the monitored test interval as specified in Eq. (5.3): $D_v = 3.67 \times 10^{-5}$ to 3.33×10^{-5} m^2/s for piezometer 4AH/4S and $D_v = 2.58 \times 10^{-5}$ to 2.80×10^{-5} m^2/s for piezometer 4AB/4S. From Eq. (5.4), with porosity of 0.60 (4AH) and 0.61 (4AB), and LE values of 0.81 (4AH) and 0.83 (4AB), S_s values of 1.42×10^{-5} m^{-1} (4AH) and 1.62×10^{-5} m^{-1} (4AB) were obtained. These estimates for S_s are similar to slightly lower than that determined for the well 2S-based piezometer network. As it was the case for site 2, nearly identical vertical hydraulic conductivities were derived for each of the clay aquitard piezometer locations: $K_v = 5.22 \times 10^{-10}$ to 4.74×10^{-10} m/s for piezometer 4AH and $K_v = 4.17 \times 10^{-10}$ to 4.53×10^{-10} m/s for piezometer 4AB [Table (5.1)].

Table 5.1: Vertical hydraulic diffusivity and conductivity calculation in sites 2 and 4 Lachenaie. where T_P is period of the input pore pressure signal, α_z/α_s is amplitude ratio, z is the distance from top of the aquitard to top of the monitored interval, D_v is vertical hydraulic diffusivity, LE is loading efficiency, n is porosity, S_s is specific storage, and K_v is vertical hydraulic conductivity.

MW	T_P (day)	α_z/α_s	z (m)	D_v (m²/s)	LE	n	S_s (m⁻¹)	K_v (m/s)
2AH/2S	409.84 – 341.43	0.507 – 0.473	7.25	1.01E-05 – 9.98E-06	0.910	0.630	3.16E-05	3.19E-10 – 3.15E-10
2AB/2S	409.84 – 341.43	0.439 – 0.410	13.30	2.32E-05 – 2.37E-05	0.820	0.650	1.63E-05	3.78E-10 – 3.86E-10
2R/2S	409.84 – 341.43	0.044 – 0.035	24.60	5.55E-06 – 5.78E-06	0.865	0.635	2.12E-05	1.18E-10 – 1.23E-10
2R/2AH	409.84 – 341.43	0.088 – 0.075	16.43	4.05E-06 – 4.29E-06	0.865	0.635	2.12E-05	8.60E-11 – 9.10E-11
4AH/4S	409.84 – 341.43	0.784 – 0.759	4.95	3.67E-05 – 3.33E-05	0.810	0.600	1.42E-05	5.22E-10 – 4.74E-10
4AB/4S	409.84 – 341.43	0.574 – 0.558	9.46	2.58E-05 – 2.80E-05	0.830	0.610	1.62E-05	4.17E-10 – 4.53E-10

5.3.2 Barometric head response function

The development of representative BHRF plots can also be used for K_h estimation based on curve matching between a predictive numerical model and observed BHRF pattern. To improve the accuracy of observed BHRF, a direct relationship purely between pore pressure head and barometric pressure should be established. This implies that the influence of other major phenomena on pore pressure data is considered to be minimal. To accomplish this, efforts were focused on selecting a limited data subset, in which the effects of various irrelevant low- and high-frequency hydrogeological factors/events were not significant. For the Lachenaie area, frozen soil in winter was assumed to minimize groundwater recharge and discharge events. Additionally, Marefat et al. (2015b) showed that there was no visible Earth-tide effect on the pore pressure response recorded in the shallow aquifer/aquitard system in the Lachenaie study area. This is also confirmed by spectral frequency analysis of the observed pressure head responses (not shown here); there was no identifiable diurnal or semi-diurnal frequency component associated with Earth-tide stress effects. Therefore, pressure head records for winters 2013, 2014, and 2015 were used to analyze the head response to short-term barometric pressure changes in developing representative BHRF patterns. In this paper, a data subset based on measurements taken every 15-min for the time period between January 1st and April 1st, 2014 was selected for BHRF analysis. As an initial step in BHRF development, each data subset was detrended to remove the background trend. This time period corresponds to a relatively stable pressure head response for the surficial aquifer boundary at the top of the clay, as reflected in the pressure head response at well 2S. For the detrended data subset, the major external stress controlling the pore pressure response is primarily the change in atmospheric pressure.

For the selected data subset, Figure 5.12 presents the change in pressure head, well-water level, and barometric pressure as compared to their respective means calculated over the ̃ 90-day analysis period. The variations in well-water level were "deduced" from observed total pressure heads by subtracting barometric pressure from absolute pressure head (i.e., u_{abs}-B) for the same time interval. Figure 5.12a shows that the well-water level in piezometer 2S was virtually insensitive to the barometric pressure fluctuations. As would be expected for a shallow unconfined aquifer system, however, total pressure head in the surficial aquifer closely followed the changes in atmospheric pressure. This indicates that the changes in barometric stress are

transmitted immediately (i.e., <15 minutes) to both the water in the well and the shallow aquifer, where the groundwater table surface is located close to ground level. There are four noticeable abrupt "jumps/offsets" in the surficial aquifer groundwater-table elevation (Figure 5.12a), as revealed in the deduced water levels of piezometer 2S. These four jumps are directly related to the increase of air temperature. Each individual rise in the surficial groundwater aquifer pressure head was compared with monitoring site climatological data. This casual comparison (not shown), indicated that the surficial aquifer head "jumps" were associated with snowmelt recharge, due to abrupt rises in air temperature conditions. Figure 5.12a also shows the changes in absolute pressure head and deduced well-water level response within the confined aquifer (2R). The fluctuations in total aquifer pressure due to barometric pressure change are very small, indicating that the majority of the imposed barometric pressure is borne by the confined aquifer solid matrix.

Figure 5.12b presents changes in the observed and the corrected high frequency pressures head response in the clay aquitard (2AH and 2AB). Total pore pressure in both piezometers followed directly the high frequency barometric pressure fluctuations. The visual correlation between absolute pressure head and barometric pressure is obvious. That is to say, the atmospheric pressure change was the main contributor to the pressure head fluctuations within the clay aquitard during the winter measurements. Thus, the BHRF really reflects the pore pressure response to high frequency short-term loading induced by barometric pressure changes.
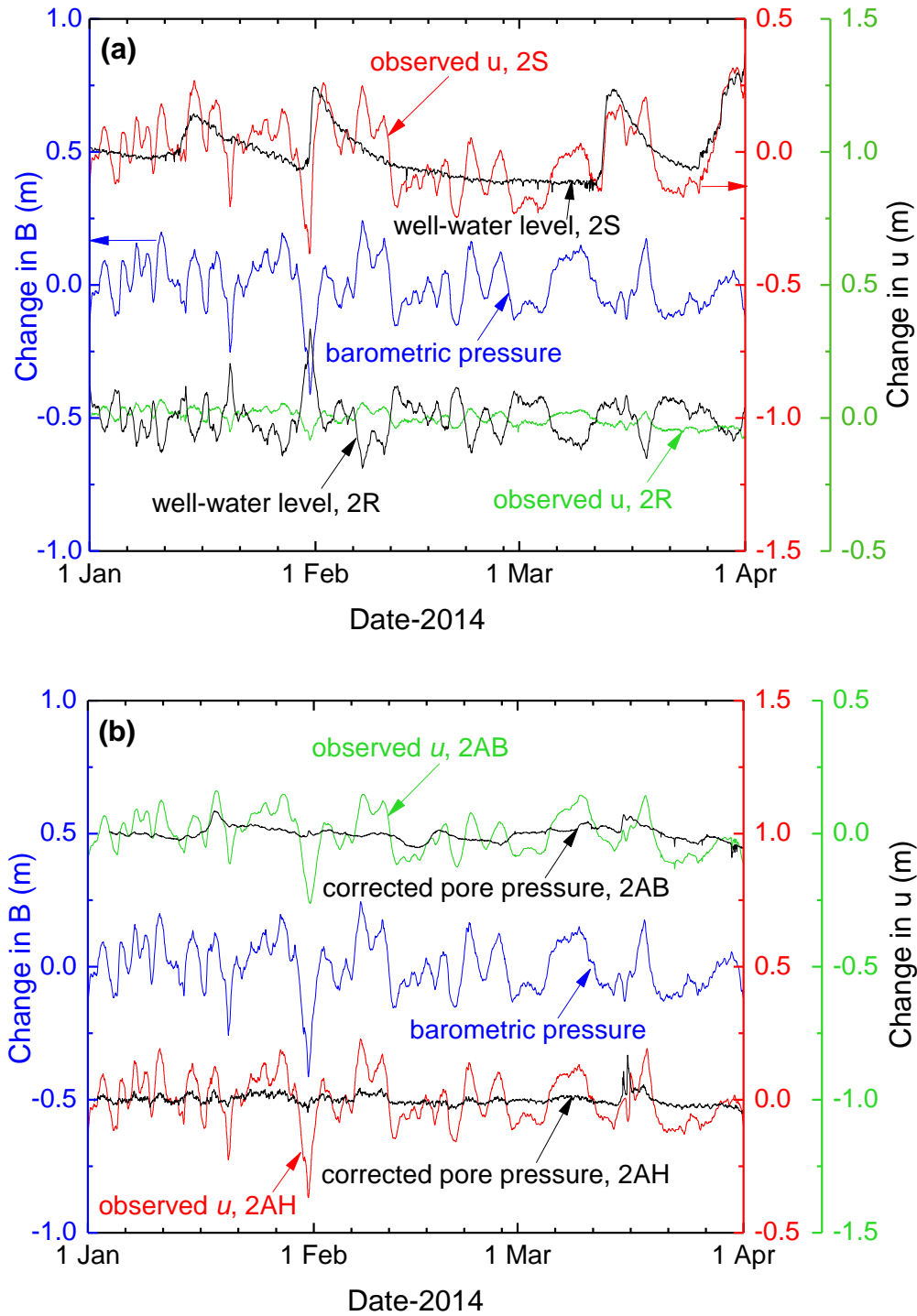
Figure 5.12: Change in barometric pressure (*B*), observed pore pressure (*u*), well-water level, and corrected pore pressure. Lachenaie site 2 between Jan. 2014 and Apr.2014: a) 2S and 2R; b) 2AH and 2AB.

5.3.3 Horizontal hydraulic conductivity

The horizontal hydraulic conductivity for Lachenaie clay was estimated by fitting the predicted numerical model response (both in type-curve format) to the observed BHRF for each closed-piezometer system. Three key parameters influence the equilibration of pore pressure imbalance between sand filter cavity and the surrounding clay layer. The sensitivity of each parameter was determined. The parameters include 1) clay horizontal hydraulic conductivity, K_h, 2) well cavity volume change, ΔV_{cavity}, and, 3) clay compressibility, m_v. The influence of these parameters was studied using the numerical model. Sensitivity analyses were conducted using the numerical model for K_h values ranging between 1×10^{-09} and 5×10^{-11} m/s, for ΔV_{cavity} between 1×10^{-05} and 5×10^{-07} m^3, and for m_v between 1×10^{-04} and 1×10^{-08} kPa^{-1}. As shown in Figure 5.13, the numerical results are most sensitive to clay hydraulic conductivity and cavity volume change. In contrast, the model results display little sensitivity to clay compressibility. For the final BHRF model matches, parameters m_v and ΔV_{cavity} were held constant. The clay compressibility was derived from calculated S_s values based on loading efficiency calculation from Eq. (5.4). For each piezometer, ΔV_{cavity} was calculated using Eq. (5.7), a relationship presented by Duhaime and Chapuis (2014) for pulse tests analysis in compressible clay. The calculated m_v and ΔV_{cavity} values were presented in Table (5.2). The best-fit result to the observed BHRF was obtained by varying values for K_h and by minimizing the sum of squared differences between the numerical results and observed BHRFs.

Observed BHRFs and best-fit type curves for piezometers 2AH, 2AB, 3AB, and 4AH are presented in Figure 5.14. The observed BHRFs were calculated based on measurements taken every 15 minutes to fit the early BHRF response of the closed-piezometers. The good correlation between the numerical type-curves and observed BHRFs is obvious. Estimated K_h values, between 2.6×10^{-10} and 7.0×10^{-10} m/s were obtained for most piezometers (Table 5.2). The slightly lower K_h value for piezometer 2AB (i.e., 6×10^{-11} m/s) in comparison with other piezometers, is not surprising given the respective BHRF response characteristics. As shown in Figure 5.14b, the observed BHRF for piezometer 2AB equilibrated after 45 hours, which is much longer than that for the other piezometers at similar depth. For example, the time needed for pressure equilibration with piezometer 3AB was about 15 hours (Figure 5.14c).

Table 5.2: Horizontal hydraulic conductivity estimation from curve fitting between BHRF and predicted numerical result. n is porosity, D_{cavity} is the cavity diameter, L_{cavity} is the cavity length, V_{cavity} is cavity volume, G is shear modulus obtained from in-situ pulse tests by Duhaime and Chapuis (2014), ΔV_{cavity} is cavity volume change obtained using Eq. (5.7), m_v is clay compressibility obtained from loading efficiency calculation, and K_h is estimated clay horizontal hydraulic conductivity.

MW	n	D_{cavity} (m)	L_{cavity} (m)	V_{cavity} (m^3)	G (Mpa)	ΔV_{cavity} (m^3)	m_v (kPa^{-1})	K_h (m/s)
2AH	0.63	0.089	0.91	6.17E-03	15.6	3.96E-07	2.61E-06	7.0E-10
2AB	0.65	0.095	1.37	7.09E-03	12	5.91E-07	1.38E-06	6.0E-11
3AB	0.66	0.085	0.89	5.63E-03	10.9	5.17E-07	1.22E-06	3.0E-10
4AH	0.60	0.086	0.94	5.85E-03	8.7	6.72E-07	1.18E-06	3.0E-10
4AB	0.61	0.091	1.02	6.53E-03	10.2	6.40E-07	1.36E-06	2.6E-10
9AH	0.62	0.077	0.69	4.71E-03	11.0	4.28E-07	1.59E-06	3.5E-10

The slow BHRF response for piezometer 2AB in comparison with the other piezometers can be assessed on the basis of the dimensionless time (T_D) and wellbore storage (C_D) constants as discussed in Bredehoeft and Papadopulos (1980) and Spane (1992). For a closed-well system the dimensionless constant ratio is $T_D/C_D = 2Tt\pi/V\beta_w\rho_w g$ where T is transmissivity, t time, V the volume of closed test system, β_w and $\rho_w g$ the compressibility and the specific weight of the test water respectively. According to this relationship, the response of a closed well can lag significantly if the test system compressibility increases (Neuzil, 1982). For the closed-piezometer system in this study, the cavity volume for piezometer 2AB is only 15% larger than that of 2AH. A very slow response for 2AB suggests that system compressibility for this well is higher than that dictated by cavity expansion and water compressiblity alone. A likely explanation for the higher compressibility for well 2AB is air entrapment within the sand filter during piezometer installation. In addition, the Lachenaie clay contains some organic matter, known to produce gas. Gas compressibility could explain the slow pore pressure response (Duhaime and Chapuis, 2014).
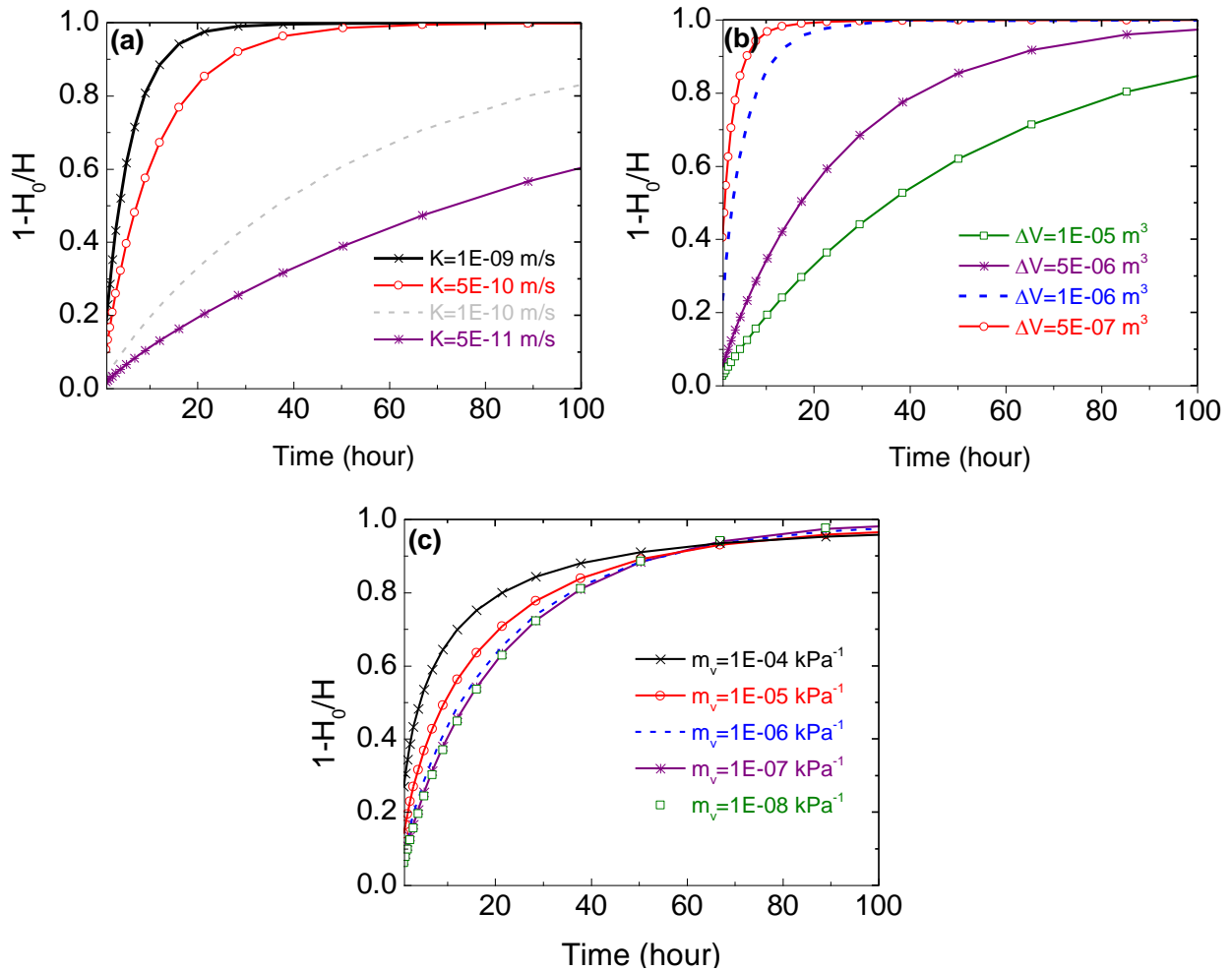
Figure 5.13: Sensitivity of the numerical model to: a) clay hydraulic conductivity; b) cavity volume change; and c) clay compressibility.

If the K_h result for piezometer 2AB is omitted on the basis of not being representative of actual in-situ test interval conditions, then the K_h values from the BHRF numerical model analysis range between 2.6×10^{-10} and 7.0×10^{-10} m/s for the clay aquitard. These results are generally slightly lower than reported in-situ K values in Lachenaie clay, based on standard field tests such as variable head tests giving from 1.2×10^{-9} to 5.7×10^{-9} m/s, by Benabdallah (2006); from 6.7×10^{-10} to 8.8×10^{-9} m/s, by GSI Environnement (2001); and from 4.0×10^{-10} to 7.0×10^{-9} m/s, by Duhaime (2012). In addition, Duhaime (2012) determined K values between 5.2×10^{-10} and 7.8×10^{-9} m/s utilizing pulse tests (i.e., pressurized slug tests) for the same study area.
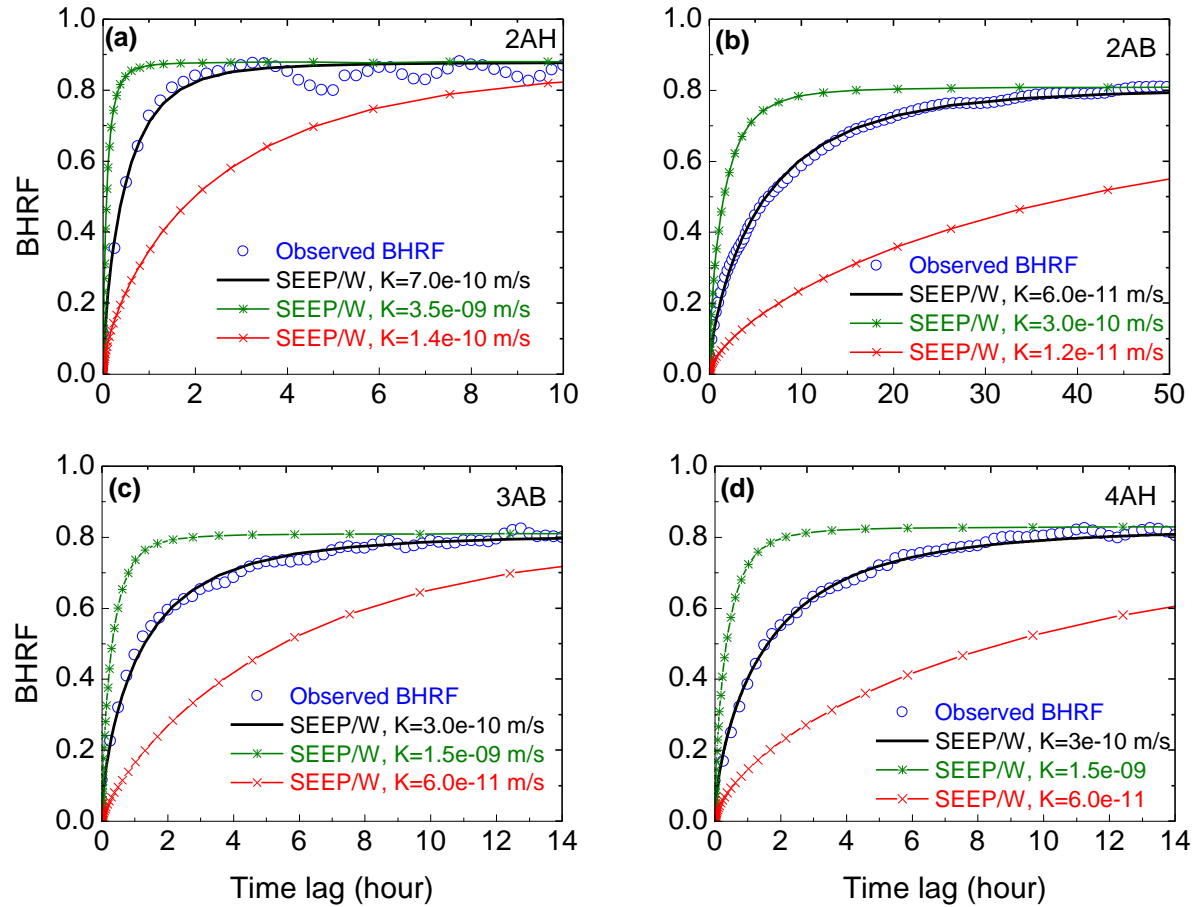
Figure 5.14: Horizontal hydraulic conductivity estimation from fitting observed BHRFs with numerically predicted type curves for piezometers: a) 2AH, b) 2AB, c) 3AB, and d) 4AH.

The K_v and K_h values calculated using the multi-timescale analysis of pressure head response are in the lower bound of previously obtained K values for the same study area. On Lachenaie, some wells installed in the bedrock are continuously degassing. The underlying methane gas-producing Utica shale and the organic matter content in the clay could both contribute to some gas production (Duhaime, 2012; Duhaime and Chapuis, 2014). The lowest hydraulic conductivity values could be explained more or less by the effects of gas compressibility within closed piezometer cavity. More complete study is required to explain these low K values by modeling composite gas-water compressibility and cavity expansion with a multiphysics FEM engine like COMSOL.

The hydraulic conductivity anisotropy for clays (tested in the laboratory) is known to increase

with consolidation (e.g., Al-Tabbaa and Wood, 1987). Chapuis and Gill (1989) Summarized some published anisotropy ratios for natural clays from the literature. The anisotropy ratio ranges from 0.7 to 4 from most experimental results of homogenous clays. For Champlain clays, within the strain range encountered in engineering applications (i.e., up to 25%), permeability anisotropy is negligible (Tavenas et al., 1983a; Leroueil et al., 1990), and that of the Lachenaie clay was found to be insignificant (Duhaime, 2012). Leroueil et al. (1990) observed an anisotropy ratio of about 1.35 for Champlain clay from small-scale laboratory tests results. A comparison between the calculated vertical and horizontal hydraulic conductivity in this study, utilizing combined analysis of pore pressure response to short and long-term loading, shows insignificant hydraulic conductivity anisotropy for Lachenaie clay (Table 5.3). This is in agreement with previous findings for the same study area (Duhaime, 2012) and for the other localities in the former Champlain Sea basin (Tavenas et al., 1983a; Leroueil et al., 1990).

Table 5.3: Hydraulic conductivity anisotropy estimation for a shallow clay aquitard in the Lachenaie area near Montreal, Quebec, Canada. K_h is obtained from curve fitting between BHRF and predicted numerical result. K^*_v is the mean vertical hydraulic conductivity for a period between 410 and 341 days (frequency between 0.00244 and 0.00293 days^{-1}).

MW	K^*_v (m/s)	K_h (m/s)	K^*_v/K_h (-)
2AH	3.17E-10	7.0E-10	0.45
2AB	3.76E-10	6.0E-11	6.26
4AH	4.98E-10	3.0E-10	1.66
4AB	4.35E-10	2.6E-10	1.67

5.4 Conclusion

The in-situ vertical and horizontal hydraulic diffusivity and conductivity of a clay aquitard in Lachenaie, near Montreal, Canada, have been determined from a multi-timescale analysis of low- to high-frequency natural pressure head responses. This approach allows the determination of clay aquitard hydraulic properties without conducting an extensive program of conventional

hydrologic tests. The obtained hydraulic diffusivity and conductivity values can be used to assess the vulnerability of underlying confined aquifer from surface or near surface contamination. The multi-timescale analysis of pore pressure response also provides an opportunity to assess in-situ the hydraulic conductivity anisotropy based solely on the analysis of associated well/piezometer responses to natural stress phenomena (i.e., long-term natural recharge events and short-term barometric pressure fluctuations.

Pressure head signals registered within the clay aquitards are reflecting various components, each with a distinct frequency or period. The high-frequency signals can be effectively filtered out by applying band-pass filtering with frequency between 0.00244 and 0.00293 day^{-1}. This allows the annual groundwater recharge cycle to be clearly captured and the amplitude ratios of downward propagating signals associated with a specific annual period be calculated. The amplitude ratios for annual groundwater recharge yield vertical hydraulic diffusivity values on the order of 1×10^{-5} m^2/s for the clay aquitard. Applying direct in-situ values of specific storage for each monitored depth interval from BHRF analysis to the vertical hydraulic diffusivity yields a vertical hydraulic conductivity on the order of 1×10^{-10} m/s for the Lachenaie clay aquitard. The specific storage values obtained based on loading efficiency calculation support previous finding. The horizontal hydraulic conductivity was estimated by fitting the observed BHRF with numerical type-curves. The horizontal hydraulic conductivity is close to the vertical component (i.e., 1×10^{-10} m/s).

Baseline pore pressure monitoring data allowed the hydraulic conductivity anisotropy for the Lachenaie clay aquitard to be measured at the field scale. A comparison between the vertical and horizontal components of hydraulic conductivity shows insignificant permeability anisotropy for Lachenaie clay, which is in a good agreement with previous works at laboratory scale. In addition, the nearly identical hydraulic conductivity values obtained for various observation sites suggest a high degree of clay integrity and uniformity for the Lachenaie clay aquitard over a distance up to 2.5 km.

5.5   Acknowledgements

research project. The help provided by Noura El-Harrak and several summer students during field work is gratefully acknowledged.

5.6 References

Al-Tabbaa, A., Wood, D.M., 1987. Some measurements of the permeability of kaolin. Geotechnique, 37(4): 499-514.

Anochikwa, C.I., van der Kamp, G., Barbour, S.L., 2012. Interpreting pore-water pressure changes induced by water table fluctuations and mechanical loading due to soil moisture changes. Can. Geotech. J. 49(3): 357-366. DOI:10.1139/t11-106

Benabdallah, E.M., 2006. Caractérisation de la perméabilité d'une argile sensible de Lachenaie, MS thesis, department of CGM, École polytechnique de Montréal, Quebec, Canada.

Bendat, J.S., Piersol, A.G., 1971. Random data: analysis and measurement procedures. John Wiley & Sons, New York.

Benson, C.H., Gunter, J.A., Boutwell, G.P., Trautwein, S.J., Berzanskis, P.H., 1997. Comparison of four methods to assess hydraulic conductivity. J. geotech. geoenviron. eng. 123(10): 929-937. DOI:10.1061/(Asce)1090-0241(1997)123:10(929)

Benson, C.H., Hardianto, F.S., Motan, E.S., 1994. Representative specimen size for hydraulic conductivity assessment of compacted soil liners. ASTM Special Technical Publication, 1142: 3-3. DOI:10.1520/Stp23883s

Bradbury, K.R. et al., 2006. Contaminant transport through aquitards: technical guidance for aquitard assessment. Awwa Research Foundation, Denver, Colorado.

Bradbury, K.R., Muldoon, M.A., 1990. Hydraulic conductivity determinations in unlithified glacial and fluvial materials. Ground water and vadose zone monitoring, ASTM STP, 1053: 138-151.

Bredehoeft, J.D., Neuzil, C.E., Milly, P.C.D., 2008. Regional flow in the Dakota aquifer : a study of the role of confining layers. U.S. Geological Survey water-supply paper;no. 2237. U.S.D.I., Alexandria.

Bredehoeft, J.D., Papadopulos, S.S., 1980. A method for determining the hydraulic properties of tight formations. Water Resour. Res. 16(1): 233-238. DOI:10.1029/WR016i001p00233

Butler, J.J., Jr., Jin, W., Mohammed, G.A., Reboulet, E.C., 2011. New insights from well responses to fluctuations in barometric pressure. Groundwater, 49(4): 525-533. DOI:10.1111/j.1745-6584.2010.00768.x

Chan, H., Kenney, T.C., 1973. Laboratory investigation of permeability ratio of New Liskeard varved soil. Can. Geotech. J. 10(3): 453-472.

Chapuis, R., 2009a. Monitoring a well in a clay layer: revisiting the time lag problem. Bull. Eng. Geol. Environ. 68(3): 387-395. DOI:10.1007/s10064-009-0210-5

Chapuis, R.P., 1998. Overdamped slug test in monitoring wells: review of interpretation methods with mathematical, physical, and numerical analysis of storativity influence. Can. Geotech. J. 35(5): 697-719. DOI:10.1139/Cgj-35-5-697

Chapuis, R.P., 2002. The 2000 R.M. Hardy Lecture: Full-scale hydraulic performance of soil–bentonite and compacted clay liners. Can. Geotech. J. 39(2): 417-439. DOI:10.1139/t01-092

Chapuis, R.P., 2005. Numerical modeling of rising-head permeability tests in monitoring wells after lowering the water level down to the screen. Can. Geotech. J. 42(3): 705-715. DOI:10.1139/t05-003

Chapuis, R.P., 2009b. Field variable-head test in low-permeability materials: Assessing the effects of trapped gas pocket and cavity expansion. Can. Geotech. J. 46(1): 81-92. DOI:10.1139/T08-106

Chapuis, R.P., 2010. Influence of Element Size in Numerical Studies of Seepage: 1. Large-Scale of Regional Studies. Geotech. News, 28(4): 31-34.

Chapuis, R.P., Chenaf, D., 2002. Slug tests in a confined aquifer: experimental results in a large soil tank and numerical modeling. Can. Geotech. J. 39(1): 14-21. DOI:10.1139/t01-070

Chapuis, R.P., Gill, D.E., 1989. Hydraulic anisotropy of homogeneous soils and rocks: influence of the densification process. Bull. International Association of Engineering Geology-Bulletin de l'Association Internationale de Géologie de l'Ingénieur, 39(1): 75-86.

Chapuis, R.P., Gill, D.E., Baass, K., 1989. Laboratory permeability tests on sand: influence of the compaction method on anisotropy. Can. Geotech. J. 26(4): 614-622.

Cherry, J. et al., 2004. Role of aquitards in the protection of aquifers from contamination: a "state of the science" report.

Chien, Y., Bryce, R., Strait, S., Yeatman, R., 1986. Elimination of frequency noise from groundwater measurements, Rockwell International Corp., HC Burkholder, pp. 389–400, Battelle Press, Richland, Washington.

Cooper, H.H., Bredehoeft, J.D., Papadopulos, I.S., 1967. Response of a finite-diameter well to an instantaneous charge of water. Water Resour. Res. 3(1): 263-269. DOI:10.1029/WR003i001p00263

Duhaime, F., 2012. Mesure de la conductivité hydraulique du dépôt d'argile Champlain de Lachenaie, Québec: théorie et applications, PhD thesis, department of CGM, École Polytechnique de Montréal., Quebec, Canada.

Duhaime, F., Benabdallah, E.M., Chapuis, R.P., 2013. The Lachenaie clay deposit: some geochemical and geotechnical properties in relation to the salt-leaching process. Can. Geotech. J. 50(3): 311-325. DOI:10.1139/cgj-2012-0079

Duhaime, F., Chapuis, R.P., 2014. A coupled analysis of cavity and pore volume changes for pulse tests conducted in soft clay deposits. Int. J. Numer. Anal. Methods Geomech. 38(9): 903-24. DOI:10.1002/nag.2238

Evans, K., Beavan, J., Simpson, D., Mousa, S., 1991. Estimating aquifer parameters from analysis of forced fluctuations in well level: An example from the Nubian Formation near Aswan, Egypt: 3. Diffusivity estimates for saturated and unsaturated zones. J. Geophys. Res. Solid Earth (1978–2012), 96(B7): 12161-12191.

Ferris JG., 1952. Cyclic fluctuations of water level as a basis for determining aquifer transmissibility. U.S. Geological Survey, Ground-Water Hydraulics Section, Contribution No. 1, 17 p.

Ferris JG., 1963. Cyclic fluctuations of water level as a basis for determining aquifer transmissibility. Water-Supply Paper 1536-I, U.S. Geological Survey, pp. 305–318.

Furbish, D.J., 1991. The response of water level in a well to a time series of atmospheric loading under confined conditions. Water Resour. Res. 27(4): 557-68. DOI:10.1029/90WR02775

GSI Environnement, 2001. Étude géotechnique, agrandissement du secteur nord, lots parties 77 a` 87, 90, 93, 94, 99 et 100.

Hantush, M.S., 1966. Wells in homogeneous anisotropic aquifers. Water Resour. Res. 2(2): 273-279.

Hydrotechnique Associates., 1984. Evaluation of barometric and earth tide effects in well records: documentation. Report prepared for Rockwell Hanford Operations, by Hydrotechnique Associates, Berkeley, California.

Hussein, M.E., Odling, N.E., Clark, R.A., 2013. Borehole water level response to barometric pressure as an indicator of aquifer vulnerability. Water Resour. Res. 49(10): 7102-7119. DOI:Doi 10.1002/2013wr014134

Hvorslev, M.J., 1951. Time lag and soil permeability in ground-water observations, Waterways Experiment Station, Corps of Engineers, Vicksburg, Miss.

Jacob, C., 1940. On the flow of water in an elastic artesian aquifer. Transactions, American Geophysical Union, 21(2): 574-586. DOI:10.1029/TR021i002p00574

Jacob, C., 1950. Flow of Groundwater. Engineering Hydraulics, Chapter 5 in Engineering Hydraulics, ed. H Rouse. John Wiley & Sons, New York, pp. 321-386.

Keller, C.K., Van Der Kamp, G., Cherry, J.A., 1989. A multiscale study of the permeability of a thick clayey till. Water Resour. Res. 25(11): 2299-2317.

Krahn, J., 2004. Seepage modeling with SEEP/W: An engineering methodology. GEO-SLOPE International Ltd. Calgary, Alberta, Canada.

Leroueil, S., Bouclin, G., Tavenas, F., Bergeron, L., Rochelle, P.L., 1990. Permeability anisotropy of natural clays as a function of strain. Can. Geotech. J. 27(5): 568-579. DOI:10.1139/t90-072

Marefat, V., Duhaime, F., Chapuis, R.P., 2015a. Pore pressure response to barometric pressure change in Champlain clay: Prediction of the clay elastic properties. Eng. Geol. 198: 16-29. DOI:dx.doi.org/10.1016/j.enggeo.2015.09.005

Marefat, V., Duhaime, F., Chapuis, R.P., 2015b. Fully grouted piezometers: Implications for pore pressure monitoring in clay layers. Eng. Geol. Submitted.

MATLAB(™)., 2010. The MathWorks, Inc. 3 Apple Hill Drive, Natick, Massachusetts.

McKenna, G.T., 1995. Grouted-in installation of piezometers in boreholes. Can. Geotech. J. 32(2): 355-363.

Mitchell, J.K., 1956. The fabric of natural clays and its relation to engineering properties, Highway Research Board, Washington, D.C., vol. 35 (1956), pp. 693–713

Neuman, S.P., Gardner, D.A., 1989. Determination of Aquitard/Aquiclude Hydraulic Properties from Arbitrary Water-Level Fluctuations by Deconvolution. GroundWater, 27(1): 66-76. DOI:10.1111/j.1745-6584.1989.tb00009.x

Neuzil, C.E., 1982. On conducting the modified 'Slug' test in tight formations. Water Resour. Res. 18(2): 439-441. DOI:10.1029/WR018i002p00439

Neuzil, C.E., 1994. How permeable are clays and shales? Water resources research, 30(2): 145-150.

Odling, N.E., Perulero Serrano, R., Hussein, M.E.A., Riva, M., Guadagnini, A., 2015. Detecting the vulnerability of groundwater in semi-confined aquifers using barometric response functions. J. Hydrol. 520(0): 143-156. DOI: http:10.1016/j.jhydrol.2014.11.016

Rasmussen, T.C., Crawford, L.A., 1997. Identifying and removing barometric pressure effects in confined and unconfined aquifers. Groundwater, 35(3): 502-511.

Rojstaczer, S., 1988. Determination of fluid flow properties from the response of water levels in wells to atmospheric loading. Water Resour. Res. 24(11): 1927-38. DOI:10.1029/WR024i011p01927

Scholes, O., Clayton, S., Hoadley, A., Tiu, C., 2007. Permeability anisotropy due to consolidation of compressible porous media. Transport in porous media, 68(3): 365-387.

Smerdon, B.D. et al., 2014. Estimating the hydraulic properties of an aquitard from in situ pore pressure measurements. Hydrogeol. J. 22(8): 1875-1887. DOI:10.1007/s10040-014-1161-x

Smith, L.A., Van Der Kamp, G., Hendry, J.M., 2013. A new technique for obtaining high-resolution pore pressure records in thick claystone aquitards and its use to determine in situ compressibility. Water Resour. Res. 49(2): 732-743. DOI:10.1002/wrcr.20084

Spane, F.A., 1999. Effects of barometric fluctuations on well water-level measurements and aquifer test data. Pac. Northwest Natl. Lab., Dep. of Energy., Richland, Wash.

Spane, F.A., 2002. Considering barometric pressure in groundwater flow investigations. Water Resour. Res. 38(6): 14-1-14-18.

Spane, F.A.J., 1992. Applicability of slug interference tests under Hanford Site test conditions: Analytical assessment and field test evaluation. Pacific Northwest laboratory, Richland, WA. PNL-8070.

Tavenas, F., Jean, P., Leblond, P., Leroueil, S., 1983. The permeability of natural soft clays. Part II: Permeability characteristics. Can. Geotech. J. 20(4): 645-660. DOI:10.1139/t83-073

Timms, W.A., Acworth, R.I., 2005. Propagation of pressure change through thick clay sequences: an example from Liverpool Plains, NSW, Australia. Hydrogeol. J. 13(5-6): 858-870. DOI:10.1007/s10040-005-0436-7

van der Kamp, G., 2001. Methods for determining the in situ hydraulic conductivity of shallow aquitards – an overview. Hydrogeol. J. 9(1): 5-16. DOI:10.1007/s100400000118

van der Kamp, G., Gale, J.E., 1983. Theory of Earth tide and barometric effects in porous formations with compressible grains. Water Resour. Res. 19(2): 538-44. DOI:10.1029/WR019i002p00538

van der Kamp, G., Maathuis, H., 1991. Annual fluctuations of groundwater levels as a result of loading by surface moisture. J. Hydrol. 127(1): 137-152.

Weeks, E.P., 1979. Barometric fluctuations in wells tapping deep unconfined aquifers. Water Resour. Res. 15(5): 1167-1176.

Witt, K.-J., Brauns, J., 1983. Permeability-anisotropy due to particle shape. J. Geotech. Eng. 109(9): 1181-1187.

Zienkiewicz, O.C., Taylor, R.L., Zhu, J.Z., 2005. The finite element method: its basis and fundamentals. Elsevier Butterworth-Heinemann.

CHAPTER 6   SUMMARY AND GENERAL DISCUSSION

The introduction and the literature review have presented gaps and uncertainties regarding pore pressure measurement with fully grouted piezometers and the analysis of natural pore pressure changes for clay aquitard piezometers. Some of these gaps were addressed in this dissertation. The following points list the main contributions for the three papers:

- The performance, capacity and limitations of fully grouted piezometers for natural pore pressure measurements in clay aquitards was evaluated using analytical and numerical solutions.

- The real clay aquitard BRF/BHRF provided loading efficiency values for clay layer.

- The multiple-regression method was used to remove barometric pressure effects on pore pressure time series registered by closed piezometers in clay aquitards.

- The clay aquitard BRF/BHRF was applied to estimate in-situ horizontal hydraulic conductivity of a clay aquitard.

- Spectral frequency analyses provided pressure head amplitude associated with an annual period cycle.

- A combined low- and high-frequency analysis of natural pore pressure fluctuation measured the in-situ hydraulic conductivity anisotropy.

The first objective in this thesis was to assess the performance of fully grouted piezometers deployed in clay aquitards. To do so, a closed-form solution was derived and verified with a finite element code. The analytical solution allows the piezometric error to be calculated for fully grouted piezometers under steady-state seepage conditions. Various factors influencing the piezometeric error were studied analytically and numerically. These factors include the permeability ratio, the ratio of grout permeability to clay permeability (K_g/K_c), the vertical hydraulic gradient in the clay layer (i_v), and the ratio of borehole length within the clay layer to the total clay layer thickness (L/b).

Results show that the permeability ratio is not the sole factor controlling the piezometric error. The error is also influenced by the natural vertical hydraulic gradient and the borehole depth within the clay layer. For a given vertical hydraulic gradient, the error increases with the

permeability ratio. The analytical solution of Vaughan (1969) and the numerical simulations of Contreras et al. (2008) found insignificant piezometric errors for permeability ratios of 100 and 1000 respectively. Our results show, however, this claim might only be true for small values of the hydraulic gradient (i.e., $i^* \approx 0.1$). Results also show that in all cases the error increases when $K_g/K_c > 1$.

The vertical hydraulic gradient has a fundamental impact on fully grouted piezometer performance. The infuence of the vertical hydraulic gradient on piezometric error was not taken into account by Vaughan (1969) and Contreras et al. (2008). The vertical hydraulic gradient changes with seasons or any variation in the groundwater table or underlying aquifer hydraulic head. This was observed during the baseline pore pressure monitoring in the Lachenaie clay deposit. Baseline pore pressure monitoring displayed a significant seasonal change in vertical hydraulic gradient for some of the observation sites. For example, at a test site next to the Mille-Îles River, the vertical hydraulic gradient changed by about two orders of magnitude during one year. Our results reveal that for a given permeability ratio, the piezometric error increases linearly with the vertical gradient. According to the analytical and numerical results, the grout permeability must be similar or one order of magnitude greater than the surrounding clay permeability to have an acceptable hydraulic head measurement, for most field conditions with a vertical hydraulic gradient of less than unity. This is consistent with the conclusion of McKenna (1995).

The performance of fully grouted piezometer is also influenced by the borehole geometry. In this study, the impact of borehole penetration depth, L/b, on piezometric error was studied. The error increases with L/b ratio, especially for permeability ratios, K_g/K_c, higher than 100. For $K_g/K_c > 100$, a very good correlation was found between analytical and numerical results. However, for smaller permeability ratios (i.e., $K_g/K_c = 10$), the numerical simulations revealed that L/b has no significant influence on the piezometric error and the error was larger than that predicted by the analytical solution. This is related to one of the hypotheses on which the analytical solution is based: it is assumed that the unit flow rate increases linearly along the borehole. The numerical results confirmed that this hypothesis was only true for $K_g/K_c \geq 100$.

Natural loading phenomena or human activities induce short to long-term transient groundwater flow which sometimes need to be measured with piezometers. If fully grouted piezometers are

planned to measure these transient pressure changes, the grout and surrounding formation storativity/elastic properties may also have some impact on the piezometer response time and the measurement accuracy. These are not addressed in the current study. More complete studies are required to fully assess the fully grouted piezometers performance when subjected to transient flow conditions.

Unfortunately, information on cement-bentonite grout properties and on the performance of fully grouted piezometers is lacking. The available data mostly concern the properties of cement-bentonite mixes that include sand, soil, or other materials for specific geotechnical applications such as cut-off walls, clay liners and so forth. Moreover, previous studies regarding the performance of fully grouted piezometers only present case studies for specific applications (McKenna, 1995; Simeoni et al., 2011; Contreras et al., 2012). More experimental and in-situ studies are needed to systematically appraise the performance of fully-grouted piezometers.

The primary goal behind this study of analysis methods for natural loading phenomena was to improve baseline natural pore pressure monitoring. This thesis demonstrates how a combined analysis of natural well water-level/pore pressure fluctuations in a shallow aquifer and aquitard system covers the above-mentioned gaps. A multi timescale natural pore pressure response to barometric pressure change and annual groundwater recharge events was used to determine in-situ clay elastic and hydraulic properties and its permeability anisotropy without conducting conventional in-situ tests.

Five (5) observation sites, covering an area of 50 km^2, were established in the Lachenaie area, near Montreal, Quebec, Canada. They have been monitored for pore pressure since November 2012. The stratigraphy of the study area comprises an intact Champlain clay deposit. The intact clay layer is located between two aquifers on top and bottom. The top aquifer is composed of either sand of alluvial or eolian origin, or up to 5 m of fissured and oxidized clay. Under the top aquifer, the unoxidized part of the clay deposit has a thickness varying between 11 and 25 m depending on the site. Below the intact clay is a till layer and the fractured upper portion of the shale bedrock with a thickness of 6 to 10 m.

On each observation site, two pressure transuducers (PT) and two vibrating wire pressure transducers (VWP) were installed for pressure head monitoring in the surficial and confined aquifers and in the clay aquitard respectively. Barometric pressure fluctuations were measured

on each site with an atmospheric pressure transducer (APT). In the surficial aquifer, a PT was installed within an open standpipe piezometer to measure hydraulic head fluctuations in this aquifer. In the confined aquifer, a PT was installed within a pre-existing MW, fully sealed in the clay layer. In the clay aquitard, two VWPs were sealed at the upper and lower third of the clay aquitard to monitor the short- to long-term pore pressure changes.

The Champlain clay mechanical properties (e.g., compressibility, specific storage) were calculated based on the in-situ loading efficiency (LE). The LE was determined using three methods: linear regression, visual inspection and BHRF analysis. To obtain representative LE values, the effect of other natural phenomena on pore pressure data were limited. A period during winter was selected because of the limited recharge/discharge due to frozen soil. In addition, for shallow piezometers, Earth-tide stress effects were found to be negligible. This was verified with a spectral frequency comparison between pore pressure response and synthetic Earth tide data. A comparison of frequency spectrum between Earth tide fluctuations and pore pressure responses on site 2 during winter 2014 (from January 1st to April 1st) is presented in Figure 6.1.
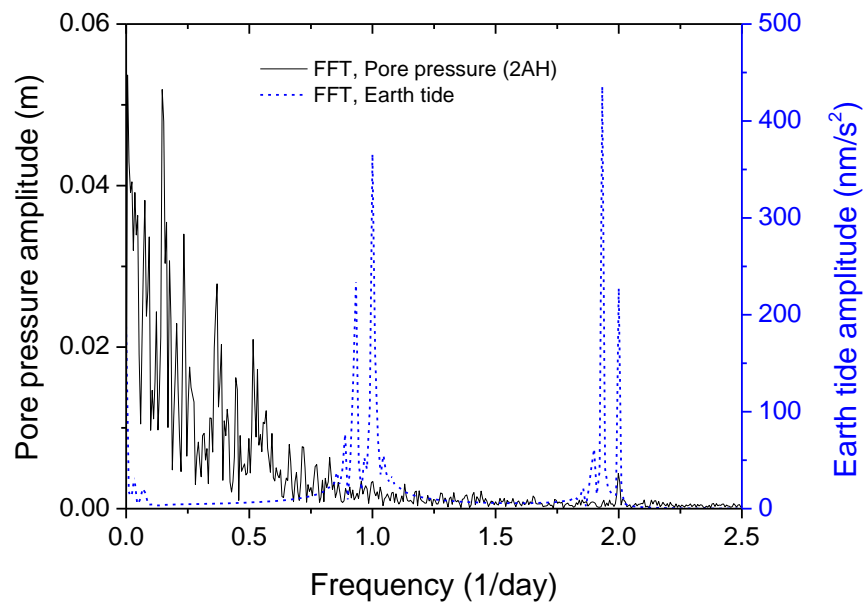
Figure 6.1: Frequency spectrum comparison between Earth tide fluctuations and pore pressure response, piezometer 2AH (data from January 1st to April 1st 2014).

As shown in Figure 6.1, earth tide fluctuations are not responsible for pore pressure change during winter measurement. Pore pressure only slightly responded for an earth tide component with frequency of 2 day^{-1}. A similar FFT comparison between earth tide fluctuations and pore pressure responses for other clay piezometers was obtained (not shown here). Therefore, for winter measurement the reaming natural loading on pore pressure fluctuations is barometric stress changes. Figure 6.2 presents a relationship between barometric loading and pore pressure response for winter 2014 data.
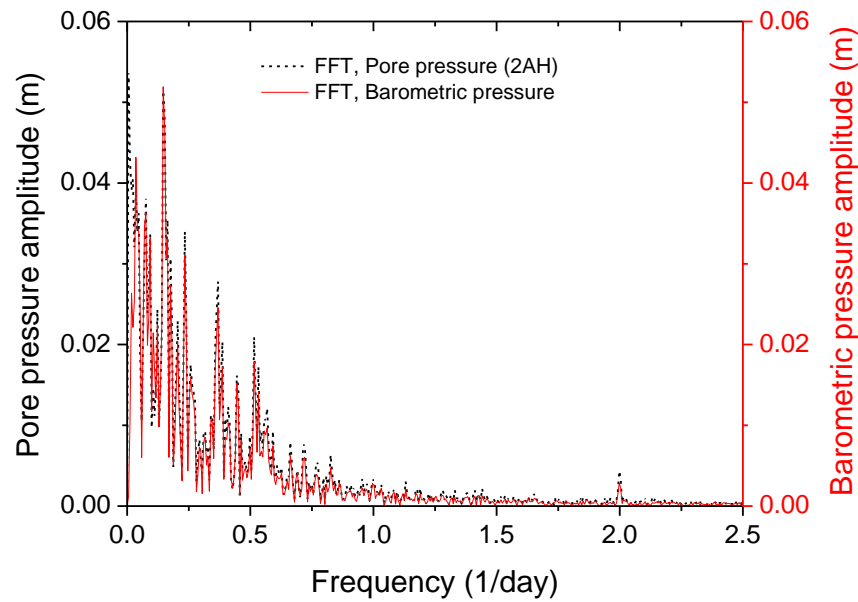
Figure 6. 2: Frequency spectrum comparison between barometric loading and pore pressure response, piezometer 2AH (data from January 1st to April 1st 2014).

For winter measurement, pore pressure fluctuations were completely explained by barometric loading (Figure 6.2). As shown for the pore pressure component with frequency of 2 day^{-1} barometric loading change is also contributed in the pore pressure fluctuation. Therefore, for data subsets acquired during winter, the major external stress controlling the pore pressure response is the change in barometric pressure. Thus, analysis of natural pore pressure response during winter provides representative LE values for the clay aquitard.

Three methods provided LE values between 0.80 and 0.95. For each well, LE values obtained

with each method differed by less than 10%. The linear regression method usually gave higher LE values than the other methods. For confined conditions with an instantaneous response, without any time lag between barometric pressure change and pore pressure response, the linear regression method provided a good fit. However, for a well with a significant time lag in the pore pressure response, the best fit between barometric pressure change and pore pressure response was poor. For such cases, the BHRF is a more robust method to describe a stabilized LE. The BHRF analysis confirmed that LE is time lag dependent for low permeability Lachenaie clay. Loading efficiency is also frequency dependent: LE decreases with increasing signal frequencies (Weeks, 1979). Our results showed a 5% decrease in LE decreasing the measurement frequency from 0.0567 to 0.0167 min^{-1} (i.e., measurement intervals from 15 to 60 min).

The maximum barometric pressure change registered during winter in the study area (i.e.,~6 kPa for winter measurements) was well below the difference between preconsolidation pressure (σ'_p = 180 to 580 kPa) and the in situ stress conditions. Thus, barometrically induced strains are very small and governed by the theory of elasticity. Accordingly, the values obtained for clay elastic properties, using the in situ LE method, correspond to the elastic and very small strain in-situ properties which are needed for the dynamic analyses of soil behaviour (e.g., Karray and Lefebvre, 2008, Lefebvre et al., 1994 and Youd et al., 2001).

Clay compressibility, m_v, and S_s on the order of 1.0×10^{-6} kPa^{-1} and 1.0×10^{-5} m^{-1} were respectively found based on the in-situ LE calculation for the standard values of freshwater density and compressibility, and the test interval porosity values. The m_v values obtained in this study are approximately one order of magnitude lower than previous results obtained with pulse tests, and approximately two orders of magnitude lower than those obtained with oedometer tests (Duhaime, 2012; Duhaime and Chapuis, 2014). However, the values obtained for m_v and S_s in this study fall within the range of slightly overconsolidated fluvial clay deposits and shallow overconsolidated formations as reported respectively in Timms and Acworth (2005) and Smith et al. (2013) based on similar in-situ LE analyses. Comparing the clay elastic parameters obtained by in-situ LE analyses with those from conventional tests confirms that the clay elastic properties are strain dependent.

This study used natural pore pressure fluctuations in various time scales to assess the Lachenaie clay hydraulic diffusivity and conductivity. Short-term pore pressure fluctuations caused by high

frequency barometric pressure changes was analyzed in terms of BHRF to estimate the clay horizontal hydraulic conductivity. Similar to in-situ variable head tests in MWs, the estimated horizontal hydraulic conductivity represents permeability condition for immediate vicinity of the borehole which is categorized as a medium scale in this study. On the other hand, analyses of the long-term pore pressure fluctuations provided vertical hydraulic diffusivity and conductivity of the clay deposit for large scale. Table 6.1 compares various permeability tests for a clay deposit in terms of scale and direction of the measurement.

Table 6.1: Comparison between various permeability tests in terms of scale and direction of the measurement. H = horizontal, V = vertical, S = small, M = medium, L = large, MW = monitoring well, PWP = pore water pressure, BP = barometric pressure, GW = groundwater.

Test/method	Direction		Scale			Anisotropy
	H	V	S	M	L	
Laboratory tests (core samples)	×	×	×			Yes
In-situ variable head tests in MW	×			×		No
In-situ slug/pulse test	×			×		No
Natural pore pressure analyses (short-term PWP response to barometric pressure change)	×			×		Yes
Natural pore pressure analyses (Long-term PWP response to downward GW recharge cycles)		×			×	
Aquifer pumping test with considering leakage from clay aquitard		×			×	No

This study analyzed actual clay aquitard pressure responses obtained from partially penetrating wells within clay as a basis for estimating in-situ clay aquitard hydraulic and elastic properties. This type of analysis was not conducted in previous BRF analyses performed by Butler et al.

(2011) and Hussein et al. (2013). Both studies fitted BRF from a confined aquifer response with an analytical model to determine the vertical hydraulic diffusivity for the overlying confining layer/clay aquitard system.

In the time domain, BHRF is an impulse function that can be determined from slug test solutions (Furbish, 1991; Rasmussen and Crawford, 1997). For Lachenaie clay, the general BHRF shape conforms to the composite confined aquifer model with wellbore storage as proposed by Spane (1999, 2002). Rasmussen and Crawford (1997) and Spane (2002) used the Hvorslev (1951) and Cooper et al. (1967) slug test solutions to describe the BRF/BHRF of a well/aquifer system. However, both solutions have limiting assumptions. The former solution does not take into account the formation storativity/elasticity and the latter solution is not able to take into account the horizontal deformation of the borehole cavity which is significant in compressible clay (Duhaime and Chapuis, 2014). The finite-element code SEEP/W (Krahn, 2004) which provides greater latitude that is not easily addressed with those analytical methods, was used to model a slug test as an analogue to BHRF. The clay horizontal hydraulic conductivity was determined by curve fitting between observed BHRF and the predicted numerical model, both in type-curve format.

The numerical simulations were carried out in three steps. The first step was to model a steady-state condition by applying an arbitrary constant total head of 25 m as a boundary condition. This step was used as an initial condition for the subsequent transient simulation. The second step was to model a first transient using a total head versus time boundary condition. This first transient corresponds to a sudden pressure increase of 1 kPa in 1 second within the sealed sand cavity. The final step was to model the dissipation through time of the hydraulic head difference between the sand cavity and the clay formation. This step was initiated using a hydraulic head versus water volume outflow H(V) boundary condition. The slope of the H(V) boundary condition was calculated using the relationship between change in cavity volume and cavity pressure through the shear modulus described in Duhaime and Chapuis (2014).

Three key parameters including clay horizontal hydraulic conductivity, cavity volume change and clay compressibility influence the equilibration of the pore pressure imbalance between the sand filter cavity and surrounding clay layer. The sensitivity of the BHRF with respect to each parameter was determined. The numerical results demonstrated that the model was most

sensitive toward clay hydraulic conductivity and cavity volume change while, it displayed little sensitivity toward clay compressibility.

Curve matching between the observed BHRF and the numerical type-curves yielded K_h values between 2.6×10^{-10} and 7.0×10^{-10} m/s for most piezometers. A lower K_h value of 6×10^{-11} m/s was obtained for the lower piezometer on site 2 (i.e., 2AB). This is related to its very slow BHRF response in comparison to the other piezometers. Comparing BHRF response for the piezometers showed that for this piezometer the system compressibility appears to be higher than that dictated by cavity expansion and water compressiblity alone. A possible explanation for the higher compressibility and slow BHRF response for this well could be air entrapment within the sand filter during piezometer installation. In addition, the Lachenaie clay contains some organic matter known to produce gas (Duhaime and Chapuis, 2014).

The K_h values obtained in this study are slightly lower than those based on conventional in-situ tests. Variable head tests resulted in K values between 9×10^{-10} and 8.8×10^{-9} m/s (GSI Environnement, 2001; Benabdallah, 2006; Duhaime, 2012). The lowest hydraulic conductivity values could be explained by the effects of gas compressibility within the closed piezometer cavities. Air compressibility slows piezometric responses. More complete study is required to explain these low K values by modelling composite gas-water compressibility and cavity expansion with a multiphysics FEM engine like COMSOL.

The analysis of long-term natural groundwater recharge provided the clay vertical hydraulic diffusivity. Cyclic groundwater recharge events imposed by the surficial aquifer attenuates and delays while propagating downward within the clay layer toward the underlying confined aquifer. Observed hydrographs for open wells and closed piezometers exhibited that various components with variable frequencies are embedded within the well/piezometer responses. The measured pressure head data in this study only represents seasonal recharge and discharge for around 2 years. A longer-term data (i.e., 10-20 years) would provide enhanced understanding of seasonal pore pressure behaviour of the Lachenaie clay aquitard. To identify the effects of various natural loading sources on pore pressure responses, time series were converted from time domain to frequency domain by applying FFT. Figure 6.3 shows a frequency spectrum comparison between long-term pore pressure cycles in clay and groundwater cycle in shallow aquifer. As shown, for periods of less than 85 days, pore pressure changes within clay are

completely explained by barometric pressure fluctuations. However, the downward groundwater recharge within the shallow aquifer was responsible for the low frequency fluctuations on pore pressure within clay layer (Figure 6.3).
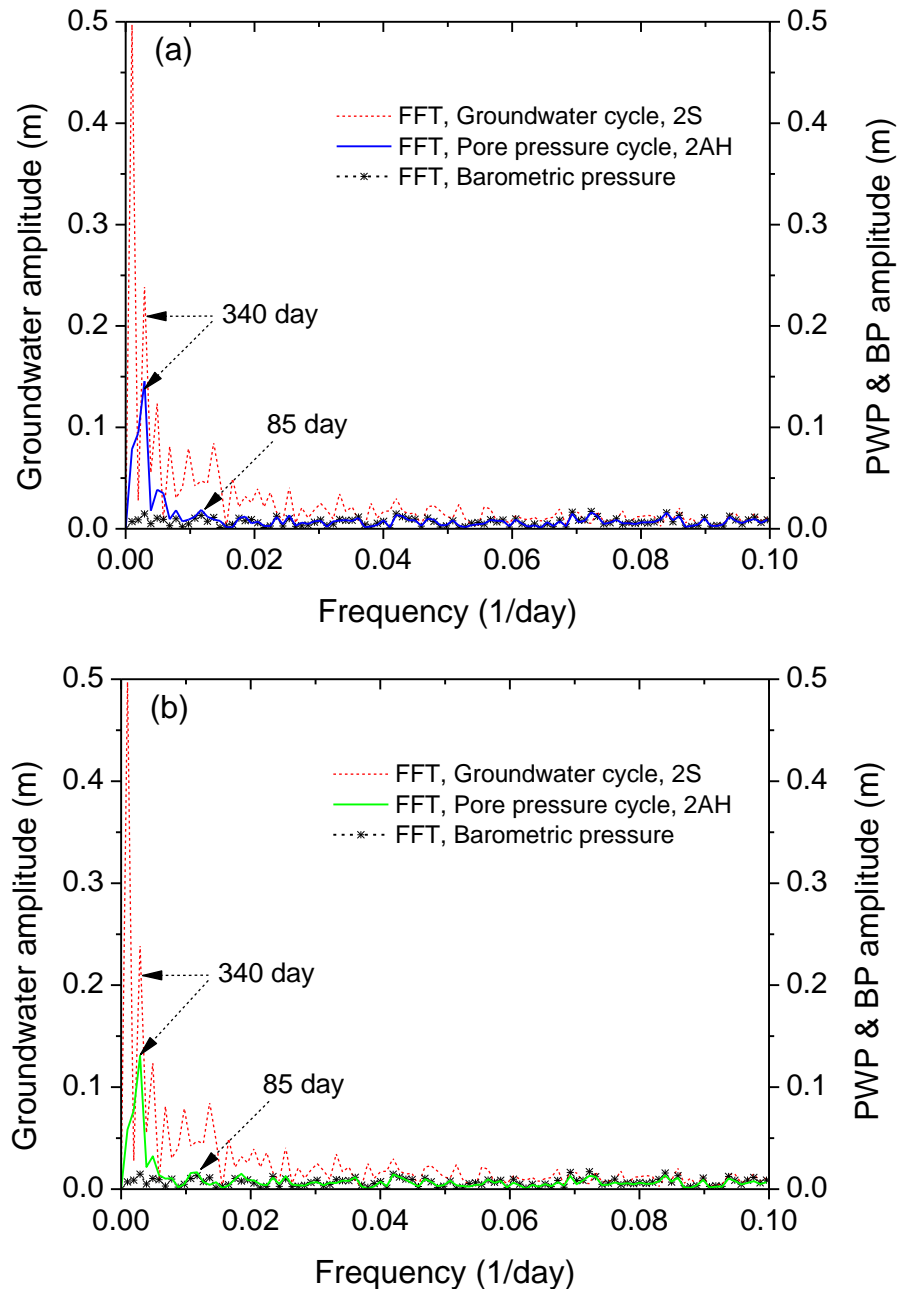
Figure 6. 3: Frequency spectrum comparison between long-term pore pressure cycles in clay and groundwater cycle in shallow aquifer, data from Nov. 2012 to Jul. 2015 (site 2, Lachenaie).

The fluctuations caused by changes in the total moisture above the clay formation, including moisture and snow loading, were considered as a high-frequency loading. Therefore, their immediate effect to pore pressure fluctuations was filtered out by applying band-pass filtering application. However, their accumulative effect to pore pressure fluctuations is not addressed in this study.

As shown on Figure 6.3 clay piezometers substantially responded for the component of downward groundwater recharge with a period that is close to an annual cycle. Therefore, efforts were focused on isolating the well/piezometer responses for frequencies bounding an annual cycle. To do so, band-pass filtering with band width frequency range of 0.0024 to 0.00328 day^{-1} (i.e., periods of 425 to 305 days) was applied to pressure head data series. With band-pass filtering, only the frequency content within the specified frequency range can pass through. In the filtered well/piezometer response, the frequency signals which were higher and lower than the specified frequency range were effectively removed. The filtered responses of clay aquitard piezometers displayed a good but attenuated correlation for annual groundwater recharge with respect to surficial aquifer responses. However, the correlation was poor for the filtered annual head cycle for the underlying confined aquifer. In addition, filtered response for piezometer 2AB showed an out of phase response. The cause for this phase difference for piezometer 2AB is not currently known. However, a phase lag analysis of the downward groundwater cycle may provide an appropriate information about the cycles phase response.

The pressure head amplitude associated with the specified frequency range for each clay aquitard location were calculated by performing spectral frequency analysis on the filtered data using the ETFFT software program, as described in Hydrotechnique Associates (1984). It should be noted that the same spectral frequency and filtering analysis can also be generated using various commercially-available mathematical software programs. In this study the spectral frequency analysis was also conducted using MATLAB^{TM} (2010). The spectral frequency analysis also exhibited correlated, but attenuated amplitude profile for clay aquitard piezometers with respect to that for surficial well. This indicates that their response characteristics are largely influenced by the annual vertical/recharge cycle. However, this high degree of correspondence does not appear in the underlying confined aquifer well response. This may imply that hydrologic phenomena other than vertical annual recharge may be included in the annual confined aquifer response pattern (e.g., areal/lateral groundwater flow/recharge).

The vertical hydraulic diffusivities and conductivities of the clay aquitard were calculated for the band width frequencies of 0.0024 to 0.00328 day^{-1}. Applying the associated amplitude ratios and the depth from the top of the clay aquitard to the top of the monitored test interval in Eq. (5.3) yields a D_v value of about 1.0×10^{-5} m^2/s for the Lachenaie clay aquitard. This is slightly higher than the value obtained by Keller et al. (1989) for a dense clayey till in Saskatchewan, using the analysis of cyclic groundwater recharge events. However, the D_v values obtained for Lachenaie clay agree with that for smectitic clay on the Liverpool Plains, Australia calcualted from downward groundwater recharge analysis (Timms and Acworth, 2005). Comparing the pressure wave penetration depth in the Lachenaie study area (i.e., 25 m) with that for the test site of Keller et al. (1989) (i.e., 10 m) supports the slightly higher hydraulic diffusivity obtained in this study for the Lachenaie clay.

The vertical hydraulic diffusivity is a function of both vertical hydraulic conductivity and storativity (or elasticity) of the formation. The in-situ clay aquitard vertical hydraulic conductivity was derived by applying direct measurement of in-situ S_s values (on the basis of LE analysis utilizing the BHRF method) in the D_v calculation. Vertical hydraulic conductivity values of about 1.0×10^{-10} m/s were obtained for the Lachenaie clay aquitard. The obtained in-situ K_v values from analysis of natural groundwater recharge cycle are at the lower bound of previously obtained K values from standard laboratory and in-situ tests for the same study area.

Conventional in-situ test (e.g., variable head-test in MW) and the high-frequency BRF analysis provides hydraulic properties in the immediate vicinity of the borehole intake zone (e.g., Keller et al., 1989; Hussein et al., 2013). Analysis of low-frequency pore pressure response (e.g., propagation of the annual groundwater recharge cycle) gives hydraulic properties in large-scale involving fractures and high flow pathways. The nearly identical hydraulic conductivity values obtained from combined low- and high-frequency analysis for various observation sites over a distance up to 2.5 km indicates a high degree of clay integrity for the Lachenaie clay aquitard. An additional study is required to assess Lachenaie clay aquitard integrity and the underlying confined aquifer vulnerability using the natural pore pressure response as an indicator which is not addressed in the current study.

The combined analysis of pore pressure response to high-frequency barometric pressure and low-frequency annual groundwater recharge was used to assess the in-situ anisotropy of hydraulic

conductivity. The combined analysis approach yields a low anisotropy for the Lachenaie clay aquitard. This agrees with previous findings for the same study area (Duhaime, 2012) and for other localities in the former Champlain Sea basin (Tavenas et al., 1983a; Leroueil et al., 1990). In addition, the obtained anisotropy ratios fall within the range for various homogenous clays (from 0.7 to 4) as reported previously in Chapuis and Gill (1989).

The study of this thesis showed that a baseline pore pressure monitoring program provides noteworthy data which can be used alone to assess the clay aquitard hydraulic and elastic properties. A longer pore pressure monitoring would be helpful to investigate the impact of climate change on some hydrogeological and geotechnical issues; for example, predicting of groundwater recharge and discharge, groundwater contamination, and the stability of natural slopes. However, baseline pore pressure monitoring to estimate clay aquitard vertical hydraulic conductivity is time consuming. It may take more than 1 year to collect enough data to analyze a cyclic groundwater recharge event. The multi-timescale method could be used in conjunction with slug tests to gather progressively more valuable in-situ data on the permeability of a clay aquitard. Furthermore, the baseline pore pressure monitoring is a valuable practice for contaminated sites which undergoing remediation programs.

CHAPTER 7   CONCLUSION AND RECOMMENDATION

The first part of this chapter presents the results of the thesis for each of the objectives that were presented in Chapter 1. The second part presents recommendations for future works.

7.1 Conclusion

This section reviews the results of the thesis for each of the objectives that were listed in the introduction.

Objective 1: Determining the capacity of the fully grouted installation method when it is deployed for pore pressures measurement within clay layers.

A closed-form solution was developed to determine the limitations of fully grouted piezometers installed within clay layers or aquitards under steady state conditions. The analytical solution has been verified using the finite element code SEEP/W. More than 300 numerical simulations were completed. The influence on the performance of fully grouted piezometers of the permeability ratio (ratio of grout permeability to surrounding aquitard permeability), natural vertical hydraulic gradient, and borehole length within the aquitard were studied. For steady state seepage conditions, the piezometeric error ε was found to be strongly related to the permeability ratio and the vertical hydraulic gradient.

For field conditions with $i^*<1$, the numerical and analytical results showed that the error ε is insignificant for grouts with a permeability up to one order of magnitude greater than the surroundig soil permeability. For field conditions with a very low vertical hydraulic gradient ($i^* \approx 0.1$), the ε value is small but the maximum theoretical error is also small. Borehole geometry influences fully grouted piezometer performance only for $K_g/K_c \geq 100$. For a low permeability ratio ($K_g/K_c < 10$), the piezometric error does not change significantly with borehole depth.

Objective 2: Estimating the in situ elastic parameters of compressible Lachenaie clay for very small strain utilizing the natural pore pressure response to barometric pressure change.

In-situ natural pore pressure analyses yield values for m_v and S_s on the order of 1.0×10^{-6} kPa^{-1} and 1.0×10^{-5} m^{-1} respectively based on loading efficiency calculations. These values highlight

some practical implications regarding the elastic parameters of the Lachenaie clay associated with very small strains. The m_v values obtained in this study are one order of magnitude lower than previous results obtained with pulse tests, and approximately two orders of magnitude lower than those obtained with oedometer tests. The constrained modulus values obtained in this study were also compared with those obtained from G values in the literature by assuming a Poisson's ratio between 0.3 and 0.5. Comparing clay elastic parameters obtained from various laboratory and in-situ methods revealed that the elastic parameters are strain-dependent. The loading efficiency calculations provided a high modulus for very small strains (undisturbed conditions), whereas the field and laboratory tests provided a lower modulus because either the wall of the borehole or the tested specimen have been slightly remoulded before testing, which decreases the modulus.

Objective 3: Calculating the loading efficiency for a soft clay aquitard using BHRF analysis.

Results show that the pore pressure response within low permeability Lachenaie clay is delayed and becomes time-lag dependent. Therefore, BHRF analysis was applied to determine representative LE values. The BHRF explicitly shows that the LE increases with time-lag up to a certain value and then stabilizes. The obtained LE values were also compared with those obtained from the linear regression and visual inspection methods. The three methods provided values for LE within a 10% range for a given piezometer.

Objective 4: Investigating the capability of multiple-regression for the removal of barometric pressure effects on pore pressure response in a soft clay aquitard.

The multiple regression and visual inspection methods were used to remove barometric pressure fluctuations from data series. For most piezometers, both methods provided similar corrected pore pressure time series. However, for deep piezometers with slow BHRF response, the multiple regression technique provided smoother pore pressure time series than the visual inspection method.

Objective 5: Calculating long-term variations of vertical hydraulic gradient within Champlain

clay.

The vertical hydraulic gradient was not constant for the 3-year monitoring period in this study. The variation in vertical hydraulic gradient was very high on some sites because of their hydrogeological characteristics. On most observation sites, the natural hydraulic gradient changed by around one order of magnitude from 0.01 to 0.1 during this study. On site 6, even larger variations in natural hydraulic gradient from -0.01 to 0.9 were observed. These natural gradient variations could potentially have a large influence on contaminant migration and salt leaching through the clay.

Objective 6: Estimating the in-situ vertical and horizontal hydraulic diffusivity and conductivity using a combined low to high-frequency analysis of associated well/piezometer response to barometric pressure change and cyclic groundwater recharge.

This study used a multi-timescale analysis of low- and high-frequency natural pore pressure responses to calculate vertical and horizontal hydraulic diffusivities and conductivities for the Lachenaie clay deposit. This approach allows the determination of clay aquitard hydraulic properties without conducting conventional hydrologic tests. Pressure head signals registered within the clay aquitards are reflecting various components, each with a distinct frequency or period. Band-pass filtering with a frequency range between 0.00244 and 0.00293 day^{-1} was applied to pressure time series in order to capture the pressure cycles with a period close to a year. This allowed the annual groundwater recharge cycle to be clearly captured and the amplitude ratios of this cycle as it propagated downward to be calculated. Applying the Fourier Transformation analysis to the filtered data yields amplitude ratios for annual groundwater recharge at each piezometer location. Vertical hydraulic diffusivity values on the order of 1×10^{-5} m^{2}/s were obtained for the clay aquitard.

Vertical and horizontal hydraulic conductivities on the order of 1×10^{-10} m/s were obtained for the Lachenaie clay aquitard. Vertical hydraulic conductivity was determined by substituting direct in-situ values of specific storage for each monitored depth interval from the BHRF analysis in the definition of the vertical hydraulic diffusivity. The horizontal hydraulic conductivity was estimated by matching the observed BHRF with the numerical type-curves that were prepared using SEEP/W.

Objective 7: Assessing the in-situ hydraulic conductivity anisotropy of clay aquitard from the multi-timescale analysis of naturally occurring groundwater/pressure head fluctuations without conducting conventional hydrologic tests.

Baseline pore pressure monitoring allowed the hydraulic conductivity anisotropy for the Lachenaie clay aquitard to be determined at the field scale. A comparison between the vertical and horizontal components of hydraulic conductivity obtained from combined analysis of natural pressure head response shows insignificant permeability anisotropy for Lachenaie clay. This is in a good agreement with previous works at the laboratory scale on Champlain clays.

7.2 Recommendation

Chapter 7 discusses the issues that were not addressed in this thesis. The following recommendations are provided for further research on fully grouted piezometer performance and natural pore pressure analysis:

- A laboratory investigation of cement-bentonite hydraulic and elastic properties for various mix recipes.

Information on cement-bentonite grout properties is lacking. A laboratory study is needed to investigate hydraulic conductivity for a wide recopies of cement-bentonite grout. Falling-head permeability test using a flexible wall permeameter can be conducted. Meanwhile, compressibility values for grout can be investigated with the oedometer test. Hydraulic diffusivity of grout as a significant controlling factor for fully-grouted piezometer installation can be introduced.

- Comprehensive laboratory, in-situ, and numerical studies to investigate fully grouted piezometer performance.

Fully grouted piezometers performance is still questioned. A laboratory test set-up controlling hydraulic gradient and borehole geometry can be established. For a various range of grout properties, the piezometer performance depends on hydraulic gradient and borehole geometry can be studies thoroughly. Large-scale in-situ tests are also important. Performance

of fully grouted piezometers can be compared with conventional piezometers for various grout properties. Numerical modeling in conjunction with laboratory and in-situ results can be used to investigate the fully grouted installation method for various cases.

- A complete study by modelling composite gas-water compressibility and cavity expansion with a multiphysics FEM engine like COMSOL to calculate accurate hydraulic conductivity values from BHRF results.

Entrapped gas within sand filter of a sealed piezometer slows pore pressure response and BHRF. This phenomenon cannot be studied with SEEP/W. However, with a multiphysics FEM engine like COMSOL, a domain can be added to sand filter or an ordinary differential equation can be tie at the boundary to study the influence of gas-water compressibility on BHRF.

- A study to take into account phase lag analyses of the downward groundwater recharge cycles after having removed the effect of other natural loading including barometric pressure changes, Earth tide fluctuations, and accumulated effect of moisture and snow loading.

The current study considered an homogenous clay aquitard and analyzed only attenuation of the downward groundwater recharge cycles. The accumulated effect of moisture and snow loading to long-term pore pressure fluctuations was ignored. This accumulated loading effect can be studied by applying vertical water balance. To do so, the terms of water balance equation i.e., input water (precipitation) and output water (actual evapotranspiration) for the study area should be determined. An investigation by considering phase lag analyses of the long-term pore pressure cycles is needed to properly understand the cycles phase behaviour and estimate the clay vertical properties.

- A composite numerical and analytical study to investigate links between groundwater vulnerability and natural pore pressure response in Lachenaie aquifer/aquitard system.

Clay aquitards are poorly understood constituent of groundwater system in terms of vulnerability assessment. Analysis of natural pore response is a worthwhile approach to assess clay aquitard integrity. An aquifer/aquitard system with and without heterogeneity can be numerically simulated. The model boundary conditions are high-and low-frequency

pressure head response for the upper unconfined aquifer and barometric pressure change at ground surface respectively. The numerical model allows pore pressure response imposed by the boundaries to be measured within the clay layer and in the underlying confined aquifer. Analysis of BHRF, amplitude, and phase shift between in-situ data and simulated response for both homogenous and heterogeneous cases highlights influence of the heterogeneity on BHRF and groundwater recharge cycle.

- A study of BHRF, elastic, and hydraulic parameters of the Lachenaie clay based on frequency domain analysis approach.

This thesis characterised time-domain BHRF to measure horizontal hydraulic conductivity for the clay aquitard. BHRF can also be analyzed with frequency domain approach. Analysis of BHRF for underlying confined aquifer wells provides also vertical hydraulic diffusivity-conductivity for the overlying clay aquitard.

BIBLIOGRAPHY

Al-Tabbaa, A., and Wood, D. M. 1987. Some measurements of the permeability of kaolin. Geotechnique, 37(4): 499-514.

Anderson, D. G., and Richart Jr., F. E. 1976. Effects of straining on shear modulus of clays. Journal of Geotechnical and Geoenvironmental Engineering, 102(GT9): 975-987.

Anochikwa, C. I., van der Kamp, G., and Barbour, S. L. 2012. Interpreting pore-water pressure changes induced by water table fluctuations and mechanical loading due to soil moisture changes. Canadian Geotechnical Journal, 49(3): 357-366.

ASTM. (2012a). *Standard Test Methods for One-Dimensional Consolidation Properties of Soils Using Incremental Loading* (D2435). West Conshohocken, PA: ASTM.

ASTM. (2012b). *Standard test methods for measurement of hydraulic conductivity of saturated porous materials using a flexible wall permeameter* (D5084). West Conshohocken, PA: ASTM.

Arnold, M. D., Gonzalez, H., and Crawford, P.B. 1962. Estimation of reservoir anisotropy from production data. Journal of Petroleum Technology, 14(08): 909-912.

Bardet, J.-P. 1997. *Experimental Soil Mechanics*. Upper Saddle River, NJ: Prentice Hall.

Bayrd, G. 2011. Evaluating Practices for Installation of Vibrating Wire Piezometers. Geotechnical News, 27(4): 26-29.

Benabdallah, E. M. 2006. *Caractérisation de la perméabilité d'une argile sensible de Lachenaie*. M.Sc.A., École Polytechnique de Montréal, Montréal, Canada.

Bendat, J. S., and Piersol, A. G. 1991. *Random data: analysis and measurement procedures*. John Wiley & Sons, Chichester.

Benson, C. H., Gunter, J. A., Boutwell, G. P., Trautwein, S. J., and Berzanskis, P. H. 1997. Comparison of four methods to assess hydraulic conductivity. Journal of geotechnical and geoenvironmental engineering, 123(10): 929-937.

Benson, C. H., Zhai, H., and Rashad, S. M. 1994. Statistical Sample Size for construction of Soil Liners. ASCE - Journal of Geotechnical Engineering, 120(10): 1704-1724.

Biot, M. A. 1941. General Theory of Three-Dimensional Consolidation. Journal of Applied Physics, 12(2): 155-164.

Bjerrum, L. 1972. Embankments on soft ground. *In Proceedings of the ASCE Specialty Conference on Performance of Earth and Earth-Supported Structures, Purdue University, Lafayette, Ind.,* (2): 1–54.

Black, D. K., and Lee, K. L. 1973. Saturating Laboratory Samples by Back Pressure. ASCE-Journal of the Soil Mechanics and Foundations Division, 99(SM1): 75-93.

Bolton, A. J., Maltman, A. J., and Fisher, Q. 2000. Anisotropic permeability and bimodal pore-size distributions of fine-grained marine sediments. Marine and Petroleum Geology, 17(6): 657-672.

Bouchard, R., Dion, D., and Tavenas, F. 1983. Origine de la préconsolidation des argiles du Saguenay, Québec. Canadian Geotechnical Journal, 20(2): 315-328.

Bozozuk, M. 1963. The Modulus of Elasticity of Leda Clay from Field Measurements. Canadian Geotechnical Journal, 1(1): 43-51.

Bradbury, K. R., Gotkowitz, M. B., Hart, D. J., Eaton, T. T., Cherry, J. A., Parker, B. L., and Borchardt, M. A. 2006. *Contaminant transport through aquitards: technical guidance for aquitard assessment.* Awwa Research Foundation, Denver, Colorado.

Bradbury, K. R., and Muldoon, M. A. 1990. Hydraulic conductivity determinations in unlithified glacial and fluvial materials. ASTM- In Ground water and vadose zone monitoring, 1053: 138-151.

Bredehoeft, J. D. 1967. Response of well-aquifer systems to Earth tides. Journal of Geophysical Research, 72(12): 3075-3087.

Bredehoeft, J. D., Neuzil, C. E., and Milly, P. C. D. 2008. *Regional flow in the Dakota aquifer : A study of the role of confining layers* (Water-Supply Paper 2237). U.S. Geological Survey.

Bredehoeft, J. D., and Papadopulos, S. S. 1980. A method for determining the hydraulic properties of tight formations. Water Resources Research, 16(1): 233-238.

Brigham, E. O. 1988. *The Fast Fourier Transform and its applications*. Engelwood Cliffs: Prentice Hall.

Brown, S. H. 2009. Multiple linear regression analysis: a matrix approach with MATLAB. Alabama Journal of Mathematics, 34: 1-3.

Burland, J. B. 1989. Ninth Laurits Bjerrum Memorial Lecture: "Small is beautiful" - the stiffness of soils at small strains. Canadian Geotechnical Journal, 26(4): 499-516.

Butler, J. J., Jr, Jin, W., Mohammed, G. A., and Reboulet, E. C. 2011. New insights from well responses to fluctuations in barometric pressure. Groundwater, 49(4): 525-533.

Canadian Geotechnical Society, 2006. *Canadian Foundation Engineering Manual (4th ed.).* Richmond, Canada : BiTech Publisher.

Casagrande, A. 1936. The determination of the pre-consolidation load and its practical significance, *In the Proceedings of the international conference on soil mechanics and foundation engineering*. Harvard University Cambridge, 60-64.

Chan, H., and Kenney, T. C. 1973. Laboratory investigation of permeability ratio of New Liskeard varved soil. Canadian Geotechnical Journal, 10(3): 453-472.

Chapuis, R. P., Paré, J.-J., and Loiselle, A. A. 1984. Laboratory test results on self-hardening grouts for flexible cutoffs. Canadian Geotechnical Journal, 21(1): 185-191.

Chapuis, R. P. 1989. Shape Factors for Permeability Tests in Boreholes and Piezometers. Groundwater, 27(5): 647-654.

Chapuis, R. P., and Gill, D. E. 1989. Hydraulic anisotropy of homogeneous soils and rocks: influence of the densification process. Bulletin of the International Association of Engineering Geology, 39(1): 75-86.

Chapuis, R. P., Gill, D. E., and Baass, K. 1989. Laboratory permeability tests on sand: influence of the compaction method on anisotropy. Canadian Geotechnical Journal, 26(4): 614-622.

Chapuis, R. P., and Sabourin, L. 1989. Effects of installation of piezometers and wells on groundwater characteristics and measurements. Canadian Geotechnical Journal, 26(4): 604-613.

Chapuis, R. P. 1998. Overdamped slug test in monitoring wells: review of interpretation methods with mathematical, physical, and numerical analysis of storativity influence. Canadian Geotechnical Journal, 35(5): 697-719.

Chapuis, R. P. 2002. The 2000 R.M. Hardy Lecture: Full-scale hydraulic performance of soil–bentonite and compacted clay liners. Canadian Geotechnical Journal, 39(2): 417-439.

Chapuis, R. P. and Cazaux, D. 2002. Pressure-pulse test for field hydraulic conductivity of soils: Is the common interpretation method adequate? Evaluation and Remediation of Low Permeability and Dual Porosity Environments ASTM, STP 1415: 66-82.

Chapuis, R. P., and Chenaf, D. 2002. Slug tests in a confined aquifer: experimental results in a large soil tank and numerical modeling. Canadian Geotechnical Journal, 39(1): 14-21.

Chapuis, R. P., and Aubertin, M. 2003. On the use of the Kozeny Carman equation to predict the hydraulic conductivity of soils. Canadian Geotechnical Journal, 40(3): 616-628.

Chapuis, R. P. 2005. Numerical modeling of rising-head permeability tests in monitoring wells after lowering the water level down to the screen. Canadian Geotechnical Journal, 42(3): 705-715.

Chapuis, R. P. 2009a. Monitoring a well in a clay layer: revisiting the time lag problem. Bulletin of Engineering Geology and the Environment, 68(3): 387-395.

Chapuis, R. P. 2009b. Field variable-head test in low-permeability materials: Assessing the effects of trapped gas pocket and cavity expansion. Canadian Geotechnical Journal, 46(1): 81-92.

Chapuis, R. P. 2010. Influence of Element Size in Numerical Studies of Seepage: Large-Scale of Regional Studies. Geotechnical News, 28(4): 31-34.

Chapuis, R. P. 2012. Predicting the saturated hydraulic conductivity of soils: a review. Bulletin of Engineering Geology and the Environment, 71(3): 401-434.

Chapuis, R. P., Duhaime, F., and Benabdallah, E. 2012. Monitoring wells in clay: the apparently static water level and its influence during variable-head permeability tests. Bulletin of Engineering Geology and the Environment, 71(4): 663-678.

Chapuis, R. P. 2015. Overdamped Slug Tests in Aquifers: The Three Diagnostic Graphs for a User-Independent Interpretation. Geotechnical Testing Journal, 38(4): 20140250.

Cherry, J., Parker, B., Bradbury, K., Eaton, T., Gotkowitz, M., Hart, D., and Borchardt, M. 2004. *Role of aquitards in the protection of aquifers from contamination:* a "state of the science" report. Awwa Research Foundation.

Chien, Y., Bryce, R., Strait, S., and Yeatman, R. 1986. *Elimination of frequency noise from groundwater measurements*. Rockwell International Corp., HC Burkholder, Battelle Press, Richland, Washington.

Clark, J. I. 1998. The settlement and bearing capacity of very large foundations on strong soils: 1996 R.M. Hardy keynote address. Canadian Geotechnical Journal, 35(1): 131-145.

Clark, W. E. 1967. Computing the barometric efficiency of a well. Journal of the Hydraulics Division, 93(4): 93-98.

Contreras, I. A., Grosser, A. T., and VerStrate, R. H. 2008. The use of the fully-grouted method for piezometer installation. Geotechnical Instrumentation News, 26: 30-37.

Contreras, I. A., Grosser, A. T., and Ver Strate, R. H. 2012. Update of the fully-grouted method for piezometer installation. Geotechnical News, 30(2): 20.

Cooper, H. H., Bredehoeft, J. D., and Papadopulos, I. S. 1967. Response of a finite-diameter well to an instantaneous charge of water. Water Resources Research, 3(1): 263-269.

Crawford, C. B. 1964. Interpretation of the consolidation test. Journal of the Soil mechanics and Foundations Division, 90(5): 87-102.

Crawford, C. B., and Burn, K. N. 1963. Discussion of Settlement studies of the Mount Sinai Hospital, Toronto. Engeenirng Geology Journal, 46(5): 31-37.

Crooks, J. H. A., and Graham, J. 1976. Geotechnical properties of the Belfast estuarine deposits. Géotechnique, 26(2): 293-315.

D'Appolonia, D. J., Poulos, H. G., and Ladd, C. C. 1971. Initial settlement of structures on clay. Journalof the Soil Mechanics and Foundations Division, ASCE, 97(SM10): 1359-1376.

Dagan, G. 1967. A method of determining the permeability and effective porosity of unconfined anisotropie aquifers. Water Resources Research, 3(4): 1059-1071.

Davis, S. N., and DeWiest, R. J. M. 1966. *Hydrogeology*. John Wiley, New York.

De Rienzo, F., Oreste, P., and Pelizza, S., 2008. Subsurface geological-geotechnical modelling to sustain underground civil planning. Engineering Geology, 96(3–4): 187-204.

Demers, D., and Leroueil, S. 2002. Evaluation of preconsolidation pressure and the overconsolidation ratio from piezocone tests of clay deposits in Quebec. Canadian Geotechnical Journal, 39(1): 174-192.

Desaulniers, D. E., and Cherry, J. A. (1989). Origin and movement of groundwater and major ions in a thick deposit of Champlain Sea clay near Montreal. Revue canadienne de géotechnique, 26(1), 80-89.

Domenico, P.A., and Schwartz, F.W. 1997. *Physical and chemical hydrogeology*. John Wiley, New York.

Duhaime, F. 2012. Mesure de la conductivité hydraulique du dépôt d'argile Champlain de Lachenaie, Québec: théorie et applications. P.hD., École Polytechnique de Montréal, Montréal, Canada.

Duhaime, F., Benabdallah, E. M., and Chapuis, R. P. 2013. The Lachenaie clay deposit: some geochemical and geotechnical properties in relation to the salt-leaching process. Canadian Geotechnical Journal, 50(3): 311-325.

Duhaime, F., and Chapuis, R. P. 2014. A coupled analysis of cavity and pore volume changes for pulse tests conducted in soft clay deposits. International Journal for Numerical and Analytical Methods in Geomechanics, 38(9): 903-24.

Dunnicliff, J., 1988. *Geotechnical Instrumentation for Measuring Field Performance*. John Wiley, New York.

Evans, K., Beavan, J., Simpson, D., and Mousa, S. 1991. Estimating aquifer parameters from analysis of forced fluctuations in well level: An example from the Nubian Formation near Aswan, Egypt: 3. Diffusivity estimates for saturated and unsaturated zones. Journal of Geophysical Research: Solid Earth (1978–2012), 96(B7): 12161-12191.

Ferris, J. G. 1952. Cyclic fluctuations of water level as a basis for determining aquifer transmissibility. U.S. Geological Survey, Ground-Water Hydraulics Section, Contribution, (1): 17p.

Ferris J. G. 1963. Cyclic fluctuations of water level as a basis for determining aquifer transmissibility. Water-Supply Paper 1536-I, U.S. Geological Survey, 305–318.

Furbish, D. J. 1991. The response of water level in a well to a time series of atmospheric loading under confined conditions. Water Resources Research, 27(4): 557-68.

Galloway, D., and Rojstaczer, S. 1988. Analysis of the frequency response of water levels in wells to earth tides and atmospheric loading. *In the proceding of 4th annual Canadian/American conference on hydrology, fluid flow, heat transfer, and mass transport in fractured rocks*, Alberta, Canada.

GSI Environnement, 2001. Étude géotechnique, agrandissement du secteur nord, lots parties 77 a` 87, 90, 93, 94, 99 et 100.

Gustin, E. J. G., Karim, U. F. A., and Brouwers, H. J. H. 2007. Bleeding characteristics for viscous cement and cement-bentonite grouts. Geotechnique, 57(4): 391-395.

Hamilton, J., and Crawford, C. 1960. Improved determination of preconsolidation pressure of a sensitive clay. ASTM Special Technical Publication, (254): 254-271.

Hamouche, K. K. 1995. Comportement des argiles Champlain sollicitées horizontalement. P.hD., Université Laval, Quebec, Canada.

Hantush, M. S. 1956. Analysis of data from pumping tests in leaky aquifers. Eos, Transactions American Geophysical Union, 37(6):

Hantush, M. S. 1966. Wells in homogeneous anisotropic aquifers. Water Resources Research, 2(2): 273-279.

Hare, P. W., and Morse, R. E. 1997. Water-Level Fluctuations Due to Barometric Pressure Changes in an Isolated Portion of an Unconfined Aquifer. Groundwater, 35(4): 667-671.

Hare, P. W., and Morse, R. E. 1999. Monitoring the hydraulic performance of a containment system with significant barometric pressure effects. Groundwater, 37(5): 755-763.

Helwany, S. 2007. *Applied Soil Mechanics: with ABAQUS Applications*. John Wiley and Sons, New York.

Holtz, R. D., Jamiolkowski, M. B., and Lancellotta, R. 1986. Lessons From Oedometer Tests on High Quality Samples. J Geotech Eng-Asce, 112(8): 768-776.

Holtz, R. D.,and Kovacs, W. D. 1981. *An introduction to geotechnical engineering*. Prentice Hall, Englewood Cliffs, New Jersey.

Hsieh, P. A., Bredehoeft, J. D., and Farr, J. M. 1987. Determination of aquifer transmissivity from Earth tide analysis. Water Resources Research, 23(10): 1824-1832.

Hsieh, P. A., and Neuman, S. P. 1985. Field Determination of the Three-Dimensional Hydraulic Conductivity Tensor of Anisotropic Media: 1. Theory. Water Resources Research, 21(11): 1655-1665.

Hydrotechnique Associates. 1984. *Evaluation of barometric and earth tide effects in well records: documentation*. Report prepared for Rockwell Hanford Operations, by Hydrotechnique Associates, Berkeley, California.

Hussein, M. E., Odling, N. E., and Clark, R. A. 2013. Borehole water level response to barometric pressure as an indicator of aquifer vulnerability. Water Resources Research, 49(10): 7102-7119.

Hvorslev, M. J. 1951. *Time-lag and soil permeability in ground water observation* (Bulletin 36). Vicksburg, MS : U.S. Army Engineering Waterways Experimental Station.

Isenhower, W. M. 1979. Torsional simple shear-resonant column properties of San Francisco Bay mud. M.Sc.A., University of Texas at Austin.

Jacob, C. 1940. On the flow of water in an elastic artesian aquifer. Transactions, American Geophysical Union, 21(2): 574-586.

Jacob, C. 1950. Flow of groundwater. In H. Rouse (dir.), In *Engineering Hydraulics* (pp. 321-386). New-York, NY: John Wiley and Sons.

Janbu, N. 1969. The resistance concept applied to deformations of soils. *Proceedings of the European Conference on Soil Mechanics and Foundation Engineering*, 1: 19-25.

Jardine, R. J., Symes, M. J., and Burland, J. B. 1984. The Measurement of soil stiffness in the triaxial apparatus. Géotechnique, 34(3): 323-340.

Jurado, A., De Gaspari, F., Vilarrasa, V., Bolster, D., Sánchez-Vila, X., Fernàndez-Garcia, D., and Tartakovsky, D. M. 2012. Probabilistic analysis of groundwater-related risks at subsurface excavation sites. Engineering Geology, 125: 35-44.

Karray, M., and Lefebvre, G. 2001. *Étude parasismique pour l'agrandissement du secteur nord-BFI usine de triage Lachenaie LTEE*. Report GEO-01-07, Varennes, Québec.

Karray, M., and Lefebvre, G. 2008. Significance and evaluation of Poisson's ratio in Rayleigh wave testing. Canadian Geotechnical Journal, 45(5): 624-635. DOI:10.1139/T08-016

Keller, C. K., van Der Kamp, G., and Cherry, J. A. 1989. A multiscale study of the permeability of a thick clayey till. Water Resources Research, 25(11): 2299-2317.

Kiyama, T., Kita, H., Ishijima, Y., Yanagidani, T., Aoki, K., and Sato, T. 1996. Permeability in anisotropic granite under hydrostatic compression and triaxial compression including post-failure region. *2nd North American Rock Mechanics Symposium*. American Rock Mechanics Association.

Klohn, E. J. 1965. The Elastic Properties of a Dense Glacial Till Deposit. Canadian Geotechnical Journal, 2(2): 116-128.

Krahn, J. 2004. *Seepage modeling with SEEP/W: An engineering methodology*. GEO-SLOPE International Ltd. Calgary, Alberta, Canada.

La Rochelle, P., Chagnon, J. Y., and Lefebvre, G. 1970. Regional geology and landslides in the marine clay deposits of eastern Canada. Canadian Geotechnical Journal, 7(2): 145-156.

La Rochelle, P., and Lefebvre, G. 1971. Sampling disturbance in Champlain clays. *Sampling of Soil and Rock.* ASTM, STP, 483: 143-163.

La Rochelle, P., Sarrailh, J., Tavenas, F., Roy, M., and Leroueil, S. 1981. Causes of sampling disturbance and design of a new sampler for sensitive soils. Canadian Geotechnical Journal, 18(1): 52-66.

Lambe, T., and Whitman, R. 1969. *Soil Mechanics*. Wiley. New York.

Lefebvre, G., Leboeuf, D., Rahhal, M. E., Lacroix, A., Warde, J., and Stokoe, K. H. 1994. Laboratory and field determinations of small-strain shear modulus for a structured Champlain clay. Canadian Geotechnical Journal, 31(1): 61-70.

Lefebvre, G., and Poulin, C. 1979. A new method of sampling in sensitive clay. Canadian Geotechnical Journal, 16(1): 226-233.

Lefebvre, G., Bozozuk, M., Philibert, A., and Hornych, P. 1991. Evaluating Ko in Champlain clays with hydraulic fracture tests. Canadian Geotechnical Journal, 28(3): 365-377.

Leroueil, S. 1996. Compressibility of Clays: Fundamental and Practical Aspects. ASCE-Journal of Geotechnical Engineering, 122(7): 534-543.

Leroueil, S., Roy, M., La Rochelle, P., Brucy, F., and Tavenas, F.A. 1979. Behavior of destructured natural clays. Journal of the Geotechnical Engineering Division, 105(6): 759-778.

Leroueil, S., Tavenas, F., Samson, L., and Morin, P. 1983. Preconsolidation pressure of Champlain clays. Part II. Laboratory determination. Canadian Geotechnical Journal, 20(4): 803-816.

Leroueil, S., Kabbaj, M., Tavenas, F., and Bouchard, R. 1985. Stress–strain–strain rate relation for the compressibility of sensitive natural clays. Géotechnique, 35(2): 159-180.

Leroueil, S., Bouclin, G., Tavenas, F., Bergeron, L., and Rochelle, P. L. 1990. Permeability anisotropy of natural clays as a function of strain. Canadian Geotechnical Journal, 27(5): 568-579.

Leroueil, S., Hamouche, K., Ravenasi, F., Boudali, M., Locat, J., Virely, D., Tan, T., Phoon, K., Hight, D., and Leroueil, S. 2003. Geotechnical characterization and properties of a sensitive clay from Quebec. Characterization and engineering properties of natural soils, 1: 363-394.

Mansur, C. I., and Dietrich, R. J. 1965. Pumping test to determine permeability ratio. Journal of the Soil Mechanics and Foundations Division, 91(4): 151-186.

Marefat, V., Duhaime, F., and Chapuis, R. P. 2013. Measuring pore pressure change in the Lachenaie clay deposit, Quebec. *Proceedings of the 66th Canadian Geotechnical Conference,* Montreal, Canada, October 2013. Canadian Geotechnical Society, 8 pages.

Marefat, V., Chapuis, R. P., and Duhaime, F. 2014. Piezometric error for fully grouted piezometers Installed in clay layers. *Proceedings of the 67th Canadian Geotechnical Conference,* Regina, Canada, October 2014. Canadian Geotechnical Society, 8 pages.

Marefat, V., Duhaime, F., and Chapuis, R. P. 2015a. Pore pressure response to barometric pressure change in Champlain clay: Prediction of the clay elastic properties. Engineering Geology, 198: 16-29.

Marefat, V., Duhaime, F., and Chapuis, R. P. 2015b. Fully grouted piezometers: Implications for pore pressure monitoring in clay layers. Submitted to Engineering Geology.

Marefat, V., Duhaime, F. and Chapuis, R. P. 2015c. Performance of fully grouted piezometers subjected to transient flow conditions. *Proceedings of the 68th Canadian Geotechnical Conference,* Quebec, Canada, September 2015. Canadian Geotechnical Society, 8 pages.

Marefat, V., Chapuis, R. P., and Duhaime, F. 2015d. In-situ investigation of Champlain clay integrity. *Proceedings of the Joint Seminar in Geoenvironmental Engineering (GEE),* Montreal, Canada.

Marefat, V., Duhaime, F., and Chapuis, R. P., Spane, F. A. 2016. Estimates of in-situ vertical and horizontal hydraulic diffusivity and conductivity for a shallow clay aquitard, using a combined natural recharge and barometric pressure response approach. Submitted to Journal of Hydrogeology.

Mbonimpa, M., Aubertin, M., Chapuis, R. P., and Bussière, B. 2002. Practical pedotransfer functions for estimating the saturated hydraulic conductivity. Geotechnical and Geological Engineering, 20(3): 235-259.

McKenna, G. T. 1995. Grouted-in installation of piezometers in boreholes. Canadian Geotechnical Journal, 32(2): 355-363.

Mesri, G., and Olson, R. E. 1971. Mechanisms controlling the permeability of clays. clays clay minerals journal, 19(3): 151–158.

Mikkelsen, P., and Green, G. E. 2003. Piezometers in fully grouted boreholes. FMGM-Field Measurements in Geomechanics, Oslo, Norway.

Mikkelsen, P. E. 1999. Grouting in Piezometers - An Experiment at Slope Indicator, In Technical Note at www.slope.com, 2 pages.

Mikkelsen, P. E. 2002. Cement-bentonite grout backfill for borehole instruments. Geotechnical News, 20(4): 38-42.

Mitchell, J. K. 1956. The fabric of natural clays and its relation to engineering properties. Highway Research Board Proceedings (pp. 693-713).

Mitchell, R. J. 1970. On the yielding and mechanical strength of Leda clays. Canadian Geotechnical Journal, 7(3): 297-312.

Montgomery, D. C., and Peck, E. A. 1992. *Introduction to linear regression analysis*. John Wiley and Sons, New York.

Nagaraj, T. S., Murthy, B. R. S., Vatsala, A., and Joshi, R. C. 1990. Analysis of Compressibility of Sensitive Soils. Journal of Geotechnical Engineering, 116(1): 105-118.

Neuman, S. P., and Gardner, D.A. 1989. Determination of Aquitard/Aquiclude Hydraulic Properties from Arbitrary Water-Level Fluctuations by Deconvolution. Ground Water, 27(1): 66-76.

Neuzil, C. E. 1982. On conducting the modified 'Slug' test in tight formations. Water Resources Research, 18(2): 439-441.

Neuzil, C. E. 1994. How permeable are clays and shales? Water resources research, 30(2): 145-150.

Nur, A., and Byerlee, J. D. 1971. An exact effective stress law for elastic deformation of rock with fluids. Journal of Geophysical Research, 76(26): 6414-6419.

O'Shaughnessy, V., and Garga, V. K. (1994). The hydrogeological and contaminant-transport properties of fractured Champlain Sea clay in Eastern Ontario. Part 1. Hydrogeological properties. Revue canadienne de géotechnique, 31(6), 885-901.

Odling, N. E., Perulero Serrano, R., Hussein, M. E. A., Riva, M., and Guadagnini, A. 2015. Detecting the vulnerability of groundwater in semi-confined aquifers using barometric response functions. Journal of Hydrology, 520(0): 143-156.

Olson, R., Daniel, D., 1981. Measurement of the hydraulic conductivity of fine-grained soils. Permeability and groundwater contaminant transport, ASTM STP, 746: 18-64.

Portland Cement Association. 1984. Cement-Bentonite Slurry Trench Cutoff Walls, USA.

Pujades, E., Carrera, J., Vázquez-Suñé, E., Jurado, A., Vilarrasa, V., Mascuñano-Salvador, E. 2012. Hydraulic characterization of diaphragm walls for cut and cover tunnelling. Engineering Geology, 125: 1-10.

Pujades, E., Vázquez-Suñé, E., Carrera, J., Vilarrasa, V., De Simone, S., Jurado, A., Ledesma, A., Ramos, G., Lloret, A. 2014. Deep enclosures versus pumping to reduce settlements during shaft excavations. Engineering Geology, 169 : 100-111.

Quigley, R. M. 1980. Geology, mineralogy, and geochemistry of Canadian soft soils: a geotechnical perspective. Canadian Geotechnical Journal, 17(2): 261-285.

Rasmussen, T. C., and Crawford, L. A. 1997. Identifying and removing barometric pressure effects in confined and unconfined aquifers. Groundwater, 35(3): 502-511.

Rasmussen, T. C., and Mote, T. L. 2007. Monitoring Surface and Subsurface Water Storage Using Confined Aquifer Water Levels at the Savannah River Site, USA. Vadose Zone Journal, 6(2): 327-335.

Rice, J. R., and Cleary, M.P. 1976. Some basic stress diffusion solutions for fluid-saturated elastic porous media with compressible constituents. Reviews of Geophysics, 14(2): 227-241.

Ritzi, R.W., Sorooshian, S., and Hsieh, P. A. 1991. The estimation of fluid flow properties from the response of water levels in wells to the combined atmospheric and Earth tide forces. Water Resources Research, 27(5): 883-893.

Rojstaczer, S. 1988a. Determination of fluid flow properties from the response of water levels in wells to atmospheric loading. Water Resources Research, 24(11): 1927-38.

Rojstaczer, S. 1988b. Intermediate Period Response of Water Levels in Wells to Crustal Strain: Sensitivity and Noise Level. Journal of Geophysical Research: Solid Earth, 93(B11): 13619-13634.

Rojstaczer, S., and Agnew, D. C. 1989. The influence of formation material properties on the response of water levels in wells to Earth tides and atmospheric loading. Journal of Geophysical Research: Solid Earth (1978–2012), 94(B9): 12403-12411.

Rojstaczer, S., and Riley, F. S. 1990. Response of the water level in a well to earth tides and atmospheric loading under unconfined conditions. Water Resources Research, 26(8): 1803-1817.

Scholes, O., Clayton, S., Hoadley, A., and Tiu, C. 2007. Permeability anisotropy due to consolidation of compressible porous media. Transport in porous media, 68(3): 365-387.

Schulze, K. C., Kümpel, H.-J., and Huenges, E. 2000. In-situ petrohydraulic parameters from tidal and barometric analysis of fluid level variations in deep wells: some results from KTB, Hydrogeology of Crystalline Rocks. Springer, pp. 79-104.

Seo, H. H. 1999. Modeling the response of ground-water levels in wells to changes in barometric pressure. P.hD., Iowa State University, Ames, IA.

Shibuya, S. 2000. Assessing Structure of Aged Natural Sedimentary Clays. Soils and Foundations, 40(3): 1-16.

Shibuya, S., Hwang, S. C., and Mitachi, T. 1997. Elastic shear modulus of soft clays from shear wave velocity measurement. Geotechnique, 47(3): 593-601.

Shih, D. C.-F., Lee, C.-D., Chiou, K.-F., and Tsai, S.-M. 2000. Spectral analysis of tidal fluctuations in ground water level. Journal of the American Water Resources Association, 36(5): 1087-1099.

Shih, D. C.-F., Lin, G.-F., Jia, Y.-P., Chen, Y.-G., Wu, and Y.-M. 2008. Spectral decomposition of periodic ground water fluctuation in a coastal aquifer. Hydrological Processes, 22(12): 1755-1765.

Silvestri, V. 1980. The long-term stability of a cutting slope in an overconsolidated sensitive clay. Canadian Geotechnical Journal, 17(3): 337-351.

Silvestri, V. 2000. Performance of shallow foundations on clay deposits in Montréal Island. Canadian Geotechnical Journal, 37(1): 218-237.

Silvestri, V. 2003. Assessment of self-boring pressuremeter tests in sensitive clay. Canadian Geotechnical Journal, 40(2): 365-387.

Silvestri, V., Soulié, M., Lafleur, J., Sarkis, G., and Bekkouche, N. 1992. Foundation problems in Champlain clays during droughts. II. Case histories. Canadian Geotechnical Journal, 29(2): 169-187.

Silvestri, V., and Abou-Samra, G. 2008. Analysis of instrumented sharp cone and pressuremeter tests in stiff sensitive clay. Canadian Geotechnical Journal, 45(7): 957-972.

Simeoni, L. 2012. Laboratory tests for measuring the time-lag of fully grouted piezometers. Journal of Hydrology, 438-439: 215-222.

Simeoni, L., De Polo, F., Caloni, G., and Pezzetti, G. 2011. Field performance of fully grouted piezometers, *Proceedings of the FMGM Congress*.

Skempton, A. 1954. The pore-pressure coefficients A and B. Geotechnique, 4(4): 143-147.

Smerdon, B. D., Smith, L. A., Harrington, G. A., Gardner, W. P., Delle Piane, C., and Sarout, J. 2014. Estimating the hydraulic properties of an aquitard from in situ pore pressure measurements. Hydrogeology Journal, 22(8): 1875-1887.

Smith, L. A., Van Der Kamp, G., and Hendry, J. M. 2013. A new technique for obtaining high-resolution pore pressure records in thick claystone aquitards and its use to determine in situ compressibility. Water Resources Research, 49(2): 732-743.

Spane, F. A. 1999. Effects of barometric fluctuations on well water-level measurements and aquifer test data. Pac. Northwest Natl. Lab., Department of Energy, Richland, Washington.

Spane, F. A. 2002. Considering barometric pressure in groundwater flow investigations. Water resources research, 38(6): 14-1-14-18.

Spane, F. A., and Mackley, R.D. 2011. Removal of River-Stage Fluctuations from Well Response Using Multiple Regression. Groundwater, 49(6): 794-807.

Spane, F. A. 1992. Applicability of slug interference tests under Hanford Site test conditions: Analytical assessment and field test evaluation. Pacific Northwest laboratory, Richland, WA. PNL-8070.

Supardi, S. S. 1993. *Repeatability of slug test results in Wisconsinan age Glacial Till in Iowa*. M.Sc.A., Iowa State University.

Tavenas, F., and Leroueil, S. 1977. The effect of stresses and time on yielding of clays. *Proceding of 9th International Conference Soil Mechanics and Foundation Engineering*, Tokyo, pp. 319-326.

Tavenas, F., Chapeau, C., La Rochelle, P., and Roy, M. 1974. Immediate Settlements of Three Test Embankments on Champlain Clay. Canadian Geotechnical Journal, 11(1): 109-141.

Tavenas, F., Jean, P., Leblond, P., and Leroueil, S. 1983a. The permeability of natural soft clays. Part II: Permeability characteristics. Canadian Geotechnical Journal, 20(4): 645-660.

Tavenas, F., Leblond, P., Jean, P., and Leroueil, S. 1983b. The permeability of natural soft clays. Part I: Methods of laboratory measurement. Canadian Geotechnical Journal, 20(4): 629-644.

Tavenas, F., Tremblay, M., Larouche, G., & Leroueil, S. (1986). In Situ Measurement Of Permeability In Soft Clays. Proceedings of In Situ 86, a Speciality Conference sponsored by the Geotechnical Engineering Division (pp. 1034-1048). ASCE Geotechnical Special Publication No. 6.

Tavenas, F., Diene, M., and Leroueil, S. (1990). Analysis of the in situ constant-head permeability test in clays. Revue canadienne de géotechnique, 27(3), 305-314.

Taylor, D. W. 1948. *Fundamentals of soil mechanics*. New-York, NY : John Wiley and Sons.

Terzaghi, K., and Peck, R. 1948. *Soil mechanics in engineering practice*. John Wiley and Sons Inc, New York.

Terzaghi, K., Peck, R., and Mesri, G. 1996. *Soil mechanics in engineering practice*. John Wiley and Sons Inc, New York.

Terzaghi, R. 1936. Theshearing resistance of sdaturated soils. *Proceding of the 1st International Conference on Soil Mechanics* (pp. 54-56). Cambridge, Mas.

Timms, W. A., and Acworth, R. I. 2005. Propagation of pressure change through thick clay sequences: an example from Liverpool Plains, NSW, Australia. Hydrogeology Journal, 13(5-6): 858-870.

Toll, N. J., and Rasmussen, T. C. 2007. Removal of barometric pressure effects and earth tides from observed water levels. Groundwater, 45(1): 101-105.

van der Kamp, G. 2001a. Methods for determining the in situ hydraulic conductivity of shallow aquitards - an overview. Hydrogeology Journal, 9(1): 5-16.

van der Kamp, G. 2001b. Methods for determining the in situ hydraulic conductivity of shallow aquitards – an overview. Hydrogeology Journal, 9(1): 5-16.

van der Kamp, G., and Gale, J. E. 1983. Theory of Earth tide and barometric effects in porous formations with compressible grains. Water Resources Research, 19(2): 538-44.

van der Kamp, G., and Maathuis, H. 1991. Annual fluctuations of groundwater levels as a result of loading by surface moisture. Journal of Hydrology, 127(1): 137-152.

van der Kamp, G., and Schmidt, R. 1997. Monitoring of total soil moisture on a scale of hectares using groundwater piezometers. Geophysical Research Letters, 24(6): 719-722.

Vaughan, P. R. 1969. A Note on Sealing Piezometers in Boreholes. Geotechnique, 19(3): 405-413.

Viggiani, G., and Atkinson, J. H. 1995. Stiffness of fine-grained soil at very small strains. Geotechnique, 45(2): 249-265.

Weeks, E. P. 1979. Barometric fluctuations in wells tapping deep unconfined aquifers. Water Resources Research, 15(5): 1167-1176.

Witt, K.-J., ad Brauns, J. 1983. Permeability-anisotropy due to particle shape. ASCE-Journal of Geotechnical Engineering, 109(9): 1181-1187.

Wood, D. M. 2010. *Soil Behaviour and critical state soil mechanics*. Cambridge University Press, New York.

Xu, Y.-S., Shen, S.-L., and Du, Y.-J. 2009. Geological and hydrogeological environment in Shanghai with geohazards to construction and maintenance of infrastructures. Engineering Geology, 109(3–4): 241-254.

Yong, R. N., and Silvestri, V. 1979. Anisotropic behaviour of a sensitive clay. Canadian Geotechnical Journal, 16(2): 335-350.

Youd, T. L., Idriss, I. M., Andrus, R. D., Arango, I., Castro, G., Christian, J. T., Dobry, R., Finn, W. D .L., Harder, L. F., Hynes, M. E., Ishihara, K., Koester, J. P., Liao, S. S. C., Marcuson, W. F., Martin, G. R., Mitchell, J. K., Moriwaki, Y., Power, M. S., Robertson, P. K., Seed, R. B., and Stokoe, K. H. 2001. Liquefaction Resistance of Soils: Summary Report from the 1996 NCEER and 1998 NCEER/NSF Workshops on Evaluation of Liquefaction Resistance of Soils. Journal of Geotechical and Geoenvironmental Engineering, 127: 817-833.

Yungwirth, G., Preene, M., Dobr, M., and Forero Garcia, F. 2013. Practical Application and Design Considerations for Fully Grouted Vibrating Wire Piezometers in Mine Water Investigations. *Proceding of annual International Mine Water Association Conference - Reliable Mine Water Technology* (pp. 229 – 237), Golden, Colorado, USA.

Zawadzki, W., and Chorley, D. 2014. Grouted-in Pressure Transducers: Implications for Hydrogeological Testing and Monitoring in Bedrock. Mine Water Environ, 33(3): 289-292.

Zienkiewicz, O. C., Taylor, R. L., and Zhu, J. Z. 2005. *The finite element method: its basis and fundamentals* (6th ed.). Boston, MA: Elsevier Butterworth-Heinemann.

Zimmie, T., Doynow, J., and Wardell, J. 1981. Permeability testing of soils for hazardous waste disposal sites. *Proceedings of the Tenth International Conference on Soil Mechanics and Foundation Engineering* (pp. 403-406).

APPENDIX A   MATLAB SCRIPT FOR BRF/BHRF CALCULATION AND REMOVING BAROMETRIC PRESSURE EFFECTS

The current values of pore pressure changes can be predicted based on both the current and lagged values of barometric pressure changes (explanatory variables). For absolute pore pressure measurement a linear set of multiple regression equations can be written as follows (Spane, 1999; Spane, 2002):

$$\Delta u_{\mathbf{t}} = \delta_0 + \delta_1 (\Delta B)_t + \delta_2 (\Delta B)_{t-1} + ... + \delta_k (\Delta B)_{t-k} + \varepsilon \tag{A1}$$

where Δu_t is the change in pore water pressure $u_t - u_{t-1}$, $(\Delta B)_t$ is the change in barometric pressure $B_t - B_{t-1}$, $(\Delta B)_{t-1}$ is the change in barometric pressure for the previous time step, $(\Delta B)_{t-k}$ is the change in barometric pressure for the kth previous time step, δ_0 is the regression intercept, δ_1 ...δ_k are the regression coefficients which can be calculated with ordinary leas squares (OLS) method.

The least square $\hat{\delta}_j$ estimators should be obtained to fit $\Delta \hat{u}_t$ to Δu_t.

$$\Delta \hat{u}_{\mathbf{t}} = \hat{\delta}_0 + \hat{\delta}_1 (\Delta B)_t + \hat{\delta}_2 (\Delta B)_{t-1} + ... + \hat{\delta}_k (\Delta B)_{t-k} \tag{A2}$$

Solving the least squares equation minimizes the sum of the squared error:

$$\Delta \mathbf{B}^{\mathbf{T}} \Delta \mathbf{B} \hat{\boldsymbol{\delta}} = \Delta \mathbf{B}^{\mathbf{T}} \Delta \mathbf{u} \tag{A3}$$

The least square estimators can be calculated as follows (Montgomery and Peck, 1992):

$$\hat{\boldsymbol{\delta}} = \left[\Delta \mathbf{B}^{\mathbf{T}} \Delta \mathbf{B} \right]^{-1} \Delta \mathbf{B}^{\mathbf{T}} \Delta \mathbf{u} \tag{A4}$$

The barometric head response function is constructed by gradually summing up the regression coefficients to k number of the associated time lag.

$$BRF/BHRF = \sum_{j=1}^{k} \delta_j \tag{A5}$$

Following equations provide corrected pore pressure (u_c) for n number of data:

$$u_c = u_t - \sum_{i=1}^{n} \Delta u_{t-i} \tag{A6}$$

And

$$\sum_i^n \Delta u_{t-i} = \Delta u_t + \Delta u_{t-1} + \cdots + \Delta u_{t-n} \tag{A7}$$

A MATLAB script was provided to calculate multiple regression coefficients, construct BHRF, and correct observed pore pressure to barometric pressure fluctuations.

```matlab
clc, clear, close all
%This script calculates multiple-regression coefficients using OLS method,
%construcs BHRF from pore pressure response to barometric pressure change,
% and removes the barometric pressure effects from observed pore
%pressure data series.

data = load('Pdata.txt');
t = data(:,1); % Time record (15 min)
u = data(:,2); % Observed pore pressure, m
b = data(:,3); % Observed barometric pressure change, m
clear data

t = t + 693960; % convert from excel to matlab time format

figure
plot(t,u,t,b)
ylabel('Change in pressure, m')
xlabel('Date/time, day')
legend('Observed pore pressure','Barometric Pressure change')
datetick('x',5)
 db = diff(b); % DELTA B
du = diff(u); % DELTA u
 lag = 100; % Number of lag
j = (lag+1):length(db);% j takes data after lag+1 to creat explanatory matrix (here DELTA B)

y = du(j);
x = ones(size(db(j)));% function to creat independent matrix (X)
for i=0:lag;
   x = [x db(j-i)];
end

c = x\y; % calculate regression coefficients (DELTA)
pt = t(j);
tc = 0:lag;
bhrf = cumsum(c(tc+1));%calculate BHRF
uc = u(j) - cumsum(x(:,tc+2)*c(tc+2)); %correct pore pressure to barometric pressure change
figure
plot(tc/4,bhrf)%divided by 4 because the time interval was 1/4 of an hour
xlabel('Time Lag (hours)')
```

```
ylabel('BHRF')
ylim([0 1]);
figure
plot(t,u,pt,uc)
datetick('x',5)
ylabel('Pressure Head, m')
xlim([min(t)-2,max(t)+2])
```

A simple example is given to show the steps to calculate BHRF for a 4 number of lag and to remove barometric pressure effect from pore pressure response.

Table A.1: Raw pore pressure and barometric pressure change data from 01/01/2013 to 02/01/2013, Lachenaie area (2AH).

Date/time	u(m)	B(m)
01/01/2013 0:01	14.54122	10.224
01/01/2013 1:01	14.54122	10.228
01/01/2013 2:01	14.54122	10.244
01/01/2013 3:01	14.54467	10.257
01/01/2013 4:01	14.54812	10.269
01/01/2013 5:01	14.55157	10.283
01/01/2013 6:01	14.55847	10.298
01/01/2013 7:01	14.56537	10.311
01/01/2013 8:01	14.56882	10.322
01/01/2013 9:01	14.57227	10.322
01/01/2013 10:01	14.57572	10.331
01/01/2013 11:01	14.57917	10.329
01/01/2013 12:01	14.57917	10.328
01/01/2013 13:01	14.57917	10.32
01/01/2013 14:01	14.57917	10.319
01/01/2013 15:01	14.57917	10.323
01/01/2013 16:01	14.58262	10.319
01/01/2013 17:01	14.58262	10.323
01/01/2013 18:01	14.58607	10.328
01/01/2013 19:01	14.58952	10.337
01/01/2013 20:01	14.59297	10.337
01/01/2013 21:01	14.59297	10.332
01/01/2013 22:01	14.59297	10.334
01/01/2013 23:01	14.59641	10.336

The first step in BRF calculation is to prepare the **Δu** and **ΔB** matrixes. **Δu** is a matrix describes observed pore pressure changes. **ΔB** is a matrix describes barometric pressure changes and its lagged components from zero up to k number of lag.

$Δu =$ $ΔB =$

Δu		$ΔB_t$	$ΔB_{t-1}$	$ΔB_{t-2}$	$ΔB_{t-3}$	$ΔB_{t-4}$
0.0034	1.0000	0.0140	0.0120	0.0130	0.0160	0.0040
0.0069	1.0000	0.0150	0.0140	0.0120	0.0130	0.0160
0.0069	1.0000	0.0130	0.0150	0.0140	0.0120	0.0130
0.0035	1.0000	0.0110	0.0130	0.0150	0.0140	0.0120
0.0034	1.0000	0	0.0110	0.0130	0.0150	0.0140
0.0035	1.0000	0.0090	0	0.0110	0.0130	0.0150
0.0034	1.0000	-0.0020	0.0090	0	0.0110	0.0130
0	1.0000	-0.0010	-0.0020	0.0090	0	0.0110
0	1.0000	-0.0080	-0.0010	-0.0020	0.0090	0
0	1.0000	-0.0010	-0.0080	-0.0010	-0.0020	0.0090
0	1.0000	0.0040	-0.0010	-0.0080	-0.0010	-0.0020
0.0035	1.0000	-0.0040	0.0040	-0.0010	-0.0080	-0.0010
0	1.0000	0.0040	-0.0040	0.0040	-0.0010	-0.0080
0.0034	1.0000	0.0050	0.0040	-0.0040	0.0040	-0.0010
0.0035	1.0000	0.0090	0.0050	0.0040	-0.0040	0.0040
0.0034	1.0000	0	0.0090	0.0050	0.0040	-0.0040
0	1.0000	-0.0050	0	0.0090	0.0050	0.0040
0	1.0000	0.0020	-0.0050	0	0.0090	0.0050
0.0034	1.0000	0.0020	0.0020	-0.0050	0	0.0090

Gaussian elimination calculates regression coefficient. MATLAB simply perform this by backslash operator "\":

$\hat{δ} = ΔB \backslash Δu =$

Timelag	BHRF
	0.0013
0	0.0932
1	0.3635
2	0.3031
3	0.2327
4	0.3227

$\hat{δ} = ΔB \backslash Δu =$
0.0013
0.0932
0.2703
-0.0604
-0.0704
0.0900

Corrected pore pressure data series can be calculated as follows:

$$\sum_{i=1}^{n} \Delta u_{t-i} =$$

$u_c=$

$\sum_{i=1}^{n} \Delta u_{t-i} =$	$u_c=$
0.0030	14.5451
0.0080	14.5436
0.0127	14.5457
0.0165	14.5489
0.0188	14.5500
0.0195	14.5528
0.0221	14.5536
0.0219	14.5573
0.0204	14.5588
0.0191	14.5600
0.0196	14.5596
0.0209	14.5583
0.0193	14.5634
0.0207	14.5619
0.0233	14.5628
0.0248	14.5648
0.0237	14.5692
0.0224	14.5706
0.0242	14.5687

APPENDIX B   MATLAB SCRIPT FOR FFT CALCULATION AND FILTERING

```
% This script creates a bandpass filter for a specified frequencies between 0.00244 and 0.00293.
%Then, is calculates the FFT for the %filtered data.
clc
close all
clear all
%% Loading the data
data = xlsread('Data.xlsx');
% Generating the time variable
t = 1:size(data,1);
% Plotting the original data set
figure; hold on;
plot(t,data)
% Removing the mean value
dataMean = data - mean(data);
plot(t,dataMean,'k')
%% Creating a band pass filter
lowFreq = 0.00244;      % Low cut off frequency
hiFreq = 0.00293;      % High cut off frequency
fs = 1;              % Sampling frequency
order = 3;            % order of the butterworth filter
[b,a] = butter(order, [lowFreq hiFreq]/(fs/2), 'bandpass'); % Forming the filter
dataMeanFiltered = filter(b,a,dataMean);  % Filtering the signal
% plotting the filtered signal
plot(t,dataMeanFiltered,'r')
legend('Original data','data after removing the mean','filtered data')
xlabel('time [Day]');
ylabel ('amplitude [?]')
%% Performing FFT
% fft length
N = 4096;
L=size(data,1)
dataMeanFFT = fft(dataMean,N)/L;    dataMeanFFT(1) = [];
dataMeanFilteredFFT = fft(dataMeanFiltered,N)/L;    dataMeanFilteredFFT(1) = [];
%% Plotting fft (power versus frequency)
% frequency axis vector
freq = linspace(0,fs,N);
% Max frequency to visualize
maxFreq = N/16;
figure; hold on;
n = length(dataMeanFFT);
powerdataMeanFFT = abs(dataMeanFFT(1:maxFreq)).^2;
powerdataMeanFilteredFFT = abs(dataMeanFilteredFFT(1:maxFreq)).^2;
subplot(211); hold on;
```

```matlab
plot(freq(1:maxFreq),powerdataMeanFFT,'k')
title('Original Signal')
subplot(212); hold on;
plot(freq(1:maxFreq),powerdataMeanFilteredFFT,'r')
% xlabel('cycles/year')
title('Filtered Signal')
```